EFFECTIVENESS OF ADAPTIVE FLIGHT PLANNING IN THE OCCURRENCE OF TOTAL LOSS OF THRUST DUE TO BIRD STRIKE

BY

KIVANÇ A. AVRENLİ

DISSERTATION

Submitted in partial fulfillment of the requirements
for the degree of Doctor of Philosophy in Civil Engineering
in the Graduate College of the
University of Illinois at Urbana-Champaign, 2015

Urbana, Illinois

Doctoral Committee:

Professor William Buttlar, Chair
Professor Barry Dempsey, Director of Research
Associate Professor Paolo Gardoni
Assistant Professor Lavanya Marla

ABSTRACT

As of today, more than 96 percent of air travelers are transported on twin-engine jets. Although contemporary twin-engine jets are more reliable and efficient than yesterday's three- and four-engine jets, they have reduced engine redundancy. A statistical analysis of the FAA Wildlife Strike Database shows that contemporary twin-engine jets are approximately 15 times more likely to undergo total loss of thrust in the event of a bird strike compared to yesterday's three- and four-engine jets. To address the total-loss-of-thrust emergency, quick reference handbooks are designed to enable speedy and successful recovery of at least one engine. Airliner type-rating programs assume that total loss of thrust culminates in at least one engine recovery. If an engine restart cannot be achieved in a real-life emergency, airline pilots are left with virtually no guidance on how to manage the emergency situation.

This dissertation hypothesizes that "an adaptive flight planner can significantly increase the odds of safe landing in the occurrence of total loss of thrust". The objective is to test the research hypothesis through a designed experiment. To construct the experimental conditions, the FAA Wildlife Strike Database is statistically analyzed, and the most hazardous bird strike conditions are identified in terms of engine failure. The findings show that engine failure due to bird strike is significantly most likely to occur during the initial climb out at a low altitude (i.e. below 5,000 ft AGL). Using the findings, five realistic bird strike scenarios are generated to be simulated in the designed experiment.

Next, an adaptive flight planner is architecturally designed for the two best-selling commercial jets: the Airbus

A320-200 and Boeing 737-800. The function of the adaptive flight planner is to compute the optimum landing trajectory in the occurrence of total loss of thrust, and then to guide the flight crew over the optimum trajectory using standard oral ATC* commands that are easy to interpret. However, the idea of engines-out landing trajectory optimization has not been developed for commercial jets due to the unavailability of aircraft-specific aerodynamic-coefficient data. To fill in this gap, a kinematic approach is adopted to develop a trajectory optimization algorithm, which is based on pure motion characteristics without making reference to the aerodynamic forces involved. The kinematic approach requires minimal amount of aircraft-specific aerodynamic data that can be effortlessly collected in a full flight simulator. Using the kinematic method, the adaptive flight planner is architecturally designed for the A320-200 and 737-800 aircraft, and its accuracy is verified through flight simulation tests.

Subsequently, the designed experiment is conducted with 12 type-rated pilots. Five total-loss-of-thrust scenarios are simulated in the A320-200 and 737-800 full flight simulators. For each scenario, the adaptive flight planning architecture is used to compute the optimum landing trajectory and the ATC commands for guiding the pilots over the optimum trajectory. Every scenario is simulated twice with each of the 12 pilots in command. First, the pilot in command is asked to attempt engines-out landing on a runway of his/ her own preference. Second, the pilot in command is guided with the ATC commands over the optimum landing trajectory. The outcomes are recorded as “success” if the pilot achieves safe touchdown on a runway,

* Air traffic control.

and “failure” otherwise. The results are analyzed using a generalized linear mixed model approach. The findings present strong evidence in favor of the research hypothesis that the adaptive flight planner can significantly increase the probability of safe touchdown in the occurrence of total loss of thrust. The results are synthesized into design recommendations which summarize the proposed application of the adaptive flight planning architecture.

This study is the first of its type to address commercial jets, and the findings can open the door for how commercial aircraft manufacturers address the total-loss-of-thrust hazard through innovative cockpit technologies.

DISCLAIMER

The accuracy of the findings presented in this dissertation is not verified by Airbus Industrie and the Boeing Company. Therefore, the findings are not intended for real flight purposes. The results are merely based on the findings of the authors in the full flight simulator, are intended to test for the research hypothesis in this study. The authors also contacted Airbus Industrie and the Boeing Company, and asked about the manufacturers' opinion on the findings. However, both manufacturers declined to provide any propriety data regarding the findings on the grounds that the University of Illinois at Urbana-Champaign does not hold a contractual agreement with them.

ACKNOWLEDGEMENTS

Foremost, I would like to express profound gratitude to my Ph.D. advisor, Prof. Barry J. Dempsey, who has been exceptionally supportive since the very beginning of this study. His expertise in aviation, his broad experience in academic research, his dedication to his profession, and his intense commitment to the academia has thoroughly impressed me. I have enjoyed working with him at every stage of this study, and his private pilot knowledge has particularly provided valuable insight into the research process. I am also aware that very few faculty advisors would display the exceptionally supportive attitude that he has shown to me, and I have been truly fortunate to have him as my advisor. Prof. Dempsey also provided extensive support in finding travel grants for the flight simulator experiments. I am very honored and proud to be the most recent Ph.D. student of Prof. Dempsey, and I will always be grateful to him for his priceless guidance and support. What I have learnt from Prof. Dempsey will continue to inspire me in my future career.

I would also like to express my sincere gratitude to Prof. Buttlar, Associate Dean in the College of Engineering, who is the chair of my dissertation committee. Despite his extremely busy schedule, he gladly accepted to be the chair of dissertation committee, and has been extremely supportive as well. I was also honored to serve as one of his teaching assistants in “CEE 405: Asphalt Materials Design I” as part of the “CEE Alumni Award for Teaching Excellence”. I am inspired by the high standards that he sets for himself and those around him, and I have learnt a lot while I worked with him.

I am also grateful to my employer, Prof. Bullock, with whom it was an absolute pleasure to work with. I also learnt a lot from him on academic teaching, particularly in the field of Statistics. I would also like to thank Prof. Gardoni and Prof. Marla for their valuable guidance and feedback, which allowed me to gain significant insight into the research process.

Finally, I am very grateful to Ms. Mary Medearis for her substantial guidance and support throughout my Ph.D. studies, and the Graduate College at the University of Illinois, and the Transportation Faculty at the Department of Civil and Environmental Engineering, particularly Prof. Roesler and Prof. Al-Qadi, for the dissertation travel grants that they provided for this study. Without the dissertation travel grants, I would not be able to complete the flight simulator experiments in Europe.

I would like to dedicate this dissertation primarily to Prof. Dempsey, who made it possible for me to focus on aircraft operational safety in my dissertation study. His expertise and his commitment to the academia will always inspire me in my future career. I would also like to dedicate this dissertation to Prof. Buttlar and Prof. Bullock, both of whom have also provided substantial insight and support in this dissertation study although I am not a member of their research teams.

TABLE OF CONTENTS

LIST OF SYMBOLS

a_v, b_v, c_v, d_v	Coefficients of cubic spline.
B_1, B_2	Dummy variables for bird size.
C_1, C_2, C_3	Dummy variables for number of birds struck.
C_j	Circular segment j.
$\cot(\gamma)$	Engines-out glide ratio.
$\cot(\gamma)_{v,\phi}$	Engines-out glide ratio at calibrated airspeed v, and bank angle ϕ.
D	Total drag force acting on the aircraft.
D_i	Dummy variables for daylight conditions.
$\bar{d}$	Average relative difference for true airspeed between two consecutive iterations.
E_i	Dummy variables for engine position on aircraft.
$E_{Touchdown}$	Elevation of the intended touchdown point.
$\bar{E}_{C_j}$	Average elevation of circular segment j.
$\bar{E}'_{C_j}$	Average elevation of circular segment j expressed in *feet*.
g	Gravitational acceleration.
k	Iteration number.
L	Total lift force acting on the aircraft.
L_i	Linear segment i.
L/D	Lift-to-drag ratio.
M_i	Dummy variables for aircraft mass.
N_i	Dummy variables for number of engines on aircraft.
P_i	Dummy variables for flight phase.
R^2	Coefficient of determination for a statistical model.
S	Wing area.
S_i	Dummy variables for season of the year.

S_{L_1}	Length of linear segment i.
$T_{j,j}$	The transition segment connecting linear segment j to circular segment j.
$T_{j,j+1}$	The transition segment connecting linear segment $j+1$ to circular segment j.
v	Calibrated airspeed.
v_E	Equivalent airspeed.
V_{FE}	Maximum flap extended airspeed/ flap placard speed.
$V_{LO\ EXT}$	Maximum operating speed for landing gear extension.
V_{LS}	Lowest selectable airspeed.
V_{S1g}	The airspeed corresponding to the maximum lift coefficient, just before the lift starts decreasing with increasing angle of attack in a given aircraft configuration.
v_T	True airspeed.
V_x	Best angle-of-climb speed.
V_y	Best rate-of-climb speed.
$\bar{v}_{T,j}$	Average true airspeed along circular segment j.
X_0	Abscissa of the aircraft position at the start of the engines-out landing maneuver.
X_i	Dichotomous predictor variable.
$X_{Touchdown}$	Abscissa of the intended touchdown point.
Y_0	Ordinate of the aircraft position at the start of the engines-out landing maneuver.
$Y_{Touchdown}$	Ordinate of the intended touchdown point.
β_i	Coefficient for a predictor variable in a linear statistical model.
$\hat{\beta}_i$	Coefficient estimate for a predictor variable in a linear statistical model.

γ	Flight path angle.
ΔX_{C_j}	Change in abscissa along circular segment j.
ΔX_{L_i}	Change in abscissa along linear segment i.
$\Delta X_{T_{j,j}}$	Change in abscissa along the transition segment connecting linear segment j to circular segment j.
$\Delta X_{T_{j,j+1}}$	Change in abscissa along the transition segment connecting linear segment $j+1$ to circular segment j.
ΔY_{C_j}	Change in ordinate along circular segment j.
ΔY_{L_i}	Change in ordinate along linear segment i.
$\Delta Y_{T_{j,j}}$	Change in ordinate along the transition segment connecting linear segment j to circular segment j.
$\Delta Y_{T_{j,j+1}}$	Change in ordinate along the transition segment connecting linear segment $j+1$ to circular segment j.
ΔZ_{C_j}	Altitude loss along circular segment j.
ΔZ_{L_i}	Altitude loss along linear segment i.
$\Delta Z_{T_{j,j}}$	Altitude loss along the transition segment connecting linear segment j to circular segment j.
$\Delta Z_{T_{j,j+1}}$	Altitude loss along the transition segment connecting linear segment $j+1$ to circular segment j.
$\Delta\theta_j$	Total change in aircraft heading (°) along circular segment j and the adjacent transition segments.
$\Delta\theta_{C_j}$	Change in aircraft heading (°) along circular segment j.
$\Delta\theta_{T_{j,j}}$	Change in aircraft heading (°) along the transition segment connecting linear segment j to circular segment j.

$\Delta\theta_{T_{j,j+1}}$	Change in aircraft heading (°) along the transition segment connecting linear segment $j+1$ to circular segment j.
θ_0	Aircraft heading (°) at the start of the engines-out landing maneuver.
$\theta_{Touchdown}$	Intended aircraft heading (°) at touchdown.
θ_i	Aircraft heading (°) along linear segment i.
P	Probability of a given event.
$\hat{\mathrm{P}}$	Predicted probability of a given event.
ρ	Air density at the altitude that the aircraft is flying.
ρ_0	Air density at sea level on a standard day.
$\dot{\phi}$	Roll rate (°/s).
ϕ	Bank (roll) angle (°).
ϕ_j	Bank angle (°) for circular segment j.
ϕ_{max}	Maximum bank angle (°) for engines-out landing maneuver.
χ^2	Wald statistic for a coefficient estimate.

LIST OF ACRONYMS

AGL	Altitude above ground level.
AMSL	Above mean sea level.
APU	Auxiliary power unit.
ATC	Air traffic control/ controller.
EASA	European Aviation Safety Agency.
ETOPS	Extended-range Twin-engine Operational Performance Standards, which is a regulation permitting turbine-powered aircraft operators to fly routes that are up to a specified flying time from the nearest airport.
FAA	Federal Aviation Administration.
FCOM	Flight Crew Operating Manual.
FSTD	Flight Simulation Training Device.
ICAO	International Civil Aviation Organization.
JAA	Joint Aviation Authorities.
JAR	Joint Aviation Regulations.
KCAS	Knots in Calibrated Airspeed.
MD	McDonnell Douglas.
NG	Next Generation.
RAT	Ram Air Turbine.
TACA	Transportes Aereos Centro-Américanos.

CHAPTER 1 - INTRODUCTION

1.1 Problem Definition

1.1.1 The Growing Threat of Bird Strikes

Bird strikes pose a growing threat to aviation. There has recently been a significant increase in the annual number of reported bird strikes. For example:

- The annual number of reported bird strikes increased over five times in the last three decades [1].
- Since 2008, the annual number of reported bird strikes has increased by up to 45 percent at major US airports [2].
- Between 2011 and 2012, the annual number of reported bird strikes increased by 11 percent [1].

The number of bird strikes is projected to continue to increase on an annual basis [2]. The losses due to bird strikes are alarming as well. Between 1990 and 2012, bird strikes led to 24 fatalities, 276 injuries, 815,997 hours of aircraft downtime, and $639.4 million monetary losses on civil aircraft [1].

Bird strikes are particularly perilous if they lead to engine failure. Single or multiple engine failure may occur when birds are ingested into aircraft engines. For example, on September 15, 1988, an Ethiopian Airlines Boeing 737-260 ingested a flock of pigeons into both engines shortly after take-off from Bahir Dar Airport, Ethiopia. The aircraft had dual engine failure and attempted a gear-up landing at Bahir Dar Airport. During the landing roll, it caught fire and 31 people aboard were killed [3]. On September 22, 1995, a military Boeing 707 ingested multiple Canada geese shortly after take-off from Elmendorf Air Force Base, Alaska. After the failure of the first

and second engines, the aircraft crashed into a wooded area and caught fire. All 26 people aboard the military 707 aircraft were killed [4]. On November 10, 2008, a Ryanair Boeing 737-800 went through several bird strikes on final approach to Ciampino Airport at Rome, Italy. The bird strikes damaged both engines and affected engine thrust, but the aircraft subsequently landed with no fatalities or serious injuries [5]. On September 29, 2009, a Ryanair Boeing 737-800 struck a flock of birds shortly after takeoff from Trapani Birgi Airport at Sicily, Italy. Both engines received damage to fan blades, but the aircraft returned uneventfully to Trapani Birgi Airport [6]. On January 15, 2009, a US Airways Airbus A320 struck multiple Canada geese and lost thrust in both engines shortly after take-off from La Guardia Airport, New York. The aircraft was ditched on the Hudson River, and one flight attendant was injured [7]. On April 19, 2010, a Dana Air MD-83 lost one of its two engines during take-off from Murtala Muhammed Airport at Ikeja, Nigeria, due to bird strike. The engine caught fire during the initial climb-out, and the aircraft made emergency landing at Murtala Muhammed Airport. All passengers were evacuated [8].

In the near future, engine failure due to bird strike is expected to occur more frequently due to the following factors:

1. There is a continuous increase in the populations of large[†] birds owing to several environmental protection actions. For example:

[†] Here, large refers to birds that weigh greater than 8.0 lb (3.6 kg) on average.

- The population of North American Canada geese[‡] increased from around 0.5 million to 3.8 million from 1980 to 2012 [1].
- The population of North American snow geese increased from around two million to six million from 1980 to 2012 [1].
- The populations of 13 other largest bird species increased significantly since 1970 [1].

2. Despite the substantial increase in large bird populations, modern-day aircraft engines are not required to be tested for birds weighing greater than 8.0 lb [9].
3. It is acceptable for a transport aircraft to lose all power due to ingestion of large[§] birds as long as the engines can be shut down and the damage is contained within the engine casing [10].
4. Air traffic is continuously increasing. From 2000 to 2012, the annual number of passengers transported on all US air carriers increased by 19.8-percent [11]. Likewise, during the same time period, the annual number of aircraft departures on all US carriers increased by 15.5 percent [12]. The commercial air traffic movements is expected to increase at an average annual rate of 1.4 percent from 2012 through 2030 [1].
5. The use of turbofan engines is being predominantly adopted. In 2013, around 97.0 percent of the passengers on all US air carriers were transported by turbofan-engine aircraft

[‡] Weigh on average 9.2 lb.

[§] Here, "large" refers to heavier than 4.0, 6.0 or 8.0 lb, depending on engine size.

[13]. Nevertheless, birds are less able to detect and avoid turbofan engines [1].

So with all these dynamics, the likelihood of engine failure in the event of a bird strike is continuously increasing.

1.1.2 The Prevalence of Twin-Engine Aircraft

In addition to the growing threat of bird strikes, there is another major factor that renders bird strikes all the more hazardous: The prevalence of twin-engine aircraft. In 1965, around 87 percent of the US commercial fleet consisted of three- and four-engine aircraft [1]. However, there has been a continuously growing trend towards twin-engine jetliners [14]. In 1989, the FAA allowed 180-minute extended operations (ETOPS) for the first time for the Boeing 767. Since then, twin-engine jets have become progressively more prevalent on the trans-Atlantic and trans-Pacific routes [14]. As of today, twin-engine jets such as the Airbus A320 aircraft family (i.e. A319/ 320/ 321) and the Boeing 737NG (Next Generation) aircraft family (i.e. 737-700/800/900) form the backbone of the commercial aviation industry. Owing to the prevalence of twin-engine jets, Airbus Industries ceased the production of its four-engine wide-body jet, the A340, in 2011 [15]. In 2013, twin-engine jetliners transported 96.5 percent of all 756.6 million passengers on US air carriers [13].

Contemporary twin-engine jets offer superior fuel efficiency and lower noise levels than three- and four-engine jets [16]. However, they have reduced number of engines, which brings about reduced engine redundancy. So compared to yesterday’s three- or four-engine aircraft, today’s twin-engine aircraft may be more susceptible to sustain damage to all

engines in the event of a bird strike. Sustaining damage to all engines can have severe impact on aircraft operational safety because it may lead to dual engine failure and total loss of thrust. Therefore, total loss of thrust due to bird strike is expected to occur more frequently in the near future due to the growing threat of bird strikes and increasing use of twin-engine aircraft. Contrary to US Airways Flight 1549, total loss of thrust may lead to more severe consequences such as the more recent Dana Air Flight 992* that resulted in 163 fatalities [17]. [17].

1.2 Motivation

The motivating idea of this study originates from the NTSB (National Transportation Safety Board) Investigations for US Airways Flight 1549. On January 15th, 2009, a U.S. Airways twin-engine Airbus A320 encountered a flock of Canada geese shortly after takeoff from New York's LaGuardia Airport. The aircraft ingested multiple birds into both engines at an altitude of 2,818 ft above ground level (AGL), and underwent total loss of thrust. The flight crew alerted the LaGuardia departure controller and spent around 35 seconds† for decision-making [7]. Although there were two airports nearby, the flight crew believed that the aircraft did not have the aerodynamic performance to return to a runway, and they successfully ditched the aircraft on the Hudson River [7].

* As of January 2015, the accident is still under investigation and has not been concluded.

† One of the reasons why the pilots spent 35 seconds trying to relight the engines was that the engines did not have diagnostic capabilities to let the pilots know that any pilot action would preclude them from turning the engines back to normal operation due to the type and extent of the damage.

While the ditching of the U.S. Airways A320 on the Hudson was hailed as a textbook example of landing on water, the subsequent NTSB investigation raised the following question: Could the accident aircraft have landed on a runway instead of ditching on the Hudson? In April 2009, NTSB ran a series of tests at the Airbus Flight Training Center, Toulouse, France. The purpose of the simulation tests was to find out if the accident plane could have touched down on a nearby runway instead of ditching on the Hudson River. The flight simulators were programmed to duplicate the same flight and weather conditions at the time of the accident. These conditions include the airplane position, thrust setting, altitude above ground level (AGL) at the beginning of the turns, thrust reduction and airspeed. The NTSB investigators performed a total of 20 simulation runs. In all runs, the pilots followed the US Airways Dual Engine Failure checklist after the loss of thrust, and then they relied on their training and experience to land the aircraft. Five of the 20 runs were later excluded from analysis due to poor data or simulator malfunction.

The simulation tests showed that the accident aircraft had indeed sufficient altitude to glide to a nearby runway at the time of the accident. In eight out of 15 runs, the pilots were able to successfully land on a runway either at the LaGuardia or Teterboro Airport. On the other hand, one run involved a 35-second delay before returning to a runway to reflect real-world conditions. The 35-second delay accounted for the time required to decide on a course of action. The attempt to land on a nearby runway was not successful when the 35-second delay was introduced [7, 18].

The following are inferred from the results of the NTSB simulations:

1. The accident aircraft had indeed sufficient altitude to return to a nearby runway at the time of the accident. Had the flight crew known this, they could have made a prompt decision to return to LaGuardia or Teterboro, and landed successfully on a runway instead of ditching on the Hudson.
2. Promptness in decision-making is of critical significance in the event of total loss of thrust. Otherwise, even a 35-second delay in decision-making could rule out a possible landing on a nearby runway.

In the event of total loss of thrust, flight crews can make more prompt decisions and can maximize the odds of a safe landing if they have access to:

- Real-time information on aircraft glide range.
- Real-time information on the optimum landing trajectory for landing on a given runway.

By using real-time information on aircraft glide range, flight crews would be able to know which runways are within aircraft glide range in the event of total loss of thrust. Knowing this, they would be able to make a prompt decision on which runway they should divert to for an emergency landing. Thereby, they would minimize the decision-making time and save critical seconds in the event of total loss of thrust.

By using real-time information on optimum landing trajectory, flight crews would be able to perform maneuvers that would minimize the required altitude loss to land on the selected runway. Consequently, this could increase the odds of a safe landing and could reduce the odds of crash landing, casualty and hull loss due to total loss of thrust.

1.3 Need for Adaptive Flight Planner

To address the total-loss-of-thrust emergency, quick reference handbooks are designed to enable speedy and successful recovery of at least one engine. Airliner type-rating programs assume that total loss of thrust culminates in at least one engine recovery, and do not require simulator training for engines-out emergency landing [19, 20].

If an engine restart cannot be achieved, the powered aircraft functions as a glider till touchdown. The relevant airworthiness regulations [21] require transport aircraft to be controllable if all engines fail. In order to meet this requirement, transport aircraft must have a source of emergency power such as auxiliary power unit (APU) and/ or ram air turbine (RAT) that can be effectively deployed in the failure of all engines. Although the aircraft is controllable in the failure of all engines, it cannot gain altitude if an engine restart is impossible. In that case, the flight crew has a single chance for landing, and there is absolutely no room for pilot error. The airworthiness regulations [21] only guarantee the controllability of the aircraft. Hence, airline pilots are left with virtually no guidance on managing engines-out emergency landing. Therefore, it is a pressing need to develop the idea of engines-out landing trajectory optimization for commercial aircraft.

In the event of dual-engine failure on a twin-engine jet, the critical task of safe landing can only be handled by pilots through effective post-failure management strategies. Effective post-failure management requires rapid selection of an appropriate landing site within the reduced flight envelope of the distressed aircraft. Once a suitable landing site is

identified, the pilots should implement energy-preserving maneuvers and follow a flyable trajectory to the intended touchdown location. Due to the inability to gain altitude and the limited time to take action, not every pilot might accomplish a safe touchdown in such an emergency situation, as in the case of Dana Air Flight 992, which resulted in 163 fatalities in June, 2012 [22]. To address this safety issue, an innovative adaptive flight planner can be developed to assist pilots in post-failure flight management. The use of the adaptive flight planner can maximize the odds of safe touchdown and minimize the odds of casualty and hull loss in the event of total loss of thrust.

1.4 Objective

The objective of this study is to test for the research hypothesis that an adaptive flight planner significantly increases the probability of safe touchdown in the occurrence of total loss of thrust due to bird strike. In this context, an adaptive flight planner is assumed to provide emergency guidance to pilots in two stages: i) guidance on landing site selection, ii) guidance on post-failure flight plan. To test for the research hypothesis, the study describes the architectural development of an adaptive flight planner, which can be integrated into flight management computers for future use. The effectiveness of the adaptive flight planner is tested through designed experiments.

1.5 Selected Commercial Jets

In the occurrence of total loss of thrust, post-failure performance characteristics depend on the specific aerodynamic design of the aircraft in question [23]. Since aerodynamic

design varies based on aircraft model, post-failure performance characteristics are specific to aircraft model. Therefore, a given aircraft model requires exclusive development of an adaptive flight planner. The budget allocated for this study allows for the consideration of up to two aircraft models. The two aircraft models are selected based on the current and projected use in the US Commercial Aviation Industry. In 2013, the top five commercial jets that transported the highest number of passengers on all U.S. air carriers are listed as follows [13]:

1. Boeing 737-700/700LR: 97.6 million passengers *(12.9 percent of all);*
2. Boeing 737-800: 82.3 million passengers *(10.9 percent of all);*
3. Airbus Industrie A320-200: 74.7 million passengers *(9.9 percent of all);*
4. Boeing 757-200: 59.6 million passengers *(7.9 percent of all);*
5. McDonnell Douglas Super 80/ MD81//82/83/88: 59.3 million passengers *(7.8 percent of all).*

In the near future, it is expected that the A320 and 737NG (next generation) aircraft families will transport a higher percentage of travelers on U.S. air carriers due to the following reasons:

- The Boeing 757 and MD80 aircraft families are out-of-production models [24].
- The aging fleet of the Boeing 757 and MD80 aircraft families are gradually getting retired [25].

- The A320 and 737NG aircraft families are currently the best-selling aircraft models of the Airbus Industrie and Boeing Company, respectively [26, 27].

In this study, the architectural design of an adaptive flight planner is designed for the Airbus A320-200 and Boeing 737-800. Although Boeing 737-700 transported more passengers on the U.S. carriers than the 737-800 did, the 737-800 is chosen as opposed to the 737-700 because:

- The 737-800 is currently the best-selling aircraft model in the 737NG aircraft family [27]. Thus, in the near future, the 737-800 is expected to transport a higher percentage of air travelers on all U.S. carriers.
- While the 737-700 can accommodate up to 149 passengers [28], the 737-800 can accommodate up to 189 passengers with a maximum range of around 3,600 miles [29]. Likewise, the A320-200 can accommodate up to 180 passengers with a maximum range of around 3,700 miles [30].

1.6 Scope and Limitations

The growing threat of bird strikes is the primary motivation in this study. Hence, bird strike hazard will be the major focus in developing and testing the adaptive flight planner. Nevertheless, the adaptive flight planner is to be still usable if total loss of thrust stems from another cause such as inclement weather or fuel starvation. It is not intended for use during a single-engine failure, engine-idle glide or partial loss of thrust. The effectiveness of the adaptive flight planner is tested through designed experiments using realistic flight simulators. Actual real-life flights are not conducted.

1.7 Significance of the Study

In the present-day U.S. commercial aviation fleet, twin-engine airliners prevail over three- and four-engine airliners. In 2013, less than 4.0 percent of the passengers were transported by three- or four-engine airliners on all US air carriers [13]. Among the twin-engine airliners, the Airbus A320 and Boeing 737NG aircraft families form the backbone of the U.S. commercial aviation industry. The A320 and Boeing 737NG are also the best-selling commercial aircraft families. In 2013, the A320 aircraft family received a total of 1,162 net orders [31], and the Boeing 737NG aircraft family received a total of 1,046 net orders [32]. Both aircraft families are expected to transport increasing number of passengers in the near future. Nonetheless, the growing threat of bird strikes renders these twin-engine airliners more prone to dual-engine failure and total loss of thrust. In addition, bird strike is not the only possible cause for total loss of thrust. In the history of commercial aviation, total loss of thrust occurred due to several other reasons such as:

- Severe weather, as in the case of Eastern Air Lines Flight 212 and TACA Flight 110 [33, 34];
- Ice ingestion, as in the case of Scandinavian Air Lines Flight 751 [35];
- Pilot error, as in the case of Delta Air Lines Flight 810 and British Midland Flight 92 [36, 37];
- Maintenance error, as in the case of PanInternational Flight DR112 [38];
- Fuel leakage, as in the case of Air Transat Flight 236 [39];

- Hijacking, as in the case of Ethiopian Air Lines Flight 961 [40];
- Volcanic ash cloud, as in the case of British Airways Flight 9 [41], and KLM Flight 867 [42].

Most of these events involved twin-engine aircraft. Therefore, it is a pressing need to adopt an innovative approach to avert grave consequences of total loss of thrust. To the author's best knowledge, there has been no study in the literature that assessed the effectiveness of an adaptive flight planner in the occurrence of total loss of thrust. A number of studies [43, 44, 45, 46, 47, 48, 49, 50, 51] addressed landing trajectory optimization in the occurrence of total loss of thrust. A vast majority of these studies involved single-engine, general aviation aircraft or fighter jets. Thus, the idea of engines-out landing trajectory optimization has not addressed commercial aircraft in detail. This study is the first of its type to addresses commercial aircraft in detail, and to test the effectiveness of emergency guidance.

1.8 Organization of this Dissertation

This dissertation describes the architectural development and simulator testing of an adaptive flight planner for engines-out emergency landings with emphasis on the bird strike hazard. The dissertation is organized as follows:

- Chapter 2 presents review of previous research on statistical analysis of aircraft-bird strikes, and the optimization of emergency landings in the occurrence of total loss of thrust.
- Chapter 3 analyzes the FAA Wildlife Strike Data to test the research hypothesis that "contemporary twin-engine

jetliners are significantly more likely to sustain damage to all engines and lose engine redundancy in the occurrence of a bird strike compared to yesterday's three- and four-engine jetliners". The findings demonstrate strong evidence to believe the research hypothesis, which justifies the development of an adaptive flight planner for engines-out emergency landings.

- Chapter 4 analyzes the FAA Wildlife Strike Data to identify statistically the most hazardous conditions for engine failure due to bird strike. The findings are later utilized to develop realistic bird strike scenarios for testing the effectiveness of the proposed adaptive flight planner.
- Chapter 5 assesses the kinematic characteristics of the Airbus A320 aircraft during engines-out flight. The A320 aircraft is one of the two commercial jets analyzed in this study. The findings are later utilized in the architectural design of the adaptive flight planner for the A320 aircraft.
- Chapter 6 assesses the kinematic characteristics of the Boeing 737NG aircraft during engines-out flight. The 737-800 aircraft is the second commercial jet analyzed in this study. The findings are later utilized in the architectural design of the adaptive flight planner for the Boeing 737NG aircraft.
- Chapter 7 derives a kinematic segmented-trajectory generation algorithm for engines-out emergency landings. Contrary to kinetic trajectory generation algorithms, the kinematic method does not make reference to aerodynamic forces involved during engines-out flight. Thereby, the kinematic method requires minimal amount of aircraft-specific aerodynamic data as input.

- Using the findings from Chapters 5 and 7, Chapter 8 demonstrates the architecture of the adaptive flight planner for the Airbus A320 aircraft, and tests its accuracy in an A320 full flight simulator.
- Using the findings from Chapters 6 and 7, Chapter 9 demonstrates the architecture of the adaptive flight planner for the Boeing 737NG aircraft, and tests its accuracy in a 737-800 full flight simulator.
- Chapter 10 describes the designed experiment to test the research hypothesis along with the findings.
- Chapter 11 finishes with the conclusions from this research and suggestions for future research.

CHAPTER 2 - LITERATURE REVIEW

2.1 Total Loss of Thrust in Commercial Aviation

Table 2-1 lists some past occurrences of total loss of thrust that involved commercial jets. As shown in Table 2-1, most of the cases involved twin-engine aircraft. A few notable examples are explained in further detail as follows:

- On April 4, 1977, a Southern Airways DC-9 had dual engine failure due to heavy water and hail ingestion in a severe thunderstorm. The aircraft glided to an emergency landing on a highway in New Hope, Georgia, killing 72 people [33].
- On May 24, 1988, a TACA Boeing 737-300 underwent dual engine flameout due to heavy water ingestion in a severe thunderstorm. The aircraft glided to an emergency landing on a grass levee near New Orleans with no fatalities or serious injuries [34].
- On December 27, 1991, a Scandinavian Airlines MD-80 lost thrust in both engines due to ice ingestion. The aircraft glided to an emergency landing in a field near Gottröra, Sweden, with no fatalities [35].
- On January 15, 2009, a US Airways Airbus A320 underwent total loss of thrust due to multiple ingestion of Canada geese. The aircraft was ditched in the Hudson River with no fatalities or serious injuries [7].
- On June 3, 2012, a Dana Air MD-83 had lost thrust in both engines on final approach to Muhammed Murtala Airport. The aircraft glided and crashed into a densely populated area in Lagos, Nigeria, killing 153 people. The crash is still under investigation [52].

Total loss of thrust may also occur due to fuel starvation as in the case of Air Canada Flight 143 [53], Indian Airlines Flight 440 [54], and Air Transat Flight 236 [39]. Lessons learnt from these events show that total loss of thrust can have varying causes. However, they all had one thing in common: all these flights were forced to engines-out glide after all engines were out. In the event of total loss of thrust, the odds of a safe landing is strongly dependent on aircraft's engines-out glide performance. A crash can be avoided if a safe touchdown point exists within aircraft glide range.

2.2 Statistical Analysis of Aircraft-Bird Strikes

Although bird strikes pose growing threat to civil and military aviation, there is a limited number of studies that statistically analyze bird strikes. Dolbeer [55] analyzed the altitude distribution of the bird strikes to civil aircraft that occurred between 1990 and 2004 in the US. He found that bird strike rates declined by a factor of around 1.5 per 1000-ft. interval from 500 ft. AGL to 20,500 ft. AGL.

In another study, Dolbeer et al. [1] analyzed the wildlife strike reports submitted to the FAA between 1990 and 2012. Based on those reports, engines were the most frequently damaged aircraft component. There were 3,935 bird strikes with one engine damaged, 132 with two engines damaged, one with three engines damaged, and one with four engines damaged [1].

Zalakevicius analyzed the bird strikes in Lithuania for the periods 1958-1978 and 1987-1991 [56]. Most of those bird strikes occurred in the month of July (27 percent) and during the phase of descent (47 percent). Moreover, Jacoby [57] analyzed the

pattern of bird strikes in Europe and discussed the possibility of using bird strike prevention measures.

Table 2-1. Some past occurrences of total loss of thrust involving commercial jets.

Aircraft Type	No. of Engines	Year	Cause of Total Loss of thrust	No. of Fatalities
DC-9	2	1970	Fuel starvation [58]	23
BAC 1-11	2	1971	Maintenance error [59]	22
Yak-40	3	1976	Fuel starvation [60]	0
DC-9	2	1977	Severe weather [33]	72
DC-8	4	1978	Fuel starvation [61]	10
Boeing 747	4	1982	Volcanic ash cloud [41]	0
Boeing 767	2	1983	Fuel starvation [53]	0
Boeing 767	2	1987	Pilot error [36]	0
Boeing 737	2	1988	Severe weather [34]	0
Boeing 737	2	1988	Bird strike [62]	35
Boeing 737	2	1989	Pilot error [63]	47
Boeing 737	2	1989	Fuel starvation [64]	13
Boeing 747	4	1989	Volcanic ash cloud [42]	0
Boeing 707	4	1990	Fuel starvation [65]	73
MD-80	2	1991	Ice ingestion [35]	0
Airbus A300	2	1993	Fuel starvation [54]	0
BAC 1-11	2	1994	Fuel starvation [66]	5
Yak-40	3	1994	Fuel starvation [67]	28
Boeing 767	2	1996	Hijacking and fuel starvation [40]	125
Airbus A310	2	2000	Fuel starvation [68]	0
Airbus A330	2	2001	Fuel leakage [39]	0
Boeing 737	2	2002	Severe weather [69]	1
CRJ200	2	2004	Engine flameout due to pilot error [70]	2
Airbus A320	2	2009	Bird strike [7]	0
MD-83	2	2012	Under investigation [52]	153

2.3 Engines-out Landing Trajectory Optimization

A number of studies have addressed landing trajectory optimization in the occurrence of total loss of thrust. However, all these studies involved single-engine general aviation aircraft or fighter jets. Rogers [43] computed the steady-state optimal turn-back maneuver to departure airport for a Beech Bonanza aircraft after engine failure during the initial climb-out. Hoffren and Raivio [44] computed the optimal trajectory of a BAe Hawk Mk.51 aircraft that maximizes the engines-out glide range in a given direction after total loss of thrust during the initial climb-out. Hyde [45] explored the non-equilibrium maneuvering required for an RV-4 aircraft to minimize altitude loss while returning to departure runway following total loss of thrust during the initial climb-out. Shapira and Ben-Asher [46] presented an algorithm to maximize the glide range of a single-engine aircraft after engine failure, and demonstrated the use of the algorithm on a Lockheed-Martin F-16 undergoing engine failure. Brinkman and Visser [48] established the conditions under which returning to departure runway is a safe option for a Lockheed-Martin F-16 aircraft if it undergoes total loss of thrust during the initial climb-out. Atkins, Portillo and Strube [47] developed a segmented-trajectory generation algorithm for real-time use in total loss of thrust emergencies, and demonstrated the application of the algorithm for general aviation aircraft. Adler, Bar-Gill and Shimkin [50] developed a 3-D trajectory planning algorithm, and conducted a simulation study to apply the algorithm to a Cessna 172 Skyhawk undergoing engine failure.

To the authors' best knowledge, there has been no study up-to-date that explored the optimization of landing trajectory for a commercial jet following total loss of thrust during the

initial climb-out. Hence, this study will be the first of its type by addressing commercial aircraft.

2.4 Adaptive Flight Planning in Total Loss of Thrust

To the author's best knowledge, there is very limited number of studies that addressed adaptive flight planning in the occurrence of total loss of thrust. Price [71] proposed an adaptive flight planner in the form of a digital moving map. In the occurrence of total loss of thrust, the moving map is to depict aircraft glide range on a real-time basis. Real-time computation of the glide range is to be accomplished by processing data gathered from various aircraft sensors and digital geographical databases. In order for the moving map to be of practical use, the map should generate intuitive symbols that are easy to interpret for pilots in such emergency situations.

Atkins, Portillo and Strube [47] designed an adaptive flight planner for engines-out emergency landings. In the occurrence of total loss of thrust, the adaptive flight planner performs two tasks, the first of which is landing site selection. To perform this task, the adaptive flight planner computes a simple approximate circular glide range of the aircraft based on its post-failure performance characteristics. Then it outputs a list of reachable runways within the glide range, and ranks them based on some quality measures such as runway width and length, cross wind speed, runway surface, type of approach, etc. Once the top-ranking runway is identified, the adaptive flight planner performs its second task, which is the generation of a feasible landing trajectory to the selected runway. The adaptive flight planner deploys a segmented

trajectory generation method, which is not computationally demanding, and is therefore appropriate for real-time applications. Later on, Peng et al. [49] conducted a similar simulation study to propose an adaptive flight planner for engines-out emergency landings.

Wu et al. [51] proposed the development of an emergency guidance module for transport aircraft. The proposed function of the emergency guidance module is to select a suitable landing site, and compute a feasible landing trajectory towards the site in the occurrence of total loss of thrust. For this purpose, Wu et al. [51] developed a dynamic programming algorithm that can generate feasible landing trajectories to an appropriate landing site in the occurrence of total loss of thrust. The landing trajectory selected by the flight crew is to be converted into pitch angle directives by flight management computers, and the directives are to be sent to either an autopilot or a flight director. Thereby, the distressed aircraft can follow the selected landing trajectory and perform a safe touchdown on the selected location. Wu et al. [51] did not test the effectiveness of the proposed emergency guidance module. Moreover, the dynamic programming algorithm to be deployed in the emergency guidance module lacked the capability of generating landing trajectories with turning maneuvers.

To the authors' best knowledge, there has been no study up to date that assessed the effectiveness of emergency guidance in the occurrence of total loss of thrust. This study will be the first of its type to accomplish this through designed experiments.

CHAPTER 3 - ARE BIRD STRIKES MORE HAZARDOUS FOR TWIN-ENGINE AIRCRAFT?

3.1 Research Question

Unlike yesterday's typical three- and four-engine commercial jets, twin-engine aircraft prevail in modern-day U.S. commercial fleet. Yet there is another major difference that distinguishes today's typical commercial aircraft from yesterday's airliners: Engine position on aircraft. In the early 1970s, a major percentage of the twin-engine jetliners in the U.S. fleet used to have aft-fuselage-mounted engines. However, since then, twin-engine jetliners with under-wing-mounted engines became progressively more predominant. For instance, in 2000, 61 percent of the 692 million passengers on all U.S. air carriers were transported by jetliners with under-wing-mounted engines. In 2012, however, 74 percent of the 751 million passengers on all U.S. air carriers were transported by jetliners with under-wing-mounted engines [13]. It is anticipated that aircraft with under-wing-mounted engines will be further predominant in the near future because:

- Several jetliners with aft-fuselage-mounted engines are not in production any more [24] (e.g. McDouglas DC-9, MD-80, Boeing 727, etc.).
- The existing older airline models such as the DC-9 and MD-80 are gradually getting retired in the U.S. fleet [25].
- As of November 2013, the best-selling twin-engine commercial aircraft are Airbus A320-200 and Boeing 737-800, both of which have under-wing-mounted engines [26, 27].

While under-wing-mounted engines have several advantages over aft-fuselage-mounted engines [72, 73], engine position on

aircraft should also be analyzed from a bird strike hazard point of view.

The objective of this chapter is to investigate:

- If twin-engine aircraft are significantly more likely to sustain damage to all engines in the event of a bird strike compared to three- and four-engine aircraft,
- If aircraft with under-wing-mounted engines are significantly more prone to sustaining damage to all engines in the event of a bird strike compared to that with aft-fuselage-mounted engines.

For this purpose, the study aims to test for the following research hypotheses:

1. "Twin-engine aircraft has significantly higher probability to sustain damage to all engines in the event of a bird strike as opposed to three- or four-engine aircraft."
2. "Engine position on aircraft is significantly associated with the probability that an aircraft will sustain damage to all engines in the event of a bird strike."

To test for the research hypotheses, the study uses the FAA Wildlife Strike Database that is publically available online [74]. Considering all available data, the study includes the following fifteen variables in statistical analysis: altitude above ground level (AGL), bird size, number of birds struck, daylight conditions, engine manufacturer, engine position on aircraft, fog, aircraft mass, number of engines, phase of flight, precipitation, season, sky conditions, airspeed and advance warning of birds. The goal of the analysis is to find out the statistical relationship between the fifteen variables and the probability that an aircraft will sustain damage to all engines in the event of a bird strike.

3.2 Significance of the Research

Using the statistical relationship built in this chapter, one can not only test for the research hypotheses, but also determine all other factors that are significantly associated with the probability that an aircraft will sustain damage to all engines in the event of a bird strike. Identifying this statistical relationship is a pressing need for the following reasons:

- Using the statistical relationship, aviation authorities can more effectively assess the bird strike hazard to typical modern-day aircraft that has reduced engine redundancy. This safety issue concerns over 730 million annual passengers that are transported via twin-engine jetliners on all U.S. carriers [75].
- Bird strike hazard mitigation strategies can be improved in view of the findings from the statistical relationship.
- The findings can be incorporated into pilot training programs so that flight crews become more knowledgeable about the risk of engine damage in the event of a bird strike.
- Aircraft engine manufacturers can consider the findings in improving future engine designs.
- The findings can help researchers understand the nature of bird strikes that result in damage to all engines of the struck aircraft. Thereby, researchers can develop a scientific approach to reduce the potential of damage to all engines and possible total loss of power in the event of a bird strike.

3.3 Data Preparation

3.3.1 Data Description

The study uses data from the FAA wildlife strike database [74]. A large sample of 70,628 bird strikes is analyzed. The sample includes all reported bird strikes that:

- occurred between January 1, 1990 (the earliest available date) and November 30, 2012;
- involved turbofan engine civil aircraft.

Thus, all findings apply to the reported aircraft-bird strikes that involved turbofan engine civil aircraft. The data in the FAA Wildlife database are collected through voluntary reporting by pilots or airlines. Table 3-1 lists the questions in the wildlife strike submission report. In view of these questions, one response variable and fifteen predictor variables are analyzed. The response (dependent) variable is called "ALL_ENG_DMG". It is of binary nature and has two possible outcomes:

1. If ALL_ENG_DMG=1, then all engines of the struck aircraft sustained damage due to the bird strike. Hence, the thrust generation of all engines were adversely affected because of the bird strike.
2. If ALL_ENG_DMG=0, then not all engines of the struck aircraft sustained damage due to the bird strike.

This response variable is chosen because when all aircraft engines sustain damage due to bird strike, the aircraft may lose all engine redundancy and may even undergo total loss of power. Among the fifteen predictor variables, thirteen of them are categorical variables. The crosstabs of the response variable vs. the categorical variables are given in Table 3-2. Variables

such as “aircraft mass” and “number of birds struck” are analyzed as categorical predictors because the FAA Wildlife Strike Database does not provide their exact value. Table 3-3 the detailed coding of the categorical predictors for statistical analysis. All categorical predictors having more than two levels have to be converted into dummy variables as shown in Table 3-3. In addition to the thirteen categorical predictors, there are two continuous predictor variables. The first one is ALTITUDE, which indicates the altitude above ground level (AGL) that the bird strike occurred. The second continuous predictor variable is AIRSPEED, which shows the indicated airspeed of the aircraft at the time of the bird strike.

3.3.2 Missing Data Mechanism

Since the data in the FAA Wildlife database are collected through voluntary reporting, some reports may contain unanswered questions. Consequently, all unanswered questions result in missing data. The amount of missing data in the study sample is as follows: ALL_ENG_DMG: 0.0%, ALTITUDE: %16.3, BIRDSIZE: 15.7%, B_STRUCK: 0.8%, DAYLIGHT: 15.2%, ENGINE_MANUFACTURER: 0.0%, ENG_POS: 0.0%, FOG: 29.2%, MASS: 3.7%, NO_ENG: 3.6%, PHASE: 5.4%, PRECIP: 28.2%, SEASON: 0.0%, SKY: 26.8%, AIRSPEED: 34.8%, WARNED: 38.0%. Overall, 14.5% of the data values are missing in the sample.

Since the data set includes extensive amount of missing data, the missing data mechanism should be explored first. There are three different types of missing data mechanism [76]:

1. Missing Completely at Random (MCAR): The missing data mechanism is not related to the value of any variables. For example, the data would be missing completely at random if

some pilots accidentally skipped questions in the wildlife strike submission report.

2. Missing at Random (MAR): The missing data mechanism is not related to the missing values, but it is related to the observed values of other variables. For instance, the missing data for BIRDSIZE may not be related to the actual bird size, but may be related to the values of DAYLIGHT. Perhaps some pilots could not clearly see the birds during nighttime, and could not report BIRDSIZE. Thus, the amount of missing data for BIRDSIZE may be greater for nighttime strikes.
3. Non-Ignorable (NI): The missing data mechanism is related to the missing values. For example, some pilots might not report the value of WARNED if they had not received advance warning. So when the actual value of WARNED is "0" (see Table 3), it is more likely to be missing.

"Little's MCAR Test" [77] and "Separate Variance t-Tests" [76] are run to determine if the data are MCAR and MAR, respectively. All tests returned p-values well below $\alpha=0.05$. Thus, there is sufficient evidence to believe that the data are neither MCAR nor MAR. Indeed, the missing data mechanism is non-ignorable.

3.3.3 Missing Data Assumptions

Since the FAA wildlife strike database relies on voluntary reporting of bird strikes, missing data occurs when respondents skip one or more questions in the FAA wildlife strike submission report. However, as shown in Table 3-1, the report consists of a single page that can be effortlessly filled out. So the question is: why are there so many skipped questions in the submitted reports?

One reason is that some wildlife strike reports might not be submitted by the flight crew. If someone other than the flight crew fills out the report, he/ she may not know all the details regarding the bird strike. However, if the report is filled out by the flight crew, what would be the major cause for skipped questions? In that case, a probable reason for missing data is explained as follows: Take the case of variable WARNED in Table 3, for instance. WARNED equals 1 if the pilots received advance warning of birds prior to the bird strike; else 0. It is assumed that pilots who had not received advance warning were more likely to skip the question *"Pilots warned of birds?"* while filling out the wildlife strike report (see Table 3-1). In other words, pilots who had received advance warning of the birds were less likely to skip the question *"Pilots warned of birds?"* while filling out the wildlife strike report (see Table 3-1). Thus, WARNED is more likely to be missing if its actual value is 0, and less likely to be missing if its actual value is 1. Likewise, take the case of the variable PRECIP in Table 3, for example. It is assumed that pilots were more likely to skip the question regarding precipitation while filling out the wildlife strike report if there had been no precipitation at the time of the bird strike. Thus, PRECIP is more likely to be missing if its actual value is 0, and less likely to be missing if its actual value is 1. So the missing values are assumed to be overall less than the observed values.

Table 3-1. Questions in the FAA Wildlife strike submission report [74].

1. Name of Operator/ Carrier	2. Aircraft Make/ Model	3. Engine Make/ Model
4. Aircraft Registration	5. Data of Incident	6. Local Time of Incident
6A. Flight Number	6B Wildlife/ Bird Remains ☐*Collected* ☐*Sent to Smithsonian*	
7. Airport Name/ ID	8. Runway Used	9. Location if En-Route and/ or Distance From Airport
10. Height (AGL) _____ *ft.*	11. Speed (IAS) _____ *kts.*	
12. Phase of Flight	13. Part(s) Struck or Damaged Struck Damaged A. Radome ☐ ☐ B. Windshield ☐ ☐ C. Nose ☐ ☐ D. Engine #1 ☐ ☐ E. Engine #2 ☐ ☐ F. Engine #3 ☐ ☐ G. Engine #4 ☐ ☐ Bird(s) Ingested? ☐	13. (Con't) Struck Damaged H. Propeller ☐ ☐ I. Wing/ Rotor ☐ ☐ J. Fuselage ☐ ☐ K. Landing Gear ☐ ☐ L. Tail ☐ ☐ M. Lights ☐ ☐ N. Other ☐ ☐ *(Specify if "N. Other is checked)*
14. Effect on Flight ☐*None* ☐*Aborted Take-Off* ☐*Precautionary Landing* ☐*Engine Shutdown* ☐*Other(specify)*	15. Sky Condition ☐*No cloud* ☐*Some cloud* ☐*Overcast*	16. Precipitation ☐*Fog* ☐*Rain* ☐*Snow* ☐*None*
17. Bird/ Other Wildlife Species	18. Number Seen and/ or Struck	19. Size of Birds ☐*Small* ☐*Medium* ☐*Large*
20. Pilots Warned of Birds/ Wildlife? ☐Yes ☐No		
22. Aircraft time out of service _____ hours	23. Estimated cost of repairs or replacement (US$)	24. Estimated other costs (US$)

Table 3-2. Crosstabs of the response variable vs. the categorical predictors.

Variable and Name of Variable	Levels	Number of bird strikes	
		Not all engines damaged	All engines damaged
Bird size *(BIRDSIZE)*	Small	32,204	32
	Medium	23,261	19
	Large	3,975	19
	Missing	*11,093*	*25*
Number of birds struck *(B_STRUCK)*	One	58,195	4
	2-10	11,041	57
	10-100	683	28
	More than 100	23	6
	Missing	*591*	*0*
Daylight conditions *(DAYLIGHT)*	Daytime	36,242	58
	Nighttime	18,640	19
	Twilight (Dusk/ Dawn)	4,946	10
	Missing	*10,705*	*8*
Engine position on aircraft *(ENG_POS)*	Under-wing	40,147	58
	Aft-fuselage	28,575	37
	Both under-wing and aft-fuselage	1,811	0
	Missing	*0*	*0*
Is there fog? *(FOG)*	No fog	48,583	70
	Fog	1,372	4
	Missing	*20,578*	*21*
Aircraft Mass (kg) *(MASS)*	Less than 2,250	560	0
	2,251 - 5,700	943	5
	5,701 - 27,000	12,124	26
	27,001 - 272,000	53,668	64
	Heavier than 272,000	656	0
	Missing	*2,582*	*0*
Number of turbofan engines *(NO_ENG)*	Two	60,127	95
	Three	6,432	1
	Four	1,436	1
	Missing	*2,536*	*0*
Flight phase *(PHASE)*	On the Ground *(i.e. Take-Off/ Landing Roll, etc.)*	24,684	39
	Climb	11,463	33
	Land (i.e. Approach/ Descent)	30,324	21
	Cruise *(i.e. En-route)*	244	2
	Missing	*3,818*	*0*
Is there precipitation? *(PRECIP)*	No precipitation	47,233	60
	Rain /Sleet /Snow	3,428	14
	Missing	*19,872*	*21*
Season *(SEASON)*	Winter	7,735	28
	Spring	15,914	17
	Summer	23,553	24
	Fall	23,331	26
	Missing	*0*	*0*
Sky Conditions *(SKY)*	Clear	25,176	32
	Some Clouds/ Overcast	26,478	46
	Missing	*18,879*	*17*
Pilots warned of birds? *(WARNED)*	No	25,895	32
	Yes	17,825	25
	Missing	*26,813*	*38*

Table 3-3. Categorical variables analyzed in this study.

Variable Name	Variable Description	Levels	Dummy variables
ALL_ENG_DMG	The aircraft sustained damage to all engines due to the bird strike	0=No 1=Yes	*Same as ALL_ENG_DMG*
BIRDSIZE	Bird size as reported by the flight crew	0=Small 1=Medium 2=Large	B_1=1 for BIRDSIZE=1; else 0. B_2=1 for BIRDSIZE=2; else 0.
B_STRUCK	Number of birds that struck the aircraft	0=One bird 1=2-10 birds 2=10-100 birds 3=More than 100 birds	C_1=1 for B_STRUCK=1; else 0. C_2=1 for B_STRUCK=2; else 0. C_3=1 for B_STRUCK=3; else 0.
DAYLIGHT	Whether the bird strike occurred during daytime, nighttime, or dusk/ dawn	0=Daytime 1=Nighttime 2=Twilight (dusk/ dawn)	D_1=1 for DAYLIGHT=1; else 0. D_2=1 for DAYLIGHT=2; else 0.
ENG_POS	Where engines are mounted on aircraft	0=All below the wing 1=All on the aft fuselage 2=Both below the wing and on the aft fuselage	E_1=1 for ENG_POS=1; else 0. E_2=1 for ENG_POS=2; else 0.
FOG	Was there fog?	0=No 1=Yes	*Same as FOG*
MASS	Aircraft mass	0=Below 2,250 kg 1=2,251 – 5,701 kg 2=5,701 – 27,000 kg 3=27,001 – 272,000 kg 4=Above 272,000 kg	M_1=1 for MASS=1; else 0. M_2=1 for MASS=2; else 0. M_3=1 for MASS=3; else 0. M_4=1 for MASS=4; else 0.
NO_ENG	Number of turbofan engines that aircraft has	0=Two 1=Three 2=Four	N_1=1 for NO_ENG=1; else 0. N_2=1 for NO_ENG=2; else 0.
PHASE	Phase of flight during which strike occurred	0=On the ground (e.g. landing roll, take-off roll, etc.) 1=Climb 2=Descent/ Approach/ Landing 3=En-route	P_1=1 for PHASE=1; else 0. P_2=1 for PHASE=2; else 0. P_3=1 for PHASE=2; else 0.
PRECIP	Was there precipitation?	0=No precipitation 1=Rain/ sleet/ snow	*Same as PRECIP*
SEASON	Did the strike occur during the birds' migration season (i.e. Spring/ Fall)?	0=Winter 1=Spring 2=Summer 3=Fall	S_1=1 for SEASON=1; else 0. S_2=1 for SEASON=2; else 0. S_3=1 for SEASON=3; else 0.
SKY	Was there any cloud cover?	0=Clear *(no cloud cover)* 1=Cloudy/ overcast	*Same as SKY*
WARNED	Were the pilots warned of birds?	0=No 1=Yes	*Same as WARNED*

3.3.4 Handling Non-Ignorable Missing Data

There are three approaches to handling missing data [76, 78]:

1. Complete-Case Analysis (List-wise Deletion): All bird strike cases with at least one missing value are excluded from analysis, and the remaining cases are analyzed.
2. Single Imputation: A plausible value is substituted for each missing value, and the filled-in data set is analyzed as if it's complete.
3. Multiple Imputation: Each missing value is substituted with a set of plausible values to represent the uncertainty about the prediction of the missing values.

In case of non-ignorable missing data, complete-case analysis produces sample selection bias [79] because the probability of a missing value depends on the variable itself. Thus, the missing data should be imputed prior to statistical analysis. Single imputation is computationally less demanding than multiple imputation. However, single imputation does not incorporate the uncertainty about the predictions of the missing values because each missing value is imputed by only one plausible value. Thus, single imputation underestimates the standard errors of the parameter estimates [78]. On the other hand, multiple imputation accounts for uncertainty about the predictions of the missing values [80]. While there are several different multiple imputation techniques, Siddique and Belin's Approximate Bayesian Bootstrap (ABB) method [80] is chosen to multiply impute the missing data because of the following reasons:

- The imputations are based on values observed elsewhere. Thereby, the method imputes realistic values that are not outside the range of the possible values [81].
- The method does not require the definition of an explicit model for the distribution of the missing values [81].
- It can properly reflect parameter uncertainty [82].
- It can incorporate all available information into the imputation model [82].
- Contrary to most other multiple imputation methods, it is capable of imputing non-ignorable missing data [80].
- Through a simulation study, Siddique and Belin showed that their ABB method can produce unbiased estimates of the true parameters when the amount of complete cases is as low as 50% [80].

Siddique and Belin's ABB method is a hot-deck imputation method that imputes one variable at a time [80]. In this study, Siddique and Belin's ABB method is used with the following modifications to create five multiply-imputed data sets:

1. In "predictive mean matching" [82], all other variables in the data set are used as predictors to make use of all available information. In addition to the variables listed in Table 3, two "auxiliary" categorical variables that are not later incorporated into the statistical analysis are used in predictive mean matching. These auxiliary variables are: i) INGESTION (i.e. whether birds are ingested into at least one engine or not); ii) ENGINE_DAMAGE (whether at least one engine is damaged or not due to bird strike). Using auxiliary variables can help minimize bias in predictive mean matching [83].

2. Based on the missing data assumptions given in section 3.3.3, missing values are deemed overall less than the observed values. Under these circumstances, Siddique and Belin [80] recommend creating five different datasets with the following "closeness parameters": $k = -3, -2, -1, 0, 1$. Negative values of k assign higher probability to donors with smaller values since the missing values are deemed overall less than the observed values. Conversely, positive values of k (i.e. $k = 1$) assign higher probability to donors with bigger values. The reason for using $k = 1$ is to account for some uncertainty about the missing data assumptions, and reduce the effect of subjectivity [80].

3.4 Statistical Model

In order to test for the research hypotheses given in section 3.1, one can simply use the sample proportions based on the raw data. However, when sample proportions are used for hypothesis testing, a very small portion of all available data would be used. Thus, the results would most likely be imprecise [84].

In order to use all available data, a different approach should be followed. Since the response variable (i.e. ALL_ENG_DMG) is binary, the five imputed data sets can be analyzed using a generalized linear model with the "logit" link function. This type of a statistical model is also called a multivariate logistic regression model, and is the most popular approach for analyzing binary response data [85]. A multivariate logistic regression model makes use of all available data. Thereby, it approximates the true probabilities more accurately than sample proportions can do [84].

3.4.1 Generalized Linear Model Approach

The general form of a generalized linear model with binary response data is given in Equation (3-1) [85]:

$$ln\left(\frac{\mathrm{P}}{1-\mathrm{P}}\right) = \beta_0 + \sum_{i=1}^{n} X_i * \beta_i \quad (3\text{-}1)$$

where

- P = The probability that the bird strike will cause damage to all engines of the struck aircraft.
- $\left(\frac{\mathrm{P}}{1-\mathrm{P}}\right)$ = The odds that the bird strike will cause damage to all engines of the struck aircraft.
- $ln\left(\frac{\mathrm{P}}{1-\mathrm{P}}\right)$ = Natural logarithm of the odds *(i.e. the "logit function" of* P*)*.
- β_0 = Intercept of the model.
- X_i = Predictor *i* (either continuous or categorical).
- β_i = Coefficient of predictor *i* in the model.

The model shown in Equation (3-1) is also called a logistic regression model, and it assumes linear relationship between the predictors (i.e. X_i) and the natural logarithm of the odds, i.e. $ln\left(\frac{\mathrm{P}}{1-\mathrm{P}}\right)$.

3.4.2 Variable Selection

Since there are five imputed data sets, each data set needs to be analyzed separately in the beginning. For each data set, all continuous and categorical dummy variables are initially included in the model in Equation (*3-1*). Then the following steps are applied to build the multivariate logistic regression model:

1. The coefficient estimates in Equation (3-1) are computed separately for each data set using Newton-Raphson Algorithm [85].
2. To select the predictor variables that significantly contribute to the model (α=0.05), a "Backward Elimination" procedure is followed based on the Wald Statistic. The Wald Statistic is adequate for analyzing large samples [84]. Based on the Wald Statistic, the following predictor variables are found significant at α=0.05 in all five data sets: Bird size, number of birds struck, engine position, number of engines, and phase of flight. These variables are also called the "main effects" in the model.
3. Once the main effects are identified, the significance of the two-way interaction terms are checked using a "Forward Elimination" procedure (α=0.05) [86]. No two-way interaction term is found significant at α=0.05.
4. The inferences across the five imputed data sets are combined following the rules of nested multiple imputation [87].

The final statistical model is given in Equation (3-2):

$$ln\left(\frac{\hat{P}}{1-\hat{P}}\right) = -9.98 + 0.89 * B_1 + 2.17 * B_2 + 4.40 * C_1 + 6.67 * C_2 + 8.84 * C_3 \quad (3\text{-}2)$$
$$-0.35 * E_1 - 0.74 * E_2 - 2.56 * N_1 - 2.72 * N_2 + 0.49 * P_1 - 0.68 * P_2 + 0.23 * P_3$$

where $\hat{P}$ is the predicted probability that the bird strike will cause damage to all engines, and the other variable definitions are given in Table 3-3. Summary statistics of the coefficient estimates are given in Table 3-4. All coefficients in the final statistical model are found significant at α=0.05.

3.4.3 Model Goodness-of-Fit

The Hosmer and Lemeshow Test [88] is widely used to assess the goodness-of-fit for logistic regression models. However, there is no standard way of applying the Hosmer and Lemeshow Test for multiply imputed data. This is because the predicted probabilities and the data groups vary across multiply imputed data sets [89]. In a recent simulation study, Sullivan and Andridge [89] compared different methods of applying Hosmer and Lemeshow Test to multiply imputed data. They found that Meng and Rubin's Likelihood Ratio Test (LRT) Combining Method [90] was the most promising in controlling the Type I Error rate if the method is applied to 3-6 multiply imputed data sets. So Meng and Rubin's LRT Combining Method is applied to the model. The test returned a p-value of 0.244, which indicates no significant difference between the observed and predicted probabilities (α=0.05). Hence, the model can accurately predict the probability that a bird strike will cause damage to all engines of the struck aircraft.

3.5 Model Interpretation

Equation (3-2) is re-arranged to compute the predicted probability $(\hat{P})$ that a given bird strike will cause damage to all engines of the struck aircraft. Table 3-5 lists these predicted probabilities for some typical commercial aircraft. Further interpretation of the results is given in the following sections.

Table 3-4. Summary of the Coefficient Estimates for the Generalized Linear Model.

Variable	Coefficient Estimate ($\hat{\beta}_i$)	Standard Error of $\hat{\beta}_i$	Wald Statistic (χ^2)	p-value* of the χ^2
Intercept	-9.98	0.24	1788.3	<0.001
B1	0.89	0.11	66.7	<0.001
B2	2.17	0.14	240.3	<0.001
C1	4.40	0.23	379.0	<0.001
C2	6.67	0.24	798.8	<0.001
C3	8.84	0.31	840.0	<0.001
E1	-0.35	0.09	14.5	<0.001
E2	-0.74	0.09	72.3	<0.001
N1	-2.56	0.42	37.9	<0.001
N2	-2.72	0.41	44.4	<0.001
P1	0.49	0.10	23.1	<0.001
P2	-0.68	0.12	34.4	<0.001
P3	0.23	0.05	18.1	<0.001

3.5.1 Number of Engines

According to the model given in Equation (3-2), a twin-engine aircraft is statistically around **12** times more likely to sustain damage to all engines in the event of a bird strike compared to a three-engine aircraft, controlling for all other covariates in Equation (3-2).

Likewise, a twin-engine aircraft is statistically around **15** times more likely to sustain damage to all engines in the event of a bird strike compared to a four-engine aircraft, controlling for all other covariates in Equation (3-2). Hence, the model in Equation (3-2) presents strong evidence to believe that today's typically twin-engine airliners are significantly more prone to sustaining damage to all engines in the event of a bird strike compared to three- or four-engine airliners.

* P-value under the null hypothesis that "the true coefficient of the given predictor in the model is 0".

Table 3-5. Predicted probability ($\hat{P}$) that a bird strike will result in damage to all engines of the struck aircraft.

(a) Twin-engine jetliner with under-wing-mounted engines *(e.g. Airbus A320, Boeing 737-NG, etc.)*

Number of birds struck	2 - 10						10 - 100						> 100					
Flight phase	Climb			Landing			Climb			Landing			Climb			Landing		
Bird size	S.	M.	L.	S.	M.	L.	S.	M.	L.	S.	M.	L.	S.	M.	L.	S.	M.	L.
$\hat{P}$ (%)	0.6	1.5	5.1	0.2	0.5	1.6	5.6	12.7	34.3	1.8	4.3	13.9	34.3	56.0	82.1	13.9	28.3	58.7

(b) Twin-engine jetliner with aft fuselage-mounted engines *(e.g. Boeing 717, CRJ 900, MD-80, ERJ 145, etc.)*

Number of birds struck	2 - 10						10 - 100						> 100					
Flight phase	Climb			Landing			Climb			Landing			Climb			Landing		
Bird size	S.	M.	L.	S.	M.	L.	S.	M.	L.	S.	M.	L.	S.	M.	L.	S.	M.	L.
$\hat{P}$ (%)	0.4	1.0	3.7	0.1	0.3	1.2	4.0	9.3	26.9	1.3	3.1	10.2	26.9	47.3	76.3	10.2	21.8	50.0

(c) Three-engine jetliner with both under-wing- and aft fuselage-mounted engines *(e.g. Boeing 727, MD-11, Lockheed L-1011, etc.)*

Number of birds struck	2 - 10						10 - 100						> 100					
Flight phase	Climb			Landing			Climb			Landing			Climb			Landing		
Bird size	S.	M.	L.	S.	M.	L.	S.	M.	L.	S.	M.	L.	S.	M.	L.	S.	M.	L.
$\hat{P}$ (%)	0.0	0.1	0.2	0.0	0.0	0.1	0.2	0.5	1.9	0.1	0.2	0.6	1.9	4.5	14.4	0.6	1.4	5.0

(d) Four-engine jetliner with under-wing-mounted engines *(e.g. Airbus A380, Boeing 747, etc.)*

Number of birds struck	2 - 10						10 - 100						> 100					
Phase of flight	Climb			Landing			Climb			Landing			Climb			Landing		
Bird size	S.	M.	L.	S.	M.	L.	S.	M.	L.	S.	M.	L.	S.	M.	L.	S.	M.	L.
$\hat{P}$ (%)	0.0	0.1	0.4	0.0	0.0	0.1	0.4	0.9	3.3	0.1	0.3	1.1	3.3	7.7	23.1	1.1	2.5	8.5

3.5.2 Engine Position on Aircraft

A twin-engine aircraft with underwing-mounted engines is statistically around **1.4** times more likely to sustain damage to both engines in the event of a bird strike compared to one with aft-fuselage-mounted engines, controlling for all other covariates in Equation (3-2). This study does not infer causality regarding this statistically significant relationship. However, the model in Equation (3-2) presents strong evidence to believe that engine position on aircraft is significantly associated with the probability that a bird strike will cause damage to all engines of the struck aircraft.

The results suggest strong evidence in favor of both research hypotheses given in section 3.1. Therefore, typical modern-day commercial aircraft that has two under-wing-mounted engines displays the highest probability to sustain damage to all engines in the event of a bird strike (controlling for bird size, number of birds struck, and phase of flight). In view of the results, aviation authorities should consider the following:

- Future turbofan engines are encouraged to be designed beyond the current FAA requirements [91].
- The FAA may consider reviewing the current turbofan engine design requirements since bird strikes are significantly more hazardous for today's "typical" commercial aircraft.

3.5.3 Phase of Flight

Based on Equation (3-2), the phase of climb is statistically the most hazardous flight phase in terms of a possible bird strike that will result in damage to all engines of the struck aircraft. Thus, although most bird strikes occur during approach or descent (see Table 3-2), bird strikes during

the phase of climb are significantly more hazardous. During the phase of climb, a bird strike is around **3.0** times more likely to cause damage to all engines of the struck aircraft compared to the phase of landing, controlling for all other covariates in Equation (3-2). Thus, aviation practitioners should consider the following:

- Airports with limited resources are recommended to prioritize the prevailing aircraft climb paths in their wildlife management programs.
- Pilot training programs should give more prominence to emergency landing procedures that may be required due to a damaging bird strike during the phase of climb.
- Generally, climb speeds closer to V_y (i.e. best rate-of-climb speed) are preferred over V_x (i.e. best angle-of-climb speed) for better fuel economy [72]. However, climb speeds closer to V_x can further improve flight safety for two reasons: i) Because V_x is always considerably lower than V_y, it can reduce the impact energy in the event of a bird strike and reduce the likelihood of damage to all engines [72]. ii) Because V_x provides steeper climb rates compared to V_y, it maximizes the altitude gain per unit distance. Consequently, maximized altitude gain per unit distance enables maximized engines-out glide range if all engines lose thrust due to a damaging bird strike during the climb [43]. The maximized glide range enhances the likelihood of safely returning to a runway.

3.5.4 Bird Size

According to Equation (3-2), a bird strike involving medium-sized bird(s) is statistically around **2.5** times more likely to cause damage to all engines of the struck aircraft

compared to one involving small-sized bird(s), controlling for all other covariates in Equation (3-2). Northern Pintail accounted for 18 percent* of the bird strikes involving medium-sized birds that resulted in damage to all engines of the struck aircraft.

Moreover, a bird strike involving large-sized bird(s) is statistically around **8.5** times more likely to cause damage to all engines of the struck aircraft compared to one involving small-sized bird(s), controlling for all other covariates in Equation (3-2). Canada geese accounted for 38 percent† of the bird strikes involving large bird species that resulted in damage to all engines of the struck aircraft, followed by snow geese (25%), and American white pelican (19%).

In view of the results and continuous increase in large bird populations, aviation practitioners should consider the following:

- Contrary to the current testing requirements, future designs of turbofan engines are strongly encouraged to be tested for large birds to provide protection against large bird ingestions [91].
- Wildlife management programs should involve species-specific means of controlling attractants, particularly for large bird species such as Canada goose, snow goose and American white pelican.

3.5.5 Number of Birds Struck

According to Equation (3-2), a bird strike involving 10-100 birds is statistically around **9.5** times more likely to cause

† Among the cases in which the bird species were identified.

damage to all engines of the struck aircraft compared to that involving 2-10 birds, controlling for all other covariates in Equation (3-2).

Furthermore, a bird strike involving more than 100 birds is statistically up to **85** times more likely to cause damage to all engines of the struck aircraft compared to that involving 2-10 birds, controlling for all other covariates in Equation (3-2). Thus, large flocks of birds present the highest degree of hazard in terms of causing damage to all engines of the struck aircraft.

The data show that gulls accounted for 39 percent* of the bird strikes that involved large (i.e. >10) flocks of birds and resulted in damage to all engines, followed by European Starling (28%) and Mourning Dove (11%). If flocks of birds are observed near the runway:

- Flight crews should delay take-off until runway is clear of birds.
- Flight crews should consider delaying landing (if fuel permits) or diverting to another runway that is clear of birds. Otherwise, if it is not possible to delay landing, they should plan on additional landing distance because damage to all engines due to a possible bird strike may disable thrust reversers [92].

3.6 Summary

The statistical analysis of the data in the FAA Wildlife Strike Database provides strong evidence that the probability that a bird strike will cause damage to all engines of the struck aircraft is significantly associated with bird size, number of birds struck, engine position on the aircraft, number

of engines, and flight phase. In terms of causing damage to all engines of the struck aircraft, a bird strike is statistically:

- 1.4 times more hazardous if the engines are mounted under the wing as opposed to on the aft fuselage,
- 12 times more hazardous if it involves twin-engine aircraft as opposed to three- engine aircraft,
- 15 times more hazardous if it involves twin-engine aircraft as opposed to four- engine aircraft,

The results show strong evidence that bird strikes are significantly more hazardous for today's "typical" commercial aircraft that has two under-wing-mounted engines. Hence, the findings warrant future development of an adaptive flight planner to assist pilots in engines-out emergency landings.

CHAPTER 4 - STATISTICAL ANALYSIS OF AIRCRAFT-BIRD STRIKES RESULTING IN ENGINE FAILURE

4.1 Research Question and Significance of Research

The objective of this chapter is to identify the statistically most hazardous conditions regarding engine failure due to bird strike. In other words, this chapter explores under what circumstances a bird strike is more likely to result in failure of the engine(s) of the struck aircraft. For this purpose, the multiply imputed data generated from the FAA Wildlife Strike Database [74] are used. The goal is to find out the statistical relationship between the 15 predictor variables listed in section 3.3.1, and the probability of engine failure in the event of a bird strike. Identification of this statistical relationship is required for creating realistic bird strike scenarios, which are to be used in designed experiments to test for the effectiveness of the proposed adaptive flight planner. In addition, the findings can help researchers understand the nature of bird strikes that result in engine failure. Thereby, researchers can develop a scientific approach to reduce the potential of engine failure in the event of a bird strike.

4.2 Data Description

This chapter uses a large sample of 42,905 bird strike cases from the FAA Wildlife Strike Database [74]. The sample includes all reported bird strikes that:

- occurred between January 1, 1990 (the earliest available date on the database) and November 30, 2012 in the US;
- involved turbofan engine civil aircraft;

- occurred while the aircraft was airborne.

Thus, all findings apply to airborne aircraft-bird strikes that involve turbofan engine civil aircraft.

The response variable is called “ENG_FAIL”. It is of binary nature and has two possible outcomes: “no engine failure” or “engine failure”. “No engine failure” means that no engine stopped running or was shut down due to the bird strike. Conversely, “engine failure” means that at least one engine stopped running or was shut down due to the bird strike. The predictor variables are the same as listed in section 3.3.1. The crosstabs of the categorical variables vs. the response variable are given in Table 4-1 (except for the “engine manufacturer”, which is the commercial manufacturer of the engines of the struck aircraft).

Since the data in the FAA Wildlife database are collected through voluntary reporting, some reports may contain unanswered questions. Consequently, all unanswered questions result in missing data. The amount of missing data in the sample is as follows: ALTITUDE: 25.1%, BIRDSIZE: 14.4%, B_STRUCK: 1.0%, DAYLIGHT: 16.5%, ENG_FAIL: 4.6%, ENGINE_MANUFACTURER: 0.0%, ENG_POS: 0.0%, FOG: 30.5%, MASS: 5.4%, NO_ENG: 5.3%, PHASE: 8.3%, PRECIP: 29.6%, SEASON: 0.0%, SKY: 28.2%, AIRSPEED: 37.1%, WARNED: 38.6%. “Little’s MCAR Test” [77] and “Separate Variance t-Tests” [76] are run to determine if the data are MCAR and MAR, respectively. All tests returned p-values well below $\alpha=0.05$. Thus, there is sufficient evidence to believe that the data are neither MCAR nor MAR. It is concluded that the missing data mechanism is non-ignorable. In order to minimize the amount of bias due to non-ignorable missing data, Siddique and Belin’s [80] Approximate Bayesian Bootstrap method is applied with the same

modifications given in section 3.3.4 to create five multiply-imputed data sets for statistical analysis.

4.3 Statistical Model

Following the procedure described in section 3.4, a logistic regression model is built. The following main effects are found significant at α=0.05 in all five data sets: ALTITUDE, BIRDSIZE, B_STRUCK, DAYLIGHT, PHASE, SKY. In addition, the two-way interaction involving the predictors ALTITUDE and PHASE is found significant at α=0.05. A summary of the coefficient estimates is given in Table 4-2. The logistic regression model is presented in Equation (4-1) as follows:

$$ln\left(\frac{\hat{P}}{1-\hat{P}}\right) = -6.80 - 0.17 * a + 1.90 * b_1 + 3.51 * b_2 + 1.22 * c_1 + 2.59 * c_2 - 0.24 * d_1 \quad (4-1)$$
$$+0.68 * d_2 - 2.42 * p_1 - 14.02 * p_2 + 0.65 * s + 0.18 * a * p_1 + 0.24 * a * p_2$$

where $\hat{P}$ is the predicted probability of engine failure in the event of a bird strike, and all other variable definitions are given in Table 4-1.

To check the model goodness-of-fit, Meng and Rubin's Likelihood Ratio Test Combining Method [90] is applied to the model. The test returned a p-value of 0.798, which indicates no significant difference between the observed and predicted probabilities (α=0.05). Hence, the model can accurately predict the probability of engine failure in the event of a bird strike.

Table 4-1. Crosstabs of the categorical predictors vs. the response variable.

Variable and Name of Variable	Levels	Number of bird strike events		
		No engine failure	Engine failure	*Missing*
Bird size *(BIRDSIZE)*	Small	18,941	15	*823*
	Medium	16,132	57	*640*
	Large	2,511	62	*127*
	Missing	*6,047*	*32*	*518*
Number of birds struck *(B_STRUCK)*	One	36,981	99	1,614
	2-10	5,791	55	478
	More than 10	382	13	15
	Missing	*476*	*0*	*1*
Daylight conditions *(DAYLIGHT)*	Daytime	18,100	85	*1142*
	Nighttime	15,358	35	*779*
	Twilight (Dusk/ Dawn)	2,736	30	*56*
	Missing	*7,437*	*16*	*131*
Engine position on aircraft *(ENG_POS)*	Under-wing	26,302	87	*1009*
	Aft-fuselage	15,888	78	*1060*
	Both under-wing and aft-fuselage	1,441	1	*39*
	Missing	*0*	*0*	*0*
Is there fog? *(FOG)*	No fog	28,947	120	*2011*
	Fog	764	4	*43*
	Missing	*13,920*	*42*	*54*
Aircraft Mass (kg) *(MASS)*	Less than 2,250	300	0	*19*
	2,251 - 5,700	490	7	*26*
	5,701 - 27,000	6,274	28	*274*
	27,001 - 272,000	33,722	115	*1756*
	Heavier than 272,000	398	16	*11*
	Missing	*2,447*	*0*	*22*
Number of turbofan engines *(NO_ENG)*	Two	35,906	131	*1719*
	Three	4,404	15	*315*
	Four	903	20	*53*
	Missing	*2,418*	*0*	*21*
Flight phase *(PHASE)*	Climb	10,821	139	*536*
	Descent	28,854	27	*1464*
	Cruise *(i.e. En-route)*	242	0	*4*
	Missing	*3,714*	*0*	*104*
Is there precipitation? *(PRECIP)*	No precipitation	28,384	117	*1958*
	Rain /Sleet /Snow	1,722	9	*150*
	Missing	*13,525*	*40*	*0*
Season *(SEASON)*	Winter	4,706	31	*223*
	Spring	10,991	46	*487*
	Summer	12,118	29	*586*
	Fall	15,816	60	*812*
	Missing	*0*	*0*	*0*
Sky Conditions *(SKY)*	Clear	16,322	43	*1189*
	Some Clouds/ Overcast	14,417	87	*888*
	Missing	*12,892*	*36*	*31*
Pilots warned of birds? *(WARNED)*	No	16,696	65	*1239*
	Yes	9,615	44	*511*
	Missing	*17,320*	*57*	*358*

Table 4-2. Summary of the coefficient estimates for the final model.

Variable	Coefficient Estimate ($\hat{\beta}_i$)	Estimated Standard Error	Wald Statistic (χ^2)	p-value* of the χ^2
Intercept	-6.80	0.40	283.5	0.000
ALTITUDE	-0.17	0.07	5.9	0.015
B1	1.90	0.39	23.7	0.000
B2	3.51	0.37	91.4	0.000
C1	1.22	0.25	23.5	0.000
C2	2.59	0.90	8.3	0.004
D1	-0.24	0.32	0.6	0.451
D2	0.68	0.31	4.7	0.030
P1	-2.42	0.34	50.3	0.000
P2	-14.02	0.67	439.8	0.000
SKY	0.65	0.24	7.2	0.007
*ALTITUDE*P1*	0.18	0.10	3.4	0.065
*ALTITUDE*P2*	0.24	0.09	6.7	0.009

4.4 Model Interpretation

Equation (*4-1*) can be rearranged to estimate the probability of engine failure ($\hat{\mathrm{P}}$) in the event of a bird strike as follows:

$$\hat{\mathrm{P}} = \frac{e^{-6.80-0.17a+1.90b_1+3.51b_2+1.22c_1+2.59c_2-0.24d_1+0.68d_2-2.42p_1-14.02p_2+0.65s+0.18ap_1+0.24ap_2}}{1+e^{-6.80-0.17a+1.90b_1+3.51b_2+1.22c_1+2.59c_2-0.24d_1+0.68d_2-2.42p_1-14.02p_2+0.65s+0.18ap_1+0.24ap_2}} \quad (4\text{-}2)$$

Using Equation (4-2), the predicted probability of engine failure in the event of a bird strike is plotted versus altitude AGL in Figure 4-1 for certain combinations of predictors. With the help of Figure 4-1, the following sections explain the statistical relationship between each predictor and the predicted probability of engine failure in the event of a bird strike.

* P-value under the null hypothesis that "the true coefficient of the given predictor in the model is 0".

It should be noted that Figure 4-1 illustrates the predicted probabilities up to an altitude of 7,000 ft. AGL. This is because more than 95% of the observed bird strikes occurred below this altitude. Hence, the results inferred in this section typically apply up to an altitude of 7,000 ft. AGL.

4.4.1 Altitude above Ground Level (AGL)

The results in Table 4-2 indicate significant interaction between altitude and flight phase. So for each flight phase, there is a different pattern of relationship between altitude AGL and the probability of engine failure in the event of a bird strike. Figure 4-1a illustrates this relationship for the flight phases of climb and descent, assuming medium-sized birds, 2-10 birds struck, daytime and clear sky conditions. The predicted probability of engine failure in the event of a bird strike declines by around **15%** with every 1,000-ft altitude gain during climb, controlling for bird size, number of birds struck, daylight and sky conditions. Comparison of the observed[†] and predicted probabilities illustrated in Figure 4-1a confirms the accuracy of the estimated pattern. During the phase of climb, lower altitudes are significantly more hazardous in terms of engine failure in the event of a bird strike. Therefore:

- Wildlife management programs should particularly focus on airport environments.
- During the initial climb-out, which is statistically the most hazardous period of flight in terms of engine failure due to bird strike, flight crews should be extremely vigilant.

[†] Observed probabilities are computed from all five imputed data sets.

- The more hazardous lower altitudes should be cleared as rapidly as possible. This can be achieved by using speeds closer to V_x or V_y, and flap settings that provide higher rate of climb. For instance, if there is sufficient runway length, Boeing 737-800 pilots can use flaps 1 instead of flaps 5 to increase the rate of climb.

Contrary to the phase of climb, the predicted probability of engine failure in the event of a bird strike remains virtually constant with altitude AGL during approach/ descent (see Figure 4-1a), controlling for bird size, number of birds struck, daylight and sky conditions. Comparison of the observed and predicted probabilities plotted in Figure 4-1a confirms this fairly constant pattern.

4.4.2 Flight Phase

Figure 4-1a shows the statistical relationship between the flight phase and probability of engine failure in the event of a bird strike. Although most bird strikes occur during approach/ descent (see Table 2), bird strikes during climb are significantly more likely to result in engine failure. At lower altitudes (i.e. <1,000 ft. AGL), a bird strike during climb is statistically around **11** times more likely to result in engine failure than that during approach. At higher altitudes such as 6,000 ft. AGL, a bird strike during climb is statistically around **four** times more likely to cause engine failure than that during descent. Therefore, bird strikes during climb are substantially more hazardous in terms of engine failure than those during approach/ descent. Hence, the following should be considered by aviation experts:

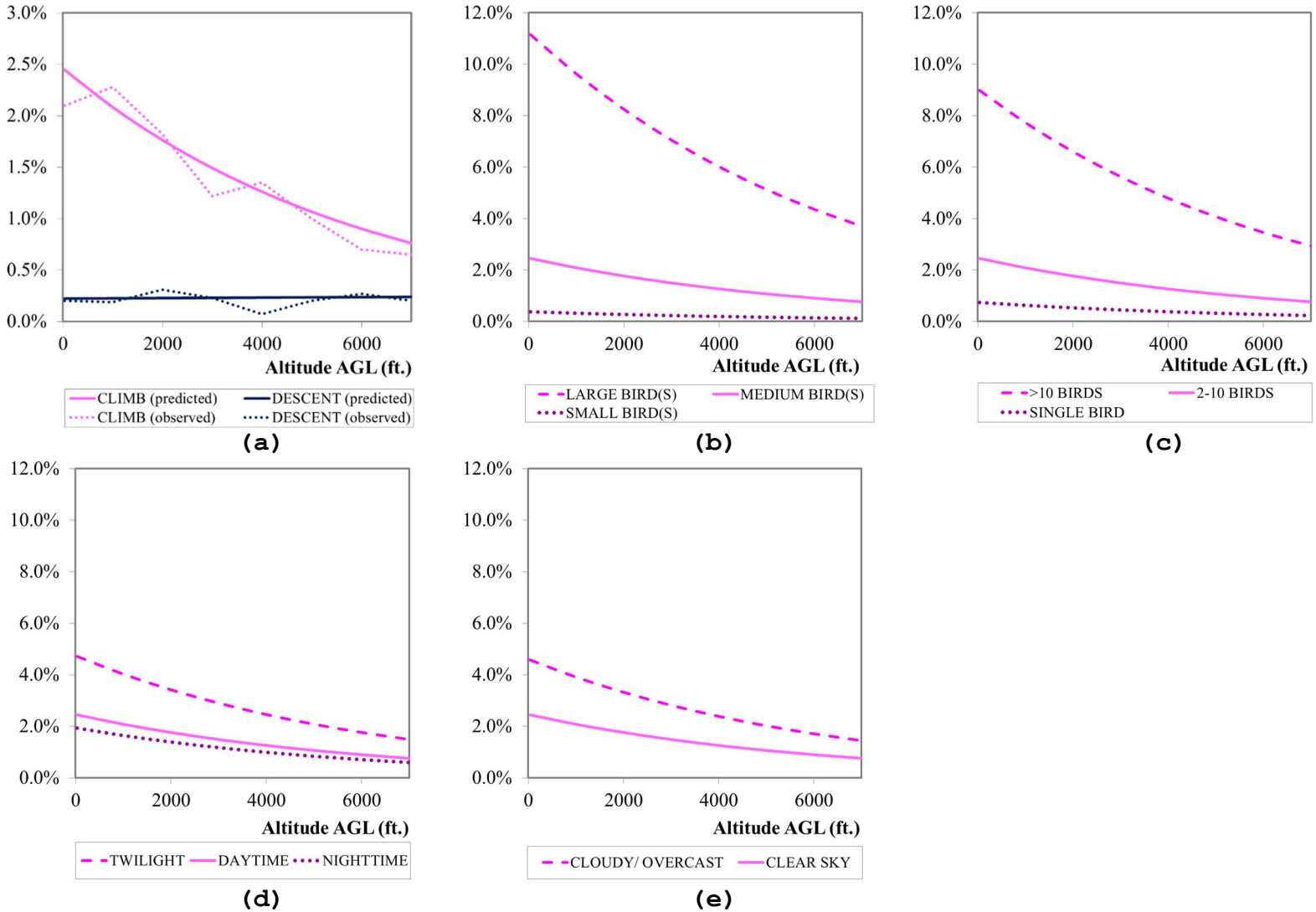

Figure 4-1. Probability of engine failure (vertical axis) vs. altitude AGL, highlighting the statistical associations with: (a) Flight phase (b) Bird size, (c) Number of birds struck, (d) Sky conditions, (e) Daylight conditions.

- Airports with limited resources are recommended to prioritize the prevailing aircraft climb paths in their wildlife management programs.
- While climb speeds closer to V_y minimize the time spent at the more hazardous lower altitudes, climb speeds closer to V_x can better improve flight safety than V_y for the reasons outlined in section 3.5.3.
- Pilot training programs should give more prominence to emergency landing procedures initiated after single or dual engine failure due to bird strike during climb.
- Since engine failure due to bird strike is expected to occur more frequently in the near future, more bird strikes can result in dual engine failure as in the case of Ethiopian Airlines Flight 604 or US Airways Flight 1549. Thus, adaptive flight planners can be developed to optimize the emergency landing trajectory of twin-engine aircraft on a real-time basis in case of a post-bird strike dual engine failure.

4.4.3 Bird Size

Assuming phase of climb, 2-10 birds struck, daytime and clear sky conditions, Figure 4-1b exemplifies the relationship between the bird size and predicted probability of engine failure in the event of a bird strike. A bird strike involving medium-sized bird(s) is statistically around **six** times more likely to lead to engine failure than that involving small-sized bird(s), controlling for altitude AGL, number of birds struck, flight phase, daylight and sky conditions. Mallard and herring gull accounted for 14 and 11 percent* of the bird strikes with engine failure, respectively, involving medium-sized birds.

A bird strike involving large (i.e. > 8.0 lb.) bird(s) is statistically around **30** times more likely to bring about engine failure than that involving small-sized bird(s), controlling for altitude AGL, number of birds struck, flight phase, daylight and sky conditions. Thus, large birds are extremely hazardous. Canada geese accounted for 38 percent[‡] of the bird strikes with engine failure involving large bird species, followed by double-crested cormorant (14%), snow goose (12%), black vulture (6%) and turkey vulture (6%). These bird species are similar to the hazardous species identified in section 3.5.4. Hence, wildlife management programs at airport environments should involve species-specific means of controlling attractants, particularly for the large bird species identified herein and in section 3.5.4.

4.4.4 Number of Birds Struck

Figure 4-1c illustrates the relationship between the number of birds struck and predicted probability of engine failure in the event of a bird strike, assuming phase of climb, medium-sized birds, daytime and clear sky conditions. A bird strike involving 2-10 birds is statistically around **three** times more likely to result in engine failure than that involving a single bird, controlling for altitude AGL, bird size, flight phase, daylight and sky conditions. If the bird strike involves more than 10 birds, it is statistically around **12** times more likely to result in engine failure that that involving a single bird. Flocks of gulls and Canada geese accounted for 26 and 21 percent[*] of the bird strikes, respectively, that involved multiple birds and led to engine failure. In view of the findings, flight crews are encouraged to follow the recommendations given in section 3.5.5.

[‡] Among the cases in which the bird species were identified.

4.4.5 Daylight and Sky Conditions

Assuming phase of climb, medium-sized birds, 2-10 birds struck, and clear sky conditions, Figure 4-1d exemplifies the relationship between the daylight conditions and predicted probability of engine failure in the event of a bird strike. While most bird strikes occur during daytime (see Table 4-1), the predicted probability of engine failure in the event of a bird strike is the highest during twilight (i.e. dusk/ dawn), controlling for the other predictors in the model. Statistically, the probability of engine failure in the event of a bird strike is around **90 percent** higher during twilight than during daytime, controlling for altitude, flight phase, bird size, number of birds struck and sky conditions. Canada geese, though not particularly known for being crepuscular[§] [93], were involved in 20 percent[**] of the bird strikes with engine failure during twilight, followed by mourning doves (15%) and gulls (15%).

Figure 4-1e illustrates the relationship between the sky conditions and predicted probability of engine failure in the event of a bird strike, assuming phase of climb, medium-sized birds, 2-10 birds struck, and daytime. Statistically, the probability of engine failure in the event of a bird strike is around **80 percent** higher during cloudy sky conditions than during daytime, controlling for altitude, flight phase, bird size, number of birds struck and daylight conditions. Gulls account for 21 percent[*] of the bird strikes with engine failure in cloudy sky conditions, followed by Canada geese (18%) and double-crested cormorant (7%).

[§] Active at dawn or dusk.

[**] Among the cases in which the bird species is identified.

It is not known why there is such a significant increase in the probability of engine failure in the event of a bird strike during twilight and/ or cloudy sky conditions. However, the FAA Wildlife Strike Data [74] provide strong evidence for this since the coefficient estimates for both *D2* and *SKY* in Equation (*4-1*) return p-values well below α=0.05 (see Table 4-2).

As for the nighttime, Canada geese and snow geese accounted for 27 and 15 percent[††] of the bird strikes with engine failure, respectively. Although many bird species are not nocturnal [93], bird strikes can still occur at night and result in engine failure. Equation (*4-1*) suggests that a bird strike during nighttime is statistically 20 percent less likely to result in engine failure compared to a daytime strike, controlling for altitude, bird size, number of birds struck, flight phase and sky conditions. However, there is not strong evidence to justify this because the coefficient estimate for *D1* in Equation (*4-1*) returns a p-value of 0.451, which is considerably higher than α=0.05 (see Table 4). Nevertheless, the results are noteworthy in that they invalidate a number of wide misconceptions such as *"Birds don't fly in poor visibility such as in clouds, etc."* or *"Birds don't fly at night"* [92]. Indeed, the results confirm that bird strikes during reduced visibility conditions are no less perilous than those during good visibility conditions, and flight crews should be extremely vigilant when visibility drops.

4.5 Summary

The data from the FAA Wildlife Strike Database are statistically analyzed to identify the factors that are significantly associated with the probability of engine failure

[††] Among the cases in which the bird species is identified.

in the event of a bird strike. The findings indicate significant statistical relationship between the probability of engine failure in the event of a bird strike versus altitude AGL, bird size, number of birds struck, flight phase, daylight and sky conditions. Among these factors, altitude AGL, flight phase, daylight and sky conditions are of particular interest for flight simulator testing. The results show that:

- Statistically, the probability of engine failure in the event of a bird strike declines by around 15% every 1,000-ft. altitude gain during the phase of climb, but it remains fairly constant with altitude AGL during the phase of approach/ descent, controlling for the other predictors in the model.
- A bird strike during climb is statistically up to 11 times more likely to result in engine failure compared to one during approach/ descent, controlling for the other predictors in the model.
- A bird strike during twilight is statistically around 90 percent more likely to result in engine failure compared to a daytime strike. Likewise, a bird strike during cloudy sky conditions is statistically 80 percent more likely to result in engine failure compared to one during clear sky conditions. Contrary to the wide misconception that "Bird do not fly in poor visibility", bird strikes not only can happen during reduced visibility conditions, but also are no less perilous than those during good visibility conditions.

The findings will be used to generate realistic bird strike scenarios for testing the effectiveness of the proposed adaptive flight planner in full flight simulators. Based on the findings, the bird strike scenarios will be simulated during the phase of climb at an altitude below 5,000 ft. in twilight conditions.

CHAPTER 5 - ENGINES-OUT FLIGHT PERFORMANCE OF THE AIRBUS A320

5.1 About the Airbus A320 Aircraft

The Airbus A320 competes directly with the Boeing 737-800. It made its maiden flight in 1987, and pioneered the use of full digital fly-by-wire controls and side-stick controllers in jetliners [94]. The A320 has two models: A320-100 and A320-200. Only 21 A320-100s were manufactured so far. The A320-100 is currently out of production [95], and does not exist in the US Fleet. The A320-200 has either wingtip fences or "sharklets" as well as increased fuel capacity compared to the A320-100. Through January 2015, the A320 aircraft received 7,577 orders with 3,867 of them delivered [26].

5.2 Research Question and Significance of Research

In the occurrence of total loss of thrust, if an engine restart is not possible, the odds of a safe landing depends several factors, including the aircraft's engines-out glide performance. A crash can be avoided if a safe touchdown location exists within the aircraft glide range. In order to accurately estimate aircraft glide range, flight crews should have sufficient knowledge on aircraft's engines-out glide performance. However, flight crew operating manuals (FCOM) scarcely present any information on aircraft glide performance [96, 97]. Flight management computers of contemporary glass cockpits do not

present such information[‡‡] either [97]. Thus, it is essential for flight crews, particularly those of twin-engine jetliners, to have sufficient knowledge on aircraft glide performance in the occurrence of total loss of thrust.

The objective of this chapter is to assess the engines-out glide performance the Airbus A320 aircraft, which is one of the two commercial jets analyzed in this study. To fulfill the objective, this chapter presents a simulation study to estimate the relationship between steady-speed[§§] engines-out glide ratio vs airspeed at varying wing configurations of the Airbus A320. The findings will be used to identify the post-failure performance of the Airbus A320. Following this task, the architectural design of an adaptive flight planner will be developed specifically for the A320 aircraft based on its engines-out glide performance. In addition, the findings from this chapter can also be incorporated into pilot training programs to help airline pilots better understand the engines-out glide performance of commercial jets.

To the author's best knowledge, there is no publically available study that assessed the engines-out glide performance of the Airbus A320 or any other comparable commercial jet. Hence, this study is the first of its type to analyze the engines-out glide performance of a commercial jet.

[‡‡] For the Airbus A320-200, the only exception is that the primary flight display indicates the best glide (i.e. "green dot") speed if the aircraft is in "clean" configuration (i.e. flaps and landing gear up).

[§§] Here, "steady speed" refers to constant calibrated airspeed.

5.3 Review of Theory

5.3.1 Mechanics of Engines-out Glide

Figure 5-1 shows the forces acting on an aircraft body during engines-out descent. The force acting perpendicular to the flight path is called lift. The magnitude of the lift force is found from Equation (5-1) as follows:

$$L = \frac{1}{2} * \rho * {v_T}^2 * S * C_L \quad (5\text{-}1)$$

where

- L= Magnitude of the lift force.
- ρ= Air density.
- S= Wing area.
- v_T= True airspeed, which is the physical speed of the aircraft in relation to the air around it [98].
- C_L= Lift coefficient of the aircraft.

On the other hand, the force shown in Figure 5-1 acting parallel to the flight path is called drag. The total magnitude of the drag force is found from Equation (*5-2*) as follows:

$$D = \frac{1}{2} * \rho * {v_T}^2 * S * C_D \quad (5\text{-}2)$$

where

- D= Magnitude of the total drag force.
- ρ= Air density.
- S= Wing area.
- v_T= True airspeed.
- C_D= Total drag coefficient of the aircraft.

For a given aircraft body, both the lift (C_L) and drag coefficients (C_D) depend on the Mach Number[***], angle of attack[†††], Reynolds Number[‡‡‡] and aircraft configuration (i.e. wing configuration, landing gear position, etc.) [72]. At Mach Numbers below 0.50, where typical engines-out glide speeds fall within, the change in C_L and C_D with respect to the Mach and Reynolds Numbers can be neglected [99].

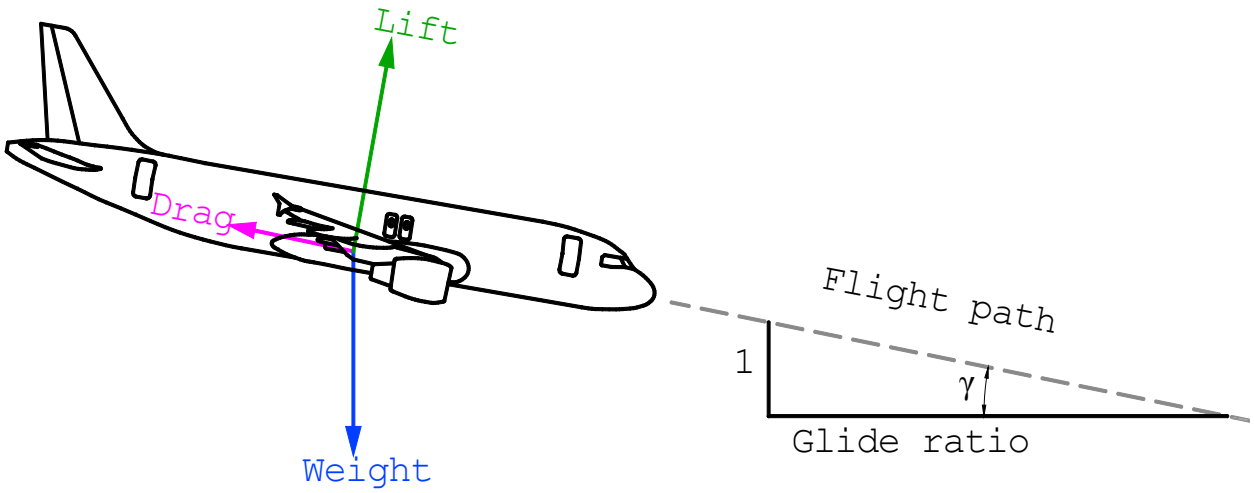

Figure 5-1. Forces acting on aircraft body during engines-out descent.

Figure 5-2 illustrates the relationship between drag force vs. airspeed. As shown in Figure 5-2, there are two types of drag force acting on an aircraft body [72]:

[***] The ratio of true airspeed to the speed of sound.

[†††] The angle between the wing chord line and the dimension of airflow.

[‡‡‡] A dimensionless parameter that indicates how rapid the effects of viscosity spread away from a surface.

- Parasite drag, which results from skin friction, roughness and pressure drag. The greater the airspeed is, the greater the parasite drag becomes in a given aircraft configuration as shown in Figure 5-2.
- Induced drag, which results from wingtip vortices due to pressure difference between the top and bottom of the wing surfaces. The greater the airspeed is, the lower the induced drag becomes in a given aircraft configuration as illustrated in Figure 5-2.

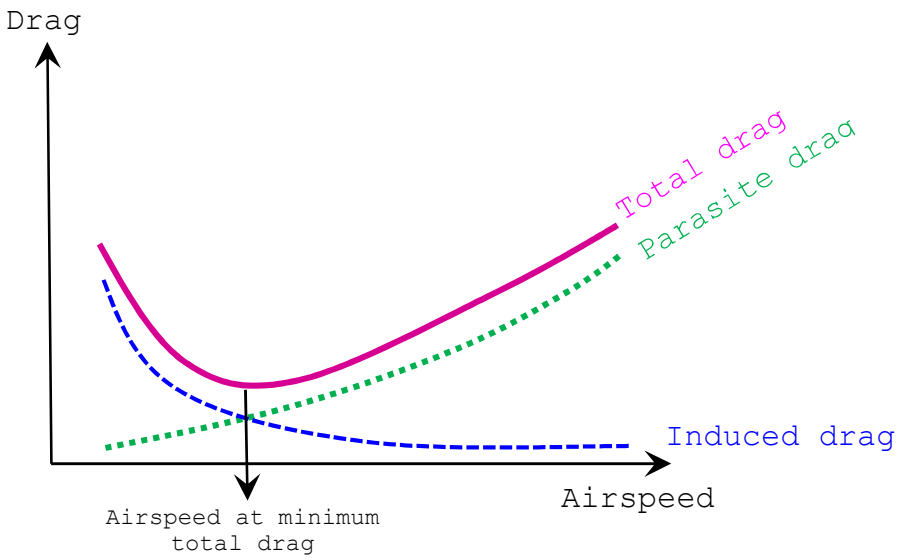

Figure 5-2. Parasite and induced drag vs. airspeed.

5.3.2 Engines-out Glide Ratio

The angle γ in Figure 5-1 is called the glide path angle. While it is an important flight parameter, flight crews may prefer using glide ratio for practical purposes. Glide ratio is the cotangent of angle γ in Figure 5-1, and defines the ratio of

the horizontal distance travelled by the aircraft to the altitude loss. Knowing the glide ratio and altitude above ground level (AGL), flight crews can estimate aircraft glide range in the occurrence of total loss of thrust.

During engines-out descent, if the lift, weight and drag forces shown in Figure 5-1 exactly balance each other, the aircraft is in equilibrium, and descends at constant angle and constant equivalent airspeed. The steady-speed engines-out glide ratio, which stems from constant angle of descent, is simply equal to the lift (L) over Drag (D) ratio (i.e. L/D) when the lift, weight and drag forces exactly balance each other [72, 100]. For a given aircraft configuration, the maximum steady-speed engines-out glide ratio is achieved at or slightly greater than the airspeed that corresponds to the minimum total drag shown in Figure 5-2 [72].

5.3.3 Types of Airspeed

The quantity $\frac{1}{2} * \rho * {v_T}^2$ is called "dynamic pressure" [98], and it affects the magnitude of the lift and drag forces acting on the aircraft as Equations (5-1) and (5-2) illustrate. As the aircraft descends during engines-out descent, the air density (ρ) increases. However, if the flight crew maintains constant "equivalent airspeed" (v_E), the dynamic pressure acting on the aircraft remains constant because a given v_E always produces the same dynamic pressure regardless of altitude and atmospheric conditions. Equivalent airspeed is defined as the true airspeed not corrected for "density error". The relationship between equivalent airspeed and true airspeed is given in Equation (5-3) [98]:

$$v_E = v_T * \sqrt{\frac{\rho}{\rho_0}} \tag{5-3}$$

where

- v_T= True airspeed of the aircraft.
- v_E= Equivalent airspeed of the aircraft.
- ρ= Air density at the altitude that the aircraft is flying.
- ρ_0= Air density at the sea level on a standard day (i.e. air pressure=101.3 kPa and air temperature=15˚C [101]).

In a given aircraft configuration, the aircraft maintains constant engines-out glide ratio if the pilots maintain constant equivalent airspeed. However, contemporary aircraft cannot display equivalent airspeed correctly at varying altitudes. Instead, they indicate "calibrated airspeed", which is defined as the equivalent airspeed not corrected for "altitude error". Calibrated airspeed and equivalent airspeed are precisely equal at the sea level on a standard day[§§§] [98]. However, the relative difference between calibrated airspeed and equivalent airspeed increases with increasing altitude and increasing airspeed as shown in Figure 5-3. Nonetheless, Figure 5-3 shows that the difference between calibrated airspeed and equivalent airspeed is always less than 1.0 kt below 5,000 ft for $v_E \leq 250\,kt$. Hence, calibrated airspeed and equivalent airspeed are virtually equal to each other below 5,000 ft. The study utilizes this fact in estimating the steady-speed engines-out glide ratio of the A320.

[§§§] On a standard day, the air pressure equals 101.3 kPa and air temperature equals 15˚C at the sea level.

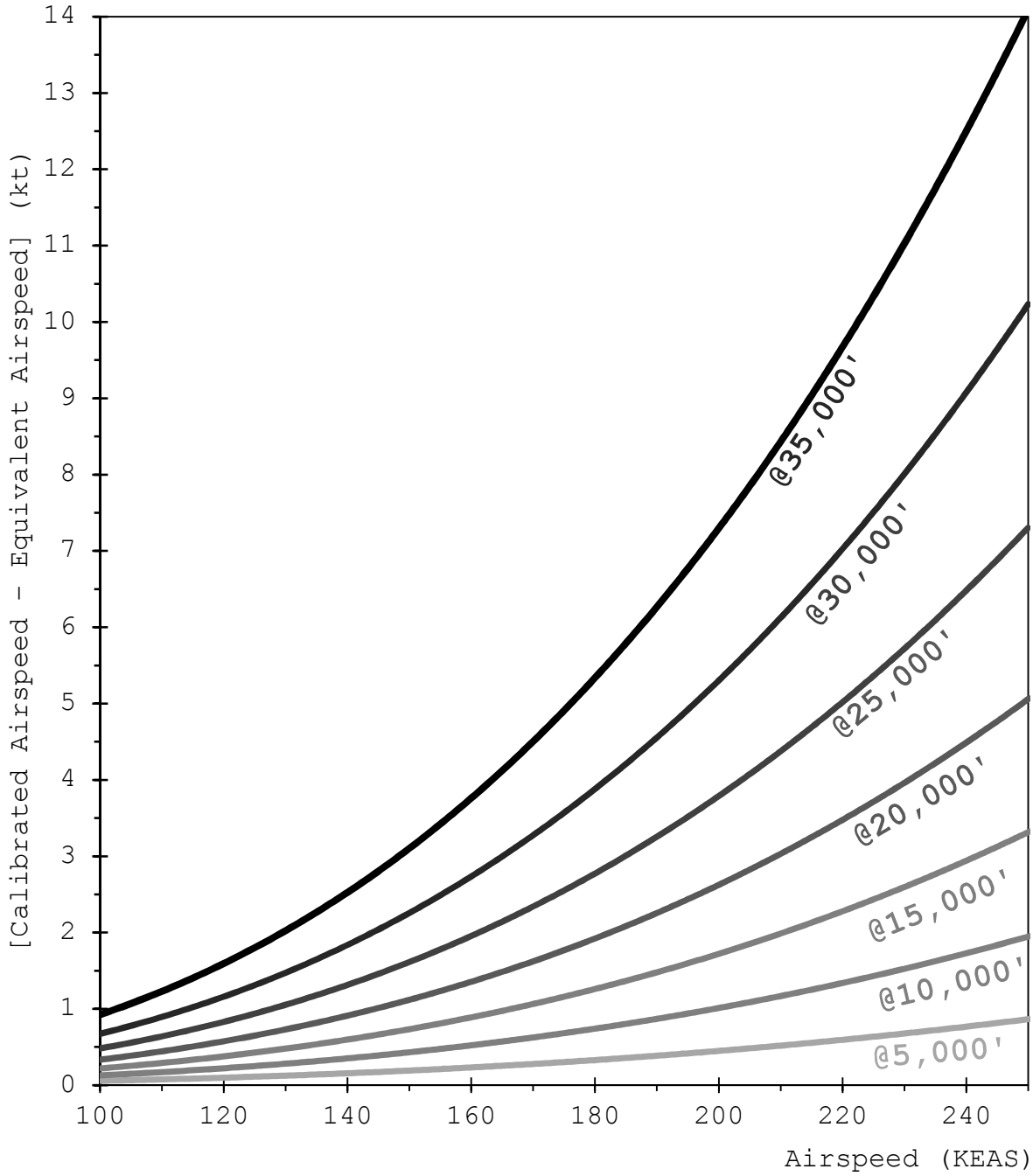

Figure 5-3. Relationship between the difference of calibrated airspeed from equivalent airspeed vs. equivalent airspeed at different pressure altitudes on a standard day.

5.4 Flight Simulation Tests

5.4.1 Testing Facilities

The engines-out glide performance of the A320 is assessed through realistic flight simulations. The flight simulations are conducted in a JAR-FSTD A, Level D full flight simulator that is certified under the European Aviation Safety Agency (EASA) and Joint Aviation Authorities (JAA). The full flight simulator simulates the Airbus A320-232, which is equipped with IAE 2527-A5 engine fit and wing-tip fences as shown in Figure 5-4. Some features of the full flight simulator are listed as follows [102, 103]:

- A full scale, fully enclosed replica of the flight deck including all flight controls, panels and switches,
- Official Airbus flight dynamics model that simulates actual flight conditions including the effect of change in aircraft attitude, sideslip, thrust, drag, altitude, temperature, and gross weight,
- Realistic aircraft mass properties including mass, center of gravity and moments of inertia as a function of payload and fuel loading,
- Aerodynamic programming including ground effect, ground reaction, ground handling characteristics and wind shear models,
- Control feel dynamics that replicate the simulated aircraft,
- A force cueing synergistic platform motion system with six degrees of freedom,
- Characteristic motion vibrations that result from operation of the aircraft,

- Continuous, cross-cockpit, minimum collimated visual field of view providing each pilot with a minimum of 180° horizontal and 40° vertical field of view.

Figure 5-4. Wing-tip fence of the Airbus A320 aircraft [104].

5.4.2 Description of a Typical Simulation Run

Several flight simulation runs are conducted to predict the engines-out glide ratio of the A320 at varying airspeeds and wing configurations. All runs start at an altitude of 5,000 ft. above sea level in standard day conditions and calm weather (i.e. no

wind). The ground is located at sea level in all runs. A typical run has the following steps:

1. The aircraft starts wings-level flight at an altitude of 5,000 ft with both engines running at the given configuration for that run. The aircraft gross weight is frozen at a particular value in each run.
2. Soon after the flight simulation starts, dual-engine failure occurs at 5,000 ft. The aircraft starts losing altitude, and then the dual-engine failure results in complete loss of thrust in both engines.
3. By the time the aircraft reaches 3,200 ft above ground level (AGL), the flight crew stabilizes the calibrated airspeed at the given value for that run.
4. From 3,200 ft AGL on, the aircraft glides at the given constant airspeed until it “crashes”. The position of the rudder is fixed at neutral during the engines-out glide.
5. The simulator plots the descent profile of the aircraft between 3,200 ft. AGL and 200 ft. AGL. The engines-out glide ratio is directly read from the plot.

The schematic representation of a typical run is illustrated in Figure 5-5.

5.5 Wing Configurations

Table 5-1 lists the wing configurations of the A320. Table 5-1 shows that as the wing configuration changes from wing configuration “1” to “FULL”, the flaps and/ or the slats are extended more. Extending the flaps and/ or slats increases the wing area and improves the lift acting on the aircraft. The more the flaps and/ or slats are extended, the lower the stall speed becomes. Thereby, aircraft can stay aloft at lower speeds and safely slow down, for instance prior to landing. However,

extending the flaps and/ or slats increases the total drag acting on the aircraft. Consequently, the overall lift over drag ratio (and thus, the engines-out glide ratio) decreases as the flaps and/ or slats are extended [97].

Table 5-1. Wing configurations of the A320-200 considered in this study [7, 105].

Wing Configuration	Position of the Slats	Position of the Flaps	Typical Use
UP	0°	0°	Cruise/ Climb/ Descent
1	18°	0°	Holding
1+F	18°	10°	Takeoff
2	22°	15°	Takeoff / Approach
3	22°	20°	Takeoff / Approach/ Landing
FULL	27°	40°	Landing

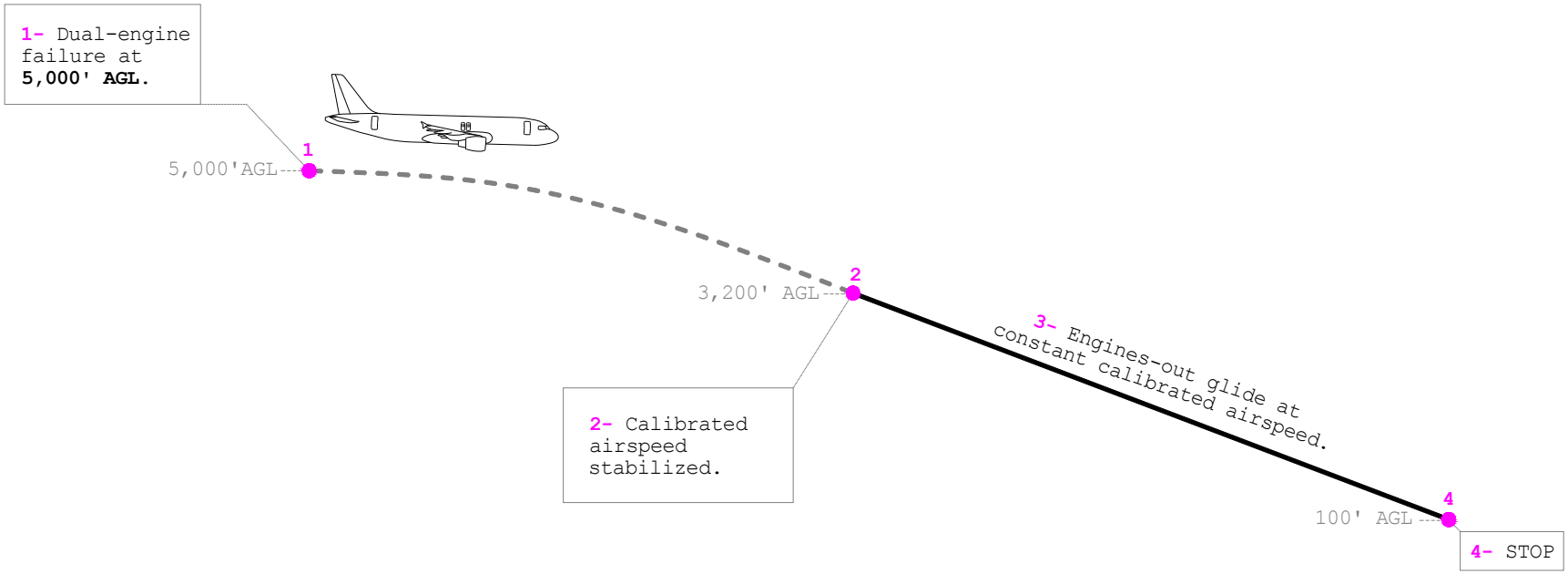

Figure 5-5. Schematic representation of a typical simulation run.

5.6 Results

5.6.1 Typical Takeoff Configurations

The findings from Chapter 4 demonstrate that engine failure due to bird strike is statistically most likely to occur during climb, particularly at low altitudes. Hence, a commercial jet is statistically most likely to undergo bird-strike-induced loss of thrust when it is in takeoff configuration. Therefore, it is essential to explore the post-failure performance of the A320 aircraft in a typical takeoff configuration. As shown in Table 5-1, the A320 aircraft has three possible takeoff configurations that are explained as follows [7, 105]:

1. Wing configuration "1+F", which is preferable when runway length for takeoff roll is not an issue, particularly when obstacle clearance is required. Wing configuration 1+F induces less drag than the other takeoff configurations, and hence, gives a better climb gradient and reduces fuel consumption on takeoff.
2. Wing configuration "2", which is preferable when a compromise between runway length and obstacle clearance is requested.
3. Wing configuration "3", which is preferable on short runways when obstacle clearance is not an issue.

An air carrier survey conducted by the International Civil Aviation Organization (ICAO) found that wing configurations "1+F" and "2" are the most commonly deployed takeoff configurations on the A320 aircraft [106]. In this section, the engines-out glide performance of the A320 aircraft is assessed for wing configuration "1+F". When runway length for takeoff roll is not an issue, wing configuration "1+F" is favorable over

wing configurations "2" and "3" because it induces less drag, which results in better lift-to-drag ratio, improved climb performance and fuel efficiency compared to wing configurations "2" and "3". Wing configurations "2" and "3" are not considered in this section due to budget constraint.

Figure 5-6 illustrates the flight simulation results for the A320 in wing configuration "1+F". The results presented in Figure 5-6 are assessed for an aircraft gross weight of 70.0 tons, which is slightly below the maximum allowable take-off weight of 73.5 tons for this particular aircraft [30]. As shown in Figure 5-6 the steady-state engines-out glide ratio of the Airbus A320 aircraft is assessed at a minimum of five different airspeeds at a given bank angle. Based on the author's observations in the full flight simulator, these airspeeds are briefly explained as follows:

- The highest airspeed for a given wing configuration approximately equals the maximum flap extended speed (V_{FE}). For the Airbus A320, V_{FE} equals 215 KCAS for wing configuration "1+F" [107].
- The lowest airspeed for a given wing configuration approximately equals the lowest selectable airspeed (V_{LS}) for that particular configuration. V_{LS} is defined as the minimum calibrated airspeed to be maintained during landing down to a height of 50 ft above the intended touchdown point. V_{LS} provides an appropriate margin to the stall speed in the given aircraft configuration. For fly-by-wire aircraft like the A320, V_{LS} equals 1.23 times V_{S1g} where V_{S1g} is the airspeed corresponding to the maximum lift coefficient, just before the lift starts decreasing with

increasing angle of attack in a given aircraft configuration [108].

The results plotted in Figure 5-6 are briefly interpreted as follows:

- For a given wing configuration, the relationship between engines-out glide ratio vs. airspeed is approximately represented by a concave-down curve. The engines-out glide ratio reaches its maximum value at or slightly above the airspeed where the minimum total drag occurs for the given setting (see Figure 5-2). As the airspeed deviates from that airspeed, the engines-out glide ratio decreases.
- The best glide ratio is predicted as approximately 14.8 for wing configuration “1+F”. So in the absence of wind, the aircraft is expected to glide a horizontal distance of around 14,700 ft for every 1,000-ft altitude loss in wing configuration “1+F” if it is flown at the best angle of glide speed.
- For a given bank angle, the relationship between engines-out glide ratio versus airspeed is typically represented by a concave downward curve. As mentioned in section 5.3.1, there is an optimum calibrated airspeed which results in the maximum lift-to-drag ratio in a given setting. This airspeed primarily depends on aircraft weight as well as the altitude at which the aircraft is flying [23].

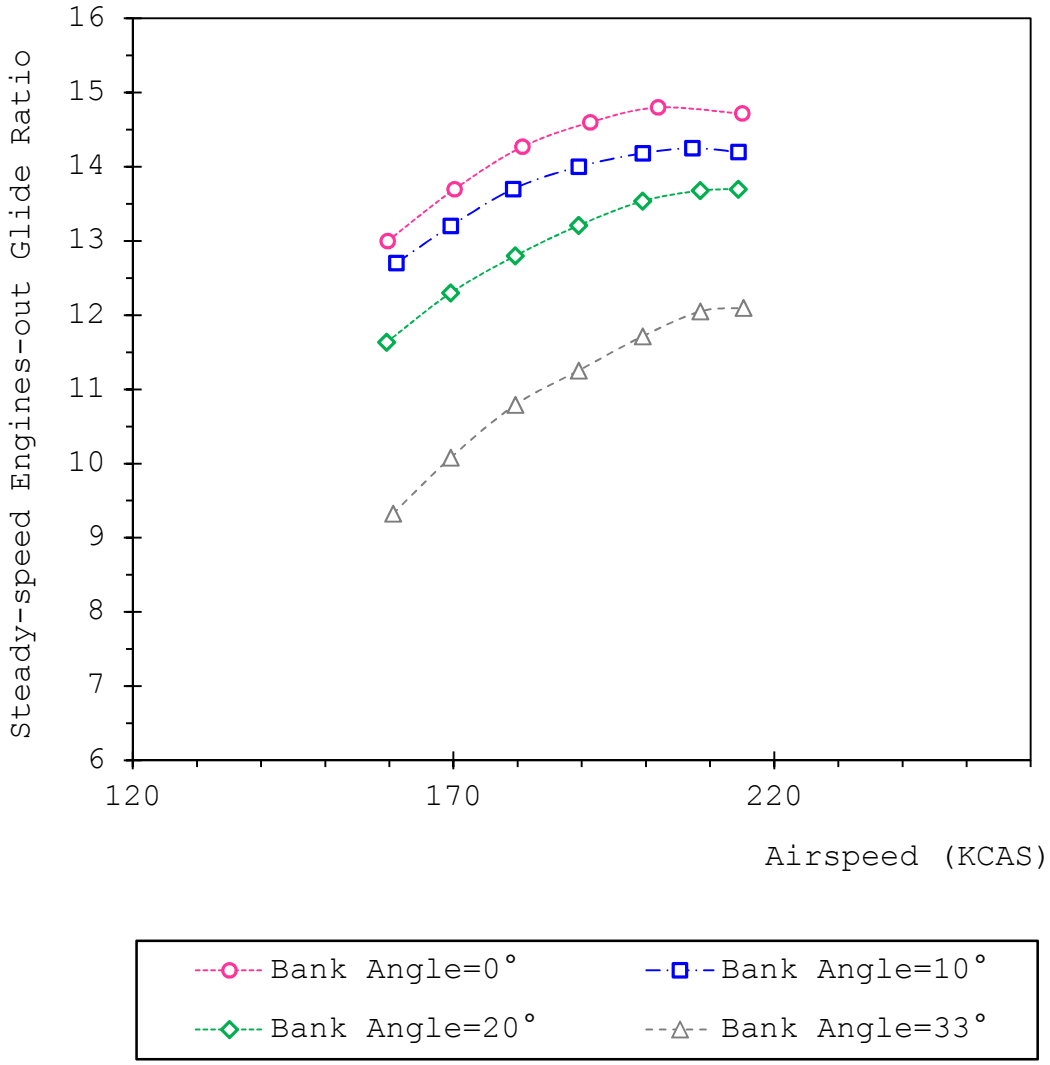

Figure 5-6. Steady-speed engines-out glide ratio vs. airspeed observed in the Airbus A320-200 full flight simulator (wing configuration 1+F, landing gear up, aircraft gross weight=70.0 tons).

5.6.2 "Clean" Configuration

During climb, slat/ flap retraction on the A320 aircraft may start as early as 400 ft AGL [109]. However, slat/ flap retraction can occur at much higher altitudes in case of noise abatement regulations or obstacle clearance requirements. After

slat/ flap retraction, the aircraft typically remains in "clear configuration" until approach to destination airport.

Figure 5-8 illustrates the flight simulation results for the A320 in "clean" configuration. The results shown in Figure 5-8 are assessed for an aircraft gross weight of 70.0 tons, which is slightly below the maximum allowable take-off weight of 73.5 tons for this particular aircraft [30]. As shown in Figure 5-8, the steady-state engines-out glide ratio of the Airbus A320 aircraft is assessed at five different airspeeds in "clean" configuration. These airspeeds are 205, 215, 225, 235, and 245 KCAS. Based on the author's observations in the full flight simulator, these airspeeds are briefly explained as follows:

- The lowest airspeed of 205 KCAS approximately equals the lowest selectable airspeed (V_{LS}) when the aircraft is in clean configuration with a gross weight of 70 tons and is in 33°-bank
- The median airspeed of 225 KCAS approximately equals the "green dot" speed at the given weight of 70.0 tons. For the Airbus A320 aircraft family, the "green dot" speed is the airspeed that corresponds to the maximum engines-out glide ratio in "clean" configuration (i.e. flaps, slats and landing gear are fully retracted). It is represented by a green dot on the primary flight display of the A320 as shown in Figure 5-7. At altitudes below 10,000 ft, the "green dot" speed primarily depends on aircraft weight, and typically ranges from 200 to 235 KCAS for the A320-200 aircraft model [110].
- The highest airspeed of 245 KCAS is slightly lower than the maximum operating speed for landing gear extension, which equals $V_{LO\,EXT} = 250$ KCAS for the A320-200 aircraft [110].

- The other airspeeds of 215 and 235 KCAS are intermediary speeds that are included in analysis to better demonstrate the relationship between the engines-out glide ratio versus airspeed.

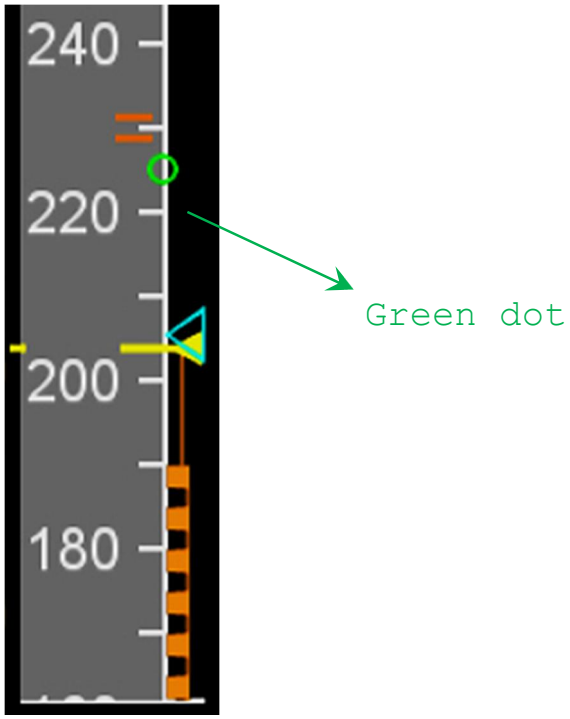

Figure 5-7. "Green dot" speed on the primary flight display of the Airbus A320.

The results plotted in Figure 5-8 are interpreted as follows:

- For wings-level flight (i.e. bank angle=0°), the engines-out glide ratio of the A320-200 increases with increasing airspeed up to the "green dot" speed of 225 KCAS. When the airspeed equals the "green dot" speed, the engines-out glide ratio of the A320 is observed as slightly above 17. In other words, the aircraft is expected to glide a

horizontal distance of slightly greater than 17,000 ft for every 1,000-ft altitude loss at the "green dot" speed in "clean configuration" in the absence of wind. After the "green dot" speed, the observed glide ratio slightly decreases with increasing airspeed.

- For a given airspeed, the engines-out glide ratio decreases with increasing bank (roll) angle. This is because a banked turn results in reduced lift and increased drag acting on the aircraft [23].
- The maximum bank (roll) angle is limited to 33° because bank angle is one of the flight dynamics parameters limited by the Airbus' fly-by-wire system. If the bank angle exceeds 33° with side-stick input from the pilot, the aircraft automatically reduces the bank angle to 33° upon side-stick release in "normal control law". Thus, it is *not* practically possible**** to maintain a constant bank angle greater than 33° on the A320 aircraft when the aircraft is in "normal control law" [111].

The accuracy of the findings presented in Figure 5-6, Figure 5-8, and Figure 5-9 are *not* verified by Airbus Industrie. The results are merely based on the authors' study in the full flight simulator, and will be used to test for the research hypotheses on the A320 aircraft.

**** In the "normal law", the maximum achievable bank angle equals 45° or 67°, depending on the particular flight conditions. In the "normal control law", if the side-stick is not released, the bank angle keeps increasing up to 45° or 67° and then remains constant at this value until the side-stick is released. With the release of the side-stick, the bank angle returns to 33° in the "normal control law". It is also possible to exceed the 33°-bank angle if the aircraft is in "alternate law".

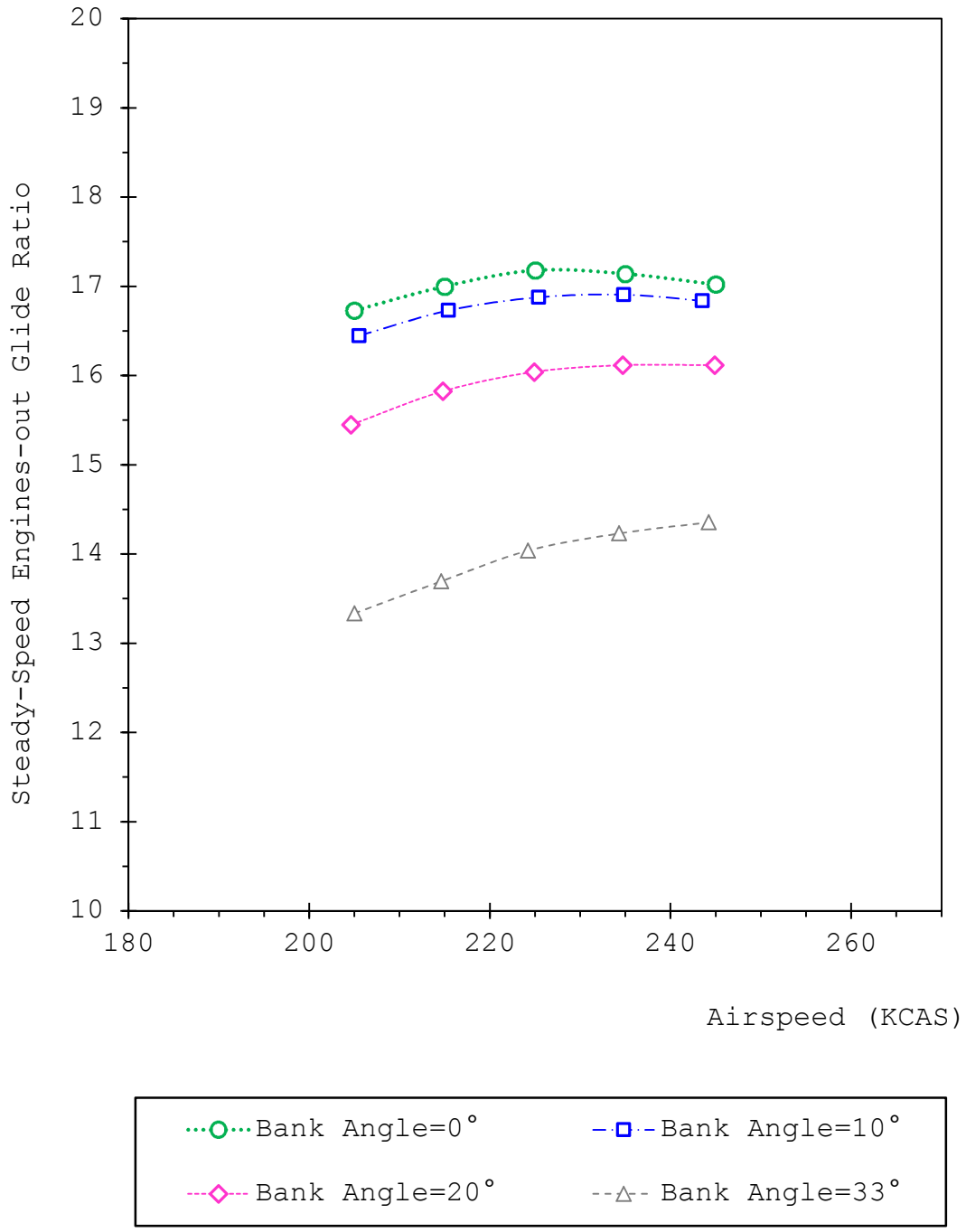

Figure 5-8. Steady-speed engines-out glide ratio vs. airspeed observed in the Airbus A320-200 full flight simulator ("clean" configuration, landing gear up, aircraft gross weight=70.0 tons).

5.6.3 Typical Landing Configurations

Table 5-1 shows that the A320 aircraft has two typical landing configurations [7, 105]:

1. Wing configuration 3, which may be preferable when runway length is not an issue for landing roll.
2. Wing configuration FULL, which induces more drag than wing configuration 3, but may be preferable when there is limited runway length for landing roll.

During final approach to destination airport, either wing configuration is typically deployed as the aircraft follows the glide slope [112]. In this phase of flight, the landing gear is already extended and locked. Since the aircraft follows the glide slope to destination airport, typically no banked turn occurs. Therefore, the engines-out glide performance in wing configurations "3" and "FULL" is assessed for wings-level flight (i.e. 0°-bank angle) with the landing gear fully extended and locked. The results from the flight runs are plotted in Figure 5-9. The aircraft gross weight is frozen at 62.0 tons in each run, which is slightly below the maximum landing weight of 64.5 tons for this particular aircraft [30]. As shown in Figure 5-9, the steady-state engines-out glide ratio of the Airbus A320 aircraft is assessed at a minimum of five different airspeeds in each wing configuration. Based on the author's observations in the full flight simulator, these airspeeds are briefly explained as follows:

- The highest airspeed for a given wing configuration approximately equals the maximum "flap extended speed" (V_{FE}). For the Airbus A320, V_{FE} equals 185 KCAS for wing configuration 3, and 177 KCAS for wing configuration FULL [107].

- The lowest airspeed for a given wing configuration approximately equals the lowest selectable airspeed (V_{LS}) for that particular configuration.

The results presented in Figure 5-9 are predicted for altitudes below 5,000 ft, and are briefly interpreted as follows:

- The best engines-out glide ratio of the A320 is predicted as approximately 10.0 for wing configuration 3 and landing gear down. So in the absence of wind, the aircraft is expected to glide a horizontal distance of around 10,000 ft for every 1,000-ft altitude loss in wing configuration "3" and landing gear down if it is flown at the best angle of glide speed.
- The best engines-out glide ratio of the A320 is predicted as 8.7 for wing configuration FULL and landing gear down. So in the absence of wind, the aircraft is expected to glide a horizontal distance of around 8,700 ft for every 1,000-ft altitude loss in wing configuration "FULL" and landing gear down if it is flown at the best angle of glide speed.
- During final approach to destination runway in normal operating conditions, commercial aircraft typically follows an approximately 3°-glide path, whose gradient equals approximately 19:1 as shown in Figure 5-10 [72]. During this phase of flight, the A320 normally deploys either wing configuration 3 or FULL with the landing gear fully extended and locked [97]. In either configuration, the best engines-out glide ratio of the A320 is well below the typical glide slope for normal operations as shown in Figure 5-10. Therefore, a dual-engine failure on final

approach to destination airport would most likely rule out reaching the destination runway, as in the case of Kegworth Air Disaster [113]. So in such an emergency situation during the final approach, flight crews should promptly find an alternative landing site within the current aircraft heading.

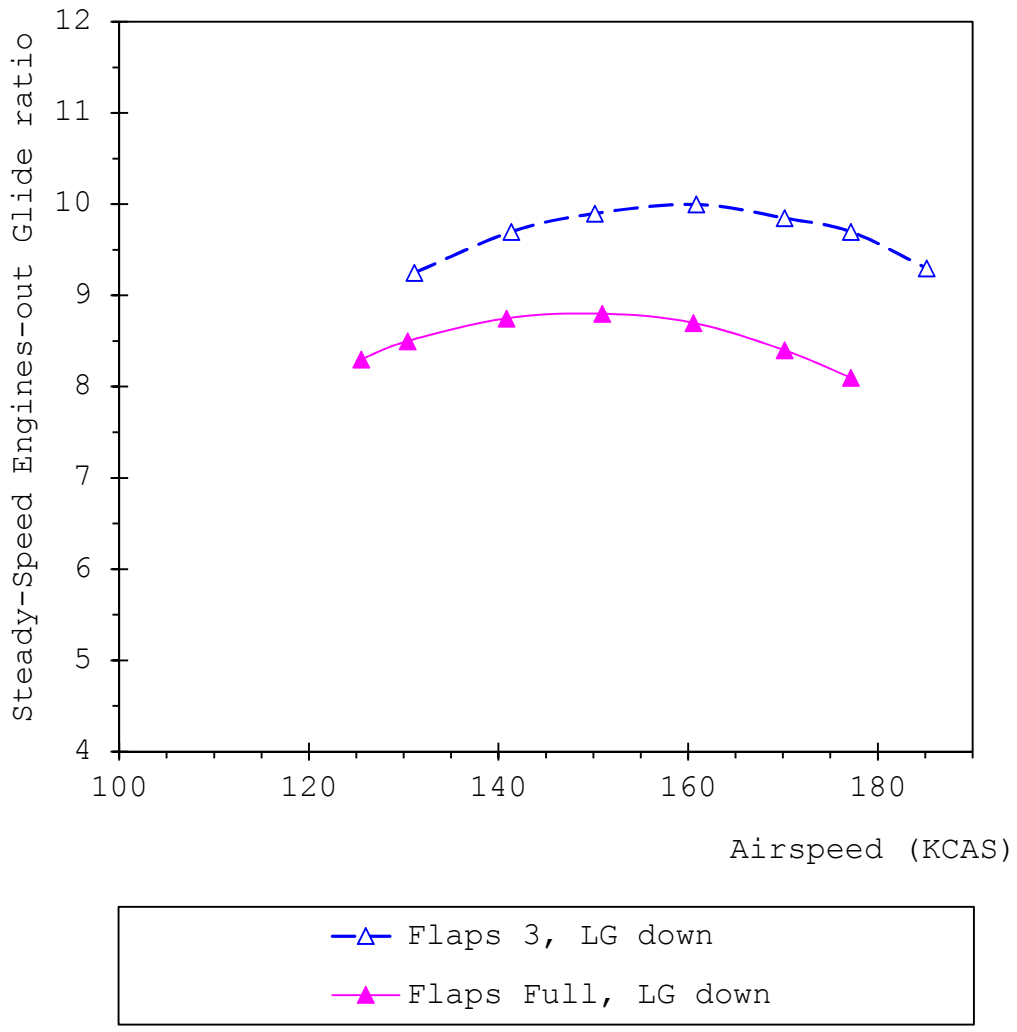

Figure 5-9. Steady-speed engines-out glide ratio vs. airspeed observed in the Airbus A320-200 full flight simulator (aircraft gross weight=62.0 tons).

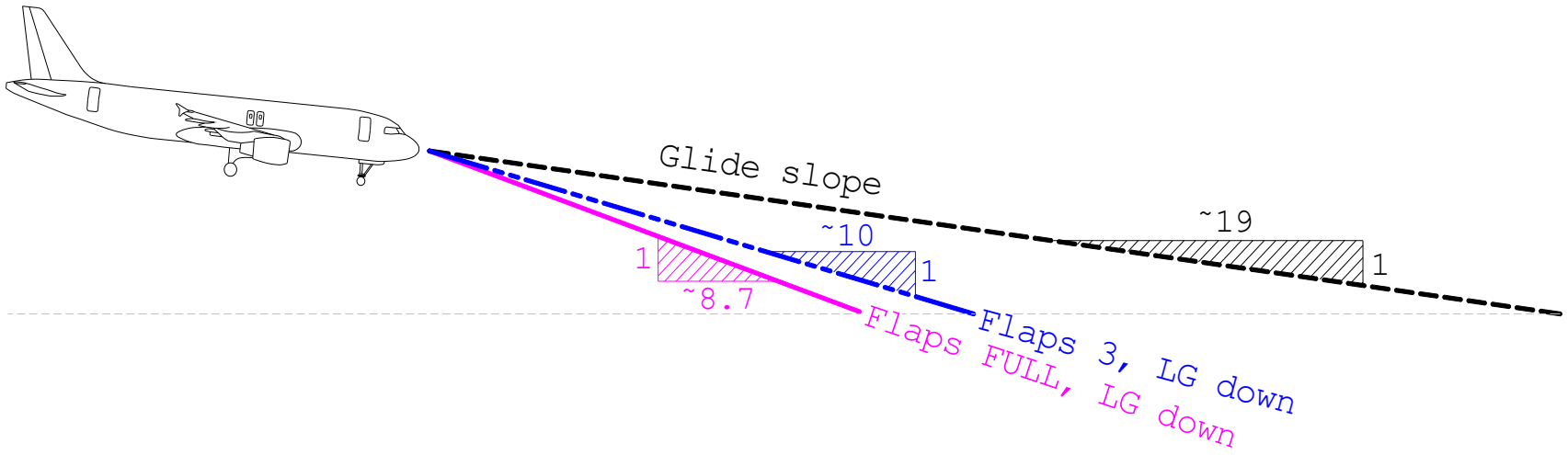

Figure 5-10. Predicted best steady-speed engines-out glide ratio of the A320 for flaps=3 and flaps=FULL vs. typical glide slope on final approach to destination runway *(LG=Landing gear)*.

5.6.4 Effect of Aircraft Weight on Engines-out Glide Ratio

The results presented in Figure 5-6 and Figure 5-7 are assessed for a 72.0-ton A320 aircraft. Likewise, the results presented in Figure 5-9 are assessed for a 62.0-ton A320 aircraft. If the aircraft gross weight differs from the test weights, the best possible glide ratio in a given configuration does not change. However, the calibrated airspeed at which the best engines-out glide ratio occurs changes. This airspeed can be estimated from Equation (5-4) as follows [56]:

$$v' = v * \sqrt{\frac{W'}{W}} \tag{5-4}$$

where

- W= Test weight of the aircraft.
- W'= Gross weight of the aircraft in question (tons).
- v= Calibrated airspeed corresponding to a given steady-state engines-out glide ratio found from Figure 5-6, Figure 5-8 or Figure 5-9.
- v'= Calibrated airspeed of the aircraft that weighs W'. If the aircraft in question maintains v', it achieves the same steady-state engines-out glide ratio as the one achieved by the 62.0-ton aircraft at v.

For example, in this study, the "green dot" speed is predicted as approximately 210 KCAS for the 62.0-ton A320 for altitudes below 5,000 ft. If the A320 weighs 70.0 tons, the best estimate for the "green dot" speed for altitudes below 5,000 ft would be $210 * \sqrt{70/62} \approx 224$ KCAS based on the results from this study.

It should be noted that the official flight crew operating manual (FCOM) for the A320 presents a different and simplified method for estimating the "green dot" speed. Using that method, the "green dot" speed for the 70-ton A320 would be predicted as 225 KCAS for altitudes below 5,000 ft. Since Airbus Industrie does not allow the use of the FCOM as a reference, details regarding that method are not given in this study.

5.7 Summary

This chapter assessed the post-failure flight performance of the Airbus A320 aircraft in the occurrence of total loss of thrust. Flight simulation tests are conducted in an A320 full flight simulator to predict the relationship between engines-out glide ratio versus airspeed at different wing configurations and bank angles. The findings are merely based on the author's observations in the full flight simulator. The accuracy of the findings are not verified by Airbus Industrie. Thus, the findings are not intended for real flight purposes. The findings will be used to test for the research hypotheses on the Airbus A320 aircraft.

CHAPTER 6 - ENGINES-OUT FLIGHT PERFORMANCE OF THE BOEING 737NG

6.1 About the Boeing 737NG Aircraft Family

As of 2014, the Boeing 737NG is the leading aircraft family in terms of the number of passengers transported on all US carriers [13]. Unlike the Airbus A320 aircraft family, the Boeing 737NG aircraft is not fly-by-wire. The variants of the 737NG aircraft family include the 737-600, 737-700, 737-800, and 737-900 aircraft models [114]. The 737-600 variant made its first flight in 1999 [115], and is the smallest model of the 737NG family [116]. As of 2014, the 737-600 does not exist in the U.S. commercial fleet [13]. The 737-700 variant is the second smallest model of the 737NG family, and can accommodate up to 149 passengers [28]. The 737-800 variant is a stretched version of the 737-700, and can accommodate up to 189 passengers. Both the 737-700 and 737-800 variants made their first flights in 1997. The longest variant of the 737NG family is the 737-900ER. It made its first flight in 2005 [115], and can accommodate up to 220 passengers [117].

Table 6-1 shows the total number of orders and deliveries through January 2015 for each variant of the 737NG aircraft family. As shown in Table 6-1, the 737-800 is the best-selling variant of the 737NG aircraft family. It also competes directly with the Airbus A320-200 aircraft, which received 7,577 orders through January 2015 with 3,867 of them delivered [26]. Therefore, the Boeing 737-800 is the second commercial jet considered in this dissertation.

Table 6-1. The orders and deliveries for the Boeing 737NG aircraft family through January 2015 [118].

Aircraft Model	Total Orders (through January 2015)	Total Deliveries (through January 2015)
Boeing 737-600	69	69
Boeing 737-700/700C/700W	1,238	1,140
Boeing 737-800/800A/800W	4,844	3,556
Boeing 737-900/900ER	560	345

6.2 Flight Simulation Tests

6.2.1 Testing Facilities

The engines-out glide performance of the Boeing 737-800 aircraft is assessed through realistic flight simulations. The flight simulations are conducted in a JAR-FSTD A, Level D full flight simulator that is certified under the European Aviation Safety Agency (EASA) and Joint Aviation Authorities (JAA). The full flight simulator simulates the Boeing 737-800W, which is equipped with CFM56-7B engine fit and blended winglets as shown in Figure 6-1. The full flight simulator has the same features outlined in section 5.4.1. In order to assess the steady-speed engines-out glide ratio of the Boeing 737-800 aircraft at different airspeeds and bank angles, the same simulation methodology outlined in section 5.4.2 is followed.

6.2.2 Flap Settings

Table 6-2 lists the most commonly deployed flap settings of the 737-800. In addition to the flap settings given in Table 6-2, the 737-800 has other flap settings called “1”, “2”, and “25”. While some air carriers may allow the use of flap setting

"1" for takeoff, wing configurations "2" and "25" are not deployed in typical takeoff and approach profiles [119, 120].

Figure 6-1. Blended winglet of the Boeing 737-800 aircraft [121].

Table 6-2 shows that as the flap setting changes from "5" to "40", the flaps and/ or the slats are extended more, which results in increased wing area, increased lift, and increased drag. The overall lift over drag ratio (and thus, the engines-out glide ratio) decreases as the flaps and/ or slats are extended [97].

Table 6-2. Flap settings of the Boeing 737-800 [119, 120].

Flap setting	Position of the Slats	Position of the leading edge Flaps	Position of the trailing edge flaps	Typical Use
UP	UP	UP	UP	Cruise/ Climb/ Descent
5	Extend	Full extended	5	Takeoff/ Approach
10	Extend	Full extended	10	Takeoff
15	Full extended	Full extended	15	Takeoff/ Approach*
30	Full extended	Full extended	30	Approach/ Landing
40	Full extended	Full extended	40	Approach/ Landing

6.3 Results

6.3.1 Typical Takeoff Configurations

As shown in Table 6-2, there are three widely-used takeoff configurations on the 737-800. These takeoff configurations involve flap settings "5", "10", and 15 [120], and are briefly explained as follows:

1. Flap setting "5", which may be preferable on long runways, particularly when a better climb gradient is preferred.
2. Flap setting "10", which may be preferable when a compromise between runway length and climb gradient is requested.
3. Flap setting "15", which is preferable on short runways when obstacle clearance is not an issue.

In addition to these flap settings, some air carriers may allow the use flap setting "1" for takeoff. An air carrier

* Flap setting 15 may also be used in landing during single-engine operations.

survey conducted by ICAO found that flap settings "5", "1" and "15" are the most commonly deployed takeoff configurations on the 737-800 aircraft [106]. In this study, flap setting "5" is considered because it is favorable over flap settings "10" and "15" in terms of climb gradient and fuel efficiency [120]. Flap Settings "1", "10" and "15" are not considered in this study due to budget constraints.

To assess the engines-out glide performance of the Boeing 737-800 in flap setting "5", the flight simulation methodology outlines in section 5.4 is followed. The results from the flight simulation tests are plotted in Figure 6-2 for an aircraft gross weight of 70.0 tons, which is below the maximum allowable take-off weight of 79.0 tons for this particular aircraft [29]. As shown in Figure 6-2, the steady-state engines-out glide ratio of the 737-800 aircraft is assessed at a minimum of five different airspeeds at a given bank angle. Based on the author's observations in the full flight simulator, these airspeeds are briefly explained as follows:

- The highest airspeed approximately equals the "flap placard speed" for that wing configuration (V_{FE}). In order to prevent structural damage to the flaps, flap placard speed is not allowed to be exceeded in a given wing configuration. The flap placard speeds on the 737 aircraft are analogous to the maximum flap extended speeds on the A320 aircraft. On the Boeing 737NG, these speeds are called "flap placard speeds" because they are written on a placard near the landing gear lever in the cockpit [122]. The flap placard speed equals 250 KCAS for flap setting "5.
- The lowest airspeed is slightly greater than the "minimum maneuver airspeed" (i.e. V_{LS}) for that particular configuration. For the 737-800, which is not a fly-by-wire

aircraft, the minimum maneuver speed equals 1.30 times V_{s1g} and provides adequate maneuver margin to stick shaker (i.e. stall warning). In other words, the minimum maneuver speed enables the 737-800 aircraft to perform banked turns at up to 40°-bank angles without stalling [122].

A brief interpretation of the results plotted in Figure 6-2 is given as follows:

- For a given bank angle, the relationship between the engines-out glide ratio versus airspeed typically displays a concave-downward pattern, as mentioned in section 5.3.1. There is an optimum calibrated airspeed that results in the maximum engines-out glide ratio in a given setting, and that optimum calibrated airspeed primarily depends on aircraft weight as well as the altitude at which the aircraft is flying.
- For flap setting “5”, the best engines-out glide ratio is predicted as approximately 16. So in the absence of wind, the aircraft is expected to glide a horizontal distance of around 16,000 ft for every 1,000-ft altitude loss in flap setting “5” if it is flown at the best angle of glide speed.

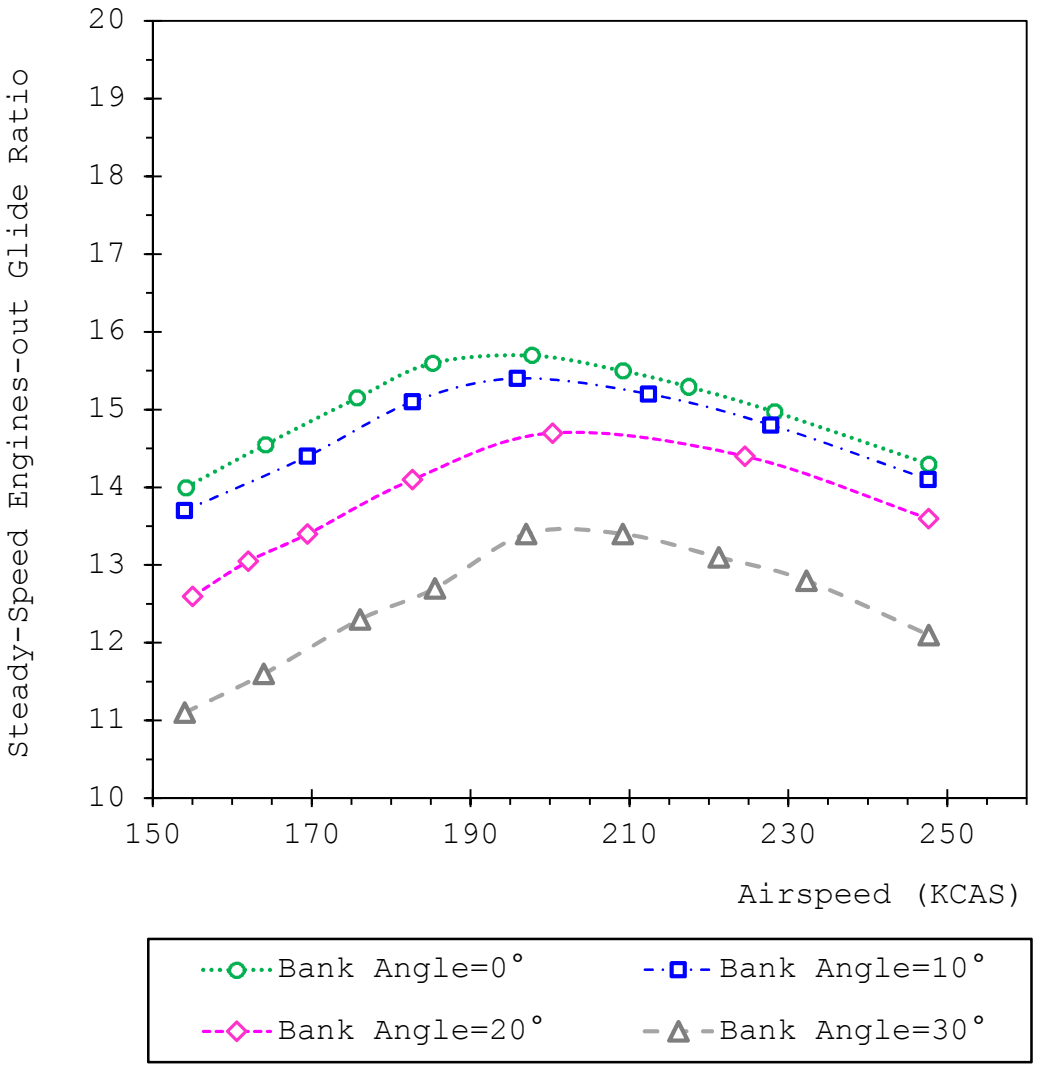

Figure 6-2. Steady-speed engines-out glide ratio vs. airspeed observed in the Boeing 737-800 full flight simulator (flaps=5, landing gear "up", aircraft gross weight=70.0 tons).

6.3.2 "Clean" Configuration

Generally, flap retraction on the Boeing 737-800 does not begin below 1,000 ft AGL during the climb-out phase. A noise climb-out procedure requires that flap retraction begins at 1,000 ft AGL for far-out noise monitors, and at 3,000 ft AGL for close-in noise monitors [120]. Following flaps retraction, the

aircraft typically remains in “clear configuration” until approach to destination airport.

Figure 6-3 illustrates the flight simulation results for the 737-800 in “clean” configuration. The results shown in Figure 6-3 are assessed for an aircraft gross weight of 70.0 tons, which is below the maximum allowable take-off weight of 79.0 tons for this particular aircraft [29]. As shown in Figure 6-3, the steady-state engines-out glide ratio of the Boeing 737-800 aircraft is assessed at a minimum of five different airspeeds for a given bank angle. The upper and lower bound of these airspeeds are briefly explained as follows:

- The lowest airspeed approximately equals the minimum maneuver speed in this particular configuration. The minimum maneuver speed is illustrated by the top of an amber bar in the speed tape of the 737-800.
- The highest airspeed of 250 KCAS equals the maximum allowable airspeed below 10,000 ft mean sea level (MSL), unless otherwise is authorized by an air traffic controller [123].

The results plotted in Figure 6-3 are interpreted as follows:

- For wings-level flight (i.e. bank angle=0°), the steady-speed engines-out glide ratio of the 737-800 increases with increasing airspeed up to the best angle-of-glide speed in the given configuration. At this airspeed, the best engines-out glide ratio of the 737-800 is observed as slightly above 18.5. In other words, the aircraft is expected to glide a horizontal distance of slightly greater than 18,500 ft for every 1,000-ft altitude loss at the best angle-of-glide speed. The calibrated airspeed that results

in the best angle-of-glide varies with aircraft gross weight and altitude. In this particular configuration, the best angle-of-glide speed is predicted as approximately 205 to 210 KCAS based on the study in the full flight simulator.

- For a given airspeed, the steady-speed engines-out glide ratio decreases with increasing bank (roll) angle. This is because a banked turn results in reduced lift and increased drag acting on the aircraft [23].
- The maximum bank angle is limited to 30° because Boeing does not recommend using bank angles exceeding 30° in any normal or non-normal conditions [124].

The accuracy of the findings presented in Figure 6-2, Figure 6-3, and Figure 6-4 are not verified by the Boeing Company. The results are merely based on the authors' study in the full flight simulator, and will be used to test for the research hypotheses on the Boeing 737-800 aircraft.

6.3.3 Typical Landing Configurations

Table 6-2 shows that the 737-800 aircraft has two typical landing configurations:

1. Flap setting "30", which may be preferable when runway length is not an issue for landing roll.
2. Flap setting "40", which induces more drag than flap setting 30, but may be preferable when there is limited runway length for landing roll.

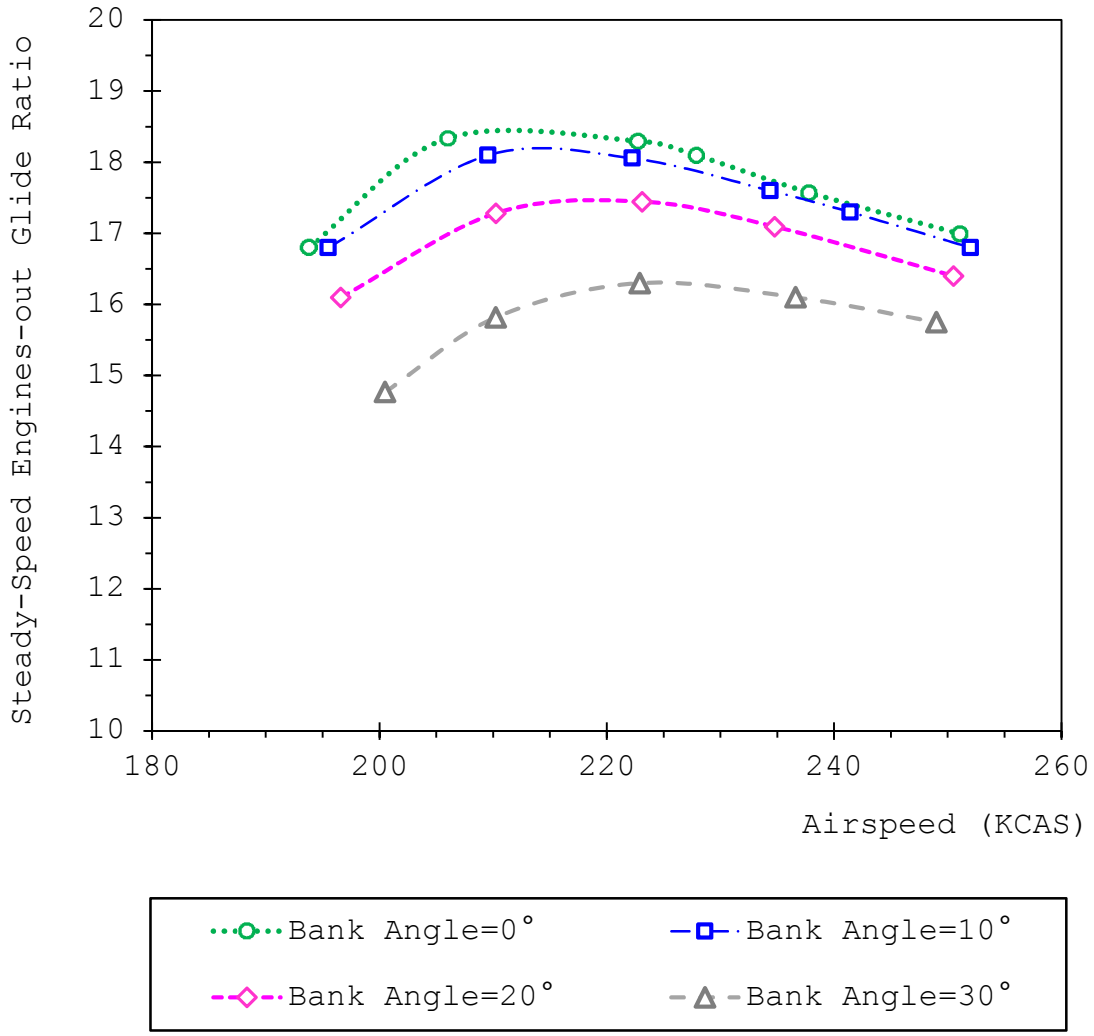

Figure 6-3. Steady-speed engines-out glide ratio vs. airspeed observed in the Boeing 737-800 full flight simulator ("clean" configuration, landing gear up, aircraft gross weight=70.0 tons).

During approach to destination airport, the 737-800 typically intercepts the glide slope at flap setting 15, and the landing gear is lowered. Following this, either flap setting is typically deployed with the landing gear fully extended and locked as the aircraft follows the glide slope [119]. Since the aircraft follows the glide slope to destination airport,

typically no banked turn occurs. Therefore, the engines-out glide performance in flap settings "30" and "40" is assessed for wings-level flight (i.e. 0°-bank angle) with the landing gear fully extended and locked. The results from the flight simulation runs are plotted in Figure 6-4. The aircraft gross weight is frozen at 60.0 tons in each run, which is below the maximum landing weight of 66.3 tons for this particular aircraft [125]. As shown in Figure 6-4, the steady-state engines-out glide ratio of the Boeing 737-800 aircraft is assessed at a minimum of five different airspeeds at a given bank angle. Based on the author's observations in the full flight simulator, these airspeeds are briefly explained as follows:

- The highest airspeed for a given flap setting approximately equals the flap placard speed for that flap setting (V_{FE}). For the 737-800, V_{FE} equals 175 KCAS for flap setting "30", and 162 KCAS for flap setting "40".
- The lowest airspeed for a given flap setting approximately equals the lowest maneuver speed for that particular configuration, which is represented by the top of an amber strip on the speed tape of the primary flight display.

The results presented in Figure 6-4 are predicted for altitudes below 5,000 ft, and are briefly interpreted as follows:

- The best engines-out glide ratio of the 737-800 is predicted as approximately 9.0 for flap setting "30" and landing gear down. So in the absence of wind, the aircraft is expected to glide a horizontal distance of around 9,000 ft for every 1,000-ft altitude loss in flap setting "30" and landing gear down if it is flown at the best angle of glide speed.

- The best engines-out glide ratio of the 737-800 is predicted as approximately 7.0 for flap setting "40" and landing gear down. So in the absence of wind, the aircraft is expected to glide a horizontal distance of around 7,000 ft for every 1,000-ft altitude loss in flap setting "40" and landing gear down if it is flown at the best angle of glide speed.
- In either configuration, the best engines-out glide ratio of the 737-800 is well below the typical glide slope of 19:1 for normal operations [72]. Therefore, in the occurrence of a dual-engine failure on final approach to destination airport, flight crews should promptly find an alternative landing site within the current aircraft heading

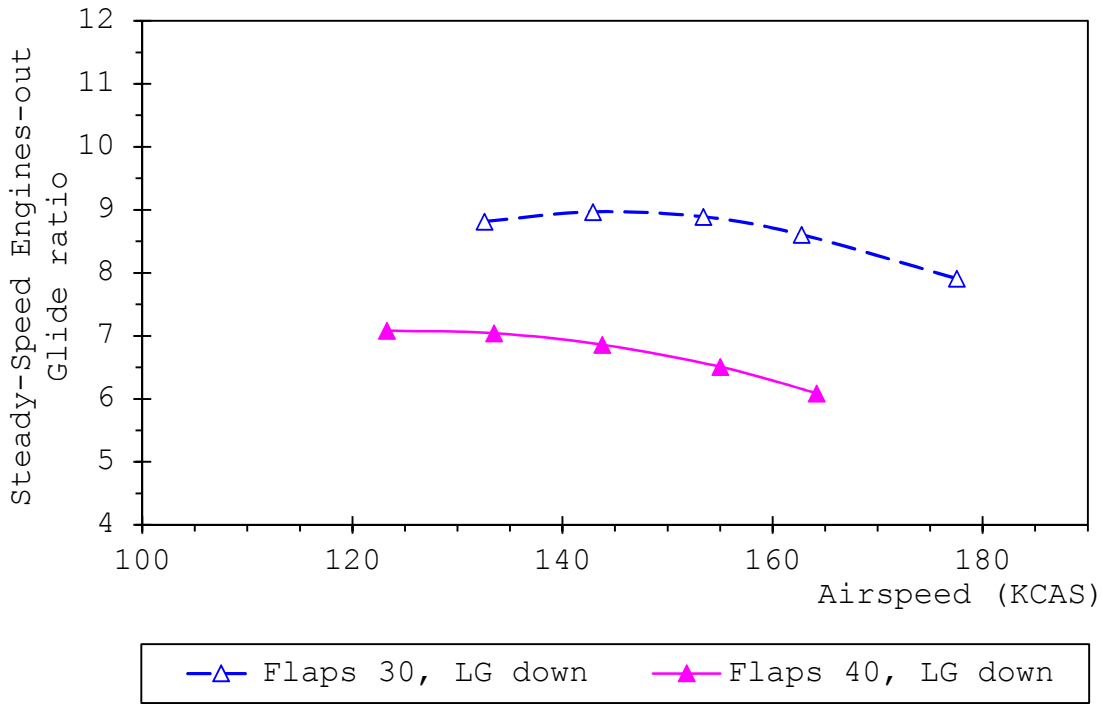

Figure 6-4. Steady-speed engines-out glide ratio vs. airspeed observed in the Boeing 737-800 full flight simulator (aircraft gross weight=60.0 tons).

6.4 Comparison with the Engines-out Glide Performance of the Airbus A320

This section briefly compares the engines-out glide performance of the 737-800 aircraft with that of the A320 aircraft. In this study, the engines-out glide ratio of the Airbus A320 aircraft is assessed for wing configurations "clean", 1+F, "3" and "FULL" whereas the engines-out glide ratio of the Boeing 737-800 aircraft is assessed for flap settings "clean", "5", "30" and "40". Each wing configuration is associated with a specific flaps/ slats position, which is listed in Table 5-1 for the A320 aircraft, and in Table 6-2 for the 737-800 aircraft. Different flaps/ slats positions lead to different lift and drag characteristics for a given aircraft. Therefore, a relevant comparison in terms engines-out glide performance can only be made between the two aircraft on condition that both aircraft are configured with the same flaps/ slats position. Table 5-1 and Table 6-2 show that the flaps/ slats are fully retracted in "clean" configuration on both the A320 and 737-800 aircraft. Besides the "clean" configuration, there is no other "common" wing configuration that leads to exactly the same flaps/ slats position on both aircraft. Thus, the A320 and 737-800 aircraft are compared in terms of engines-out glide performance in only "clean" configuration.

Figure 5-8 and Figure 6-3 illustrate the predicted relationship between engines-out glide ratio versus airspeed for the A320 and 737-800 aircraft, respectively, in "clean" configuration. The results shown in Figure 5-8 and Figure 6-3 are valid for an aircraft gross weight of 70.0 tons and for flight levels below 5000 ft AMSL. Table 6-3 summarizes the

results illustrated in Figure 5-8 and Figure 6-3. The results summarized in Table 6-3 show that:

- The best engines-out glide ratio is predicted as 17.1 for the A320 aircraft equipped with wing-tip fences, and 18.5 for the 737-800 aircraft equipped with blended winglets. Hence, the best engines-out glide ratio of the 737-800 aircraft equipped with blended winglets is found to be approximately nine percent greater than that of the A320 aircraft equipped with wing-tip fences.
- When the aircraft gross weight equals 70.0 tons, the best-angle-of-glide speed is predicted as approximately 225 KCAS for the A320 aircraft equipped with wing-tip fences, and around 205-210 KCAS for the 737-800 aircraft equipped with blended winglets. So at a given aircraft gross weight, the best-angle-of-glide speed of the 737-800 aircraft with blended winglets is less than that of the A320 aircraft with wing-tip fences.

Table 6-3. Summary of the predicted engines-out glide performance of the A320 and 737-800 aircraft in "clean" configuration and wings-level flight.

Aircraft	Aircraft Gross weight(tons)	Predicted Best Engines-out Glide Ratio	Predicted Best-Angle-of-Glide Speed* (KCAS)
Airbus A320-200 with wing-tip fences	70.0	17.1	225†
Boeing 737-800 with blended winglets	70.0	18.6	≈ 205 to 210

* Below 5,000 ft AMSL.

† "Green dot" speed in this particular configuration.

Figure 6-5 illustrates a photo of the wing-tip fence of the Airbus A320 and blended winglet of the 737-800. Both wing-tip devices shown in Figure 6-5 are intended to reduce the induced drag acting on the aircraft [99]. However, a blended winglet would generally be more effective in reducing the induced drag than a wing-tip fence. Because of this, Airbus Industrie has recently modified the wing-tip design of the A320 aircraft family. The new generation Airbus A320 aircraft family is also equipped with blended winglets similar to the one shown in Figure 6-5b, which Airbus Industrie named as "sharklets" [126].

(a) **(b)**

Figure 6-5. A photo of the (a) wing-tip fence of the Airbus A320 aircraft [104], (b) blended winglet of the Boeing 737-800 aircraft [121].

The relative effect of blended winglets on engines-out glide performance can be exemplified in Figure 6-6, which compares the magnitude of induced drag in deployment of wing-tip fences versus blended winglets for a given aircraft body. As

shown in Figure 6-6, the deployment of blended winglets would lower the induced drag compared to the deployment of wing-tip fences. The resultant reduction in induced drag would also lead to a reduction in total drag, which would in turn increase the best lift-to-drag ratio (and thus, the best engines-out glide ratio) for the given aircraft body. Moreover, Figure 6-6 also shows that the deployment of blended winglets would lower the airspeed at which minimum total drag occurs compared to the deployment of wing-tip fences. Since the airspeed at the best lift-to-drag ratio occurs at or slightly above the airspeed at minimum total drag, the deployment of blended winglets would reduce the airspeed that gives the best engines-out glide ratio compared to the deployment of wing-tip fences. The example illustrated in Figure 6-6 can in part explain why the 737-800 aircraft equipped with blended winglets has greater engines-out glide ratio and lower best-angle-of-glide speed compared to the A320 aircraft equipped with wing-tip fences at the same gross weight.

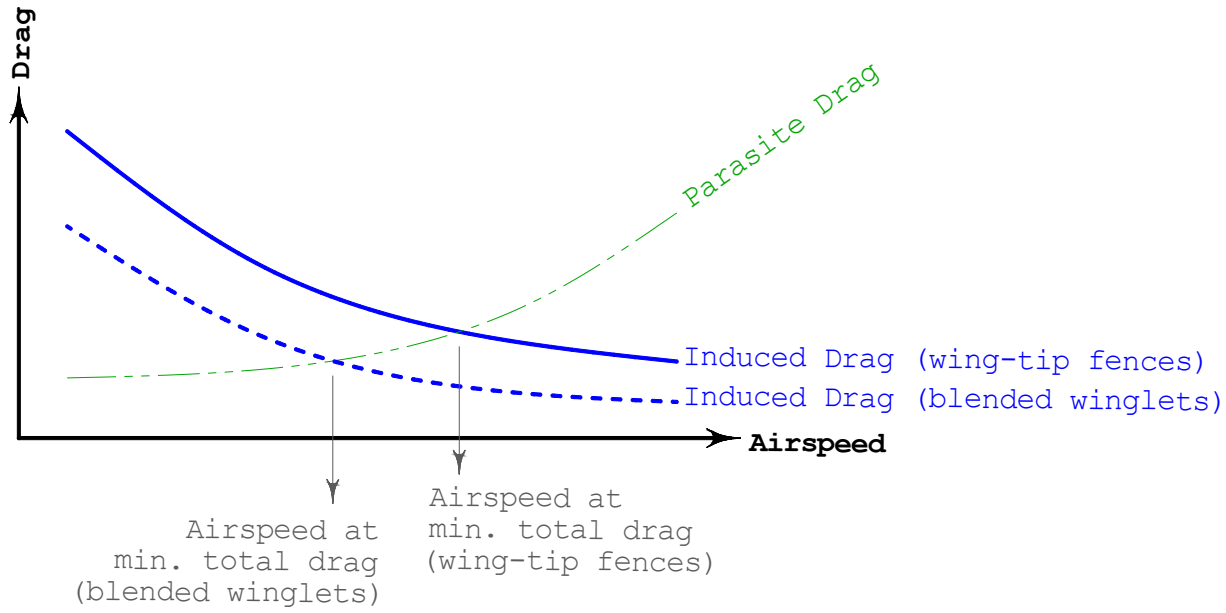

Figure 6-6. Graphical representation of induced drag in deployment of wing-tip fences versus blended winglets.

6.5 Summary

This chapter assessed the post-failure flight performance of the Boeing 737-800 aircraft in the occurrence of total loss of thrust. Flight simulation tests are conducted in a Boeing 737-800 full flight simulator to predict the relationship between engines-out glide ratio versus airspeed at different wing configurations and bank angles. The findings show that the engines-out glide ratio of the 737-800 aircraft equipped with blended winglets is predicted to be as high as 18.5, which is approximately nine percent greater than the predicted best engines-out glide ratio of the A320 aircraft equipped with wing-tip fences.

The findings presented in this chapter are merely based on the author's observations in the full flight simulator. The accuracy of the findings are not verified by the Boeing Company.

Thus, the findings are not intended for real flight purposes. The findings will be used to test for the research hypotheses on the Boeing 737-800.

CHAPTER 7 - KINEMATIC APPROACH TO TRAJECTORY OPTIMIZATION IN TOTAL LOSS OF THRUST

7.1 Research Question

The findings in Chapter 4 show that engine failure due to bird strike is most likely to occur at a low altitude below 5,000 ft. above ground level (AGL), which in turn gives flight crews limited time to avoid crash. Despite this, current airline pilot training programs do not require simulated total loss of thrust at a low altitude [19, 20]. Likewise, modern-day commercial jets do not have a checklist specifically designed for total loss of thrust at a low altitude [7]. In order to mitigate the effects of total loss of thrust at a low altitude, it is essential to explore the idea of landing trajectory optimization for commercial aircraft in the total-loss-of-thrust emergency. A number of studies [43, 44, 45, 46, 47, 48, 49, 50, 51] addressed engines-out landing trajectory optimization for general aviation aircraft and fighter jets, but *not* for commercial jets. This is primarily because conventional trajectory optimization methods require aircraft-specific aerodynamic-coefficient[‡] data for the aircraft in question, which is not released by commercial aircraft manufacturers. Assessment of aircraft-specific aerodynamic-coefficient data may be achieved in full flight simulators, but would require several hours of flight simulation tests, which would render it costly and impractical. Due to the lack of aerodynamic-coefficient data, the aerodynamic forces acting on a commercial jet cannot be accurately computed. Therefore, the idea of engines-out

[‡] For example, the lift coefficient vs. angle of attack, the drag polar, etc.

trajectory optimization has not addressed commercial jets in detail.

To fill in this gap in the literature, the objective of this chapter is to develop a kinematic method that can rapidly perform trajectory optimization in the event of total loss of thrust. Contrary to kinetic methods, a kinematic approach deals with pure motion characteristics without making reference to the aerodynamic forces involved. Hence, a kinematic approach does not require aircraft-specific aerodynamic-coefficient data. Thereby, the kinematic method will be readily applicable to commercial jets.

7.2 Significance of the Research

The kinematic method is to be employed in the architectural design of the adaptive flight planner designed for the total-loss of-thrust emergency. The findings can also enable aviation practitioners to identify safe landing maneuvers in possible total-loss-of-thrust emergencies for commercial jets. Hence, the findings can be utilized in a variety of fields such as airliner type-rating programs, design of airport environments and evaluation of aircraft-airport compatibility.

7.3 Characteristics of the Optimum Trajectory

7.3.1 Practical Feasibility

To be of practical value, the optimum landing trajectory should:

- *Not* require non-trivial and complex changes in flight path angle and bank (roll) angle [44],
- Be simple enough to follow in an emergency situation [127],

- Be compressible to standard and simple pilot and ATC (air traffic control) commands [44].

Therefore, the optimization algorithm will be formulated allowing for the following:

1. The optimum landing trajectory will be defined assuming a constant calibrated airspeed. This is because airspeed is directly related to flight path angle [23], and it would be significantly more practical and intuitive for flight crews to maintain a given airspeed rather than following a set of complex pitch attitude directives.
2. The optimum landing trajectory will not require more than three banked turns. Otherwise, too many changes in bank (roll) angle may not be practical to follow in an emergency situation.

7.3.2 Segmented Structure

In the kinematic approach, the engines-out landing trajectory is divided into three types of segments based on bank (roll) angle state as follows:

1. Linear segments, where bank angle equals 0° and wings-level flight is performed,
2. Transition segments, where bank angle changes linearly from 0° up to ϕ_{max} and vice versa,
3. Circular segments, where bank angle retains a constant positive value of $\leq \phi_{max}$.

The presumed landing trajectory consists of four linear segments (L) interconnected with three circular segments (C). Each linear segment represents wings-level, equilibrium glide whereas each circular segment represents a turning maneuver at constant bank angle. There is also one transition segment (T)

directly before and after each circular segment to simulate continuous change in bank angle. Hence, the presumed landing trajectory is a sequence of waypoints connected by segments of constant-trim states[§] as follows:

$$L_1 \rightarrow T_{1,1} \rightarrow C_1 \rightarrow T_{1,2} \rightarrow L_2 \rightarrow T_{2,2} \rightarrow C_2 \rightarrow T_{2,3} \rightarrow L_3 \rightarrow T_{3,3} \rightarrow C_3 \rightarrow T_{3,4} \rightarrow L_4$$

In the event of total loss of thrust, rapid computation of a flyable landing trajectory is required. Thus, overly complicated formulation of the optimum trajectory should be avoided. A segmented trajectory can be more quickly computed than that found by a conventional trajectory generation algorithm. Atkins et al. [47] showed that the execution time for segmented-trajectory generation can be achieved under 1.0 second in an emergency situation. A segmented trajectory can also be easily reduced to basic pilot commands. Hence, it can be more easily interpreted by pilots and air traffic controllers [47].

7.3.3 Input Data

In the failure of all engines, post-failure performance characteristics of the distressed aircraft depend on the specific aerodynamic design. Therefore, a kinematic approach to trajectory optimization still requires aircraft-specific aerodynamic data. The input data required in this study is the steady-speed[**], engines-out glide ratio of the aircraft in question. The glide ratio should be assessed at the intended landing speed for a minimum of four bank angle values (ϕ) as follows: i) 0°, ii) $\phi_{\max}$, iii) two intermediate ϕ values between 0° and ϕ_{max}. The simulation methodology described in

[§] Constant-trim state may not occur over the transition segments due to the changing roll state of the aircraft.

[**] Here, "steady-speed" refers to constant calibrated airspeed, and not constant true airspeed.

section 5.4.2 is followed to collect the required data. Once the data is collected, the least squares estimation method [128] is applied to the data to build a third-degree, piece-wise continuous polynomial function given in Equation (7-1):

$$\cot(\gamma)_{v,\phi} = a_v * \phi^3 + b_v * \phi^2 + c_v * \phi + d_v \qquad 0° \leq \phi \leq \phi_{max} \tag{7-1}$$

Equation (7-1) is the required aircraft-specific aerodynamic data for the optimization problem.

7.3.4 Adjustables

The adjustables for the optimization problem are defined as follows:

- S_{L_i}=Length of linear segment i. $S_{L_i} \geq 0$; $i = 1,2,3,4.$
- $\Delta\theta_j$=Total change in aircraft heading (°) along circular segment j and the adjacent transition segments (i.e. $T_{j,j}$, C_j, $T_{j,j+1}$). $\Delta\theta_j \geq 0°$; $j = 1,2,3.$
- ϕ_j=Bank (roll) angle for circular segment j. $\forall\ \Delta\theta_j > 0°$: $0° < \phi_j \leq \phi_{max}$; $j = 1,2,3.$

Hence, the optimization problem involves a total of 10 adjustables.

7.3.5 Objective Function

The goal of trajectory optimization is to achieve efficient energy management. In the occurrence of total loss of thrust, the energy of the distressed aircraft stems from its airspeed and altitude. To achieve efficient energy management, the objective function aims to minimize the altitude loss required for the distressed aircraft to glide to an intended landing site within the degraded flight envelope. The objective function can be simply formulated in Equation (7-2) as follows:

$$\min_{S_{L_i},\Delta\theta_j,\phi_j} \sum_{i=1}^{4} \Delta Z_{L_i} + \sum_{j=1}^{3} \Delta Z_{C_j} + \sum_{j=1}^{3} \left(\Delta Z_{T_{j,j}} + \Delta Z_{T_{j,j+1}}\right) \quad (7\text{-}2)$$

where

- $\Delta Z_{T_{j,j}} = \Delta Z_{T_{j,j+1}}$,
- $\sum_{i=1}^{4} \Delta Z_{L_i}$, $\sum_{j=1}^{3} \Delta Z_{C_j}$ and $\sum_{j=1}^{3} \left(\Delta Z_{T_{j,j}} + \Delta Z_{T_{j,j+1}}\right)$ denote the total altitude loss along all linear, circular and transition segments, respectively.

Using $\cot(\gamma)_{v,\phi}$ from Equation (7-1), the terms in Equation (7-2) can be computed by Equations (7-3a), (7-3b) and (7-3c) as follows [23]:

$$\Delta Z_{L_i} = \frac{S_{L_i}}{\cot(\gamma)_{v,0^\circ}} \quad (7\text{-}3a)$$

$$\Delta Z_{C_j} = \frac{\Delta\theta_j * \pi}{180^\circ} * \frac{v_T^2}{g * tan\phi_j} * \frac{1}{\cot(\gamma)_{v,\phi_j}} \quad (7\text{-}3b)$$

$$\Delta Z_{T_{j,j}} = \Delta Z_{T_{j,j+1}} = \frac{\phi_j}{\dot{\phi}} * v_T * \frac{2}{\cot(\gamma)_{v,\phi_j} + \cot(\gamma)_{v,0^\circ}} \quad (7\text{-}3c)$$

where:

- $\left[\frac{v_T^2}{g * tan\phi_j}\right]$ equals the radius of the banked turn for circular segment j [23],
- $\left[\frac{\phi_j}{\dot{\phi}} * v_T\right]$ equals the length of each transition segment connected to circular segment j,
- $\cot(\gamma)_{v,\phi_j}$ is computed from Equation (7-1),
- v_T is the true airspeed.

For subsonic flights at or below 10,000 ft above sea level, the difference between calibrated airspeed and equivalent airspeed can be ignored, and true airspeed (i.e. v_T) can be

computed directly from calibrated airspeed (i.e. v) using Equation (7-4) [98]:

$$v_T = v * \sqrt{\frac{\rho_0}{\rho}} \tag{7-4}$$

7.3.6 Constraints

The landing trajectory starts at the initial aircraft position, and ends at the intended touchdown point. This geometric constraint is formulated in Equations (7-5a), (7-5b), and (7-5c):

$$\sum_{i=1}^{4} \Delta X_{L_i} + \sum_{j=1}^{3} \Delta X_{C_j} + \sum_{j=1}^{3} \left(\Delta X_{T_{j,j}} + \Delta X_{T_{j,j+1}} \right) = X_{Touchdown} - X_0 \tag{7-5a}$$

$$\sum_{i=1}^{4} \Delta Y_{L_i} + \sum_{j=1}^{3} \Delta Y_{C_j} + \sum_{j=1}^{3} \left(\Delta Y_{T_{j,j}} + \Delta Y_{T_{j,j+1}} \right) = Y_{Touchdown} - Y_0 \tag{7-5b}$$

$$\sum_{j=1}^{3} \Delta \theta_{C_j} + \sum_{j=1}^{3} \left(\Delta \theta_{T_{j,j}} + \Delta \theta_{T_{j,j+1}} \right) = \theta_{Touchdown} - \theta_0 \tag{7-5c}$$

The terms ΔX_{L_i} and ΔY_{L_i} quantify the change in the aircraft's horizontal position over the linear segments. They can be computed from Equations (7-6a) and (7-6b) based on the axis conventions used in aviation:

$$\Delta X_{L_i} = S_{L_i} * sin\, \theta_i \tag{7-6a}$$

$$\Delta Y_{L_i} = S_{L_i} * cos\, \theta_i \tag{7-6b}$$

Likewise, the terms ΔX_{C_j} and ΔY_{C_j} quantify the change in the aircraft's horizontal position over the circular segments. They can be computed from Equations (7-7a) and (7-7b) based on the axis conventions used in aviation:

$$\Delta X_{C_j} = \frac{\text{Sign}(\Delta\theta_j) * (v_T)^2}{g * tan\phi_j} * \left[\sin\left(\theta_0 + \Delta\theta_{T_{j,j}} + \sum_{n=1}^{j-1} \Delta\theta_n \right) - \sin\left(\theta_0 - \Delta\theta_{T_{j,j+1}} + \sum_{n=1}^{j} \Delta\theta_n \right) \right] \tag{7-7a}$$

$$\Delta Y_{C_j} = \frac{\text{Sign}(\Delta\theta_j) * (v_T)^2}{g * tan\phi_j} * \left[\cos\left(\theta_0 - \Delta\theta_{T_{j,j+1}} + \sum_{n=1}^{j} \Delta\theta_n \right) - \cos\left(\theta_0 + \Delta\theta_{T_{j,j}} + \sum_{n=1}^{j-1} \Delta\theta_n \right) \right] \tag{7-7b}$$

In order to represent the geometry of the transition segments, the transition segments are modeled as clothoids (i.e. Euler's spiral). Clothoids can accurately represent the transition segments because a linear change in bank angle results in approximately linear change in curvature, which is the same as over a clothoid [129]. Based on clothoid properties [129], the change in aircraft heading over a transition segment is computed from Equation (7-8a):

$$\Delta\theta_{T_{j,j}} = \Delta\theta_{T_{j,j+1}} = \frac{\phi_j}{\dot{\phi}} * \frac{g*tan\phi_j}{2*v_T} \tag{7-8a}$$

Using $\Delta\theta_{T_{i,j}}$ found from Equation (7-8a), the change in aircraft heading over a circular segment is computed from Equation (7-8b):

$$\Delta\theta_{C_j} = \Delta\theta_j - 2 * \Delta\theta_{T_{j,j}} \tag{7-8b}$$

Once $\Delta\theta_{T_{j,j}}$ and $\Delta\theta_{C_j}$ are found, the terms $\Delta X_{T_{j,j}}$ and $\Delta Y_{T_{j,j}}$ are computed based on clothoid properties [129] using Equations (7-9a) and (7-9b):

$$\Delta X_{T_{j,j}} = \left[cos\left(\theta_0 + \sum_{n=1}^{j-1}\Delta\theta_n\right) * \mathbb{C}(u) + sin\left(\theta_0 + \sum_{n=1}^{j-1}\Delta\theta_n\right) * \mathbb{S}(u)\right] \tag{7-9a}$$

$$\Delta Y_{T_{j,j}} = \left[sin\left(\theta_0 + \sum_{n=1}^{j-1}\Delta\theta_n\right) * \mathbb{C}(u) - cos\left(\theta_0 + \sum_{n=1}^{j-1}\Delta\theta_n\right) * \mathbb{S}(u)\right] \tag{7-9b}$$

where

$$\mathbb{S}(u) = \int_0^{\left(\frac{\phi_j}{\dot{\phi}} * v_T\right)} sin\left(\frac{\dot{\phi}*g*tan\phi_J}{2*\phi*(v_T)^3} * u^2\right) du \quad \text{and} \quad \mathbb{C}(u) = \int_0^{\left(\frac{\phi_j}{\dot{\phi}} * v_T\right)} cos\left(\frac{\dot{\phi}*g*tan\phi_J}{2*\phi*(v_T)^3} * u^2\right) du$$

are the Sine and Cosine Fresnel integrals that can be computed using the series expansions of the Sine and Cosine functions [130]:

$$\sin x = x - \frac{x^3}{3!} + \frac{x^5}{5!} - \frac{x^7}{7!} + \frac{x^9}{9!} - \cdots \approx x - \frac{x^3}{3!} + \frac{x^5}{5!} \tag{7-10a}$$

$$\cos x = 1 - \frac{x^2}{2!} + \frac{x^4}{4!} - \frac{x^6}{6!} + \frac{x^8}{8!} - \cdots \approx 1 - \frac{x^2}{2!} + \frac{x^4}{4!} \tag{7-10b}$$

Likewise, the terms $\Delta X_{T_{j,j+1}}$ and $\Delta Y_{T_{j,j+1}}$ are computed using Equations (7-11a) and (7-11b) as follows [129]:

$$\Delta X_{T_{j,j+1}} = \left[cos\left(\theta_0 + \sum_{n=1}^{j} \Delta\theta_n\right) * \mathbb{C}(u) - sin\left(\theta_0 + \sum_{n=1}^{j} \Delta\theta_n\right) * \mathbb{S}(u)\right] \quad (7\text{-}11b)$$

$$\Delta Y_{T_{j,j+1}} = \left[sin\left(\theta_0 + \sum_{n=1}^{j} \Delta\theta_n\right) * \mathbb{C}(u) + cos\left(\theta_0 + \sum_{n=1}^{j} \Delta\theta_n\right) * \mathbb{S}(u)\right] \quad (7\text{-}11b)$$

The terms found from Equations (7-9) and (7-12) quantify the change in the aircraft's horizontal position over the transition segments.

7.3.7 Iterative Optimization Procedure

Equations (7-3), (7-7), (7-8) and (7-9) show that the altitude loss required for flying the optimal trajectory depends on v_T, i.e. the true airspeed of the aircraft. Meanwhile, Equation (7-4) shows that v_T depends on ρ, which is the air density at the flight altitude. This introduces a circular reference in the optimization problem because air density depends on altitude [131], and the flight altitude can only be determined once the optimum trajectory is computed. To overcome the circular reference, an iterative procedure is proposed as follows:

1. Replace all $\mathrm{v_T}$ (i.e. true airspeed) terms in Equations (7-3), (7-7), (7-8) and (7-9) with v (i.e. calibrated airspeed).
2. Find the preliminary solution to the optimization problem using the differential evolution algorithm, which is a fast and robust optimization algorithm for continuous domains that can handle non-differentiable, nonlinear and multimodal objective functions as in this problem [132, 133].

3. Based on the preliminary solution, compute the average elevation for each circular segment using Equation (7-13):

$$\bar{E}_{C_j} = E_{Touchdown} + \sum_{n=1}^{j} \Delta Z_{L_n} + \sum_{m=1}^{j-1} \left(\Delta Z_{T_{m,m}} + \Delta Z_{C_m} + \Delta Z_{T_{m,m+1}} \right) + \Delta Z_{T_{j,j}} + \Delta Z_{C_j}/2 \quad (7\text{-}13)$$

4. Using the average elevation of a given circular segment, find the average true airspeed (i.e. $\bar{v}_{T,j}$) over that circular segment from Equation (7-14) [47]:

$$\bar{v}_{T,j} \approx v * 1.015^{\left(\bar{E}'_{C_j}/1000'\right)} \quad (7\text{-}14)$$

where $\bar{E}'_{C_j}$ simply equals $\bar{E}_{C_j}$ expressed in feet.

Equation (7-14) is built based on the fact that the true airspeed (v_T) corresponding to a given calibrated airspeed (v) increases by approximately 1.5 percent for every 1,000-ft increase in altitude up to 10,000 ft above sea level in standard day conditions [131].

5. Replace *all* v_T terms in Equations (7-3), (7-7), (7-8) and (7-9) with the newly-computed $\bar{v}_{T,j}$ values, and find the solution to the optimization problem using the differential evolution algorithm [133].
6. Based on the latter solution, re-compute the average true airspeed ($\bar{v}_{T,j}$) over each circular segment using Equations (7-13) and (7-14).
7. Compute the average relative difference ($\bar{d}$) between the $\bar{v}_{T,j}$ values from the latter solution and the prior solution as shown in Equation (7-15):

$$\bar{d} = \frac{1}{3} * \sum_{j=1}^{3} \frac{\left| (\bar{v}_{T,j})_k - (\bar{v}_{T,j})_{k-1} \right|}{(\bar{v}_{T,j})_k} * 100 \quad (7\text{-}15)$$

where k denotes the iteration number.

8. If the average relative difference ($\bar{d}$) is greater than 1.0 percent, repeat steps 5 through 7. Otherwise, if $\bar{d}$ is less than 1.0 percent, the procedure has converged, and the latter solution is accurate enough for practical purposes.

7.4 Adaptive Flight Planning Algorithm

This section presents an adaptive flight planning algorithm that is primarily targeted for the total-loss-of-thrust emergency during the initial climb. The goal of the algorithm is to guide the flight crew to a reachable runway when total loss of thrust occurs and there is no time to attempt an engine restart. While the presented algorithm is also applicable in other flight phases, the initial climb phase is emphasized due to the following reasons:

- If total loss of thrust occurs during the flight phases other than the initial climb or final approach, the flight crew would have ample time for emergency management. Therefore, the initial climb and final approach are more critical than other flight phases.
- The findings in sections 3.5.3 and 4.4 show that total loss of thrust due to bird strike is most likely to occur during the initial climb.
- The results summarized in section 5.6.3 demonstrate that if total loss of thrust occurs during the final approach, it would most probably rule out reaching a runway, as in the case of Kegworth air disaster [113]. Even the occurrence of partial loss of thrust during the final approach may rule out reaching a runway, as in the case of British Airways Flight #38 in January, 2008 [134].

The adaptive flight planning algorithm presented in this section requires advance input of two types of data prior to takeoff:

- A database that consists of the geographical coordinates and magnetic headings of the runways and desirable touchdown points that the aircraft can divert to in the event of total loss of power.
- The pressure altitude at the departure airport, and the wind speed.

The adaptive flight planning algorithm is explained as follows:

1. Based on the present wing configuration of the aircraft, the kinematic methodology computes the minimum altitude loss required for gliding to each runway at the departure airport.
2. The adaptive flight planner lists the "reachable" runways and ranks them based on required altitude loss. The reachable runways are those that require less altitude loss than the present altitude of the aircraft.
3. The flight crew selects one of the reachable runways from the list.
4. The adaptive flight planner indicates the allowable range of airspeed that should be maintained in order to glide to the selected runway.
5. Based on the allowable range of airspeed, the flight crew inputs the intended airspeed using the speed knob on the flight control unit (FCU) panel.
6. The adaptive flight planner guides the flight crew to the selected runway through simple oral pilot commands that are easy to follow in an emergency situation.

7. At approximately 40 ft AGL, the pilot in command initiates landing flare and touches down.

In case the aircraft does not have sufficient altitude to glide to any runway, the adaptive flight planner can guide the flight crew to an alternative safe landing site as long as the geographic coordinates of the landing site are input prior to takeoff.

7.5 Limitations

While the kinematic methodology is applicable to virtually all possible events of total loss of thrust, it is primarily intended for an emergency at a low altitude. This is because engine failure due to bird strike is most likely to occur below 5,000 ft AGL. If total loss of thrust occurs at an altitude higher than 10,000 ft AMSL, compressibility correction (i.e. ΔV_C) needs to be incorporated into the methodology, which would marginally increase the required computational time [98].

Another limitation of the methodology is that the optimum landing trajectory is computed based on minimized altitude loss. However, there may occur cases in which the aircraft's altitude is greater than that required for flying the optimum trajectory. In that case, the methodology does not provide guidance on excess altitude dissipation. So in such cases, the flight crew would have to dissipate the excess altitude by applying one or more of the following strategies:

- Early extension of the landing gear.
- Flaps extension (if the aircraft has sufficient hydraulic power).
- A side-slip maneuver, as in the case of Air Canada Flight 143 [53].

- S-turn maneuvers, as in the case of Air Transat Flight 236 [39].

It should be noted that flaps extension during the engines-out landing maneuver would change the aerodynamic performance of the distressed aircraft. In that case, the optimum landing trajectory should be re-computed based on the present aerodynamic characteristics of the aircraft.

7.6 Summary

This study adopted a kinematic approach to trajectory optimization for the total-loss-of-thrust emergency, which particularly hazards contemporary twin-engine jets with reduced engine redundancy. Contrary to present trajectory optimization methods, the kinematic method does not require aircraft-specific aerodynamic-coefficient data. Hence, it is readily applicable to commercial jets, for which the aerodynamic-coefficient data is not released. In the event of total loss of thrust, the kinematic method computes the minimum-altitude-loss trajectory to an accessible landing site through an iterative procedure that rapidly converges. To guide the pilots over the optimum trajectory, the method generates standard ATC commands that are simple to follow in an emergency.

Since the kinematic method is not computationally intensive, it can be utilized to develop an adaptive flight planner for real-time trajectory generation in the occurrence of total loss of thrust. Therefore, the kinematic method is promising for real-world applications. The following chapters demonstrate the application of the segmented-trajectory generation method to the Airbus A320 and Boeing 737NG aircraft. Flight simulation tests are conducted in JAR-FSTD A, Level D

full flight simulators to verify the accuracy of the method for each aircraft.

CHAPTER 8 - ADAPTIVE FLIGHT PLANNING ARCHITECTURE FOR THE AIRBUS A320 AIRCRAFT

This chapter utilizes the segmented trajectory generation algorithm to demonstrate the architecture of the adaptive flight planner through two realistic total-loss-of-thrust scenarios for the Airbus A320 aircraft. The results presented in 4.4 show that engine failure due to bird strike is statistically most likely to occur during the initial climb-out below 5000 ft AGL. Hence, two bird strike scenarios are assumed that occur shortly after takeoff below 5000 ft AGL. The first bird strike scenario is called "flaps scenario" since total loss of thrust occurs prior to flap retraction on the Airbus A320. On the other hand, the second bird strike scenario is called "clean scenario" since total loss of thrust occurs after flap retraction when the Airbus A320 is in "clean" configuration. The chapter demonstrates how the adaptive flight planner works to compute the optimum landing trajectory and guide the pilots over the optimum landing trajectory. The chapter also describes the flight simulation tests conducted in a JAR-FSTD A Level D full flight simulator to validate the accuracy of the optimum landing trajectories.

8.1 Occurrence of Total Loss of Thrust

The "flaps scenario" is assumed to occur as follows:

1. An Airbus A320 performs a northbound takeoff from Runway 36 shown in Figure 8-1, and starts the initial climb-out. The runway is at sea level, and the assumed wing configuration of the A320 is 1+F during the take-off.
2. Although flap retraction on the A320 aircraft may occur as early as 400 ft AGL [109], it is assumed that flap

retraction is scheduled to occur at 3,000 ft AGL at the time of the departure in accordance with ICAO's noise abatement departure procedure for close-in noise monitors [120].

3. During the initial climb-out before the flaps are retracted, the A320 encounters a flock of birds, and multiple birds are ingested into both engines.
4. Both engines of the A320 undergo total loss of thrust at a distance of 2.0 nautical miles (nm) north of Runway 18 while the aircraft is heading north (i.e. 0°; see Figure 8-1). At this exact location, the aircraft weighs 70.0 tons, and the turn-back maneuver to Runway 18 is initiated.
5. It is assumed that the A320 does not have sufficient hydraulic power to change the wing configuration due to the dual-engine failure. Thus, the wing configuration remains at 1+F throughout the landing maneuver.
6. Since the flaps cannot be extended, the landing speed is greater than typical landing speeds. It is assumed that the pilots maintain 160 KCAS throughout the landing maneuver, which approximately equals the lowest selectable airspeed (i.e. V_{LS}) in this particular configuration. Flying at the lowest selectable airspeed is advantageous in that it minimizes the landing roll distance.

On the other hand, the "clean scenario" is assumed to occur as follows:

1. An Airbus A320 performs a northbound takeoff from Runway 36 shown in Figure 8-1, and starts the initial climb-out. The runway is at sea level.
2. It is assumed that flap retraction is scheduled to occur at 1,000 ft AGL at the time of the departure in accordance

with ICAO's noise abatement departure procedure for far-out noise monitors [120].

3. After the flaps are retracted, the A320 encounters a flock of birds, and multiple birds are ingested into both engines.
4. Both engines of the A320 undergo total loss of thrust at a distance of 3.0 nautical miles (nm) north of Runway 18 while the aircraft is heading north (i.e. 0°; see Figure 8-1). At this exact location, the aircraft weighs 70.0 tons, and the turn-back maneuver to Runway 18 is initiated.
5. It is assumed that the A320 does not have sufficient hydraulic power to change the wing configuration due to the dual-engine failure. Thus, the aircraft is in "clean" configuration throughout the landing maneuver.
6. Since the flaps cannot be extended, the landing speed is greater than typical landing speeds. It is assumed that the pilots maintain 205 KCAS throughout the landing maneuver, which approximately equals the lowest selectable airspeed (i.e. V_{LS}) in this particular configuration. Thereby, the pilots maximize the time aloft, and minimize the runway length requirements for landing roll.

8.2 Input Data

For the "flaps scenario", the required input data is the engines-out glide ratio of the Airbus A320 aircraft in wing configuration 1+F at 160 KCAS for the bank angles of 0°, 10°, 20°, and ϕ_{max} =33°. These data are assessed in Chapter 5, and presented in Figure 5-6. The data are re-plotted in Figure 8-2 with the engines-out glide ratio in the vertical axis, and bank angle on the horizontal axis. Likewise for the "clean scenario", the required input data is the engines-out glide ratio of the

Airbus A320 aircraft at 205 KCAS for the bank angles of 0°, 10°, 20°, and ϕ_{max} =33°. These data are assessed in Chapter 5, and presented in Figure 5-8. The data are re-plotted in Figure 8-2 with the engines-out glide ratio in the vertical axis, and bank angle on the horizontal axis.

As shown in Figure 8-2, the engines-out glide ratio at a given airspeed decreases with increasing bank angle because the aircraft loses lift in banked turns and the drag increases [23]. The total simulation time required for obtaining the aerodynamic input data plotted in Figure 8-2 is less than one hour. A piece-wise continuous, third-degree polynomial function is fitted to the data for each airspeed in Figure 8-2 using the least squares estimation method [128]. The resulting polynomial function is given in Equation (8-1) for the "flaps scenario", and in Equation (8-2) for the "clean scenario":

$$\cot(\gamma)_{v,\phi} = 0.000011 * \phi^3 - 0.004017 * \phi^2 + 0.009051 * \phi + 13.0 = f(\phi) \quad (8\text{-}1)$$
$$v = 160\ KCAS,\ 0° \leq \phi \leq 33°$$

$$\cot(\gamma)_{v,\phi} = 0.000025 * \phi^3 - 0.004333 * \phi^2 + 0.012415 * \phi + 16.7 = f(\phi) \quad (8\text{-}2)$$
$$v = 205\ KCAS,\ 0° \leq \phi \leq 33°$$

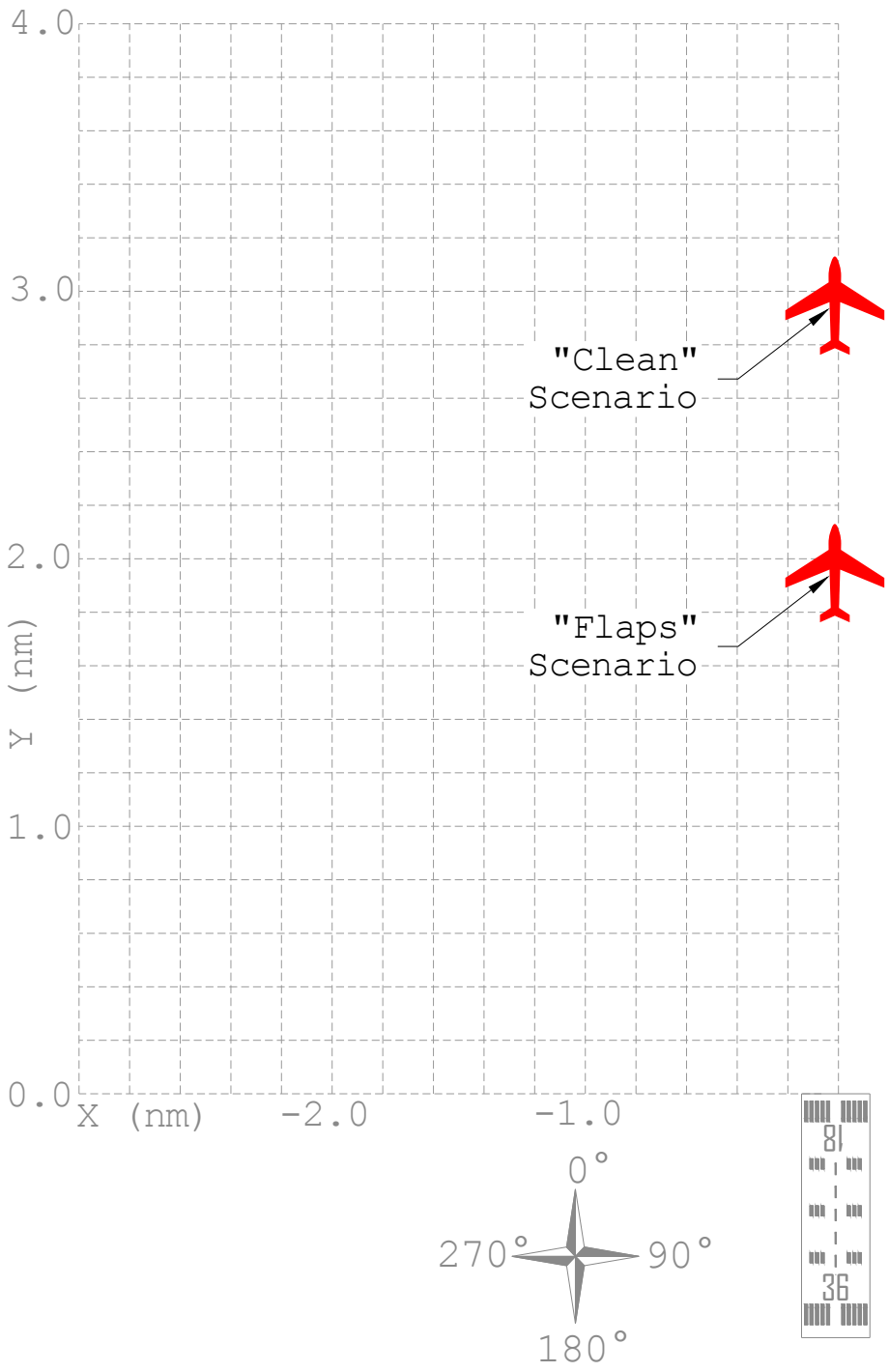

Figure 8-1. Aircraft location at the instant of total loss of thrust (aircraft and runway not drawn to scale).

Both Equation (8-1) and Equation (8-2) return a coefficient of determination, $R^2 = 1.0$. Equations (8-1) and (8-2) are plotted in Figure 8-2, and are used as the aircraft-specific aerodynamic input data to formulate the optimization problem.

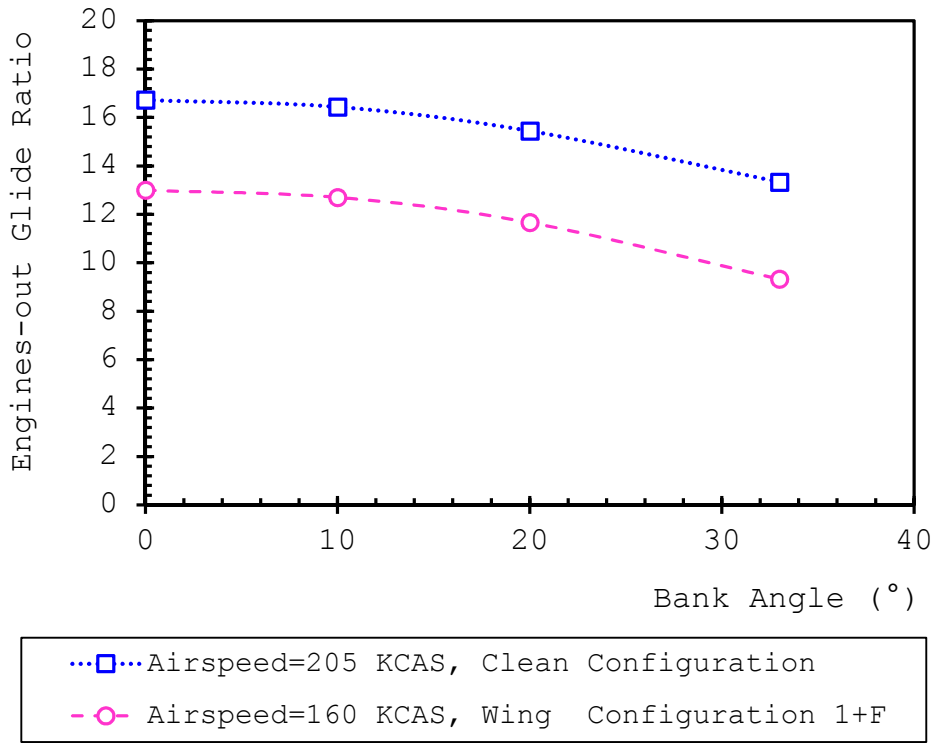

Figure 8-2. Predicted engines-out glide ratio for the A320 aircraft during steady-speed engines-out descent *(landing gear up, aircraft gross weight=70.0 tons).*

8.3 Modeling Assumptions

The following assumptions are incorporated into the optimization problem:

1. The aerodynamic roll rate of the A320 aircraft equals $\dot{\phi} = 10°/\text{sec}$.

2. Once the flight crew configures “landing gear down”, it takes no longer than 15 seconds for the landing gear to be fully extended and locked.
3. The aircraft is aligned with Runway 18 by the time it is 100 ft. above ground level. This allows for the insertion of a “final approach waypoint”, which precedes a stabilizing final approach segment. The landing trajectory is to be generated from the initial aircraft state to this “final approach waypoint”.
4. The pilots configure “landing gear down” no later than 15 seconds before the aircraft reaches the “final approach waypoint”.
5. Standard day conditions prevail during the engines-out landing, and no wind prevails during the course of landing.

The first and the second assumptions are based on the observations made in the JAR-FSTD A, Level D full flight simulator. The third assumption basically prohibits banked turns below 100 ft to prevent possible wingtip collisions with ground objects. The fourth assumption enables sufficient time for landing gear extension prior to touchdown.

It should also be noted that landing gear extension results in increased drag and reduced engines-out glide ratio [23]. When the landing gear is fully extended during wings-level flight in the full flight simulator, the resultant reduction in the engines-out glide ratio is measured as approximately 14% at 160 KCAS and wing configuration “1+F”, and approximately 15% at 205 KCAS and “clean” configuration.

8.4 Objective Functions

The objective function of the optimization problem is to minimize the altitude loss required for gliding from the initial

aircraft location to the "final approach waypoint". For the "flaps" scenario, Equation (8-3) gives the "initial" objective function, in which all v_T terms are temporarily replaced with v =160 KCAS since the v_T values are initially unknown. All equations in this chapter are presented without dimensional homogeneity for reader-friendliness:

$$\min_{S_{L_i},\Delta\theta_j,\phi_j} \sum_i \left[\frac{S_{L_i}}{13.0}\right] + \sum_j \left[\frac{\Delta\theta_j * \pi}{180°} * \frac{(160\,kt)^2}{(9.81 m/s^2) * tan\phi_j} * \frac{1}{f(\phi_j)}\right] + 2 * \sum_{j=1}^{3} \left[\frac{\phi_j}{10°/\text{sec}} * \frac{2*(160\,kt)}{f(\phi_j)+13.0}\right] \quad (8\text{-}3)$$

where $f(\phi_j)$ is given in Equation (8-1), and 13.0 equals the predicted steady-speed engines-out glide ratio in wings-level flight in this particular configuration, which is found from $f(0°)$ in Equation (8-1).

Likewise for the "clean" scenario, Equation (8-4) gives the "initial" objective function, in which all v_T terms are temporarily replaced with v =205 KCAS since the v_T values are initially unknown:

$$\min_{S_{L_i},\Delta\theta_j,\phi_j} \sum_i \left[\frac{S_{L_i}}{16.7}\right] + \sum_j \left[\frac{\Delta\theta_j * \pi}{180°} * \frac{(205\,kt)^2}{(9.81 m/s^2) * tan\phi_j} * \frac{1}{f(\phi_j)}\right] + 2 * \sum_{j=1}^{3} \left[\frac{\phi_j}{10°/\text{sec}} * \frac{2*(205\,kt)}{f(\phi_j)+16.7}\right] \quad (8\text{-}4)$$

where $f(\phi_j)$ is given in Equation (8-2), and 16.7 equals the predicted steady-speed engines-out glide ratio in wings-level flight in this particular configuration, which is found from $f(0°)$ in Equation (8-2).

8.5 Constraints

As mentioned in section 8.3, it is assumed that the aircraft is situated 100 ft above ground level by the time it is aligned with Runway 18. This state is represented by a "final approach waypoint". It is assumed that the "final approach waypoint" projects onto the beginning of Runway 18 threshold.

The engines-out landing trajectory is generated from the initial aircraft state to the "final approach waypoint". The resultant geometric constraints for the optimization problem are formulated as follows:

$$\sum_{i=1}^{4} \Delta X_{L_i} + \sum_{j=1}^{3} \Delta X_{C_j} + \sum_{j=1}^{3} \left(\Delta X_{T_{j,j}} + \Delta X_{T_{j,j+1}} \right) = 0.00\ nm \quad (8\text{-}5a)$$

$$\sum_{i=1}^{4} \Delta Y_{L_i} + \sum_{j=1}^{3} \Delta Y_{C_j} + \sum_{j=1}^{3} \left(\Delta Y_{T_{j,j}} + \Delta Y_{T_{j,j+1}} \right) = \Delta Y \quad (8\text{-}5b)$$

$$\sum_{j=1}^{3} \Delta\theta_{C_j} + \sum_{j=1}^{3} \left(\Delta\theta_{T_{j,j}} + \Delta\theta_{T_{j,j+1}} \right) = 180° \quad (8\text{-}5c)$$

where ΔY equals -2.0 nm for the "flaps" scenario, and -3.0 nm for the "clean" scenario. As mentioned in section 7.3.7, all v_T terms are initially replaced with v =160 KCAS for the "flaps" scenario, and v =205 KCAS for the "clean" scenario at this stage of the optimization problem. For instance, the term $\Delta\theta_{T_{j,j}}$ in Equation (8-5c) is formulated as $\Delta\theta_{T_{j,j}} = \frac{\phi_j}{10°/sec} * \frac{(9.81 m/s^2) * tan\phi_j}{2*(160\ kt)}$ for the "flaps" scenario where v_T in Equation (7-8a) is temporarily substituted with $v = 160\ kt$.

8.6 Solutions

The optimum solution is computed using the differential evolution algorithm [133]. Since the optimization problem is formulated over a continuous domain, the global optimum solution is computed [132, 133]. Step-by-step findings from the optimization problem are given in Table 8-1.

8.6.1 "Flaps" Scenario

To proceed with the second stage of the iterative procedure, the following steps are followed in the "flaps" scenario:

1. Using the initial solution, the terms in Equation (7-13) are computed based on Equations (7-3a), (7-3b), and (7-3c) as follows: $\Delta Z_{C_1} = 1360'$, $\Delta Z_{C_2} = 298'$, $\Delta Z_{T_{1,1}} = \Delta Z_{T_{1,2}} = 80'$, $\Delta Z_{T_{2,2}} = \Delta Z_{T_{2,3}} = 51'$, $\Delta Z_{L_2} = 463'$ and all other terms are equal to 0.
2. Since the runway is located at sea level, $E_{Touchdown} = 0$, and the mid-elevation of each circular segment is computed as follows:

   $\bar{E}'_{C_1} = 100' + 2 * 51' + 298' + 463' + 80' + 1360'/2 = 1723'$, and

   $\bar{E}'_{C_2} = 100' + 51' + 298'/2 = 300'$.

   The $100'$ is incorporated into the calculations to account for the third modeling assumption given in 8.4.
3. The average true airspeed for each circular segment is computed from Equation (7-14):

   $\bar{v}_{T,1} \approx (160\ kt) * 1.015^{(1723'/1000')} = 164.2\ kt$

   $\bar{v}_{T,2} \approx (160\ kt) * 1.015^{(300'/1000')} = 160.7\ kt$
4. The same optimization problem is formulated by replacing all v_T terms with $\bar{v}_{T,j}$. For example, Equation (7-8a) is modified as $\Delta\theta_{T_{j,j}} = \Delta\theta_{T_{j,j+1}} = \frac{\phi_j}{\dot{\phi}} * \frac{g*tan\phi_j}{2*\bar{v}_{T,j}}$.

   The second stage of the optimization problem is solved using the differential evolution algorithm [133]. The results are given in the second row of Table 8-1.
5. Using the second solution, the terms in Equation (7-13) are computed based on Equations (7-3a), (7-3b), and (7-3c) as follows: $\Delta Z_{C_1} = 1422'$, $\Delta Z_{C_2} = 175'$, $\Delta Z_{T_{1,1}} = \Delta Z_{T_{1,2}} = 84'$, $\Delta Z_{T_{2,2}} = \Delta Z_{T_{2,3}} = 81'$, $\Delta Z_{L_2} = 561'$ and all other terms are equal to 0.
6. The mid-elevation of each circular segment is computed as follows:

$\bar{E}'_{C_1} = 100' + 2 * 81' + 175' + 561' + 84' + 1422'/2 = 1793'$, and

$\bar{E}'_{C_2} = 100' + 81' + 175'/2 = 269'$.

7. The average true airspeed for each circular segment is computed from Equation (7-14):

$\bar{v}_{T,1} \approx (160\ kt) * 1.015^{(1793'/1000')} = 164.3\ kt$

$\bar{v}_{T,2} \approx (160\ kt) * 1.015^{(269'/1000')} = 160.6\ kt$

8. Using Equation (7-15), $\bar{d}$ is found as:

$\bar{d} = \frac{1}{2} * \left\{\frac{|164.2-164.3|}{164.3} * 100 + \frac{|160.7-160.6|}{160.6} * 100\right\} = 0.03\%$

Since $\bar{d} < 1.0\%$, the convergence criterion is met. The second solution for the "flaps" scenario given in Table 8-1 is the final solution to the optimization problem. Based on the solution, the altitude loss required for following the optimum trajectory equals $100' + 2 * 81' + 175' + 561' + 2 * 84 + 1422' = 2588\ ft$. However, this does not include the additional altitude loss due to landing gear extension. As mentioned in section 8.3, the flight crew should configure "landing gear down" no later than 15 seconds before the aircraft reaches the "final approach waypoint" described in section 7.3.6. As mentioned in section 8.3, extension of the landing gear is predicted to reduce the engines-out glide ratio by approximately 14 percent. To predict the additional altitude loss caused by landing gear extension, the following procedure is followed:

1. The predicted altitude AGL vs. time is plotted over the optimum trajectory without incorporating the additional altitude loss due to landing gear extension. The plot is shown in Figure 8-3. The altitude AGL at t = 0 equals 2588 ft.

2. From the plot, the time corresponding to 15 seconds before the aircraft is 100 ft AGL is computed. This is when the pilots must have configured "landing gear down". The required altitude loss from this moment on is increased by 14%. In this example, the additional altitude loss due to landing gear extension is predicted as 500*0.14=70 ft (see Figure 8-3).
3. The total altitude loss required for flying the optimum trajectory is predicted as 2,588 + 72 = 2,660 ft.

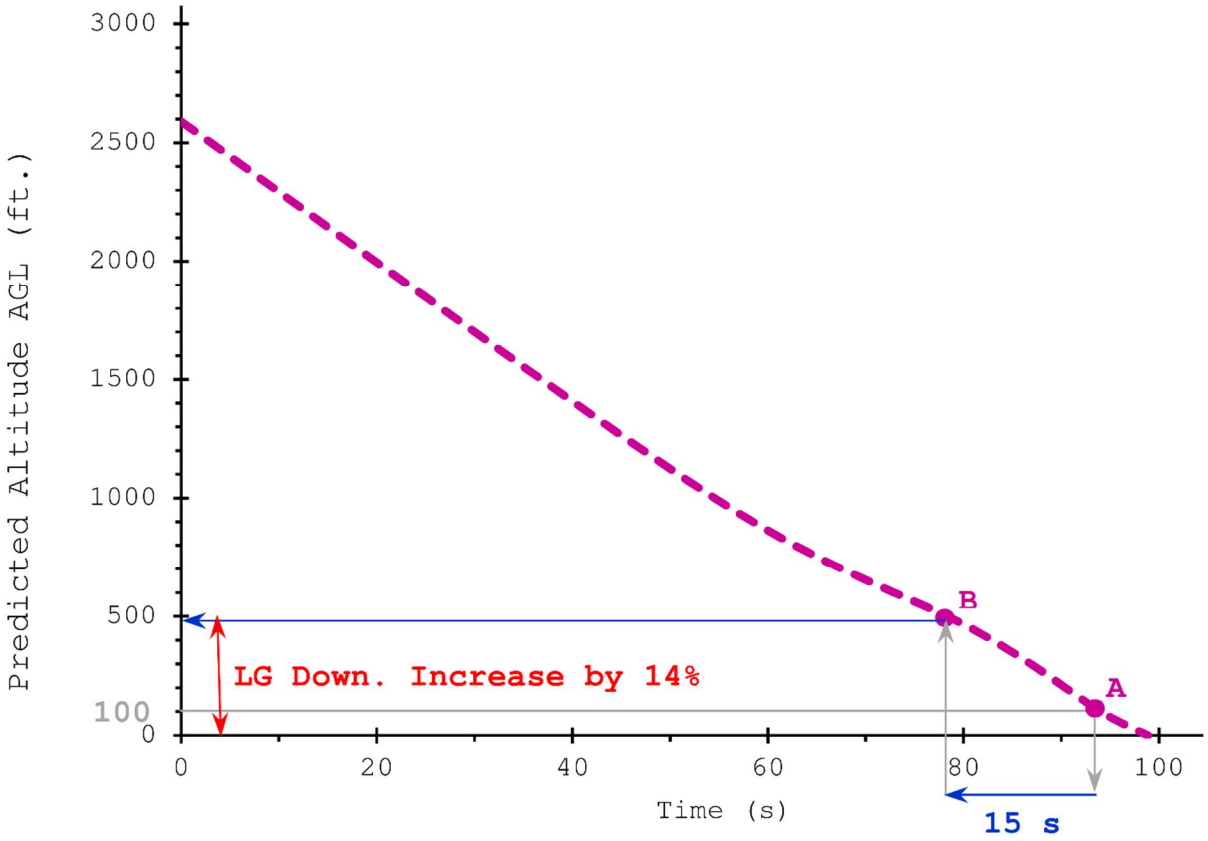

Figure 8-3. Procedure for computing the additional altitude loss due to landing gear extension.

8.6.2 "Clean" Scenario

Similarly, the following steps are followed in the "clean" scenario to proceed with the second stage of the iterative procedure:

1. Using the initial solution, the terms in Equation (7-13) are computed based on Equations (7-3a), (7-3b), and (7-3c) as follows: $\Delta Z_{C_1} = 1578'$, $\Delta Z_{C_2} = 262'$, $\Delta Z_{T_{1,1}} = \Delta Z_{T_{1,2}} = 76'$, $\Delta Z_{T_{2,2}} = \Delta Z_{T_{2,3}} = 68'$, $\Delta Z_{L_2} = 712'$ and all other terms are equal to 0.
2. Since the runway is located at sea level, $E_{Touchdown} = 0$, and the mid-elevation of each circular segment is computed as follows:

   $\bar{E}'_{C_1} = 100' + 2 * 68' + 262' + 712' + 76' + 1578'/2 = 2075'$, and

   $\bar{E}'_{C_2} = 100' + 68' + 262'/2 = 299'$.

   The $100'$ is incorporated into the calculations to account for the third modeling assumption given in 8.4.
3. The average true airspeed for each circular segment is computed from Equation (7-14):

   $\bar{v}_{T,1} \approx (205\ kt) * 1.015^{(2075'/1000')} = 211.4\ kt$

   $\bar{v}_{T,2} \approx (205\ kt) * 1.015^{(299'/1000')} = 205.9\ kt$
4. The same optimization problem is formulated by replacing all v_T terms with $\bar{v}_{T,j}$. For example, Equation (7-8a) is modified as $\Delta\theta_{T_{j,j}} = \Delta\theta_{T_{j,j+1}} = \frac{\phi_j}{\dot{\phi}} * \frac{g*tan\phi_j}{2*\bar{v}_{T,j}}$.

   The second stage of the optimization problem is solved using the differential evolution algorithm [133]. The results are given in the second row of Table 8-1.
5. Using the second solution, the terms in Equation (7-13) are computed based on Equations (7-3a), (7-3b), and (7-3c) as

follows: $\Delta Z_{C_1} = 1704'$, $\Delta Z_{C_2} = 253'$, $\Delta Z_{T_{1,1}} = \Delta Z_{T_{1,2}} = 81'$, $\Delta Z_{T_{2,2}} = \Delta Z_{T_{2,3}} = 77'$, $\Delta Z_{L_2} = 652'$ and all other terms are equal to 0.

6. The mid-elevation of each circular segment is computed as follows:

   $\bar{E}'_{C_1} = 100' + 2 * 77' + 253' + 652' + 81' + 1704'/2 = 2092'$, and

   $\bar{E}'_{C_2} = 100' + 77' + 241'/2 = 298'$.

7. The average true airspeed for each circular segment is computed from Equation (7-14):

   $\bar{v}_{T,1} \approx (205\ kt) * 1.015^{(2092'/1000')} = 211.5\ kt$

   $\bar{v}_{T,2} \approx (205\ kt) * 1.015^{(298'/1000')} = 205.9\ kt$

8. Using Equation (7-15), $\bar{d}$ is found as:

   $\bar{d} = \frac{1}{2} * \left\{ \frac{|211.4-211.5|}{211.5} * 100 + \frac{|205.9-205.9|}{205.9} * 100 \right\} = 0.02\%$

Since $\bar{d} < 1.0\%$, the convergence criterion is met. The second solution for the "clean" scenario given in Table 8-1 is the final solution to the optimization problem. Based on the solution, the altitude loss required for following the optimum trajectory equals $100' + 2 * 77' + 253' + 652' + 2 * 81' + 1704' \approx 3025\ ft$. However, this does not include the additional altitude loss due to landing gear extension. The procedure outlined in section 8.6.1 is applied to the findings to predict the additional altitude loss due to landing gear extension. The additional altitude loss due to landing gear extension is predicted as 73 ft. Hence, the total altitude loss required for flying the optimum trajectory is predicted as 3,025 + 73 = 3,098 ft.

8.7 Interpretation of the Optimum Trajectory

Figure 8-4 illustrates the ground tracks of the optimum landing trajectories, both of which indicate a tear-drop shaped

pattern. For a given total-loss-of-thrust scenario, the optimum landing trajectory is divided into four distinct flight phases. For the “flaps” scenario, these flight phases are briefly explained as follows:

1. An initial left-turn with 33° bank, where the absolute change in aircraft heading equals 221°.
2. A wings-level, equilibrium glide for a horizontal distance of 1.2 nm.
3. A final 41°-right turn at 33° bank that aligns the aircraft with Runway 18.
4. Landing flare and safe touchdown on Runway 18.

For the “clean” scenario, these flight phases are explained as follows:

1. An initial left-turn with 33° bank, where the absolute change in aircraft heading equals 225°.
2. A wings-level, equilibrium glide for a horizontal distance of 1.8 nm.
3. A final 45°-right turn at 33° bank that aligns the aircraft with Runway 18.
4. Landing flare and safe touchdown on Runway 18.

Table 8-1. Numeric solutions to the optimization problem for (a) "flaps" scenario, (b) "clean" scenario on the Airbus A320 aircraft (no wind).

		"Flaps" scenario		"Clean" scenario	
	No. of Iteration	1	2	1	2
Optimum Trajectory	S_{L_1} (nm)	0	0	0	0
	$\Delta\theta_1$ $(^\circ)$	-223	-221	-222	-225
	ϕ_1 $(^\circ)$	33	33	33	33
	S_{L_2} (nm)	1.0	1.2	2.0	1.8
	$\Delta\theta_2$ $(^\circ)$	43	41	42	45
	ϕ_2 $(^\circ)$	23	33	30	33
	S_{L_3} (nm)	0	0	0	0
	$\Delta\theta_3$ $(^\circ)$	0	0	0	0
	ϕ_3 $(^\circ)$	N/A	N/A	N/A	N/A
	S_{L_4} (nm)	0	0	0	0
Convergence Criterion	$\bar{v}_{T,1}$ (kt)	164.2	164.3	211.4	211.5
	$\bar{v}_{T,2}$ (kt)	160.7	160.6	205.9	205.9
	$\bar{v}_{T,3}$ (kt)	N/A	N/A	N/A	N/A
	$\bar{d}$ $(\%)$	N/A	0.03	N/A	0.02

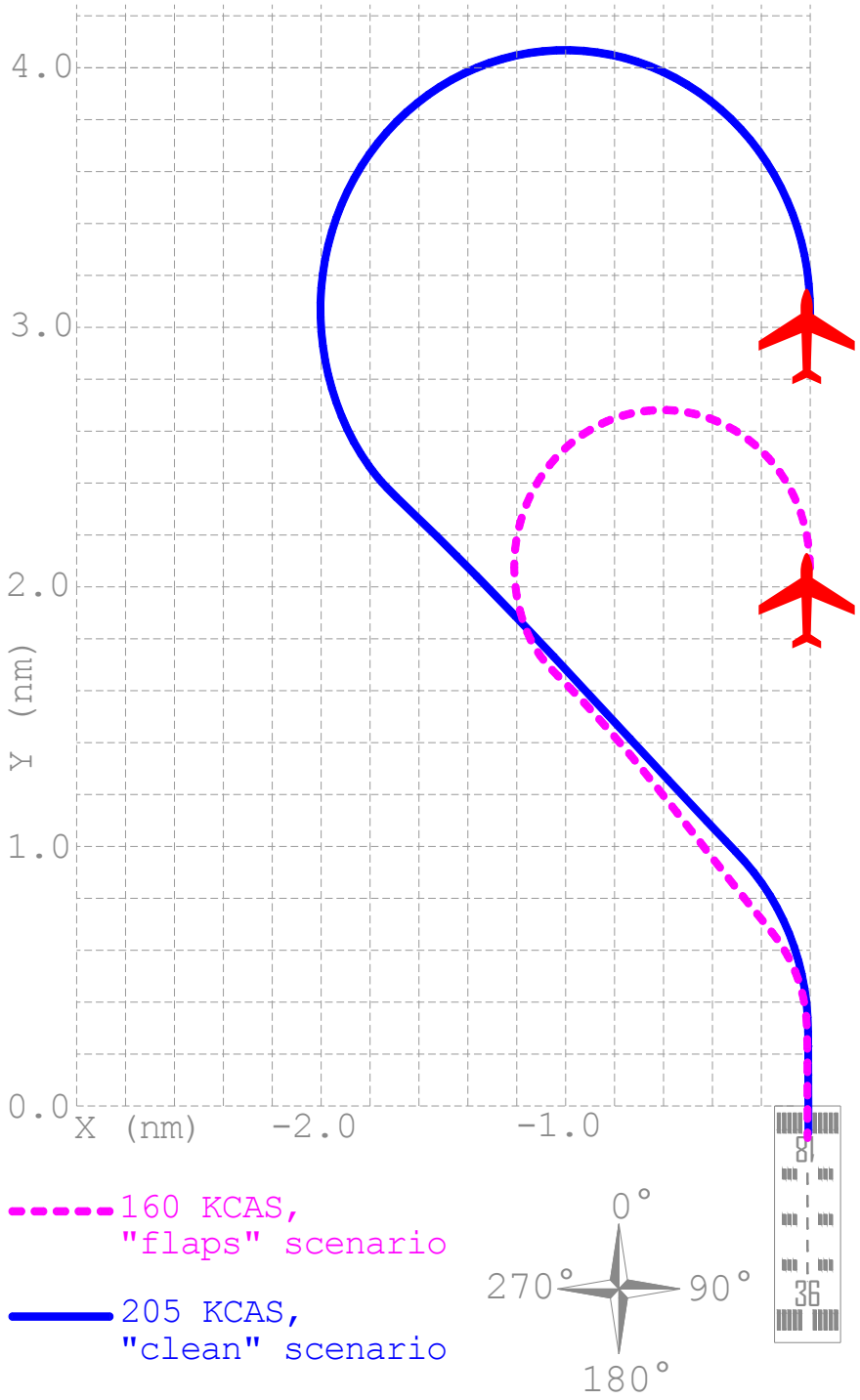

Figure 8-4. Ground tracks for the optimum engines-out landing trajectories for the Airbus A320 aircraft (no wind).

8.8 ATC Commands for the Optimum Trajectory

Since the autopilot of the A320 and 737-800 aircraft disengages in total-loss-of-thrust emergency [135], the adaptive flight planner should guide the pilots over the optimum landing trajectory. In order to be of practical value, the optimum landing trajectory must be easy to interpret and follow for pilots in an emergency situation.

The proposed adaptive flight planner is to guide the pilots over the optimum landing trajectory using standard and simple ATC commands. In order to generate the ATC commands, the following procedure is applied:

1. The altitude loss is plot versus the aircraft heading over the optimum trajectory. Figure 8-5 shows the altitude loss versus aircraft heading for both the "flaps" and "clean" scenarios.
2. Using the charts in Figure 8-5, the adaptive flight planner predicts the altitude loss values corresponding to the start of a heading change. For instance in the "flaps" scenario, the heading change from 139° to 180° should be initiated at an altitude loss of approximately 2,150 ft (see Figure 8-5a). Likewise in the "clean" scenario, the heading change from 135° to 180° should be initiated at an altitude loss of approximately 2,500 ft.
3. Using the results from the charts in Figure 8-5, the adaptive flight planner computes the altitude AGL corresponding to the start of a heading change. For example, if the start altitude is 2,700 ft AGL in the "flaps" scenario, the heading change from 139° to 180° should be initiated at approximately 2700 – 2150 = 550 ft AGL.

Likewise, if the start altitude is 3,100 ft AGL in the "clean" scenario, the heading change from 135° to 180° should be initiated at approximately 3100 – 2500 = 600 ft AGL.

4. The adaptive flight planner issues the heading change commands shortly before the aircraft descends to the predicted altitude for the start of heading change. For example, if the start altitude is 2,700 ft AGL in the "flaps" scenario, the adaptive flight planner issues "turn right heading 180° at 33°-bank" shortly before the aircraft descends to 550 ft AGL. Likewise, if the start altitude is 3,100 ft AGL in the "clean" scenario, the adaptive flight planner issues "turn right heading 180° at 33°-bank" shortly before the aircraft descends to 600 ft AGL. The adaptive flight planner can read the altitude AGL from the aircraft's radar altimeter.
5. The adaptive flight planner also issues the airspeed to be maintained to fly the optimum trajectory. For example, it commands the pilot to "maintain 160 kt" in the "flap" scenario, and "maintain 205 kt" in the "clean" scenario.

The oral ATC commands described in this section are easy to interpret and follow in an emergency situation. The procedure described in this section shows that the optimum trajectories computed from the segmented trajectory generation algorithm can be easily reduced to basic commands, which have practical value. The following section utilizes the oral ATC commands to validate the accuracy of the optimum landing trajectories in an A320 full flight simulator.

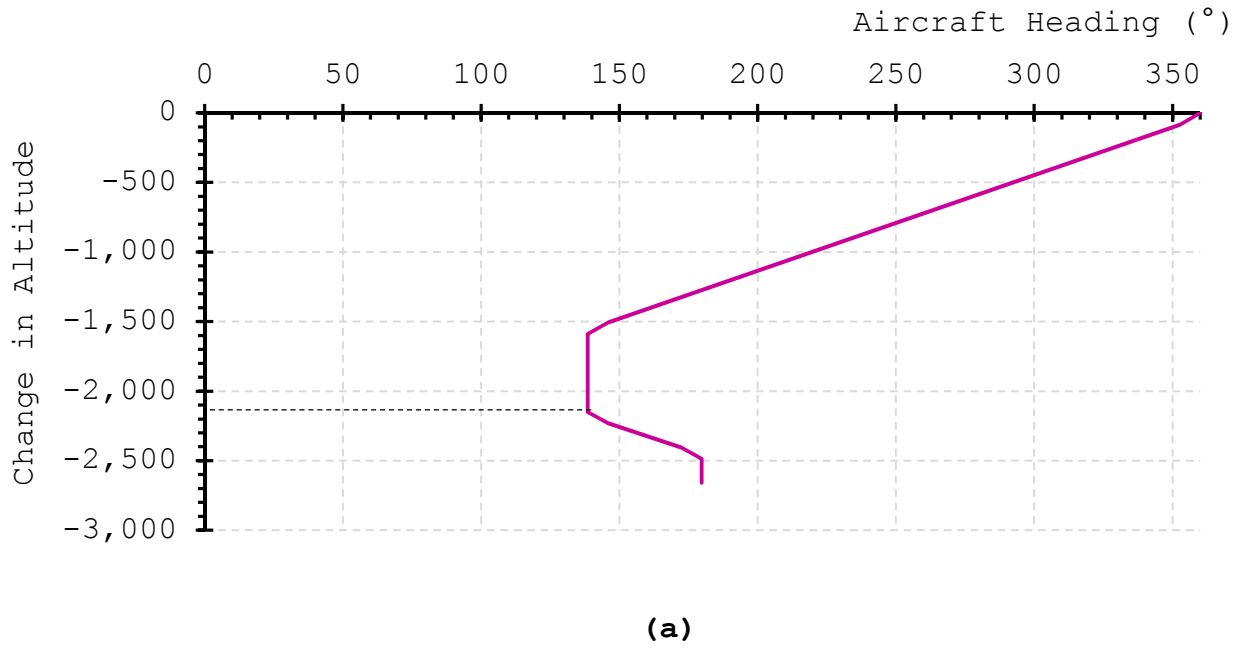

(a)

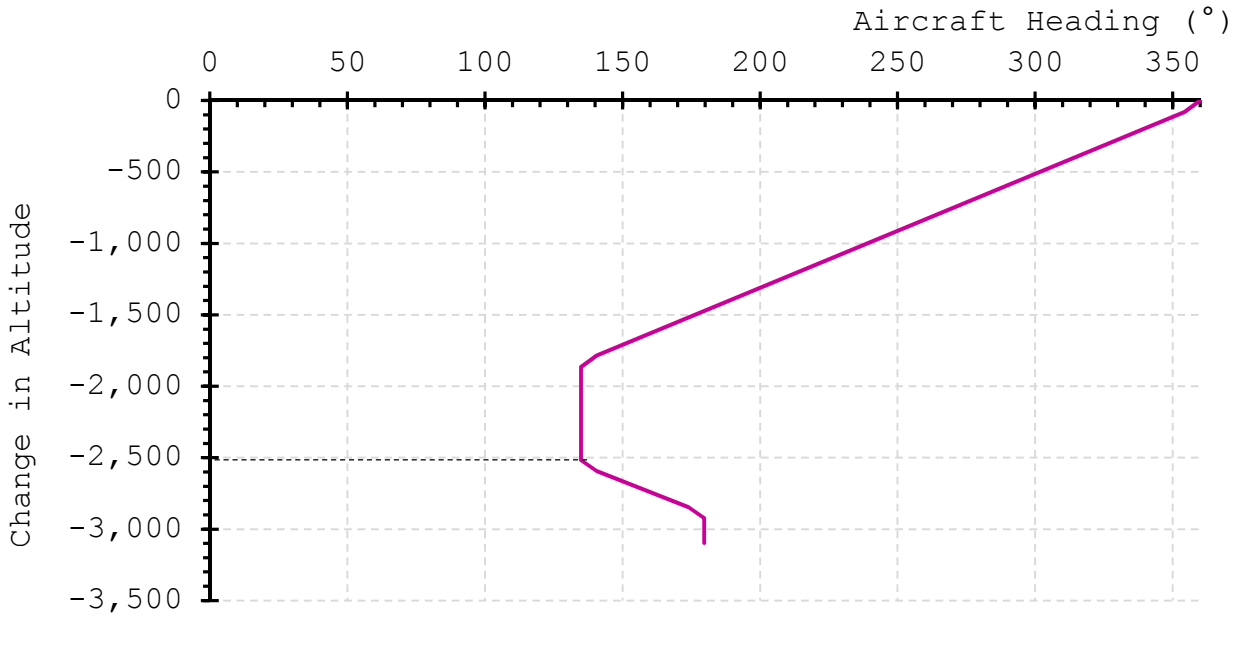

(b)

Figure 8-5. Altitude loss versus aircraft heading over the optimum landing trajectory for (a) "flaps" scenario, (b) "clean" scenario.

8.9 Validation of the Results

Flight simulation tests are conducted to find out if the kinematic approach to segmented-trajectory generation accurately estimates the required altitude loss plotted in Figure 8-4. The simulations are conducted in a JAR-FSTD A, Level D full flight simulator that is certified under the European Aviation Safety Agency (EASA) and Joint Aviation Authorities (JAA). Three type-rated A320 pilots participated in the flight simulation tests. The simulation of the "flaps" scenario starts with freezing the aircraft position at 2.0 nm north of runway 18 threshold at an altitude of 2,700 ft. AGL. On the other hand, the simulation of the "clean" scenario starts with freezing the aircraft position 3.0 nm north of runway 18 threshold at an altitude of 3,100 ft. The aircraft weight is frozen at 70.0 tons throughout the simulations. The aircraft heading is initially frozen at 0°, and the landing gear is initially fully retracted. The wing configuration is set at "1+F" in simulating the "flaps" scenario, and is set to "clean" configuration in simulating the "clean" scenario. The full flight simulator is programmed to simulate dual-engine failure on the A320. When dual-engine failure results in total loss of thrust, both the aircraft position and aircraft heading are "released", and the aircraft starts engines-out glide at 160 KCAS in simulating the "flaps" scenario, and at 205 KCAS in simulating the "clean" scenario. From this moment on, one of the three type-rated A320 pilots flies the aircraft while one member of the research team issues simplified oral commands to make the pilot follow the optimum landing trajectory illustrated in Figure 8-4. In simulating the "flaps" scenario, the following oral commands are issued to the pilot in control:

- Turn left heading 139° with 33° bank. Maintain 160 kt.
- Maintain present heading and speed.
- Descend to 550′. Landing gear down.
- Turn right heading 180° with 33° bank. Maintain 160 kt.
- Clear to land on Runway 18.

In simulating the "clean" scenario, the following oral commands are issued to the pilot in control:

- Turn left heading 135° with 33° bank. Maintain 205 kt.
- Maintain present heading and speed.
- Descend to 600′. Landing gear down.
- Turn right heading 180° with 33° bank. Maintain 205 kt.
- Clear to land on Runway 18.

After each run, the simulator plots the ground tracks and descent profile of the A320. Using the plots of the ground tracks, the research team verifies that the landing trajectory is simulated properly. Using the plots of the descent profile, the research team measures the total altitude loss (rounded up to the nearest 50′) from the initial aircraft position to the northern threshold of Runway 18. The average simulated altitude loss is found as: $\frac{2600'+2600'+2600'}{3} = 2600\,ft$ for the "flaps" scenario, which differs from the predicted altitude loss of 2,660 ft by 2.3 percent. Similarly, the average simulated altitude loss is found as: $\frac{3050'+3000'+3000'}{3} = 3017\,ft$ for the "clean" scenario, which differs from the predicted altitude loss of 3,098 ft by 2.7 percent. In both scenarios, the predicted altitude loss is marginally greater than the actual simulated altitude loss, possibly because:

- There exists no exact method to compute the additional altitude loss due to landing gear extension.
- The kinematic methodology does not incorporate the "ground effect" [23] into the calculations.

Nevertheless, the rate of error is marginal in both scenarios. In addition, since the required altitude loss is slightly overestimated, the error is on the "safe side". Hence, the kinematic trajectory optimization method described in Chapter 7 can accurately estimate the altitude loss required for gliding to an intended landing site.

8.10 Uncertainty Analysis

To be of practical value, the optimum trajectory should not be overly sensitive to assumed aerodynamic parameters [44], such as the assumed roll rate, i.e. $\dot{\phi}$. In both the "flaps" scenario and "clean" scenario, the optimum trajectory is computed assuming an aerodynamic roll rate of $\dot{\phi}=10^{\circ}$/sec. The goal of this section is to find out how the required altitude loss would change when different roll rates are assumed. For this purpose, the optimum trajectory is re-computed assuming roll rates of $\dot{\phi}=12.5^{\circ}$/sec, and $\dot{\phi}=7.5^{\circ}$/sec. The resulting altitude vs. time histories are plotted in Figure 8-6, which shows that the predicted altitude loss remains virtually the same for the assumed roll rates of $\dot{\phi}=12.5^{\circ}$/sec, $\dot{\phi}=10.0^{\circ}$/sec and $\dot{\phi}=7.5^{\circ}$/sec. The resulting relative differences in required altitude loss are in the order of ±0.6 percent, and trivial. Therefore, the proposed method is not sensitive to assumed roll rate, and is promising for real-world applications.

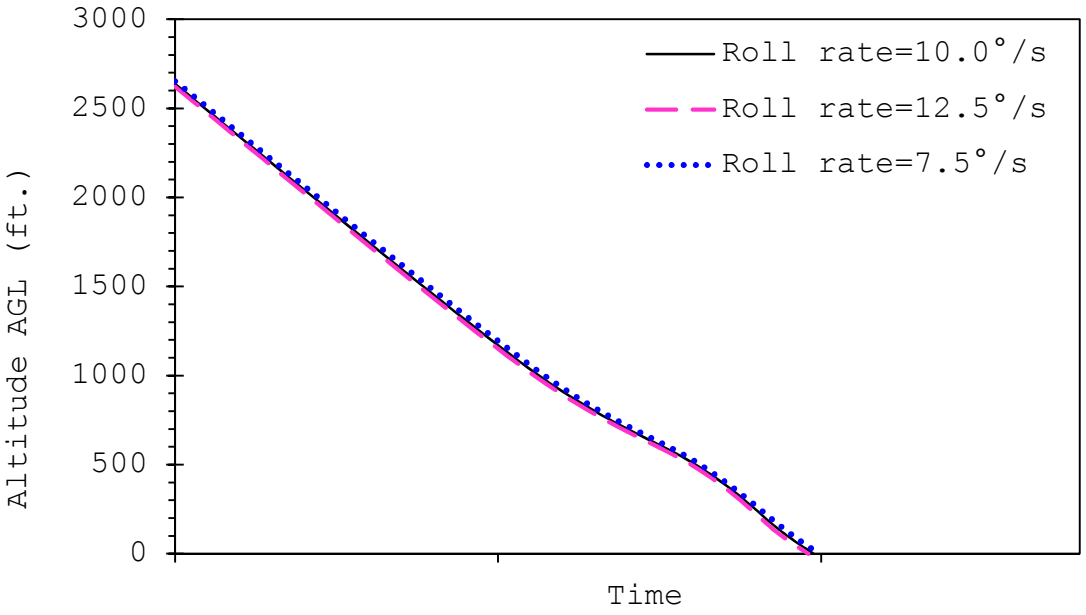

(a)

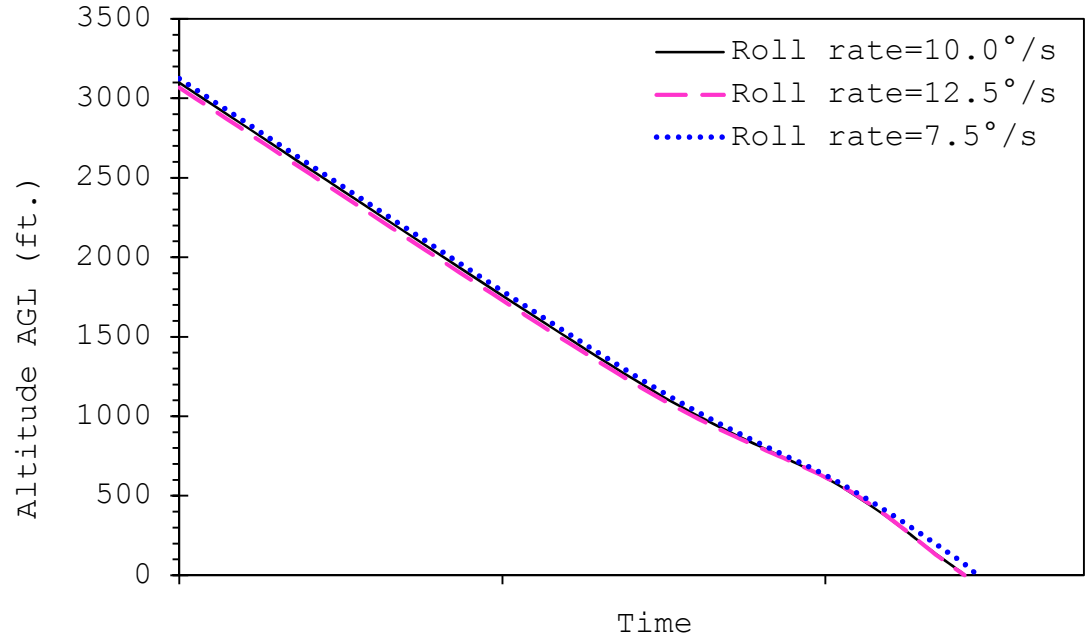

(b)

Figure 8-6. Relationship between predicted altitude above ground level vs. time for the optimum engines-out landing trajectory (a) at 160 KCAS and wing configuration "1+F", (b) at 205 KCAS in "clean" configuration (no wind).

8.11 Application of the Segmented Trajectory Generation Algorithm at Other Airspeeds

The segmented trajectory generation algorithm presented in Chapter 7 is applied to the "flaps" scenario and "clean" scenario assuming varying airspeeds to further verify its accuracy. These airspeeds are 170, 180, and 190 KCAS for the "flaps" scenario, and 215, 225, and 235 KCAS for the "clean" scenario. For each airspeed, the procedure described in sections 8.2 through 8.7 is applied to compute the optimum engines-out landing trajectory for landing on Runway 18 both in the absence of wind, and in the presence of wind. The simulated wind is 0°[††] at 10 knots, and it acts as "tailwind" during a landing maneuver on Runway 18. Since the maximum allowable tailwind component is 10 knots for the Airbus A320 aircraft during landing, the simulated tailwind speed is limited to 10 knots. Crosswind (i.e. 90°- or 270°-wind) and headwind (i.e. 180°-wind) components for landing on Runway 18 are not simulated because:

- In the presence of crosswind, the rudder of the aircraft may have to be employed. If the rudder is not in neutral position, it would result in increased drag, somewhat lowering the engines-out glide ratio of the aircraft compared to when it is in neutral position. In this study, engines-out landing maneuver in the presence of crosswind component is not simulated due to budget constraints.
- Both the "flaps" and "clean" scenarios start with takeoff from Runway 36. A headwind component for landing on Runway 18 would act as a tailwind component for takeoff from Runway 36. This would render the simulated total-loss-of-

[††] The direction from which the wind blows is 0°.

thrust scenario somewhat unrealistic because aircraft typically takes off into the wind.

The computed optimum engines-out landing trajectories at the other airspeeds are presented in section A.1 for the “flaps” scenario, and in section A.2 for the “clean” scenario. Flight simulation tests are conducted as described in section 8.8 to compare the predicted altitude loss with the simulated altitude loss required to fly a given landing trajectory. Comparison of the predicted vs. simulated altitude loss is presented for each airspeed in the last row of Tables A-1 through A-4. The results given in Tables A-1 through A-4 show that the segmented trajectory generation algorithm can predict the altitude loss required to follow a given trajectory within 1.5–3.6 percent error for the Airbus A320 aircraft. Hence, the accuracy of the segmented trajectory algorithm is promising for real-world use on the Airbus A320 aircraft.

8.12 Summary

This chapter demonstrated the adaptive flight planning architecture for the A320-200 aircraft. The adaptive flight planner generates an optimum flyable trajectory to a given runway in the occurrence of total loss of thrust. The results show that the method can compute the altitude loss required to fly the trajectory within approximately 1.6 to 3.5 percent error. An uncertainty analysis also reveals that the method is not sensitive to modeling assumptions such as the assumed roll rate. Therefore, the proposed method is promising for real-world applications on the Airbus A320 aircraft.

CHAPTER 9 - ADAPTIVE FLIGHT PLANNING ARCHITECTURE FOR THE BOEING 737-800 AIRCRAFT

This chapter demonstrates the architecture of the adaptive flight planner through two realistic total-loss-of-thrust scenarios for the 737-800 aircraft. The chapter also describes the flight simulation tests conducted in a JAR-FSTD A Level D full flight simulator to validate the accuracy of the optimum landing trajectories.

9.1 Total Loss of thrust Scenario

This chapter assumes basically the same bird strike scenarios as the ones presented in section 8.1: the "flaps" scenario and "clean" scenario. However, the aircraft type is Boeing 737-800 instead of the A320. For the Boeing 737-800 aircraft, the "flaps" scenario is assumed as follows:

1. A Boeing 737-800 performs a northbound takeoff from Runway 36 shown in Figure 8-1, and starts the initial climb-out. The runway is at sea level, and the assumed wing configuration of the 737-800 is "Flaps=5" during the take-off.
2. During the phase of climb, flap reduction on the 737-800 aircraft may occur as early as 800 ft AGL [106]. However, it is assumed that flap retraction is scheduled to occur at 3,000 ft AGL at the time of the departure in accordance with ICAO's noise abatement departure procedure for close-in noise monitors [120].
3. During the initial climb-out before the flaps are retracted, the 737-800 encounters a flock of birds, and multiple birds are ingested into both engines.

4. Both engines of the 737-800 undergo total loss of thrust at a distance of 2.0 nautical miles (nm) north of Runway 18 while the aircraft is heading north (i.e. 0°; see Figure 8-1). At this exact location, the aircraft weighs 70.0 tons, and the turn-back maneuver to Runway 18 is initiated.
5. It is assumed that the 737-800 does not have sufficient hydraulic power to change the wing configuration due to the dual-engine failure. Thus, the wing configuration remains at "Flaps=5" throughout the landing maneuver.
6. Since the flaps cannot be extended, the landing speed should be greater than typical landing speeds. It is assumed that the pilots maintain 155 KCAS throughout the landing maneuver, which approximately equals the minimum maneuver speed (i.e. V_{LS}) in this particular configuration. Thereby, the pilots maximize the time aloft, and minimize the runway length requirements for landing roll.

On the other hand, the "clean scenario" is summarized as follows:

1. A Boeing 737-800 performs a northbound takeoff from Runway 36 shown in Figure 8-1, and starts the initial climb-out. The runway is at sea level.
2. It is assumed that flap retraction is scheduled to occur at 1,000 ft AGL at the time of the departure in accordance with ICAO's noise abatement departure procedure for far-out noise monitors [120].
3. After the flaps are retracted, the 737-800 encounters a flock of birds, and multiple birds are ingested into both engines.
4. Both engines of the 737-800 undergo total loss of thrust at a distance of 3.0 nautical miles (nm) north of Runway 18 while the aircraft is heading north (i.e. 0°; see Figure

8-1). At this exact location, the aircraft weighs 70.0 tons, and the turn-back maneuver to Runway 18 is initiated.

5. It is assumed that the 737-800 does not have sufficient hydraulic power to change the wing configuration due to the dual-engine failure. Thus, the aircraft is in "clean" configuration throughout the landing maneuver.
6. Since the flaps cannot be extended, the landing speed is greater than typical landing speeds. It is assumed that the pilots maintain 200 KCAS throughout the landing maneuver, which is slightly above the minimum maneuver speed (i.e. V_{LS}) in this particular configuration. Thereby, the pilots attempt to maximize the time aloft, and minimize the runway length requirements for landing roll.

9.2 Input Data

For the "flaps scenario", the required input data is the engines-out glide ratio of the Boeing 737-800 aircraft in wing configuration "5" at 155 KCAS for the bank angles of 0°, 10°, 20°, and ϕ_{max} =30°. These data are assessed in Chapter 6, and presented in Figure 6-2. The data are re-plotted in Figure 9-2 with the engines-out glide ratio in the vertical axis, and bank angle on the horizontal axis. Likewise for the "clean scenario", the required input data is the engines-out glide ratio of the Boeing 737-800 aircraft at 200 KCAS for the bank angles of 0°, 10°, 20°, and ϕ_{max} =30°. These data are assessed in Chapter 6, and presented in Figure 6-3. The data are re-plotted in Figure 9-2 with the engines-out glide ratio in the vertical axis, and bank angle on the horizontal axis. As shown in Figure 9-2, the engines-out glide ratio at a given airspeed decreases with increasing bank angle because the aircraft loses lift in banked turns and the drag increases [23].

A piece-wise continuous, third-degree polynomial function is fitted to the data for each airspeed in Figure 9-2 using the least squares estimation method [128]. The resulting polynomial function is given in Equation (9-1) for the "flaps scenario", and in Equation (9-2) for the "clean scenario":

$$\cot(\gamma)_{v,\phi} = 0.000078 * \phi^3 - 0.006328 * \phi^2 + 0.023180 * \phi + 14.0 = f(\phi) \quad (9\text{-}1)$$
$$v = 155\ KCAS,\ 0° \leq \phi \leq 30°$$

$$\cot(\gamma)_{v,\phi} = -0.000071 * \phi^3 - 0.000026 * \phi^2 - 0.035390 * \phi + 17.7 = f(\phi) \quad (9\text{-}2)$$
$$v = 200\ KCAS,\ 0° \leq \phi \leq 30°$$

Both Equation (9-1) and Equation (9-2) return a coefficient of determination, $R^2 = 1.0$. These equations are plotted in Figure 9-2, and are used as the aircraft-specific input data to formulate the optimization problem.

9.3 Modeling Assumptions

The modelling assumptions mentioned in section 8.3 are incorporated into the optimization problem as follows:

1. The aerodynamic roll rate of the 737-800 aircraft equals $\dot{\phi}$ =10°/sec.
2. Although bank angles greater than 30° may be used on the Boeing 737-800, bank angles exceeding 30° are not considered in this study because Boeing does not recommend bank angles exceeding 30° in any normal or non-normal conditions [124]. Therefore, all results presented in this study are valid for a maximum allowable bank angle of 30° on the Boeing 737-800 aircraft.
3. Once the flight crew configures "landing gear down", it takes no longer than 15 seconds for the landing gear to be fully extended and locked.

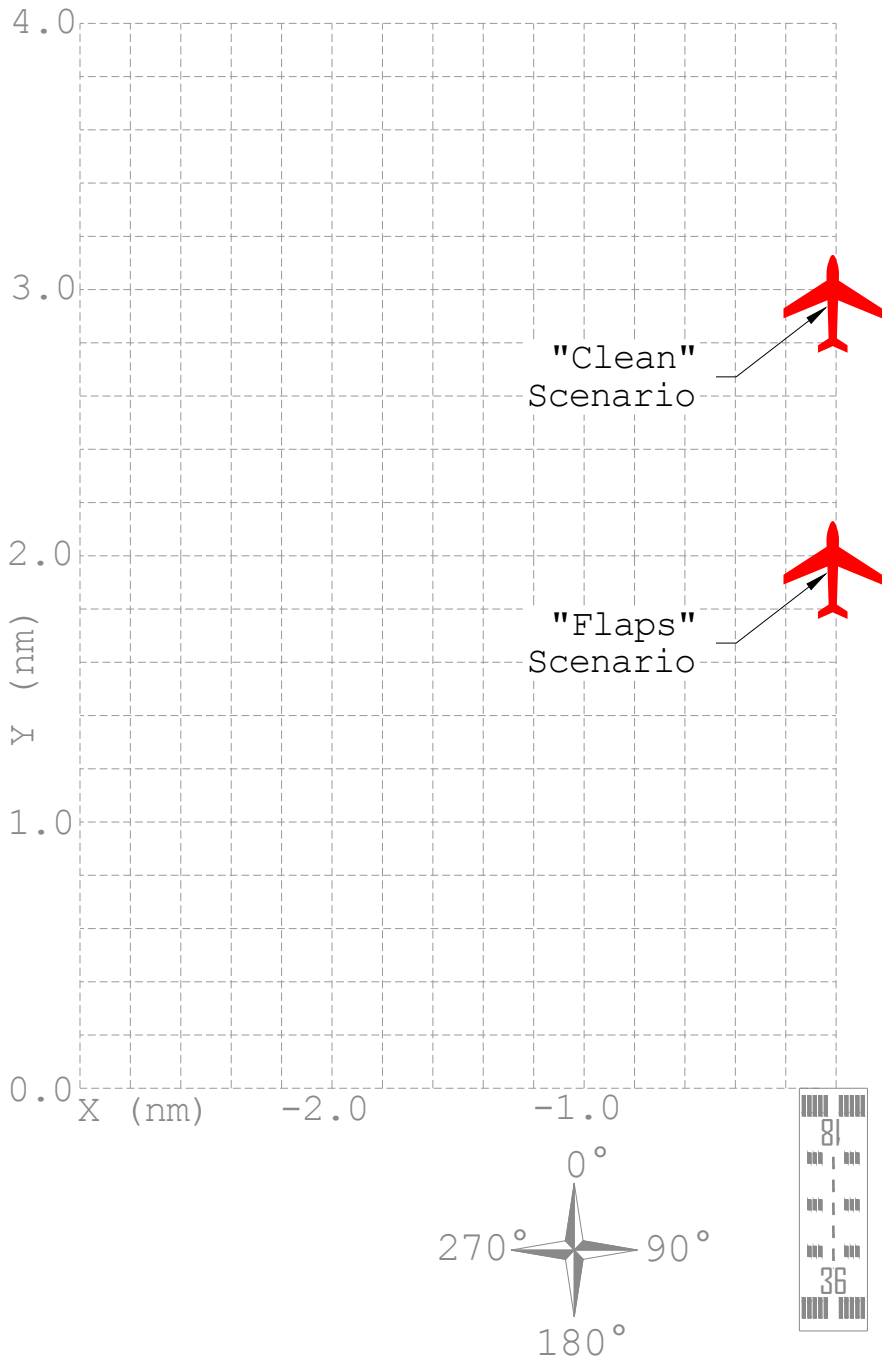

Figure 9-1. Aircraft location at the instant of total loss of thrust (aircraft and runway not drawn to scale).

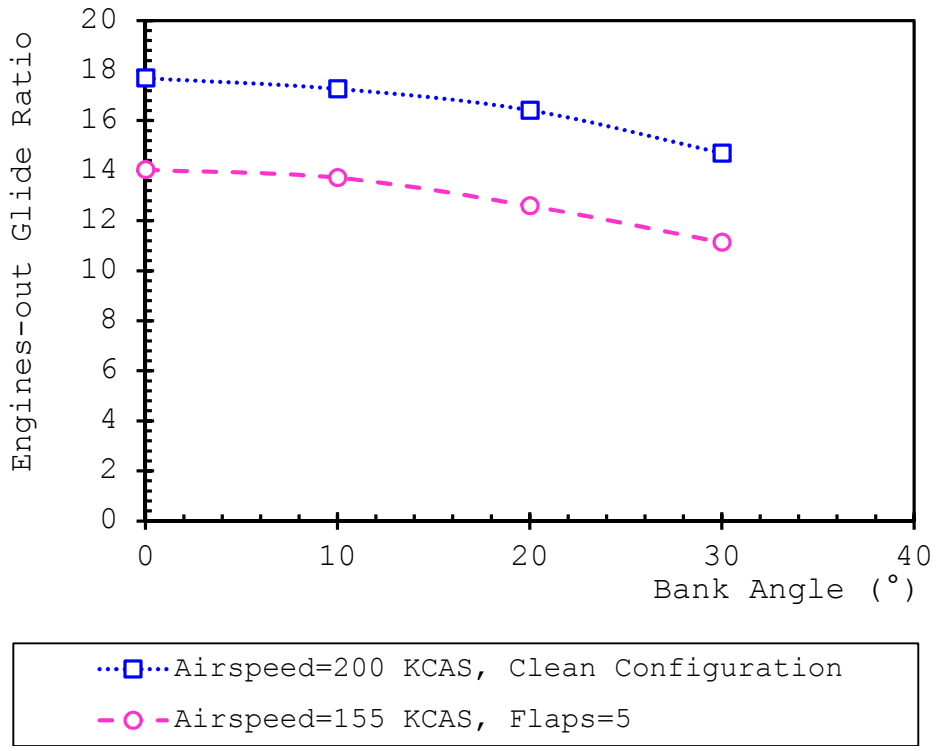

Figure 9-2. Predicted engines-out glide ratio for the 737-800 aircraft during steady-speed engines-out descent *(landing gear up, aircraft gross weight=70.0 tons).*

4. The aircraft is aligned with Runway 18 by the time it is 100 ft. above ground level. This allows for the insertion of a "final approach waypoint", which precedes a stabilizing final approach segment. The landing trajectory is to be generated from the initial aircraft state to this "final approach waypoint".
5. The pilots configure "landing gear down" no later than 15 seconds before the aircraft reaches the "final approach waypoint".
6. Standard day conditions prevail during the engines-out landing. No wind prevails during the emergency landing.

The first and the second assumptions are based on the observations made in the JAR-FSTD A, Level D full flight

simulator. The third assumption basically prohibits banked turns below 100 ft to prevent possible wingtip collisions with ground objects. The fourth assumption enables sufficient time for landing gear extension prior to touchdown. In the full flight simulator, when the landing gear is fully extended in wings-level flight, the resultant reduction in the engines-out glide ratio is measured as approximately 16% at 155 KCAS in wing configuration "5", and 17% at 200 KCAS in "clean" configuration.

9.4 Objective Function

The objective function minimizes the altitude loss required for the Boeing 737-800 to glide from the initial aircraft location to the "final approach waypoint". Equation (9-3) gives the "initial" objective function, in which all v_T terms are temporarily replaced with v =155 KCAS since the v_T values are initially unknown. All equations in this chapter are presented without dimensional homogeneity for reader-friendliness:

$$\min_{S_{L_i},\Delta\theta_j,\phi_j} \sum_i \left[\frac{S_{L_i}}{14.0}\right] + \sum_j \left[\frac{\Delta\theta_j * \pi}{180^\circ} * \frac{(155\ kt)^2}{(9.81 m/s^2) * tan\phi_j} * \frac{1}{f(\phi_j)}\right] + 2 * \sum_{j=1}^{3} \left[\frac{\phi_j}{10^\circ/\text{sec}} * \frac{2*(155\ kt)}{f(\phi_j)+14.0}\right] \quad (9\text{-}3)$$

where $f(\phi_j)$ is given in Equation (9-1), and 14.0 equals the predicted steady-speed engines-out glide ratio in wings-level flight in this particular configuration, which is found from $f(0^\circ)$ in Equation (9-1).

Likewise for the "clean" scenario, Equation (9-4) gives the "initial" objective function, in which all v_T terms are temporarily replaced with v =200 KCAS since the v_T values are initially unknown:

$$\min_{S_{L_i},\Delta\theta_j,\phi_j} \sum_i \left[\frac{S_{L_i}}{17.7}\right] + \sum_j \left[\frac{\Delta\theta_j * \pi}{180^\circ} * \frac{(200\ kt)^2}{(9.81 m/s^2) * tan\phi_j} * \frac{1}{f(\phi_j)}\right] + 2 * \sum_{j=1}^{3} \left[\frac{\phi_j}{10^\circ/\text{sec}} * \frac{2*(200\ kt)}{f(\phi_j)+17.7}\right] \quad (9\text{-}4)$$

where $f(\phi_j)$ is given in Equation (9-2), and 17.7 equals the predicted steady-speed engines-out glide ratio in wings-level flight in this particular configuration, which is found from $f(0°)$ in Equation (9-2).

9.5 Constraints

As mentioned in section 9.3, it is assumed that the aircraft is situated 100 ft above ground level by the time it is aligned with Runway 18. This state is represented by a "final approach waypoint", which projects onto the beginning of Runway 18 threshold. The engines-out landing trajectory is generated from the initial aircraft state to the "final approach waypoint". The resultant geometric constraints for the optimization problem are formulated as follows:

$$\sum_{i=1}^{4} \Delta X_{L_i} + \sum_{j=1}^{3} \Delta X_{C_j} + \sum_{j=1}^{3} \left(\Delta X_{T_{j,j}} + \Delta X_{T_{j,j+1}} \right) = 0.00\ nm \quad (9\text{-}5a)$$

$$\sum_{i=1}^{4} \Delta Y_{L_i} + \sum_{j=1}^{3} \Delta Y_{C_j} + \sum_{j=1}^{3} \left(\Delta Y_{T_{j,j}} + \Delta Y_{T_{j,j+1}} \right) = \Delta Y \quad (9\text{-}5b)$$

$$\sum_{j=1}^{3} \Delta\theta_{C_j} + \sum_{j=1}^{3} \left(\Delta\theta_{T_{j,j}} + \Delta\theta_{T_{j,j+1}} \right) = 180° \quad (9\text{-}5c)$$

where ΔY equals -2.0 nm for the "flaps" scenario, and -3.0 nm for the "clean" scenario. As mentioned in section 7.3.7, all v_T terms are initially replaced with v =155 KCAS for the "flaps" scenario, and v =200 KCAS for the "clean" scenario at this stage of the optimization problem. For example in formulating the "flaps" scenario, the term $\Delta\theta_{T_{j,j}}$ in Equation (9-5c) is initially formulated as $\Delta\theta_{T_{j,j}} = \frac{\phi_j}{10°/sec} * \frac{(9.81 m/s^2) * tan\phi_j}{2*(155\ kt)}$ where v_T in Equation (7-8a) is temporarily substituted with $v = 155\ kt$.

9.6 Solutions

The optimum solution is computed using the differential evolution algorithm [133]. Since the optimization problem is formulated over a continuous domain, the global optimum solution is computed [132]. Step-by-step findings from the optimization problem are given in Table 9-1.

9.6.1 "Flaps" Scenario

To proceed with the second stage of the iterative procedure, the following steps are followed in the "flaps" scenario:

1. Using the initial solution, the terms in Equation (7-13) are computed based on Equations (7-3a), (7-3b), and (7-3c) as follows: $\Delta Z_{C_1} = 1202'$, $\Delta Z_{C_2} = 161'$, $\Delta Z_{T_{1,1}} = \Delta Z_{T_{1,2}} = 62'$, $\Delta Z_{T_{2,2}} = \Delta Z_{T_{2,3}} = 62'$, $\Delta Z_{L_2} = 558'$ and all other terms are equal to 0.
2. Since the runway is located at sea level, $E_{Touchdown} = 0$, and the mid-elevation of each circular segment is computed as follows:

   $\bar{E}'_{C_1} = 100' + 2 * 62' + 161' + 558' + 62' + 1202'/2 = 1606'$, and

   $\bar{E}'_{C_2} = 100' + 62' + 161'/2 = 242'$. The $100'$ is incorporated into the calculations to account for the third modeling assumption given in 9.3.
3. The average true airspeed for each circular segment is computed from Equation (7-14):

   $\bar{v}_{T,1} \approx (155\ kt) * 1.015^{(1606'/1000')} = 158.7\ kt$

   $\bar{v}_{T,2} \approx (155\ kt) * 1.015^{(242'/1000')} = 155.5\ kt$

4. The same optimization problem is formulated by replacing all v_T terms with $\bar{v}_{T,j}$. For example, Equation (7-8a) is modified as $\Delta\theta_{T_{j,j}} = \Delta\theta_{T_{j,j+1}} = \frac{\phi_j}{\dot{\phi}} * \frac{g*tan\phi_j}{2*\bar{v}_{T,j}}$.
5. The second stage of the optimization problem is solved using the differential evolution algorithm [133]. The results are given in the second row of Table 9-1.
6. Using the second solution, the terms in Equation (7-13) are computed based on Equations (7-3a), (7-3b), and (7-3c) as follows: $\Delta Z_{C_1} = 1290'$, $\Delta Z_{C_2} = 189'$, $\Delta Z_{T_{1,1}} = \Delta Z_{T_{1,2}} = 65'$, $\Delta Z_{T_{2,2}} = \Delta Z_{T_{2,3}} = 63'$, $\Delta Z_{L_2} = 489'$ and all other terms are equal to 0.
7. The mid-elevation of each circular segment is computed as follows:

   $\bar{E}'_{C_1} = 100' + 2 * 63' + 189' + 489' + 65' + 1290'/2 = 1614'$, and

   $\bar{E}'_{C_2} = 100' + 63' + 189'/2 = 257'$.

8. The average true airspeed for each circular segment is computed from Equation (7-14):

   $\bar{v}_{T,1} \approx (155\ kt) * 1.015^{(1614'/1000')} = 158.8\ kt$

   $\bar{v}_{T,2} \approx (155\ kt) * 1.015^{(257'/1000')} = 155.6\ kt$

9. Using Equation (7-15), $\bar{d}$ is found as:

$$\bar{d} = \frac{1}{2} * \left\{ \frac{|158.7 - 158.8|}{158.8} * 100 + \frac{|155.5 - 155.6|}{155.6} * 100 \right\} = 0.06\%$$

Since $\bar{d} < 1.0\%$, the convergence criterion is met. The second solution for the "flaps" scenario given in Table 9-1 is the final solution to the optimization problem. Based on the solution, the altitude loss required for following the optimum trajectory equals $100' + 2 * 63' + 189' + 489' + 2 * 65 + 1290' \approx 2320\ ft$. However, this does not include the additional altitude loss due to landing gear extension. The procedure outlined in section

8.6.1 is applied to the findings to predict the additional altitude loss due to landing gear extension. The additional altitude loss due to landing gear extension is predicted as 66 ft. Hence, the total altitude loss required for flying the optimum trajectory is predicted as 2,320 + 66 = 2,386 ft.

9.6.2 "Clean" Scenario

Similarly, the following steps are followed in the "clean" scenario to proceed with the second stage of the iterative procedure:

1. Using the initial solution, the terms in Equation (7-13) are computed based on Equations (7-3a), (7-3b), and (7-3c) as follows: $\Delta Z_{C_1} = 1558'$, $\Delta Z_{C_2} = 247'$, $\Delta Z_{T_{1,1}} = \Delta Z_{T_{1,2}} = 62'$, $\Delta Z_{T_{2,2}} = \Delta Z_{T_{2,3}} = 62'$, $\Delta Z_{L_2} = 658'$ and all other terms are equal to 0.
2. Since the runway is located at sea level, $E_{Touchdown} = 0$, and the mid-elevation of each circular segment is computed as follows:

   $\bar{E}'_{C_1} = 100' + 2 * 62' + 247' + 658' + 62' + 1558'/2 = 1970'$, and

   $\bar{E}'_{C_2} = 100' + 62' + 247'/2 = 286'$. The $100'$ is incorporated into the calculations to account for the third modeling assumption given in 9.3.
3. The average true airspeed for each circular segment is computed from Equation (7-14):

   $\bar{v}_{T,1} \approx (200\ kt) * 1.015^{(1970'/1000')} = 205.9\ kt$

   $\bar{v}_{T,2} \approx (200\ kt) * 1.015^{(286'/1000')} = 200.8\ kt$
4. The same optimization problem is formulated by replacing all v_T terms with $\bar{v}_{T,j}$. For example, Equation (7-8a) is modified as $\Delta\theta_{T_{j,j}} = \Delta\theta_{T_{j,j+1}} = \frac{\phi_j}{\dot{\phi}} * \frac{g*tan\phi_j}{2*\bar{v}_{T,j}}$.

5. The second stage of the optimization problem is solved using the differential evolution algorithm [133]. The results are given in the second row of Table 9-1.
6. Using the second solution, the terms in Equation (7-13) are computed based on Equations (7-3a), (7-3b), and (7-3c) as follows: $\Delta Z_{C_1} = 1691'$, $\Delta Z_{C_2} = 288'$, $\Delta Z_{T_{1,1}} = \Delta Z_{T_{1,2}} = 66'$, $\Delta Z_{T_{2,2}} = \Delta Z_{T_{2,3}} = 63'$, $\Delta Z_{L_2} = 579'$ and all other terms are equal to 0.
7. The mid-elevation of each circular segment is computed as follows:

   $\bar{E}'_{C_1} = 100' + 2 * 63' + 288' + 579' + 66' + 1691'/2 = 2005'$, and

   $\bar{E}'_{C_2} = 100' + 63' + 288'/2 = 307'$.

8. The average true airspeed for each circular segment is computed from Equation (7-14):

   $\bar{v}_{T,1} \approx (200\ kt) * 1.015^{(2005'/1000')} = 206.1\ kt$

   $\bar{v}_{T,2} \approx (200\ kt) * 1.015^{(307'/1000')} = 200.9\ kt$

9. Using Equation (7-15), $\bar{d}$ is found as:

$$\bar{d} = \frac{1}{2} * \left\{ \frac{|205.9 - 206.1|}{206.1} * 100 + \frac{|200.8 - 200.9|}{200.9} * 100 \right\} = 0.07\%$$

Since $\bar{d} < 1.0\%$, the convergence criterion is met. The second solution for the "clean" scenario given in Table 9-1 is the final solution to the optimization problem. Based on the solution, the altitude loss required for following the optimum trajectory equals $100' + 2 * 63' + 288' + 579' + 2 * 66' + 1691' \approx 2916\ ft$. However, this does not include the additional altitude loss due to landing gear extension. The procedure outlined in section 8.6.1 is applied to the findings to predict the additional altitude loss due to landing gear extension. The additional altitude loss due to landing gear extension is predicted as 87

ft. Hence, the total altitude loss required for flying the optimum trajectory is predicted as 2,916 + 87 = 3,003 ft.

9.7 Interpretation of the Optimum Trajectory

Figure 9-3 illustrates the ground tracks of the optimum landing trajectories, both of which indicate a tear-drop shaped pattern. For a given total-loss-of-thrust scenario, the optimum landing trajectory is divided into four distinct flight phases. For the "flaps" scenario, these flight phases are briefly explained as follows:

1. An initial left-turn with 30° bank, where the absolute change in aircraft heading equals 225°.
2. A wings-level, equilibrium glide for a horizontal distance of 1.1 nm.
3. A final 40°-right turn at 30° bank that aligns the aircraft with Runway 18.
4. Landing flare and safe touchdown on Runway 18.

For the "clean" scenario, these flight phases are explained as follows:

1. An initial left-turn with 30° bank, where the absolute change in aircraft heading equals 229°.
2. A wings-level, equilibrium glide for a horizontal distance of 1.7 nm.
3. A final 49°-right turn at 30° bank that aligns the aircraft with Runway 18.
4. Landing flare and safe touchdown on Runway 18.

Table 9-1. Numeric solutions to the optimization problem for (a) "flaps" scenario, (b) "clean" scenario on the Boeing 737-800 aircraft (no wind).

		"Flaps" scenario		"Clean" scenario	
	No. of Iteration	1	2	1	2
Optimum Trajectory	S_{L_1} (nm)	0	0	0	0
	$\Delta\theta_1$ $(^\circ)$	-220	-225	-224	-229
	ϕ_1 $(^\circ)$	30	30	30	30
	S_{L_2} (nm)	1.3	1.1	1.9	1.7
	$\Delta\theta_2$ $(^\circ)$	40	45	44	49
	ϕ_2 $(^\circ)$	30	30	30	30
	S_{L_3} (nm)	0	0	0	0
	$\Delta\theta_3$ $(^\circ)$	0	0	0	0
	ϕ_3 $(^\circ)$	N/A	N/A	N/A	N/A
	S_{L_4} (nm)	0	0	0	0
Convergence Criterion	$\bar{v}_{T,1}$ (kt)	158.7	158.8	205.9	206.1
	$\bar{v}_{T,2}$ (kt)	155.5	155.6	200.8	200.9
	$\bar{v}_{T,3}$ (kt)	N/A	N/A	N/A	N/A
	$\bar{d}$ $(\%)$	N/A	0.03	N/A	0.07

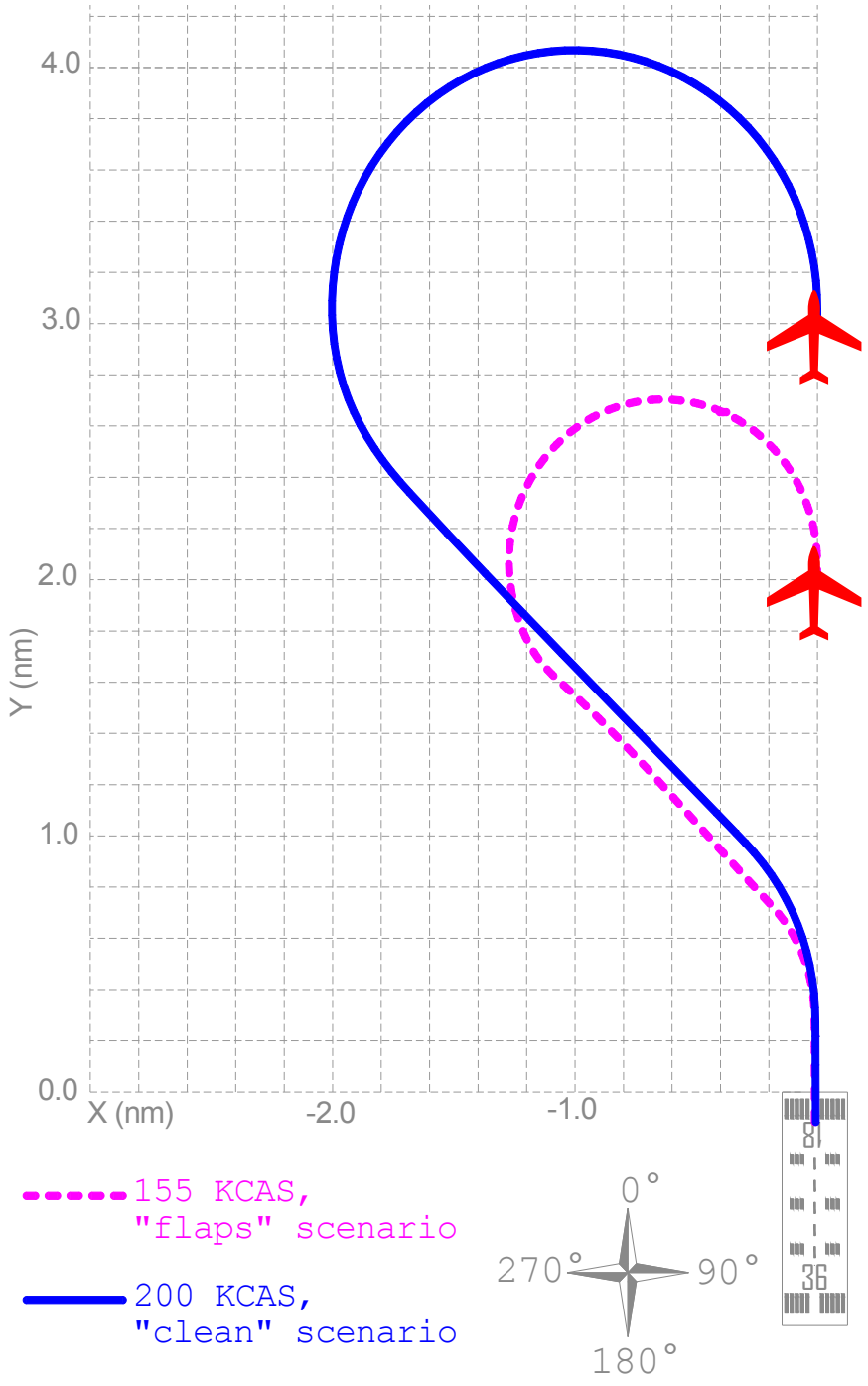

Figure 9-3. Ground tracks for the optimum engines-out landing trajectories for the Boeing 737-800 aircraft (no wind).

9.8 Validation of the Results

Flight simulation tests are conducted to find out if the kinematic approach to segmented-trajectory generation accurately estimates the required altitude loss plotted in Figure 8-4. The simulations are conducted in a JAR-FSTD A, Level D full flight simulator that is certified under the European Aviation Safety Agency (EASA) and Joint Aviation Authorities (JAA). Three type-rated Boeing 737NG pilots participated in the flight simulation tests. The simulation of the "flaps" scenario starts with freezing the aircraft position at 2.0 nm north of runway 18 threshold at an altitude of 2,400 ft. AGL. On the other hand, the simulation of the "clean" scenario starts with freezing the aircraft position 3.0 nm north of runway 18 threshold at an altitude of 3,100 ft. The aircraft weight is frozen at 70.0 tons throughout the simulations. The aircraft heading is initially frozen at 0°, and the landing gear is initially fully retracted. The wing configuration is set at "5" in simulating the "flaps" scenario, and is set to "clean" configuration in simulating the "clean" scenario. The full flight simulator is programmed to simulate dual-engine failure on the 737-800. When dual-engine failure results in total loss of thrust, both the aircraft position and aircraft heading are "released", and the aircraft starts engines-out glide at 155 KCAS in simulating the "flaps" scenario, and at 200 KCAS in simulating the "clean" scenario. From this moment on, one of the three type-rated Boeing 737NG pilots flies the aircraft while one member of the research team issues simplified oral commands to make the pilot follow the optimum landing trajectory illustrated in Figure 9-3. In simulating the "flaps" scenario, the following oral commands are issued to the pilot in control:

- Turn left heading 135° with 30° bank. Maintain 155 kt.
- Maintain present heading and speed. Descend to 500′.
- Turn right heading 180° with 30° bank. Maintain 155 kt. Landing gear down.
- Clear to land on Runway 18.

In simulating the "clean" scenario, the following oral commands are issued to the pilot in control:

- Turn left heading 131° with 30° bank. Maintain 200 kt.
- Maintain present heading and speed. Descend to 700′.
- Landing gear down. Turn right heading 180° with 30° bank. Maintain 200 kt.
- Clear to land on Runway 18.

These oral commands are generated using the procedure described in section 8.8. After each run, the simulator plots the ground tracks and descent profile of the 737-800. Using the plots of the ground tracks, the research team verifies that the landing trajectory is simulated properly. Using the plots of the descent profile, the research team measures the total altitude loss (rounded up to the nearest 50′) from the initial aircraft position to the northern threshold of Runway 18. The average simulated altitude loss is found as: $\frac{2300'+2300'+2300'}{3} = 2300\,ft$ for the "flaps" scenario, which differs from the predicted altitude loss of 2,394 ft by 4.1 percent. Similarly, the average simulated altitude loss is found as: $\frac{2900'+2850'+2850'}{3} = 2867\,ft$ for the "clean" scenario, which differs from the predicted altitude loss of 3003 ft by 4.7 percent. In both scenarios, the kinematic method marginally overestimated the required altitude loss. The probable cause for the overestimation of required altitude loss is outlined in section 8.9. Since the rate of error is marginal

and the error is on the "safe" side, it is concluded that the kinematic trajectory optimization method described in Chapter 7 can accurately estimate the altitude loss required for gliding to an intended touchdown location.

9.9 Uncertainty Analysis

The section explores how the required altitude loss would change when different roll rates are assumed. For this purpose, the optimum trajectory is re-computed assuming roll rates of $\dot{\phi}$ =12.5°/sec, and $\dot{\phi}$ =7.5°/sec. The resulting altitude vs. time histories are plotted in Figure 9-4, which shows that the predicted altitude loss remains virtually the same for the assumed roll rates of $\dot{\phi}$ =12.5°/sec, $\dot{\phi}$ =10.0°/sec and $\dot{\phi}$ =7.5°/sec. The resulting relative differences in required altitude loss are in the order of ±0.5 percent, and trivial. Therefore, the proposed method is not sensitive to assumed roll rate, and is promising for real-world applications.

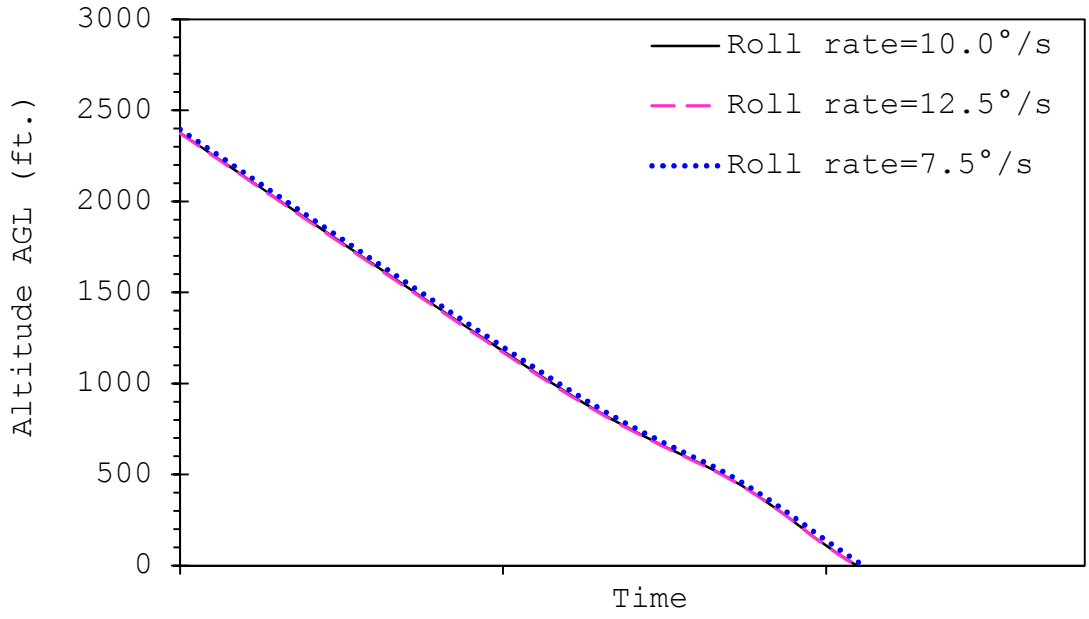

(a)

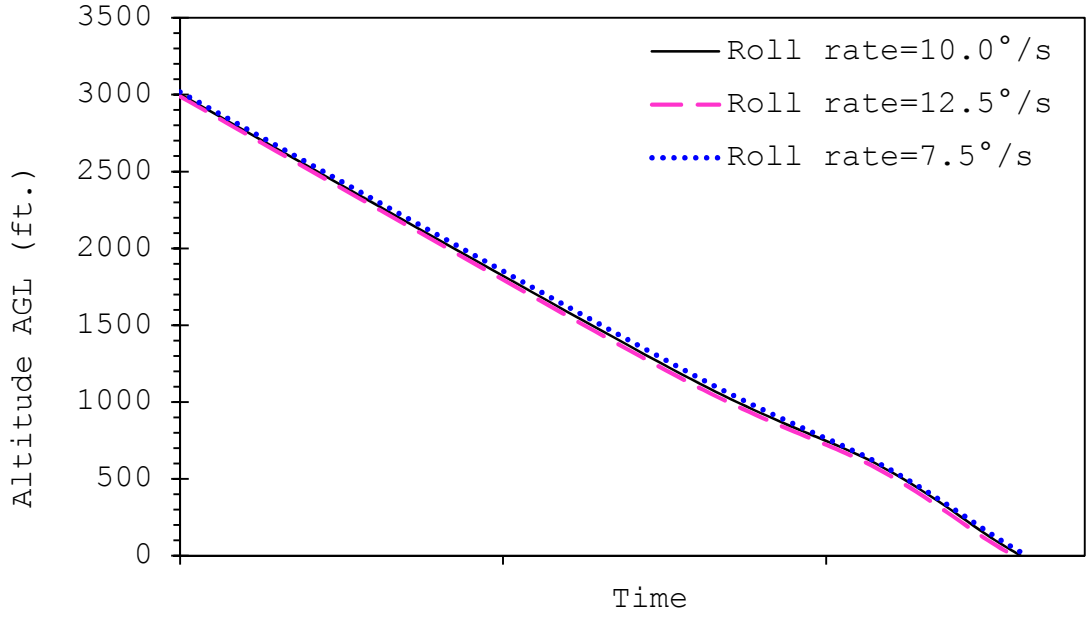

(b)

Figure 9-4. Relationship between predicted altitude above ground level vs. time for the optimum engines-out landing trajectory (a) at 155 KCAS and wing configuration "5", (b) at 200 KCAS in "clean" configuration (no wind).

9.10 Application of the Segmented Trajectory Generation Algorithm at Other Airspeeds

The segmented trajectory generation algorithm presented in Chapter 7 is applied to the "flaps" scenario and "clean" scenario assuming varying airspeeds to further verify its accuracy. These airspeeds are 165, 175, and 185 KCAS for the "flaps" scenario, and 210, 220, and 230 KCAS for the "clean" scenario. For each airspeed, the procedure described in sections 6 through 9.7 is applied to compute the optimum engines-out landing trajectory for landing on Runway 18 both in the absence of wind, and in the presence of wind. The simulated wind is 0°[‡‡] at 15 knots, and it acts as "tailwind" during a landing maneuver on Runway 18. The maximum allowable tailwind component is 15[§§] knots for the Boeing 737-800 aircraft during landing, the simulated tailwind speed is limited to 15 knots. Crosswind (i.e. 90°- or 270°-wind) and headwind (i.e. 180°-wind) components for landing on Runway 18 are not simulated because of the same reasons outlined in section 8.11.

The computed optimum engines-out landing trajectories at the other airspeeds are presented in section B.1 for the "flaps" scenario, and in section B.2 for the "clean" scenario. Flight simulation tests are conducted as described in section 9.7 to compare the predicted altitude loss with the simulated altitude loss required to fly a given landing trajectory. Comparison of the predicted vs. simulated altitude loss is presented for each airspeed in the last row of Tables B-1 through B-4. The results given in Tables B-1 through B-4 show that the segmented

---

[‡‡] The direction from which the wind blows is 0°.

[§§] For approved airfields and/ or type ratings.

trajectory generation algorithm can predict the altitude loss required to follow a given trajectory within 3.7–5.1 percent relative error for the Boeing 737-800 aircraft. Hence, the accuracy of the kinematic trajectory optimization is promising for real-world use on the Boeing 737-800 aircraft.

9.11 Summary

This chapter demonstrated the adaptive flight planning architecture for the Boeing 737-800 aircraft. The adaptive flight planner generates an optimum flyable trajectory to a given runway in the occurrence of total loss of thrust. The results show that the method can compute the altitude loss required to fly the trajectory within 3.7 to 5.1 percent error. An uncertainty analysis also reveals that the method is not sensitive to modeling assumptions such as the assumed roll rate. Therefore, the proposed method is promising for real-world applications on the Boeing 737-800 aircraft.

The purpose of the flight simulation tests explained in chapters 8 and 9 is to assess the accuracy of the kinematic trajectory optimization method. The kinematic method predicts the required altitude loss from the instant the pilots initiate the landing maneuver until touchdown occurs at the intended landing site. Therefore, variations in pilot response time are not considered in the flight simulation tests.

CHAPTER 10 - A DESIGNED EXPERIMENT TO ASSESS THE EFFECTIVENESS OF ADAPTIVE FLIGHT PLANNING

10.1 Research Question and Significance of the Research

The findings in Chapter 4 demonstrated that total loss of thrust due to bird strike is statistically most likely to occur during the initial climb-out at altitudes below 5,000 ft AGL. If aircraft undergoes total loss of thrust during the initial climb-out, it may not have sufficient altitude to return to departure runway. Consequently, the flight crew may have to search for an alternative landing site within the current heading of the aircraft, as in the case of Scandinavian Airlines Flight #751 [35] and U.S. Airways Flight #1549 [7]. However, there are circumstances where flight crews may have to attempt a turn-back maneuver to departure runway. For instance, if the airport environment is surrounded by inhospitable terrain or large bodies of water, returning to departure runway can significantly increase survivability and prevent hull loss [136]. In such emergency situations, the odds of reaching the departure runway depends on the total aerodynamic energy of the aircraft as well as the expertise of the flight crew. However, current pilot type-rating programs do not require simulated total loss of thrust at a low altitude [19, 20]. Likewise, the engine dual failure checklist of the A320 aircraft is not intended for total loss of thrust at a low altitude [7]. Therefore, this chapter hypothesizes the following:

- The current pilot type-rating programs and emergency checklists do not suffice for managing a total-loss-of-

thrust emergency that occurs at a low altitude (i.e. below 5,000 ft AGL),

- An adaptive flight planner can significantly increase the probability of a safe touchdown in the occurrence of total loss of thrust that occurs at a low altitude.

In order to test the research hypotheses, this chapter undertakes the following tasks:

- Develop realistic aircraft-bird strike scenarios that result in total loss of thrust for the struck commercial aircraft.
- Simulate the bird strike scenario in a JAR-FSTD A, Level D full flight simulator that is certified under the Joint Aviation Authorities (JAA).
- Conduct a designed experiment in the full flight simulator with real-life pilots to test the research hypotheses.

The research hypotheses tested in this chapter can open the door for commercial aircraft manufacturers approach the rising hazard of total loss of thrust. Due to the growing threat of bird strikes and the prevalence of twin-engine aircraft with reduced engine redundancy, it has become a pressing need to address this safety issue. If the use of the proposed adaptive flight planner is found effective, commercial aircraft manufacturers may undertake steps to incorporate it into glass cockpit technologies.

10.2 Simulated Scenarios for Total Loss of Thrust

As mentioned in section 4.4.1, engine failure due to bird strike is statistically most likely to occur during the phase of climb at lower altitudes *(i.e. below 5,000 ft.)* and in twilight

conditions. Considering this, all total-loss-of-thrust scenarios are simulated during the phase of climb below 5,000 ft AGL and in twilight conditions. The designed experiment involves four total-loss-of-thrust scenarios. The first and the second scenarios are simulated in virtual environment of Amsterdam Schiphol International Airport[***], which is located -11 ft AMSL [137]. The third and the fourth scenarios are simulated in virtual environment of Istanbul Atatürk International Airport[†††], which is located 163 ft AMSL [138]. These total-loss-of-thrust scenarios are explained in the following subsections.

10.2.1 Total-Loss-of-Thrust Scenario #1

The first total-loss-of-thrust scenario is assumed to occur as follows:

1. An A320 or 737-800 aircraft takes off from Schiphol Airport's runway 36C shown in Figure 10-1 in standard day conditions (no wind). The simulated wing configuration is "1+F" on the A320 aircraft, and flap setting "5" on the 737-800 aircraft. The magnetic heading of this runway is 3°, and flap retraction is scheduled to occur at 3,000 ft AGL in accordance with ICAO's noise abatement departure procedure for close-in noise monitors [120, 137].
2. During the climb prior to flap retraction, the aircraft encounters a flock of birds while it is still heading 3°. Multiple birds are ingested into both engines, and total loss of thrust occurs.
3. The flight crew initiates an engines-out emergency landing attempt at Schiphol Airport. At this instant, the aircraft

[***] IATA Code: AMS. ICAO Code: EHAM.

[†††] IATA Code: IST. ICAO Code: LTBA.

weighs 70.0 tons, and is situated at a linear distance of 2.0 nm from Runway 18C threshold as shown in Figure 10-1.

10.2.2 Total-Loss-of-Thrust Scenario #2

The second total-loss-of-thrust scenario is similar to the first scenario, and it is assumed to occur as follows:

1. An A320 or 737-800 aircraft takes off from Schiphol Airport's runway 06 shown in Figure 10-1 in standard day conditions (no wind). The simulated wing configuration is "1+F" on the A320 aircraft, and flap setting "5" on the 737-800 aircraft. The magnetic heading of this runway is 58°, and flap retraction is scheduled to occur at 3,000 ft AGL in accordance with ICAO's noise abatement departure procedure for close-in noise monitors [120, 137].
2. During the climb prior to flap retraction, the aircraft encounters a flock of birds while it is still heading 58°. Multiple birds are ingested into both engines, and total loss of thrust occurs.
3. The flight crew initiates an engines-out emergency landing attempt at Schiphol Airport. At this instant, the aircraft weighs 70.0 tons, and is situated at a linear distance of 2.0 nm from Runway 24 threshold as shown in Figure 10-1.

Both the first and second total-loss-of-thrust scenarios assume that the distressed aircraft does not have sufficient hydraulic power for flaps extension. Thus, the simulated wing configuration is "1+F" on the A320 aircraft, and the flap setting is "5" on the 737-800 aircraft throughout the engines-out landing attempt.

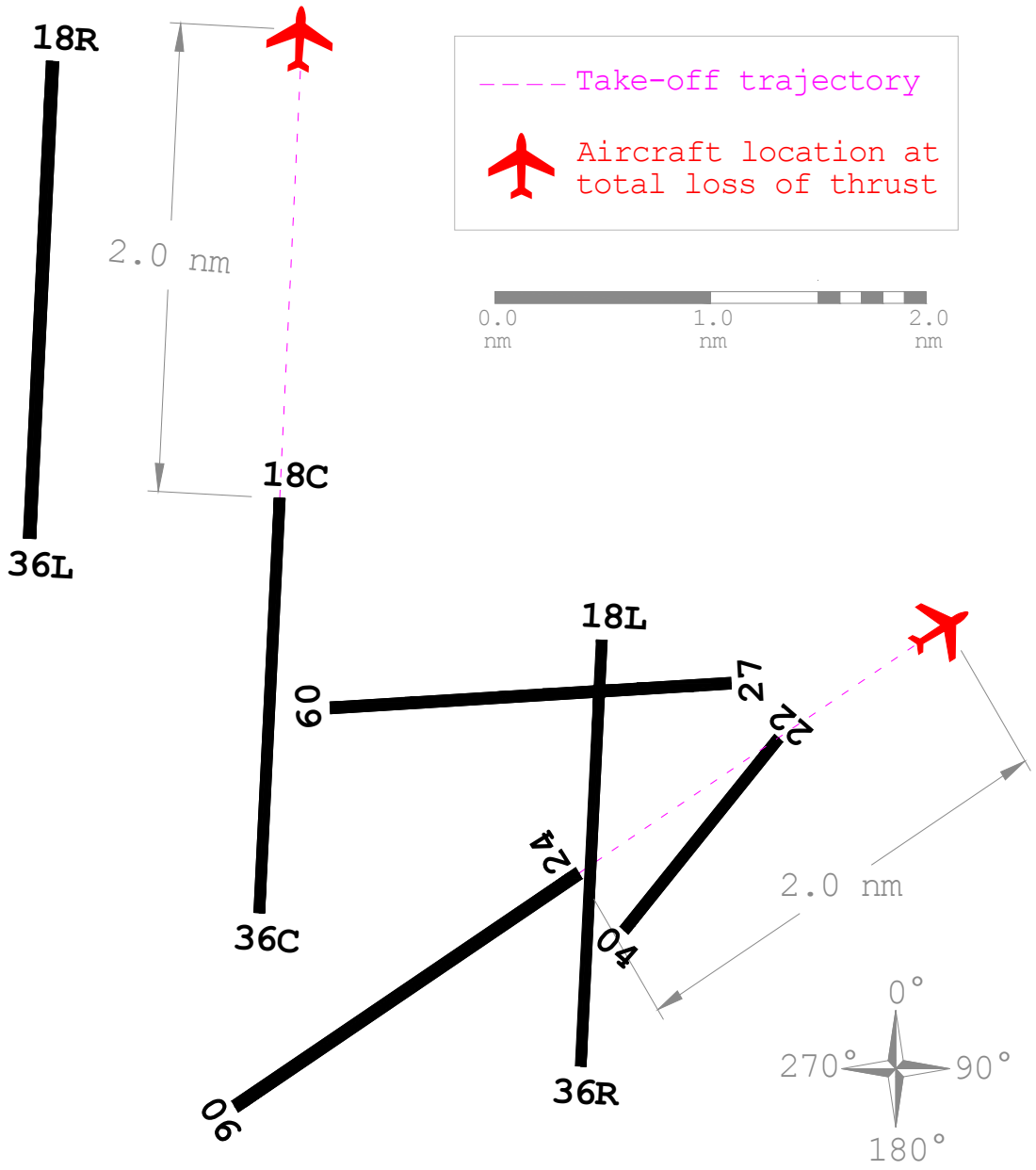

Figure 10-1. Aircraft location at the instant of total loss of thrust after takeoff from Amsterdam Schiphol International Airport (runway width not drawn to scale).

10.2.3 Total-Loss-of-Thrust Scenario #3

The third total-loss-of-thrust scenario is assumed to occur as follows:

1. An A320 or 737-800 aircraft takes off from Atatürk Airport's runway 17L shown in Figure 10-2 in standard day conditions (no wind). The magnetic heading of this runway is 174°, and flap retraction is scheduled to occur at 1,000 ft AGL in accordance with ICAO's noise abatement departure procedure for far-out noise monitors [120, 137].
2. During the climb after the flap retraction, the aircraft encounters a flock of birds while it is still heading 174°. Multiple birds are ingested into both engines, and total loss of thrust occurs.
3. The flight crew initiates an engines-out emergency landing attempt at Atatürk Airport. At this instant, the aircraft weighs 70.0 tons, and is situated at a linear distance of 3.0 nm from Runway 35R threshold as shown in Figure 10-2.

10.2.4 Total-Loss-of-Thrust Scenario #4

The fourth total-loss-of-thrust scenario is assumed to occur as follows:

1. An A320 or 737-800 aircraft takes off from Atatürk Airport's runway 05 shown in Figure 10-2 in standard day conditions (no wind). The magnetic heading of this runway is 55°, and flap retraction is scheduled to occur at 1,000 ft AGL in accordance with ICAO's noise abatement departure procedure for far-out noise monitors [120, 137].
2. During the climb after the flap retraction, the aircraft encounters a flock of birds while it is still heading 55°.

Multiple birds are ingested into both engines, and total loss of thrust occurs.

3. The flight crew initiates an engines-out emergency landing attempt at Atatürk Airport. At this instant, the aircraft weighs 70.0 tons, and is situated at a linear distance of 3.0 nm from Runway 23 threshold as shown in Figure 10-2.

Both the third and fourth total-loss-of-thrust scenarios assume that the distressed aircraft does not have sufficient hydraulic power for flaps extension. Thus, both the A320 aircraft and 737-800 aircraft are simulated in "clean" configuration throughout the engines-out landing attempt.

10.2.5 Total-Loss-of-Thrust Scenario #5

The fifth total-loss-of-thrust scenario is assumed to occur as follows:

1. An A320 or 737-800 aircraft takes off from Atatürk Airport's runway 23 shown in Figure 10-2 in standard day conditions (no wind). The magnetic heading of this runway is 235.
2. During the climb prior to flap retraction, the aircraft encounters a flock of birds while it is still heading 235°. Multiple birds are ingested into both engines, and total loss of thrust occurs.
3. The flight crew initiates an engines-out emergency landing attempt at Atatürk Airport. At this instant, the aircraft weighs 70.0 tons, and is situated at a linear distance of 2.0 nm from Runway 05 threshold as shown in Figure 10-2.

Similar to the first and second scenarios, the fifth scenario assumes that the aircraft does not have sufficient

hydraulic power to change the wing configuration during the engines-out landing attempt.

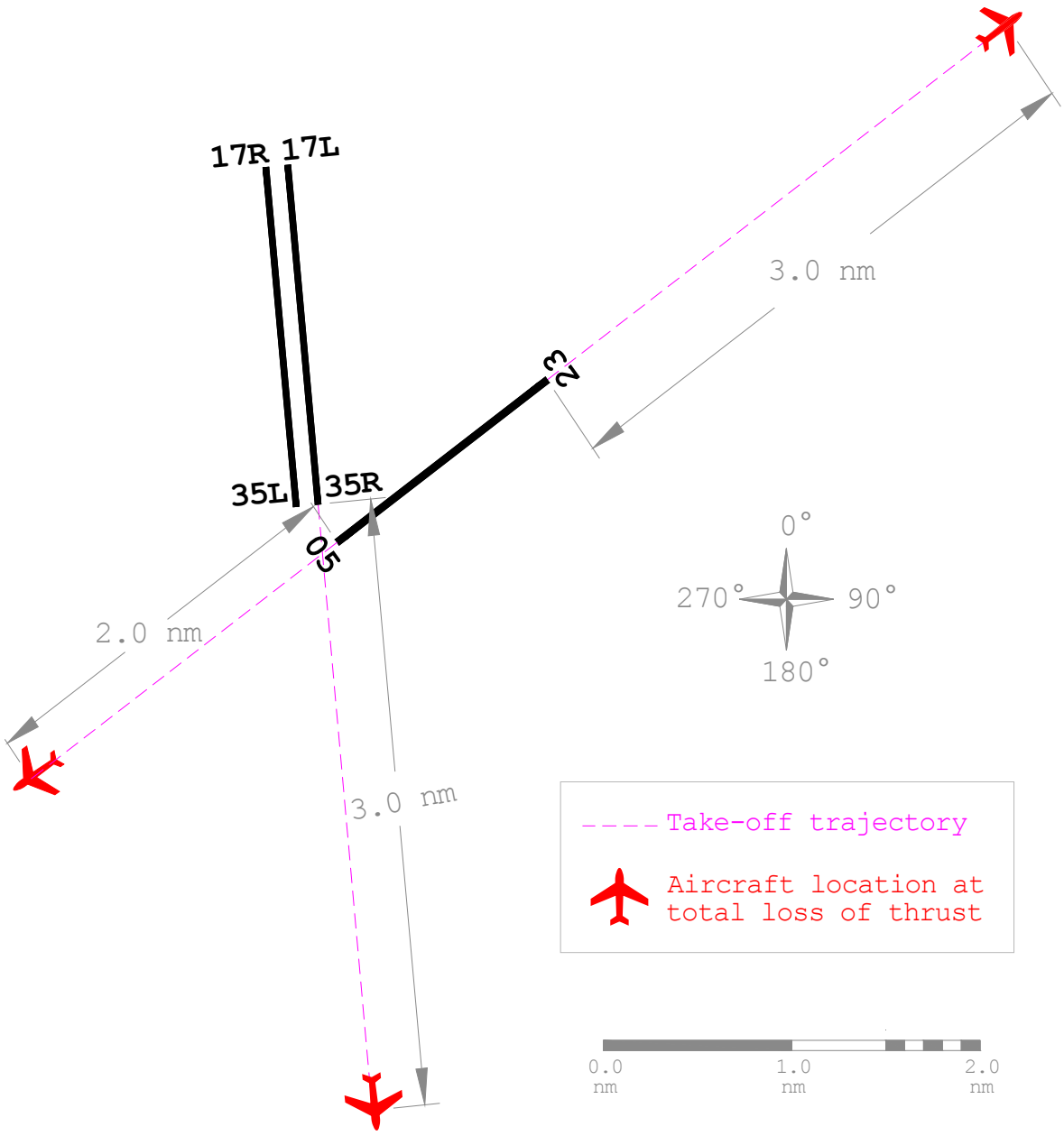

Figure 10-2. Aircraft location at the instant of total loss of thrust after takeoff from Istanbul Atatürk Airport (runway width not drawn to scale).

Although the total-loss-of-thrust scenarios are conducted in two different virtual airport environments, both airport environments are considered similar because:

- Both airport environments are situated on level terrain,
- Both airports are located approximately at mean sea level,
- All simulations are conducted in exactly the same weather and visibility conditions (i.e. standard day conditions, clear weather, no wind and twilight),
- Air traffic is ignored.

10.3 Optimum Trajectories for Landing on a Runway

To compute the optimum landing trajectory for a given total-loss-of-thrust scenario, the segmented trajectory generation algorithm presented in Chapter 7 is applied based on the modelling assumptions outlined in sections 8.3 and 9.3. For a given scenario, the altitude loss required for landing on each runway is computed at every allowable airspeed with a 5.0-knot increment. The landing trajectory that is found to require the minimum altitude loss in a given scenario is defined as the "optimum" landing trajectory for that scenario. A summary of the optimum landing trajectories is given in Table 10-1. The results in Table 10-1 are briefly interpreted as follows:

- The minimum altitude loss for landing on a runway would be achieved by diverting to Runway 18R, 18L, 05, and 17L in the first, second, third, and fourth scenarios, respectively.
- In the fifth scenario, however, the minimum altitude loss for landing on a runway would be achieved by a turn-back maneuver to Runway 05. The optimum landing trajectory for

this scenario is demonstrated thoroughly in section 8.6.1 for the A320 aircraft, and in section 9.6.1 for the 737-800 aircraft.

- In all five scenarios, the distressed aircraft should be flown at approximately V_{LS} to minimize the altitude loss required for a safe landing. This finding conflicts with the Airbus' "Engine Dual Failure" checklist, which specifies the "green dot" speed as the optimum airspeed in clean configuration if an engine restart is considered impossible [7].
- The altitude loss required for flying each optimum trajectory is computed using the kinematic methodology presented in Chapter 7. Each landing trajectory is simulated in a full flight simulator with three type-rated pilots. The last two columns of Table 10-1 show that the computed altitude loss is marginally greater than the simulated altitude loss for each trajectory. Nevertheless, the computed values are accurate enough for practical purposes.

The optimum landing trajectories are drawn in Figures 10-3 and 10-4 for the first and second simulated scenarios, and in Figures 10-5 and 10-6 for the third, fourth and fifth simulated scenarios. A detailed solution of the optimum landing trajectories are given in Appendix C.

Table 10-1. Summary of the optimum landing trajectories in the simulated total-loss-of-thrust scenarios for (a) the A320 aircraft, (b) 737-800 aircraft.

(a)

Simulated Scenario	Wing Config.	Airport	Landing Runway	Airspeed (KCAS)	Required Altitude Loss (ft)	
					Computed	Simulated*
#1	1+F	Schiphol	18R	160	1946	1900
#2	1+F	Schiphol	18L	160	2291	2217
#3	Clean	Atatürk	05	205	2844	2767
#4	Clean	Atatürk	17L	205	2949	2883
#5	1+F	Atatürk	23	160	2651	2600

(b)

Simulated Scenario	Flap Setting	Airport	Landing Runway	Airspeed (KCAS)	Required Altitude Loss (ft)	
					Computed	Simulated*
#1	5	Schiphol	18R	155	1748	1700
#2	5	Schiphol	18L	155	1981	1917
#3	Up†	Atatürk	05	200	2814	2750
#4	Up†	Atatürk	17L	200	2787	2700
#5	5	Atatürk	23	155	2394	2300

* Average result from three simulation runs. The result from each run is rounded up to the nearest 50 ft.

† "Clean" configuration.

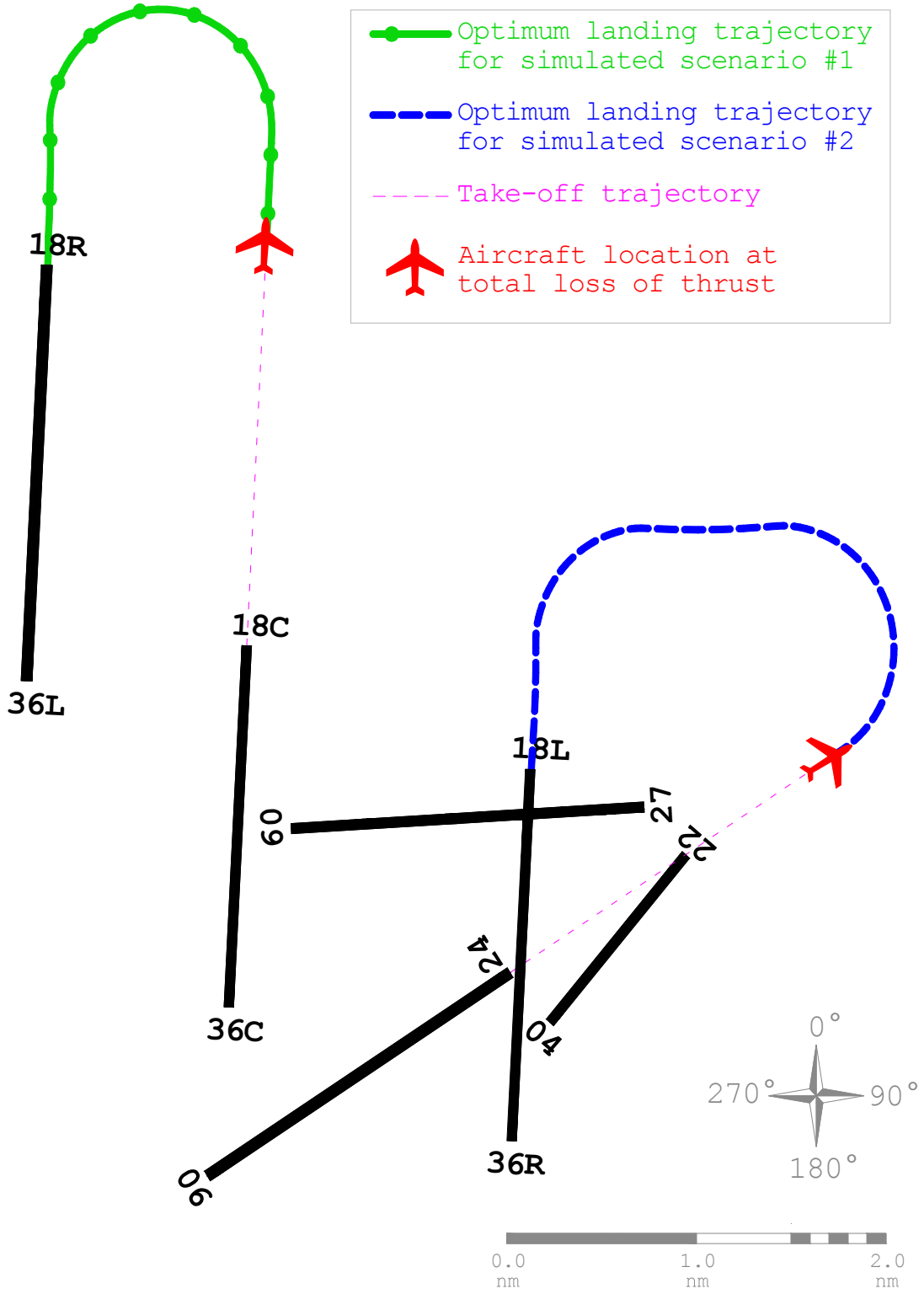

Figure 10-3. Optimum landing trajectories for the A320 aircraft in the first and second total-loss-of-thrust scenarios.

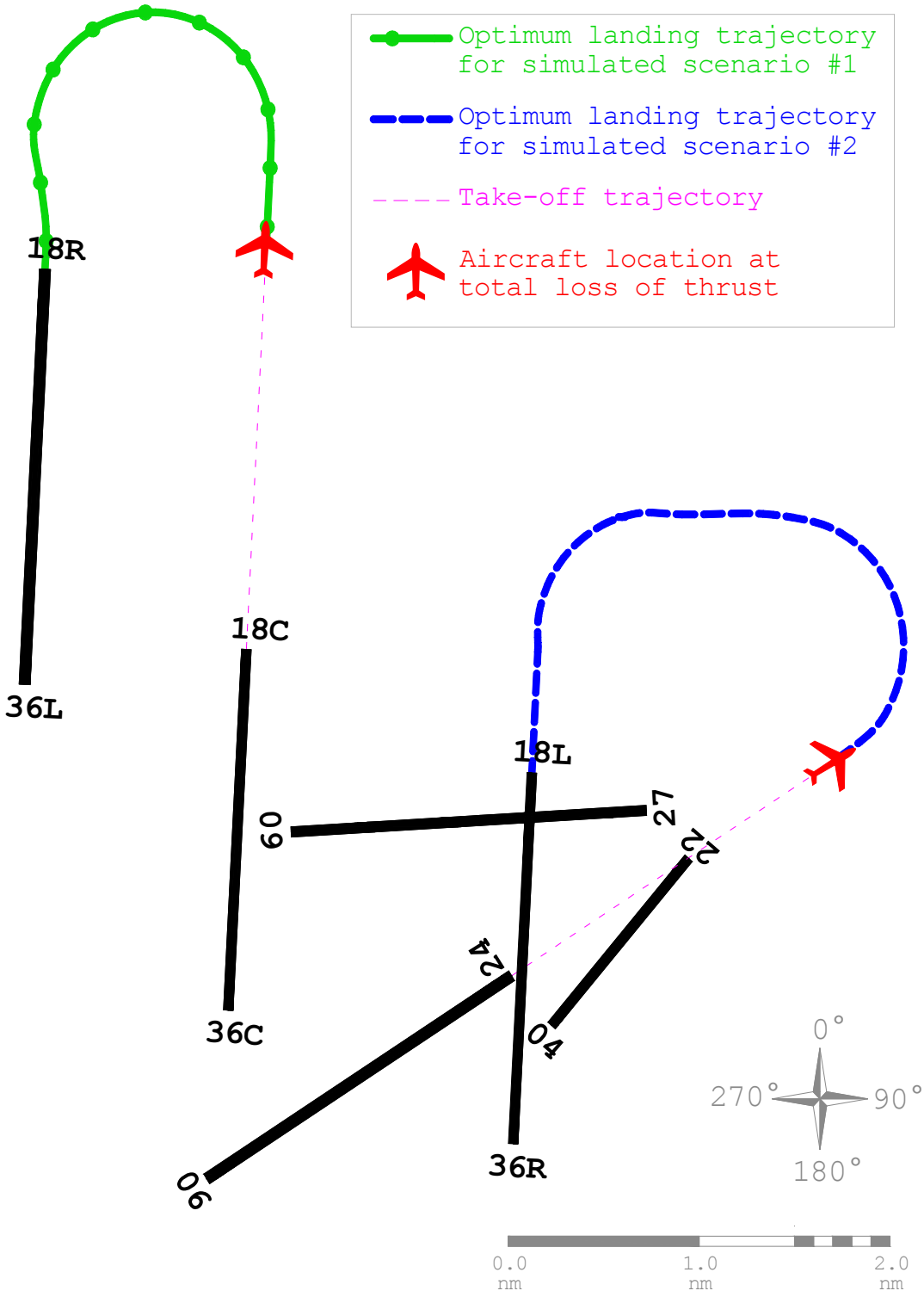

Figure 10-4. Optimum landing trajectories for the 737-800 aircraft in the first and second total-loss-of-thrust scenarios.

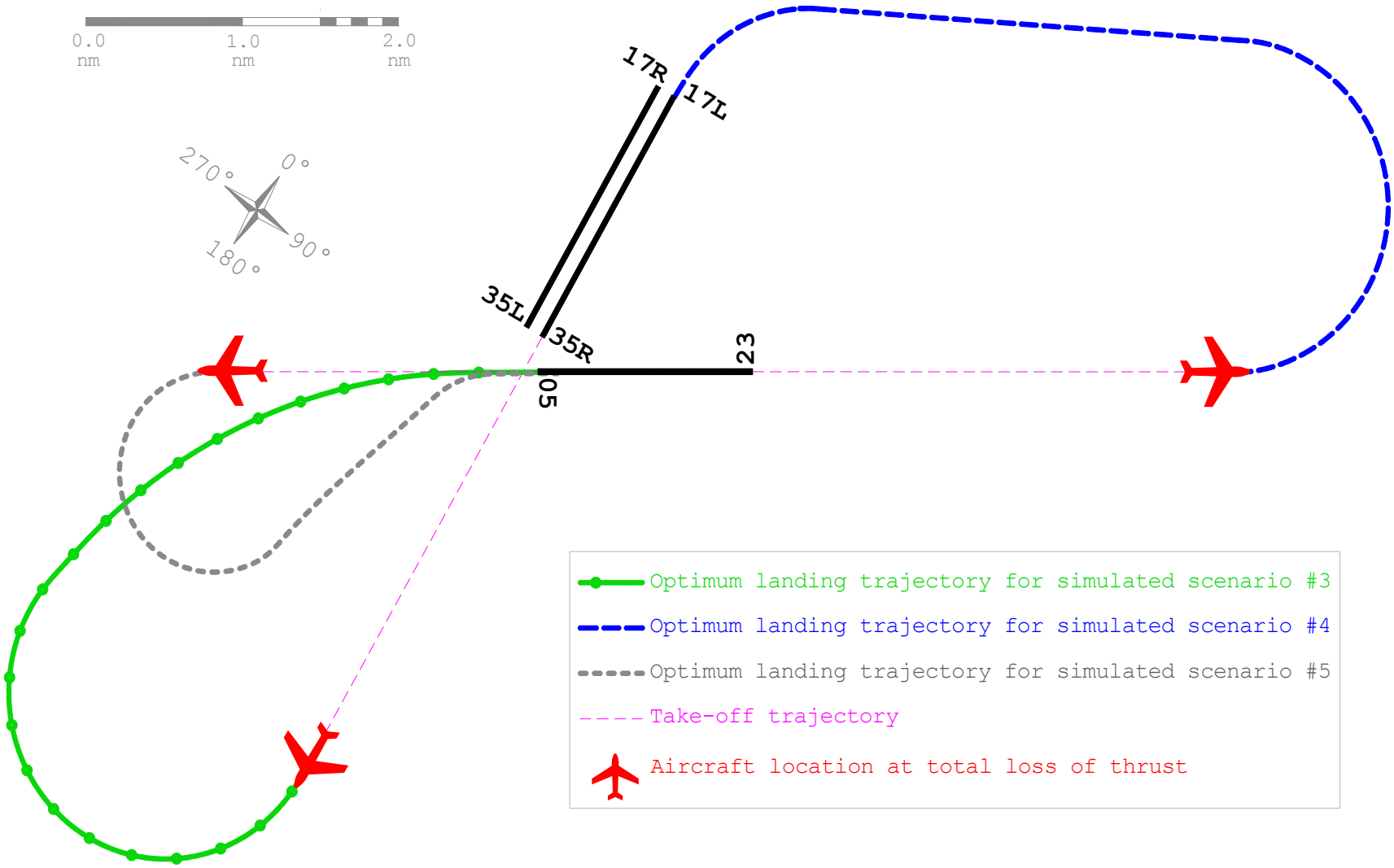

Figure 10-5. Optimum landing trajectories for the A320 aircraft in the third and fourth total-loss-of-thrust scenarios.

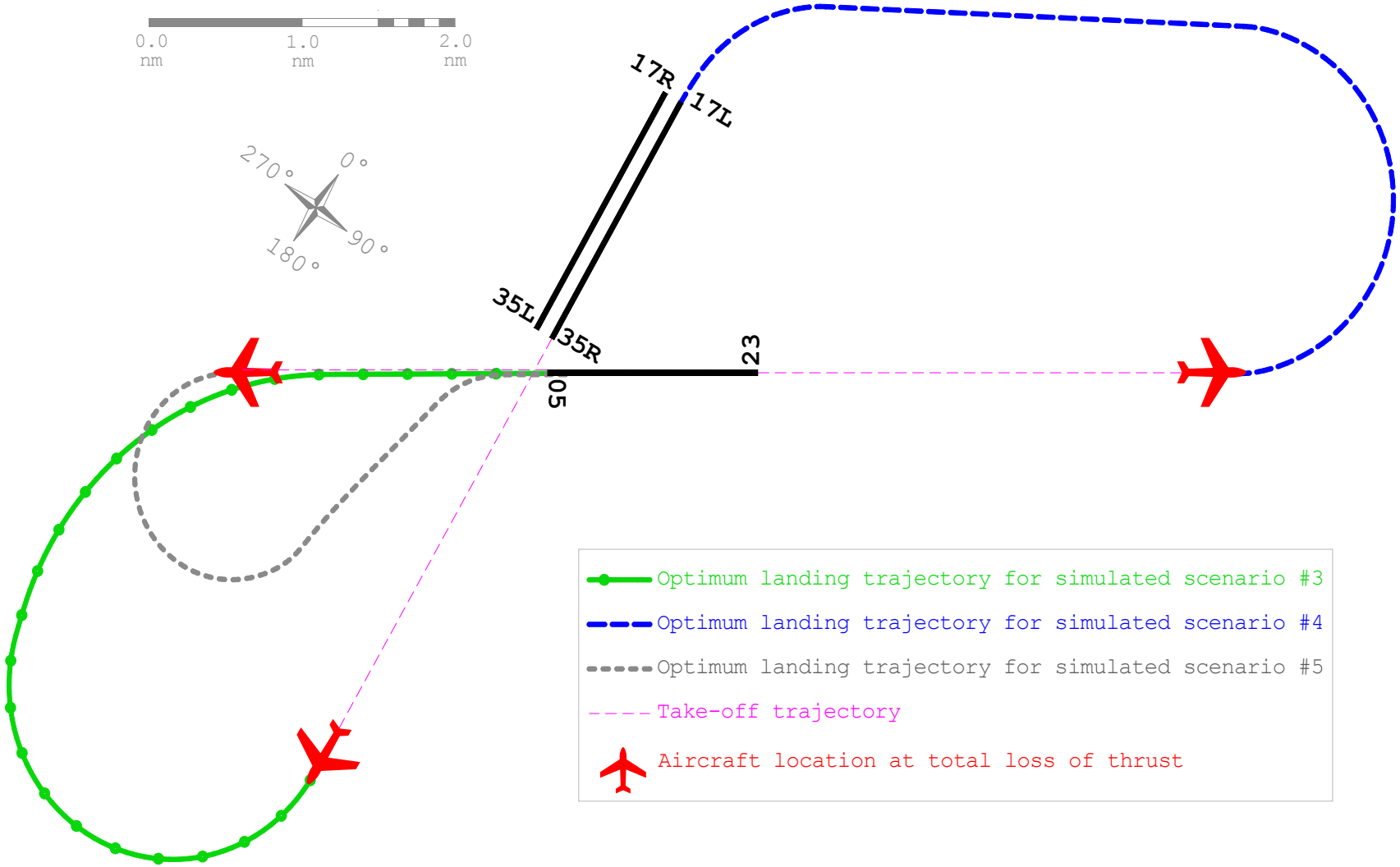

Figure 10-6. Optimum landing trajectories for the 737-800 aircraft in the third and fourth total-loss-of-thrust scenarios.

10.4 Designed Experiment

10.4.1 Initial Aircraft State in the Simulations

The flight simulation tests are conducted at Airbus A320 and Boeing 737-800 JAR-FSTD A, Level D full flight simulators that are certified under the European Aviation Safety Agency (EASA) and Joint Aviation Authorities (JAA). In each run, the aircraft position is initially frozen at the state listed in Table 10-2 and shown in Figures 10-3 through 10-6. For example, at the beginning of the first simulated scenario, the aircraft location is frozen at 3°-heading and 2.0 nm from Runway 18C threshold. The aircraft is in neutral pitch, and the landing gear is fully retracted in the beginning of each run.

The aircraft's starting altitude in a given scenario is determined based on the simulated altitude loss required for flying the optimum landing trajectory in that scenario (given in the last column of Table 10-1) plus an extra ≈50 ft margin. For example in the first total-loss-of-thrust scenario, the simulated altitude loss for flying the optimum landing trajectory is found as 1900 ft for the A320 aircraft as listed in Table 10-1. When the first total-loss-of-thrust scenario is simulated, the aircraft's starting altitude is set to 1900 + 50 = 1950 ft AGL in the A320 full flight simulator. The starting altitude in a given scenario allows for sufficient energy to follow the optimum landing trajectory in that scenario. On the other hand, if the pilot in command deviates considerably from the optimum landing trajectory in a given scenario, the total energy of the aircraft would not allow for a safe touchdown on a runway.

10.4.2 Description of a Typical Simulation Run

The following steps are followed in a given simulation run to simulate dual-engine failure and the subsequent engines-out emergency landing:

1. While the aircraft's position, altitude, pitch attitude and heading are still frozen, dual-engine failure occurs, and both engines start losing thrust.
2. When total loss of thrust takes place, the aircraft is "released". At this instant, the airspeed is approximately equal to V_{LS}, which is listed in Table 10-1 for each simulated scenario.
3. Once the aircraft is "released", a type-rated pilot takes over command of the aircraft, and is asked to make an immediate turn to a runway.

Table 10-2. Initial aircraft state at the beginning of the flight simulation runs.

Simulated Scenario	Distance from the departure runway threshold (nm)	Magnetic Heading	Altitude AGL (ft)	
			Airbus A320	Boeing 737-800
#1	2.0	3°	1950	1750
#2	2.0	58°	2300	2000
#3	3.0	174°	2850	2800
#4	3.0	55°	2950	2750
#5	2.0	235°	2650	2350

All simulations are conducted in standard day conditions, in which the air pressure equals 101.3 kPa and air temperature equals 15°C in mean sea level [101]. The weather is clear, and there is no wind during the engines-out landing attempts.

10.4.3 "Control" vs. "Treatment" Runs

A total of six type-rated A320 pilots and six type-rated Boeing 737NG pilots participated in the flight simulation tests. A given total-loss-of-thrust scenario is simulated twice with each type-rated pilot in command. These runs are explained as follows:

1. The first run of a given scenario with a particular pilot in command is called a "control" run. During the "control" run, the pilot in command is simply asked to attempt a touchdown on a runway of his/ her own preference.
2. The second run of a given scenario with the same pilot in command as in the "control" run is called a "treatment" run. During the "treatment" run, the pilot in command is given the oral ATC commands listed in Table 10-3 for the A320 aircraft, and Table 10-4 for the 737-800 aircraft. These oral commands are generated using the procedure described in section 8.8. The oral commands guide the pilot over the optimum landing trajectory in the simulated scenario.

Since there are five total-loss-of-thrust scenarios and 12 type-rated pilots, a total of 12*5=60 "control" runs and 60 "treatment" runs are conducted. For a given pilot in command, the five "control" runs are conducted in randomized order in the full flight simulator, followed by the five "treatment" runs conducted in randomized order.

The “control” runs represent the engines-out landing attempts of the type-rated pilots without the use of the adaptive flight planning architecture proposed in this dissertation. On the other hand, the “treatment” runs represent the engines-out landing attempts of the pilots under the guidance of the adaptive flight planner.

In the following sections, the outcomes of the “treatment” runs are statistically compared with the outcomes of the “control” runs. The objective is to find out if the use of the adaptive flight planning architecture significantly increases the probability of safe touchdown in the simulated scenarios. Since each type-rated pilot participated in both the “control” and “treatment” run of a given scenario, any bias that may result from the factors such as pilot age and experience is eliminated.

Table 10-3. Oral ATC commands for guiding the A320 pilots over the optimum trajectory in total-loss-of-thrust scenario (a) #1, (b) #2, (c) #3, (d) #4, (e) #5.

(a)

- Descend to 1750′. Maintain 160 kt.
- Turn left heading 181° at 33° bank. Maintain 160 kt.
- Turn* right heading 183° at 33° bank.
- Clear to land on Runway 18R.

(b)

- Turn left heading 269° at 33° bank. Maintain 160 kt.
- Descend to 950′. Maintain 160 kt.
- Turn left heading 183° at 33° bank. Maintain 160 kt.
- Clear to land on Runway 18L.

(c)

- Turn right heading 8° at 33° bank. Maintain 205 kt.
- Turn right heading 55° at 10° bank. Maintain 205 kt.
- Clear to land on Runway 05.

(d)

- Turn left heading 239° at 33° bank. Maintain 205 kt.
- Descend to 550′. Maintain 205 kt.
- Turn left heading 174° at 33° bank. Maintain 205 kt.
- Clear to land on Runway 17L.

(e)

- Turn left heading 14° at 33° bank. Maintain 160 kt.
- Descend to 500′. Maintain 160 kt.
- Turn right heading 55° at 33° bank. Maintain 160 kt.
- Clear to land on Runway 05.

* When the aircraft descends to approximately 300 ft AGL.

Table 10-4. Oral ATC commands for guiding the 737-800 pilots over the optimum trajectory in total-loss-of-thrust scenario (a) #1, (b) #2, (c) #3, (d) #4, (e) #5.

(a)

- Descend to 1600′. Maintain 155 kt.
- Turn left heading 189° at 30° bank. Maintain 155 kt.
- Turn right heading 183° at 30° bank.
- Clear to land on Runway 18R.

(b)

- Turn left heading 270° at 30° bank. Maintain 155 kt.
- Descend to 950′. Maintain 155 kt.
- Turn left heading 183° at 30° bank. Maintain 155 kt.
- Clear to land on Runway 18L.

(c)

- Turn right heading 342° at 30° bank. Maintain 200 kt.
- Turn right heading 55° at 16°[†] bank. Maintain 200 kt.
- Clear to land on Runway 05.

(d)

- Turn left heading 237° at 30° bank. Maintain 200 kt.
- Descend to 500′. Maintain 200 kt.
- Turn left heading 174° at 33° bank. Maintain 200 kt.
- Clear to land on Runway 17L.

(e)

- Turn left heading 10° at 30° bank. Maintain 155 kt.
- Descend to 450′. Maintain 155 kt.
- Turn right heading 55° at 30° bank. Maintain 155 kt.
- Clear to land on Runway 05.

[†] May be rounded form 16° to 15° since bank angles of multiples of 5° may be more easily read on the attitude indicator.

10.5 Results

10.5.1 Outcomes

The outcomes of the simulations are summarized in Table 10-5 for the A320 aircraft, and in Table 10-6 for the 737-800 aircraft. A detailed tabulation of the outcomes is presented in Appendix D. The results in Tables 10-5 and 10-6 are presented in the form of crosstabs that list the frequency of "safe landing" and "crash". A touchdown on a runway is counted as a "safe landing" unless runway overshoot occurs. On the other hand, failure to touch down on a runway or runway overshoot is counted as a "crash". For a given aircraft type, the "control" and "treatment" samples involve observations from the same subjects. The outcomes summarized in Tables 10-5 and 10-6 are briefly interpreted as follows:

- When the A320 was in clean configuration, there were nine out of 12 cases in which the pilot in command crashed the aircraft in the "control" runs, but accomplished safe landing in the corresponding "treatment" runs.
- When the A320 was in wing configuration "1+F", there were nine out of 18 cases in which the pilot in command crashed the aircraft in the "control" runs, but achieved safe landing in the corresponding "treatment" runs.
- When the 737-800 was in flap setting "5", there were 13 out of 18 cases in which the pilot in command crashed the aircraft in the "control" runs, but achieved safe landing in the corresponding "treatment" runs.
- When the 737-800 was in clean configuration, there were 11 out of 12 cases in which the pilot in command crashed the

aircraft in the "control" runs, but achieved safe landing in the corresponding "treatment" runs.

Table 10-5. Outcomes from the designed experiment for the A320 aircraft in (a) wing configuration "1+F", (b) "clean" configuration.

(a)

	Number of "Control" Runs	Number of "Treatment" Runs
Safe Landing	9	18
Crash	9	0
TOTAL	**18**	**18**

(b)

	Number of "Control" Runs	Number of "Treatment" Runs
Safe Landing	2	11
Crash	10	1
TOTAL	**12**	**12**

Table 10-6. Outcomes from the designed experiment for the 737-800 aircraft in (a) flap setting "5", (b) "clean" configuration.

(a)

	Number of "Control" Runs	Number of "Treatment" Runs
Safe Landing	5	18
Crash	13	0
TOTAL	**18**	**18**

(b)

	Number of "Control" Runs	Number of "Treatment" Runs
Safe Landing	0	11
Crash	12	1
TOTAL	**12**	**12**

10.5.2 Interpretation of the Outcomes

The distribution of the factors that led to crash during the "control" runs is illustrated in Figure 10-7 for the A320 aircraft, and in Figure 10-8 for the 737-800 aircraft. Since some of the control runs involved multiple factors such as both poor landing site selection and non-optimal airspeed, the percentages in Figures 10-7 and 10-8 may add up to more than 100 percent. Based on the results illustrated in Figure 10-7, the following are inferred:

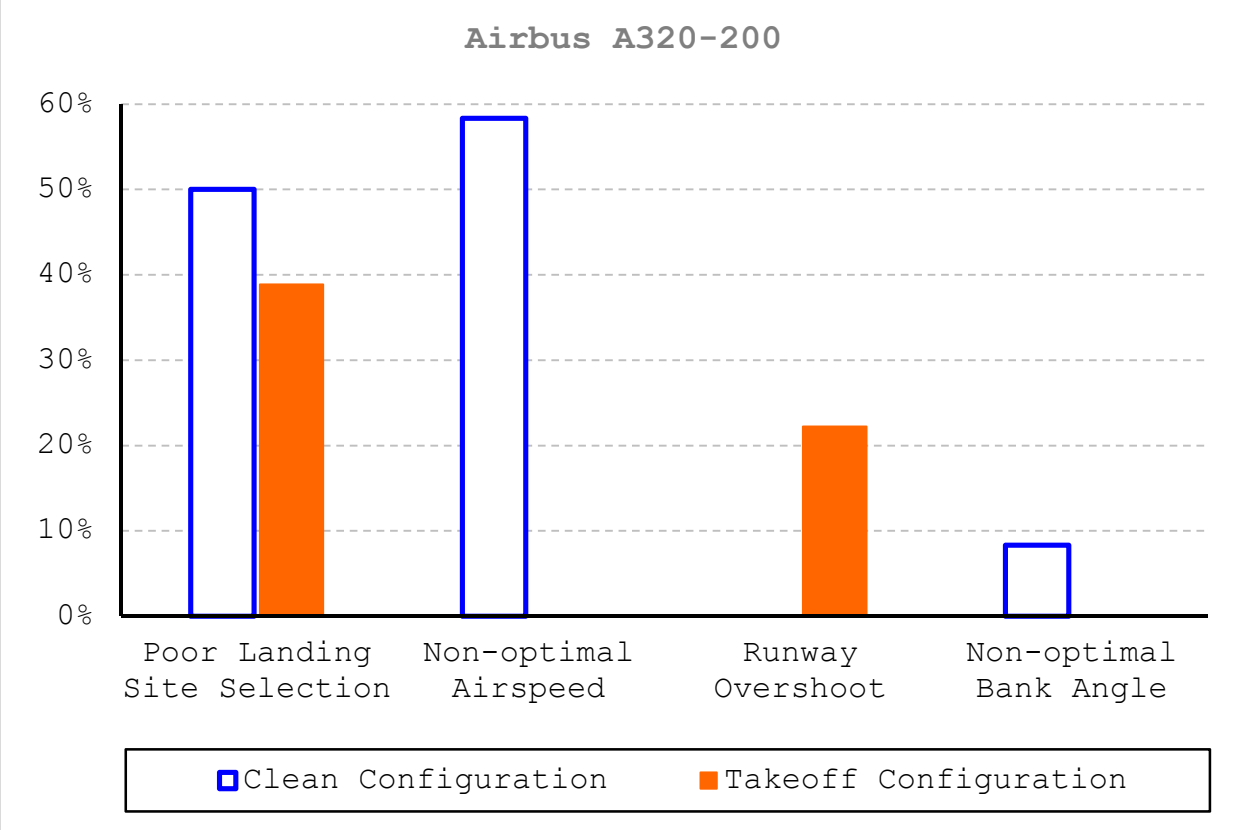

Figure 10-7. Distribution of the factors leading to crash in the "control" runs on the Airbus A320-200 aircraft.

- When the A320 was in takeoff configuration (i.e. wing configuration "1+F"), the primary crash cause during the "control" runs was the pilots' inappropriate landing site selection. Some of the pilot subjects aimed to land on runways that were in fact outside of the aircraft's glide range (see Appendix D). Having insufficient aerodynamic energy, the aircraft crashed without making it to the intended runway.
- When the A320 was in clean configuration, the prominent crash cause during the "control" runs was that some of the pilot subjects chose not to maintain V_{LS} = 205* KCAS, but rather attained the "green dot" speed of 225‡ KCAS, which is the procedure recommended in the A320 engine dual failure checklist [7] (see Appendix D). Compared to V_{LS} = 205* KCAS, the "green dot" speed of 225* KCAS required longer turning radii and resulted in increased energy loss over the banked turns. Consequently, the aircraft ran out of altitude without reaching a runway.

Contrary to the "control" runs in clean configuration, all pilot subjects maintained the optimum airspeed (i.e. V_{LS}) during the "control" runs in wing configuration 1+F. The difference in pilot control strategy between the clean configuration and wing configuration 1+F may be explained by the following:

- The Engine Dual Failure checklist of Airbus Industrie does not recommend an optimum airspeed in engines-out glide for wing configurations other than the "clean" configuration [110].

‡ At the aircraft gross weight of 70.0 tons.

- Airbus Industrie recommends the lowest selectable airspeed (i.e. V_{LS}) as the final approach speed in the absence of wind [112].

Hence, when the A320 aircraft was in wing configuration 1+F, the pilot subjects followed manufacturer's recommendation. On the contrary, when the A320 aircraft was in clean configuration, some of the pilot subjects observed the recommendation of "green dot" speed in the Engine Dual Failure Checklist whereas others chose to adhere to the lowest selectable airspeed.

Based on the results for the 737-800 aircraft illustrated in Figure 10-7, the following are inferred:

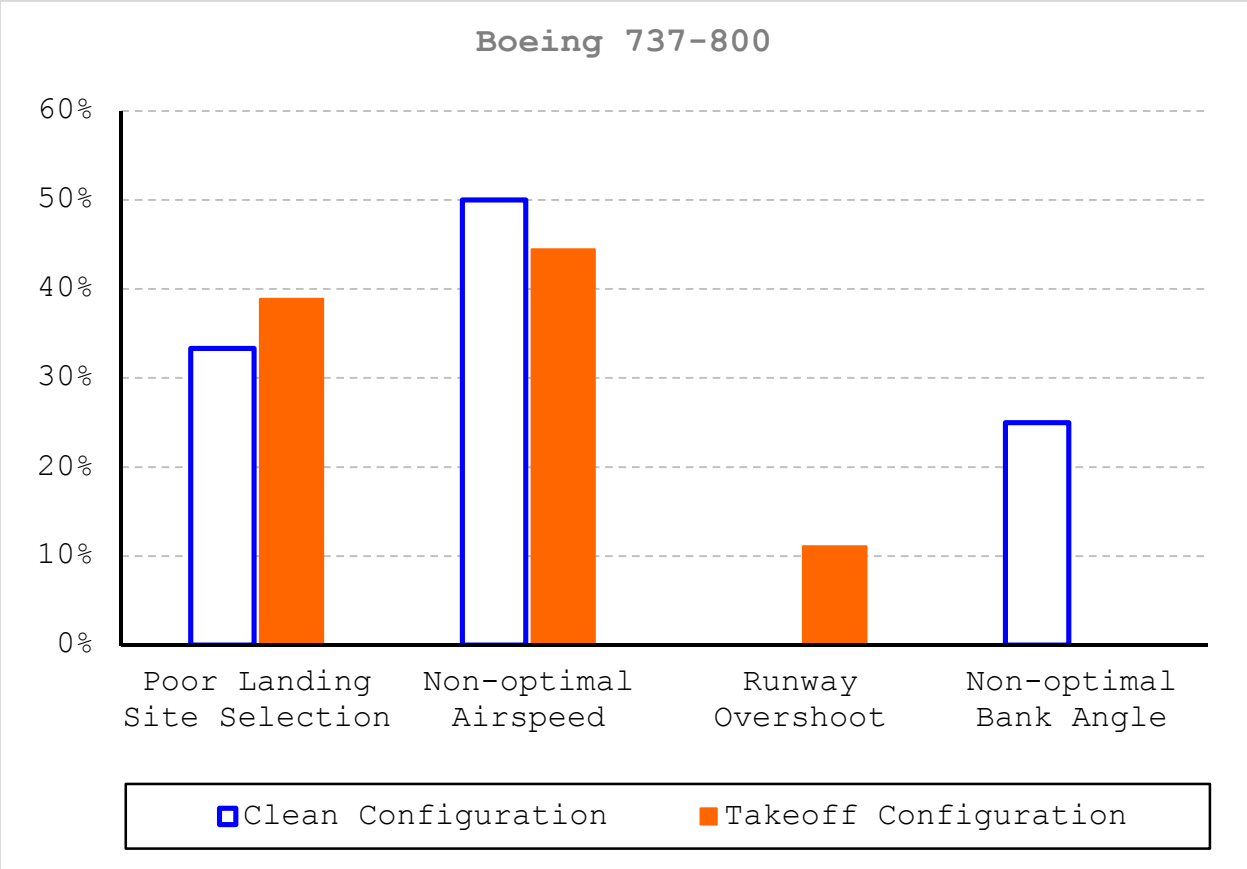

Figure 10-8. Distribution of the factors leading to crash in the "control" runs on the Boeing 737-800 aircraft.

- In both clean configuration and flap setting 5, pilots' failure to maintain the optimum airspeed was the leading crash cause on the 737-800 aircraft during the "control" runs. The Dual-Engine Failure checklist of the 737-800 aircraft does not recommend an optimum engines-out landing speed because the objective of the entire checklist is to restart at least one engine.
- When the 737-800 aircraft was in flap setting 5, some of the pilot subjects chose to maintain the flap 5 "maneuver speed" of 176* KCAS instead of the "minimum maneuver speed" (i.e. V_{LS}) of approximately 155* KCAS (see Appendix D). The "maneuver speed" is the minimum recommended airspeed at which the airplane should carry out any maneuvering after takeoff and before landing to ensure adequate margin from stall warning [122]. The "maneuver speed" is also close to the airspeed at minimum drag, and can provide enhanced lift-to-drag ratio [122]. As shown in Figure 10-9, the flap 5 "maneuver speed" is indicated by a "5" bug on the speed tape of the primary flight display after takeoff and before landing. Since the flap 5 "maneuver speed" of 176* KCAS is greater than the "minimum maneuver" speed of approximately 155* KCAS, it required longer turning radii and resulted in increased energy loss over the banked turns. Therefore, the aircraft ran out of altitude without making it to a runway (see Appendix D).
- Likewise, when the 737-800 aircraft was in clean configuration, some of the pilots chose to maintain the "maneuvering speed" of 216* KCAS instead of the "minimum

* At the aircraft gross weight of 70.0 tons.

maneuver speed" (i.e. V_{LS}) of approximately 200* KCAS (see Appendix D). As shown in Figure 10-9, the "maneuver speed" for clean configuration is indicated by an "UP" bug on the speed tape of the primary flight display after takeoff and before landing. Since the flaps up "maneuver speed" of 216* KCAS is greater than the "minimum maneuver" speed of approximately 200* KCAS, it required longer turning radii and resulted in increased energy loss over the banked turns. Therefore, the aircraft ran out of altitude without making it to a runway (see Appendix D).

Figure 10-9. Speed tape of the Boeing 737-800 aircraft on the primary flight display.

10.5.3 Generalized Linear Mixed Model

The designed experiment involves repeated observations on the subjects (i.e. pilots) because each subject participated in both the "control" and "treatment" run of a particular total-loss-of-thrust scenario. The repeated observations on a given subject are typically correlated since they involve the same subjects. Therefore, the "control" and "treatment" samples are statistically dependent for a given aircraft [139]. If the correlation is ignored in statistical analysis, the standard error estimates of model parameters can be heavily biased [140].

The repeated observations made on a given subject are referred to as a "cluster". To represent the correlation among the observations in a given "cluster", a generalized linear mixed model approach is followed. A mixed model permits both fixed effects and random effects in the linear predictors. For a fixed-effects term, the true effect size is assumed to be the same for all observations. For a random-effects term, however, the true effect size varies randomly from one cluster to the other. Equation (10-1) shows the form of a generalized linear mixed model as follows:

$$\ln\left(\frac{P}{1-P}\right) = \alpha_i + \beta_0 + \sum_i(\beta_i * X_i) \qquad (10\text{-}1)$$

where

P = Probability of a given event.

$\ln\left(\frac{P}{1-P}\right)$ = The "logit" link function.

α_i = Random effect of cluster i. All α_i's are assumed to have the normal $N(0,\sigma^2)$ distribution where σ^2 is unknown.

β_0 = Mean intercept of the model.

X_i = Predictor i.

β_i = Fixed effect of predictor i.

The random effects (α_i's) are unknown and unobserved parameters that vary randomly from one cluster to the other. Hence, the model's intercept ($\alpha_i + \beta_0$) also varies randomly from one cluster to the other. Therefore, the model in Equation (10-1) is called a "random intercept" model. Since the observations from a given cluster involve the same α_i (and thus, the same intercept), there is positive correlation among the observations within a cluster [141].

To analyze the results from the designed experiment, the pilot effects are modeled as random effects whereas the "treatment" and "wing configuration" effects are modeled as fixed effects. All observations from pilot i are assumed to have the same intercept $\alpha_i + \beta_0$ in the model. On the other hand, the fixed effect of "treatment" is assumed to represent the effects of the ATC commands on the probability of safe touchdown (see Table 10-3 and Table 10-4). Likewise, the fixed effect of "wing configuration" is assumed to represent the effect of flap setting on the probability of safe touchdown. The resultant generalized linear mixed model is given in Equation (10-2):

$$\ln\left(\frac{P}{1-P}\right) = \alpha_i + \beta_0 + \beta_1 * X_1 + \beta_2 * X_2 + \beta_3 * X_3 \qquad (10\text{-}2)$$

where

P = Probability of landing on a runway.

α_i = Random effect of pilot i. All α_i's are $N(0, \sigma^2)$.

β_0 = Mean intercept of the model.

X_1 = Dichotomous predictor variable for the "treatment" effect. $X_1 = 1$ if the pilot in command is guided with the ATC commands in Table 10-3 or Table 10-4, and $X_1 = 0$ otherwise.

β_1 = Fixed effect of predictor X_1.

X_2 = Dichotomous predictor variable for the "wing configuration" effect. $X_2 = 1$ if the aircraft is in "clean" configuration, and $X_2 = 0$ otherwise.

β_2 = Fixed effect of predictor X_2.

X_3 = Dichotomous predictor variable for the "airport location" effect. $X_3 = 1$ if the total-loss-of-thrust scenario is simulated in the virtual environment of Istanbul Atatürk Airport, and $X_3 = 0$ otherwise.

β_3 = Fixed effect of predictor X_3.

A separate model is built for each aircraft. There are 60 observations made on each aircraft. The number of observations meet the minimum sample size requirements [142] for the linear model given in Equation (10-2). To compute the coefficient estimates in the generalized linear mixed model, a Laplace approximation method [143] is applied. The results of the coefficient estimates are summarized in Table 10-7. All fixed effects that are found statistically significant at α=0.05* are included in the model. Equations (10-3) and (10-4) give the predicted models for the A320 and 737-800 aircraft, respectively:

$$\ln\left(\frac{\hat{P}}{1-\hat{P}}\right) = 0.049 + 4.647 * X_1 - 1.909 * X_2 \quad (10\text{-}3)$$

$$\ln\left(\frac{\hat{P}}{1-\hat{P}}\right) = -0.597 + 2.091 * X_1 \quad (10\text{-}4)$$

where

$\hat{P}$ = Predicted probability of landing on a runway.

Figure 10-10 plots the random effect estimates (i.e. $\hat{\alpha}_i$'s) associated with the subjects. The model estimates in Equations

(10-3) and (10-4) include the expected value of α_i, which is equal to 0 since all α_i's are assumed to follow the normal $N(0,\sigma^2)$ distribution.

The results in Table 10-7 show that the "treatment" effect is found statistically significant* for both the A320 and 737-800 aircraft. On the contrary, the "wing configuration" effect is found statistically significant* for only the 737-800 aircraft. A detailed interpretation of each statistical model is given in section 10.5.5.

Table 10-7. Summary of the coefficient estimates for the generalized linear mixed model.

Aircraft	Variable	Coefficient Estimate	Standard Error Estimate	Wald Statistic (χ^2)	p-value† of the χ^2
Airbus A320	*Intercept*	0.049	0.547	0.008	0.929
	β_1	4.647	1.330	12.208	<0.001
	β_2	-1.909	0.938	4.142	0.042
Boeing 737-800	*Intercept*	-0.597	0.471	1.607	0.205
	β_1	2.091	0.651	10.317	0.001

10.5.4 Model Assumptions and Goodness-of-Fit

The random effect estimates plotted in Figure 10-10 are assumed to have the normal $N(0,\sigma^2)$ distribution where σ^2 quantifies the variability in the random pilot effects. The

* At a type I error rate of 0.05.

† P-value under the null hypothesis that "the true coefficient of the predictor in the model is 0".

bigger the σ^2 is, the more variability there is among the pilots. While σ^2 is unknown, it can be estimated from the sample data using the Laplace Approximation method [143]. In this experiment, the variance σ^2 is estimated as 0.379 for the A320 data, and 0.370 for the 737-800 data. Using the variance estimates, Shapiro-Wilk Test [144] is applied to the random error estimates plotted in Figure 10-10. The goal is to check whether the random error effects meet the normality assumption. The results are summarized in Table 10-8. The p-values for the Shapiro-Wilk Test suggest no sufficient evidence[‡] to believe that the random effect estimates are non-normally distributed. Hence, both the A320 and 737-800 data meet the normality assumption of the random effects.

To check the model goodness-of-fit, Hosmer and Lemeshow Test [88] is run with 10 groups for each statistical model. The goal is to check whether the observed and predicted probabilities of safe landing on a runway differ significantly. The results are summarized in Table 10-8. The p-values for the Hosmer and Lemeshow Test [88] show that the predicted probabilities of safe landing on a runway do not differ significantly[*] from the observed probabilities. Hence, the models in Equations (10-3) and (10-4) can accurately predict the probability of safe touchdown on a runway in a particular setting.

[‡] At a Type I error rate of 0.05.

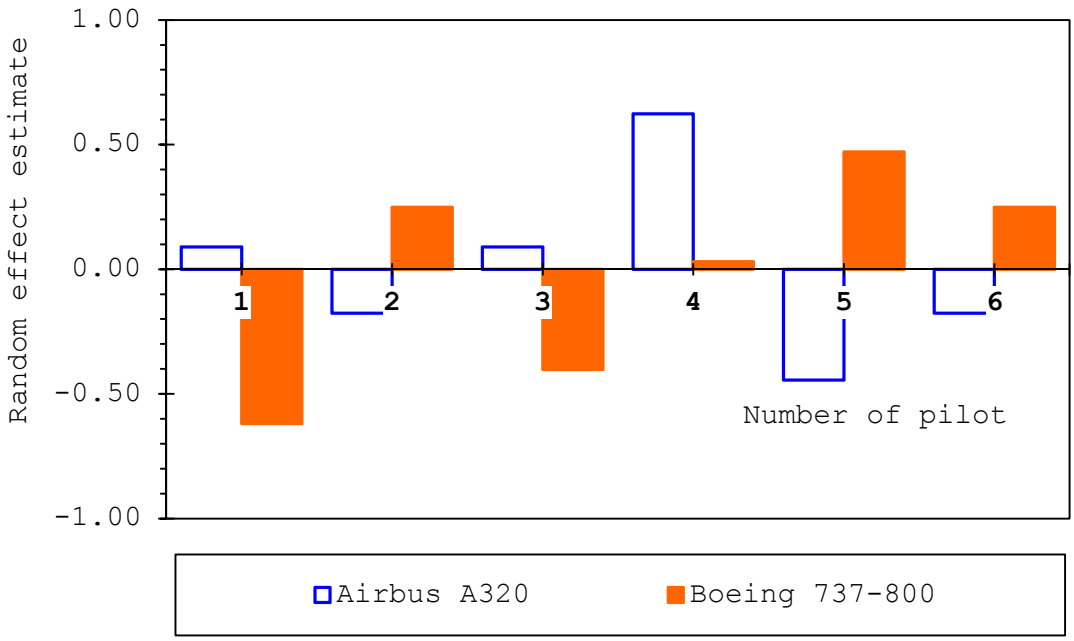

Figure 10-10. Random effect estimates ($\hat{\alpha}_i$).

Table 10-8. Results of the statistical tests on modelling assumptions and model goodness-of-fit.

	Shapiro-Wilk Test		Hosmer and Lemeshow Test	
	Airbus A320 Data	Boeing 737-800 Data	Airbus A320 Data	Boeing 737-800 Data
Test Statistic	0.927	0.914	3.382	7.630
P-value	0.556*	0.462*	0.908†	0.470†

* P-value under the null hypothesis that "the $\hat{\alpha}_i$'s are normally distributed".

† P-value under the null hypothesis that "the predicted and observed probabilities of safe landing do not differ significantly".

10.5.5 Testing for the Research Hypothesis

Equations (10-3) and (10-4) are rearranged as shown in Equation (10-5) to compute the predicted probability of safe landing on a runway in a given setting:

$$\hat{P} = \exp[\hat{\beta}_0 + \sum_i(\hat{\beta}_i * X_i)]/\{1 + \exp[\hat{\beta}_0 + \sum_i(\hat{\beta}_i * X_i)]\} \quad (10\text{-}5)$$

where

$\hat{P}$ = Predicted probability of safe touchdown on a runway.

$\hat{\beta}_0$ = Estimate for the mean intercept of the model.

$\hat{\beta}_i$ = Coefficient estimate for predictor *i*.

X_i = Predictor *i*.

Using Equation (10-5), the predicted probability of safe touchdown on a runway is computed based on the coefficient estimates in Equations (10-3) and (10-4). The results are given in Table 10-9. All predicted probabilities listed in Table 10-9 differ significantly* from each other. Based on the total-loss-of-thrust scenarios simulated in the designed experiment, the results in Table 10-9 show that:

- When the A320 pilots attempt engines-out landing on a runway of their own preference, the predicted probability of safe touchdown on a runway is 0.51 in wing configuration "1+F", and 0.13 in "clean" configuration
- When the A320 pilots are guided with the ATC commands given in Table 10-3, the predicted probability of safe touchdown on a runway increases significantly* to 0.99 in wing configuration "1+F", and to 0.94 in "clean" configuration.

* At a Type I error rate of 0.05.

- When the 737-800 pilots attempt engines-out landing on a runway of their own preference, the predicted probability of safe touchdown on a runway is 0.36.
- When the 737-800 pilots are guided with the ATC commands given in Table 10-4, the predicted probability of safe touchdown on a runway increases significantly* to 0.82.

Therefore, the results present strong evidence in favor of the hypothesis given in section 10.1 for both the A320 and 737-800 aircraft. When the ATC commands generated by the adaptive flight planner are used to guide the pilots, the probability of safe touchdown on a runway increased significantly on both aircraft. The ATC commands generated by the adaptive flight planning architecture not only directed the pilots to a reachable runway within the aircraft's glide range, but also enabled them to achieve energy-preserving maneuvers during the engines-out landing. Consequently, the probability of safe touchdown on a runway increased significantly, which in turn significantly reduced the probability of hull loss and casualty.

Table 10-9. Predicted probability of safe touchdown on a runway.

	Airbus A320		Boeing 737-800
	Wing config. "1+F"	Clean config.	
"Control" run	0.51	0.13	0.36
"Treatment" run	0.99	0.94	0.82

* At a Type I error rate of 0.05.

CHAPTER 11 - CONCLUSIONS AND RECOMMENDATIONS

11.1 Total-Loss-of-Thrust Emergency

Contrary to yesterday's three- and four-engine jets, more than 96 percent of air travelers are transported on twin-engine jets today. While twin-engine jets offer reduced noise levels and enhanced fuel efficiency compared to three- and four-engine jets, they have vulnerabilities that are not shared by yesterday's three- and four-engine aircraft. Reduced engine redundancy is one of these vulnerabilities. Commercial aircraft may undergo total loss of thrust if birds are ingested into all engines. For example in January 2009, a U.S. Airways Airbus A320 aircraft ingested multiple Canada geese into both engines at an altitude of 2,818 ft AGL shortly after takeoff from New York's LaGuardia Airport. The aircraft underwent total loss of thrust, and the flight crew failed to restart at least one engine. Believing that the aircraft did not have sufficient aerodynamic energy to return to a nearby runway, the flight crew successfully ditched the aircraft on the Hudson River with no fatalities. Total loss of thrust may also occur due to maintenance error, severe weather, ice ingestion, pilot error and fuel leakage. For instance in October 2004, a Pinnacle Airlines Bombardier CRJ-200 aircraft underwent total loss of thrust during a ferry flight from Little Rock, Arkansas, to Minneapolis, Minnesota, when the flight crew performed non-standard maneuvers and overstressed the engines. Although there were a number of airports within reach for a forced landing, the flight crew lost too much altitude trying to restart at least one engine, and failed to succeed. Consequently, the aircraft crashed near Jefferson City, Missouri, and both pilots were killed.

Total loss of thrust is a particularly critical emergency situation. Unlike single-engine failure or partial loss of thrust, the aircraft cannot gain altitude in the event of total loss of thrust. Thus, the flight crew has only one chance for landing, and there is no room for human error. Otherwise, total loss of thrust may lead to severe consequences such as the Dana Air Flight 992 that resulted in 163 fatalities after undergoing total loss of thrust on approach to Lagos Airport, Nigeria, in June 2012. With the engine redundancy cut from three or four to two, contemporary twin-engine jets are imperiled by the total-loss-of-thrust hazard.

To address the total-loss-of-thrust emergency, quick reference handbooks and airliner checklists are designed. For instance, the Airbus A320 aircraft has a checklist called “Engine Dual Failure”, which is targeted for use in the total-loss-of-thrust emergency. Likewise, the Boeing 737NG aircraft family has a checklist called “Loss of Thrust on Both Engines”. The primary objective of both checklists is to enable speedy and successful recovery of at least one engine. Neither checklist provides in-depth guidance on landing the aircraft if an engine restart cannot be achieved. Likewise, airliner type-rating programs are established based on the assumption that total loss of thrust culminates in at least one engine recovery, and therefore, they do not necessitate simulator training for engines-out emergency landing. Nonetheless, if an engine restart cannot be achieved in a real-life emergency, airline pilots are left with virtually no guidance on how to manage the emergency situation. Thus, it is a pressing need to further develop the idea of engines-out landing trajectory optimization for commercial aircraft.

A number of studies explored the idea of aircraft trajectory optimization in the total-loss-of-thrust emergency. The existing studies principally followed kinetic approaches based on equations of aircraft motion. A kinetic approach to aircraft trajectory optimization requires the input of aircraft-specific aerodynamic-coefficient data. Hence, the existing studies demonstrated the application of different trajectory optimization algorithms for some general aviation aircraft and fighter jets, for which the aerodynamic-coefficient data is available. On the contrary, the aerodynamic-coefficient data for commercial aircraft is not released by commercial aircraft manufacturers. Consequently, the existing work has not thoroughly explored the idea of engines-out trajectory optimization for commercial aircraft.

11.2 The Bird Strike Hazard for Contemporary Twin-Engine Aircraft

Bird strikes are expected to be more hazardous for aircraft engines in the near future due to continuous increase in large (i.e. > 8.0 lb) bird populations, the fact that present-day turbofan engines are not tested for birds heavier than 8.0 lb, and the increasing use of faster turbofan engines, which birds are less likely to detect and avoid compared to older turbojet engines. With the engine redundancy cut from three or four to two for contemporary commercial jets, this study tested whether contemporary twin-engine jetliners are significantly more likely to undergo total loss of thrust in the event of a bird strike compared to yesterday's three- and four-engine airliners.

To test the hypothesis, the data in the FAA Wildlife Strike Database was analyzed. The FAA Wildlife Strike Database involves data on all reported bird strikes in the U.S. since January

1990. The data analyzed in this study consisted of a large sample of 70,628 bird strike cases that occurred between January 1, 1990 and November 30, 2012, and involved turbofan engine civil aircraft. However, analysis of the data presented a challenge: Since the data wa collected through voluntary reporting of bird strikes by pilots and/ or other airline employees, not every reported bird strike included complete data. In fact, 14.5% of the data values in the sample were missing because they had not been reported. Thus, the missing data mechanism had to be determined prior to data analysis.

To determine the missing data mechanism, Little's Missing Completely at Random (MCAR) and separate-variance t-tests were conducted. The results showed that the missing data was neither missing completely at random nor missing at random. Instead, the missing data was non-ignorable, and a complete case analysis would result in sample selection bias. Therefore, the missing data values had to be multiply imputed to minimize sample selection bias. Unlike single imputation, multiple imputation accounts for uncertainty about the predictions for the missing values by imputing multiple plausible values for each missing value. To multiply impute the missing data values in the FAA Wildlife Strike data, an approximate Bayesian Bootstrap Method was employed. The method was chosen because it is applicable to non-ignorable missing data, and it was shown to provide unbiased estimates of true parameters when the amount of complete cases was as low as 50%. Using the approximate Bayesian Bootstrap Method, a total of five imputed data sets were generated to account for uncertainty in predicting the missing values.

To test whether twin-engine jetliners are significantly more likely to undergo total loss of thrust in the event of a bird strike compared to three- and four-engine jetliners, a

generalized linear model approach was followed. It was assumed that the probability of total loss of thrust was related to the probability of damage to all engines of the struck aircraft. Hence, the response variable in the generalized linear model was the probability that a bird strike will cause damage to all engines of the struck aircraft. This response variable was chosen based on the available data because the FAA Wildlife Strike Database does not provide information on whether a given bird strike resulted in total loss of thrust or the failure of all engines.

To build the generalized linear model, a multiple logistic regression model was initially fitted to each of the five imputed data sets. Each logistic regression model identified the factors that were significantly associated with the probability that an aircraft will sustain damage to all engines in the event of a bird strike. Using the five logistic regression models, the inferences across the five data sets were combined into a single statistical model based on the rules of nested multiple imputation. The goodness-of-fit of the resultant model was verified by applying Hosmer and Lemeshow's Test modified based on Meng and Rubin's Likelihood Ratio Test Combining Method for multiply imputed data.

A probabilistic interpretation of the statistical model presented strong evidence that today's "typical" jetliners with two under-wing mounted engines are significantly more likely to sustain damage to all engines in the event of a bird strike compared to three- and four-engine jetliners. More specifically, a bird strike was found to be:

- 12 times more likely to cause damage to all engines of the struck aircraft if it involves twin-engine aircraft as opposed to three- engine aircraft,
- 15 times more likely to cause damage to all engines of the struck aircraft if it involves twin-engine aircraft as opposed to four- engine aircraft,
- 1.4 times more likely to cause damage to all engines of the struck aircraft if the engines are mounted under the wing as opposed to on the aft fuselage.

The probability that a bird strike will cause damage to all engines of the struck aircraft was also found to be significantly associated with bird size, number of birds struck, and phase of flight. Large flocks of bird species heavier than 8.0 lb were found to be the most hazardous in this aspect. Furthermore, although most bird strikes occur during the phase of approach or descent, those that occur during the phase of climb were found to be significantly more hazardous in sustaining damage to all engines of the struck aircraft compared to those that occur during the phase of approach or descent.

The results pointed to the fact that today's "typical" jetliners are significantly more prone to losing engine redundancy in the event of a bird strike compared to three- and four-engine jetliners. Thus, in the near future, total loss of thrust due to bird strike may occur more frequently. The risk of total loss of thrust associated with the bird strike hazard may not be fully eliminated. Nonetheless, the consequences of the risk occurrence can be effectively mitigated through innovative strategies. One of the innovative strategies would be an adaptive flight planner that can achieve real-time trajectory optimization and guide the flight crew over the optimum trajectory in the event of total loss of thrust. This

dissertation hypothesized that an adaptive flight planner can significantly increase the probability of a safe touchdown in the event of total loss of thrust. The objective was to assess how effectively the adaptive flight planner can mitigate the consequences of the total-loss-of-thrust emergency. To fulfill the objective, an experiment was designed to be conducted with type-rated pilots in the full flight simulators of selected commercial jets. The experiment design involved the following steps:

1. Statistical analysis of aircraft-bird strikes resulting in engine failure, which enables identification of the most hazardous conditions for engine failure due to bird strike,
2. Assessment of the engines-out flight performance of the selected commercial jets in full flight simulators to provide the essential aerodynamic input data for engines-out trajectory optimization,
3. Development of a kinematic methodology for engines-out trajectory optimization, which would require minimal amount of aerodynamic input data, and would be readily applicable to the selected commercial jets,
4. Architectural design of an adaptive flight planner based on the kinematic methodology for the total-loss-of-thrust emergency,
5. Application of the kinematic methodology to the selected commercial jets and verification of its accuracy through flight simulation tests,
6. A designed experiment with type-rated pilots in full flight simulators to test if the adaptive flight planner would significantly increase the probability of a safe touchdown in a total-loss-of-thrust emergency under the hazardous conditions identified in step #1.

11.3 Statistical Analysis of Bird Strikes Resulting in Engine Failure

The designed experiment requires simulation of multiple total-loss-of-thrust scenarios in full flight simulators. This dissertation simulated multiple bird-strike scenarios resulting in total loss of thrust. In order to generate realistic bird strike scenarios, the FAA Wildlife Strike Database should be analyzed to identify the factors that are significantly associated with the probability of engine failure in the event of a bird strike. For this purpose, a large sample of 42,905 bird strike cases were analyzed. The sample included all airborne bird strike cases that involved turbofan-engine civil aircraft, and occurred between January 1, 1990 and November 30, 2013. The data were analyzed following the same approach outlined in section 11.2. The response variable in the generalized linear model was the probability of engine failure in the event of a bird strike. The results showed that the probability of engine failure in the event of a bird strike is significantly associated with the altitude AGL that the bird strike occurred, bird size, number of birds struck, flight phase, daylight and sky conditions. A probabilistic interpretation of the generalized linear model showed that the most hazardous conditions for engine failure due to bird strike was identified as follows:

- The phase of climb: A bird strike during climb is statistically up to 11 times more likely to result in engine failure compared to one during approach/ descent.
- Lower altitudes: Statistically, the probability of engine failure in the event of a bird strike was found to decline

by around 15% every 1,000-ft. altitude gain during the phase of climb.

- Twilight and cloudy/ overcast sky conditions: A bird strike during twilight is statistically around 90 percent more likely to result in engine failure compared to a daytime strike. Likewise, a bird strike during cloudy sky conditions is statistically 80 percent more likely to result in engine failure compared to one during clear sky conditions. Contrary to the wide misconception that "Bird do not fly in poor visibility", bird strikes not only can happen during reduced visibility conditions, but also are no less perilous than those during good visibility conditions.
- Large birds: A bird strike involving large (> 8.0 lb) birds is statistically around 30 times more likely to bring about engine failure compared to that involving small birds.
- Flocks of birds: A bird strike involving more than 10 birds is statistically around 12 times more likely to result in engine failure compared to one involving a single bird.

Based on the findings, the bird strike scenario leading to total loss of thrust was to be simulated during the phase of climb at a low altitude (i.e. below 5,000 ft AGL) in twilight and cloudy sky conditions.

Additional inferences concerning aviation practitioners are listed as follows:

- Future designs of turbofan engines are recommended to be tested for birds larger than 8.0 lb beyond the current FAA requirements. The FAA may also consider reviewing and/ or improving the current turbofan engine design requirements.

- In case of airports with limited resources, bird deterrent programs should give prominence to prevailing aircraft climb paths.
- Flight crews should be extremely vigilant at lower altitudes and in reduced visibility such as twilight and cloudy sky conditions.
- During climb, lower altitudes should be cleared using speeds and flap settings that provide higher rate of climb. Climb speeds around V_x are recommended as opposed to V_y since climb speeds around V_x offer enhanced flight safety benefits. Lower flap settings are recommended (if runway length permits) since they induce less drag during the initial climb-out.
- Future designs of turbofan engines are recommended to be tested for large birds beyond the current FAA requirements.
- Flight crews should delay take-off or landing if flocks of birds are reported. If landing cannot be delayed, flight crews should plan on additional landing distance because a possible bird strike may disable thrust reversers.
- Wildlife management programs should particularly focus on airport environments and involve species-specific means of controlling attractants, particularly for large bird species such as Canada goose, double-crested cormorant, snow goose and black/ turkey vulture.

11.4 Engines-out Glide Performance of the Selected Commercial Jets

When an aircraft undergoes total loss of thrust, its flight envelope is reduced due to the inability to produce thrust, and its post-failure performance characteristics primarily depend on

its aerodynamic design. Since aerodynamic design varies based on aircraft model, post-failure performance characteristics are specific to aircraft model. Therefore, a given aircraft model requires exclusive development of an adaptive flight planner. The budget allocated for this study allows for the consideration of up to two aircraft models. The selected aircraft models are the Airbus A320-200 and the Boeing 737-800, which transported 74.7 million and 82.3 million passengers in 2013 on all U.S. These aircraft models are chosen because they are currently the best-selling commercial jets manufactured by Airbus Industrie and the Boeing Company.

Since a kinematic approach to trajectory optimization deals with pure motion without reference to masses and forces involved in it, the motion characteristics of the A320 and 737-800 aircraft during engines-out descent had to be defined. An aircraft undergoing total loss of thrust should lose altitude (i.e. potential energy) to maintain the airspeed above the stall speed. In the event of total loss of thrust, aircraft motion characteristics are typically defined by “glide ratio”, which equals the horizontal distance travelled by the aircraft divided by the altitude loss. At altitudes below 10,000 ft, glide ratio primarily depends on airspeed and aircraft configuration. In order to define aircraft motion characteristics during engines-out descent, flight simulation tests are conducted in full flight simulators of the A320 aircraft with wing-tip fences, and the 737-800 aircraft with blended winglets. The goal of the flight simulator tests was to define the relationship between glide ratio versus airspeed at different aircraft configurations. The aircraft configurations analyzed in this study were as follows:

- A typical takeoff configuration, which was wing configuration “1+F” for the A320 aircraft, and flap setting “5” for the 737-800 aircraft. These takeoff configurations were chosen because they result in less drag and superior climb performance than the other typical takeoff settings on these aircraft.
- Typical landing configurations, which was wing configurations “3” and “FULL” for the A320 aircraft, and flap settings “30” and “40” for the 737-800 aircraft.
- The “clean” configuration, in which the flaps and slats were fully retracted.

The major findings from the flight simulation tests are summarized as follows:

- The relationship between glide ratio versus airspeed displayed a concave-downward pattern at a particular aircraft configuration. In other words, there is an optimum angle-of-glide speed that gives the maximum engines-out glide ratio at a given configuration. That optimum airspeed is generally slightly higher than the airspeed corresponding to minimum total drag.
- For the A320 aircraft with wing-tip fences, the optimum angle-of-glide speed and the corresponding engines-out glide ratio was found as approximately 225 KCAS and 17.1, respectively, at a gross weight of 70.0 tons in “clean” configuration. For the 737-800 aircraft with blended winglets, the optimum angle-of-glide speed and the corresponding engines-out glide ratio was found as approximately 205-to-210 KCAS and 18.5, respectively, at the same gross weight and configuration.

- The fact that the 737-800 with blended winglets had a slightly higher glide ratio and a lower optimum angle-of-glide speed than the A320 with wing-tip fences was attributed to the blended winglets, which can effectively reduce induced drag.
- For both aircraft, the engines-out glide ratio in typical landing configurations was found well steeper than the 3°-glide path. Therefore, a total loss of thrust during final approach to destination airport would most likely rule out reaching the destination runway, as in the case of Kegworth Air Disaster in January, 1989. Thus, flight crews should promptly find an alternative landing site within the current aircraft heading in such an emergency situation.

The relationship between glide ratio versus airspeed found from this phase of the study was used as aerodynamic input data for the architectural design of the adaptive flight planner.

11.5 Kinematic Approach to Engines-out Trajectory Optimization

It is not possible to compute the aerodynamic forces acting on the aircraft with the aerodynamic-coefficient data, which is not publically available for commercial jets. Therefore, a trajectory optimization method based on the principles of kinetics cannot be adopted without the aerodynamic coefficient data. Instead, this study adopted a kinematic approach to trajectory optimization, which dealt with pure motion without reference to masses and forces involved in it.

The objective of the kinematic methodology was to compute the engines-out landing trajectory that would require minimum altitude loss to reach an intended touchdown location within the

degraded flight envelope of the distressed aircraft. In order to be of practical value, the optimum trajectory should be easy to follow in the event of an emergency, and should not require erratic changes in flight path angle and bank angle. Therefore, the following assumptions were incorporated into the formulation of the optimum trajectory:

- The optimum landing trajectory was formulated based on a constant calibrated airspeed, which is directly related to flight path angle. In the event of total-loss-of-thrust emergency, it would be considerably more intuitive for flight crews to maintain a given airspeed rather than following a set of complex pitch attitude directives.
- The optimum landing trajectory would not require more than three banked turns. Otherwise, too many changes in bank angle would be impractical to follow in an emergency situation.

Based on these assumptions, the trajectory optimization problem was formulated over a continuous domain based on the principles of kinematics. The optimum trajectory was defined as a segmented trajectory that consisted of three types of segments where different segments represented different bank angle states. The three types of trajectory segments are briefly explained as follow:

1. Linear segments, where the aircraft performed equilibrium, wings-level glide with 0°-bank angle.
2. Circular segments, where the aircraft performed a turning maneuver at a constant, positive bank angle.
3. Transition segments, where the bank angle was assumed to change linearly from zero to a positive value and vice versa.

The aerodynamic input data to the optimization problem was a 3rd-degree, piece-wise continuous polynomial function that quantified the predicted relationship between engines-out glide ratio versus bank angle at the intended landing speed. To compute the solution to the trajectory optimization problem, the Differential Evolution Algorithm was employed, which is a robust and fast algorithm for continuous domains that can handle non-differentiable, nonlinear and multimodal objective functions as in this problem. The Differential Evolution Algorithm was applied in a minimum of two stages during the computation of the optimum trajectory. These stages are briefly explained as follows:

1. In the first stage, the Differential Evolution Algorithm was applied to the initial formulation of the optimization problem, which was based on calibrated airspeed instead of true airspeed. This was because true airspeed depends on the flight altitude, and the flight altitude could only be found once the optimization problem was solved. At this stage, the Differential Evolution Algorithm was applied to the initial formulation of the optimization problem, and returned a preliminary solution.
2. In the second stage, the true airspeed terms were estimated based on the preliminary solution, and the optimization problem was formulated based on the estimated true airspeed terms. Then the Differential Evolution Algorithm was applied to obtain a subsequent solution to the optimization problem, and then the true airspeed terms were computed based on the subsequent solution. If there was less than 1.0-percent relative difference between the newly-computed true airspeed terms and estimated true airspeed terms, the

optimization problem has converged, and the subsequent solution would be the final solution.

The solution to the optimization problem was a segmented trajectory, which was shown to be easily reduced to simple pilot and ATC commands. The optimization procedure is also computationally undemanding, which makes it practical for real-time applications.

In order to verify its accuracy, the kinematic methodology was applied to both the A320 and 737-800 aircraft. Multiple total-loss-of-thrust scenarios were generated, and the kinematic methodology was employed to compute the optimum landing trajectory in each scenario. A total of 16 engines-out landing trajectories were generated for each aircraft, and the altitude loss required for flying each trajectory was computed. Following this, each trajectory was simulated in a full flight simulator with three type-rated pilots. Each of the three pilots were guided over a given trajectory by means of the simple pilot and ATC commands associated with that trajectory. Once a given trajectory was simulated with the three type-rated pilots, the average simulated altitude loss required for flying that trajectory was obtained. Subsequently, the computed altitude loss was compared with the average simulated altitude loss for each trajectory. The findings showed that the kinematic methodology consistently overestimated the required altitude loss for all 32 trajectories. Nonetheless, the relative error in estimating the altitude loss was within 1.5 to 3.6 percent for the Airbus A320 aircraft, and within 3.7 to 5.1 percent for the Boeing 737-800 aircraft. Hence, the results were accurate enough for practical purposes, and the kinematic methodology is found promising for real-world applications.

11.6 Limitations of the Kinematic Approach

The kinematic methodology developed in this study is applicable to virtually all possible events of total loss of thrust. However, it is primarily intended for a total-loss-of-thrust emergency at a low altitude since engine failure due to bird strike is most likely to occur below 5,000 ft AGL. If the kinematic methodology is applied to a total-loss-of-thrust emergency that occurs above 10,000 ft AMSL, the methodology should be modified by incorporating the compressibility into the calculations, which would in turn marginally increase the required computational time.

Another limitation of the methodology stems from the formulation of the optimum trajectory. The kinematic methodology regards the optimum trajectory as the one that would require minimized altitude loss to the intended landing site. If the aircraft altitude is greater than that required for flying the optimum trajectory, the methodology does not provide guidance on excess altitude dissipation. In such cases, the pilots would have to dissipate the excess altitude by applying one or more of the following strategies:

- Early extension of the landing gear.
- A side-slip maneuver.
- S-turn maneuvers
- Flaps extension, provided that the aircraft has sufficient hydraulic power.

Should the flight crew extend the flaps, the aerodynamic performance of the aircraft would change, which would require re-computation of the optimum landing trajectory.

11.7 Assessing the Effectiveness of the Adaptive Flight Planner through a Designed Experiment

After the architectural design of the adaptive flight planner was complete, a designed experiment was conducted to test the hypothesis that the adaptive flight planner would significantly increase the odds of a safe touchdown in the event of total loss of thrust. The designed experiment was conducted in the full flight simulators of the Airbus A320 and Boeing 737-800 aircraft. The designed experiment involved the simulation of realistic total-loss-of-thrust scenarios in the full flight simulators. The findings from the statistical analysis of bird strikes showed that engine failure due to bird strike was statistically most likely to occur during the initial climb at altitudes below 5,000 ft AGL in twilight and cloudy sky conditions. Based on these findings, a total of five bird strike scenarios were generated. Two of the bird strike scenarios were simulated in the virtual environment of Amsterdam Schiphol International Airport, and the remaining three scenarios were simulated in the virtual environment of Istanbul Atatürk International Airport. The five bird strike scenarios were generated as follows:

1. The aircraft (i.e. the A320 or 737-800) took off from Schiphol Airport's runway 36C. The takeoff configuration was "1+F" for the A320 aircraft, and flap setting "5" for the 737-800 aircraft. Prior to flap retraction, the aircraft ingested multiple birds into both engines and underwent total loss of thrust. While heading 3° at a distance of 2.0 nm from runway 18C threshold, an engines-out emergency landing was initiated.

2. The aircraft took off from Schiphol Airport's runway 06. The takeoff configuration was "1+F" for the A320 aircraft, and flap setting "5" for the 737-800 aircraft. Prior to flap retraction, the aircraft ingested multiple birds into both engines and underwent total loss of thrust. While heading 58° at a distance of 2.0 nm from runway 24 threshold, an engines-out emergency landing was initiated.
3. The aircraft took off from Atatürk Airport's runway 17L. After flap retraction, the aircraft ingested multiple birds into both engines and underwent total loss of thrust. While heading 174° at a distance of 3.0 nm from runway 35R threshold, an engines-out emergency landing was initiated.
4. The aircraft took off from Atatürk Airport's runway 05. After flap retraction, the aircraft ingested multiple birds into both engines and underwent total loss of thrust. While heading 55° at a distance of 3.0 nm from runway 23 threshold, an engines-out emergency landing was initiated.
5. The aircraft took off from Atatürk Airport's runway 23. The takeoff configuration was "1+F" for the A320 aircraft, and flap setting "5" for the 737-800 aircraft. Prior to flap retraction, the aircraft ingested multiple birds into both engines and underwent total loss of thrust. While heading 235° at a distance of 2.0 nm from runway 05 threshold, an engines-out emergency landing was initiated.

Using the kinematic methodology, the optimum engines-out landing trajectory that would require the minimum altitude loss was computed for each scenario and each aircraft. Each optimum trajectory was reduced to simple oral pilot commands for use in the designed experiment.

The designed experiment was conducted with six type-rated A320 pilots, and six type-rated 737-800 pilots. All scenarios

were simulated in twilight and cloudy sky conditions. The aircraft gross weight was 70.0 tons in all scenarios. Besides, it was assumed that the aircraft did not have sufficient hydraulic power for flaps extension or retraction, so a change in wing configuration was not permitted during the landing attempts. Each scenario was simulated twice with a given pilot in command. The first landing attempt of each pilot in a given scenario was called the "control run". During the control runs, the pilot in command was simply asked to attempt engines-out landing on a runway of his/ her own preference. The second landing attempt of each pilot in a given scenario was called the "treatment run". During the treatment runs, the pilot in command was guided over the optimum trajectory through the oral pilot commands. The starting altitude in each simulation run was marginally greater than that required for flying the optimum trajectory. Thereby, a safe landing could only be achieved in a given scenario if the pilot in command were to approximately follow the optimum trajectory. A total of 120 flight simulation runs were conducted in the full flight simulator. The outcomes of the simulations are summarized as follows:

- In nine out of 12 runs, the pilot in command crashed the aircraft in the "control" run, but accomplished safe landing in the corresponding "treatment" run on the A320 aircraft in clean configuration. The crashes were predominantly caused by the pilots' preference to maintain the "green dot" speed, which is the procedure recommended in the A320 engine dual failure checklist, but was not the optimum airspeed in the simulated scenarios (see Figure D-1 in Appendix D).
- In nine out of 18 runs, the pilot in command crashed the aircraft in the "control" run, but accomplished safe

landing in the corresponding “treatment” run on the A320 aircraft in wing configuration “1+F”. The crashes were predominantly caused by the pilots’ decision to attempt landing to other runways that were in fact outside of the aircraft’s glide range (see Figure D-1 in Appendix D).

- In 13 out of 18 runs, the pilot in command crashed the aircraft in the “control” run, but achieved safe landing in the corresponding “treatment” run on the 737-800 aircraft in flap setting “5”. The crashes were predominantly caused due to the pilots’ preference to maintain the flap 5 “maneuvering speed”, which was approximately 20 knots greater than the optimum airspeed in the simulated scenarios (see Figure D-2 in Appendix D).
- In 11 out of 12 runs, the pilot in command crashed the aircraft in the “control” run, but achieved safe landing in the corresponding “treatment” run on the 737-800 aircraft in clean configuration. Similar to the simulation runs in flap setting “5”, the predominant crash cause was the preference to maintain the “maneuvering speed”, which was approximately 15 knots greater than the optimum airspeed in the simulated scenarios (see Figure D-2 in Appendix D).

The outcomes of the designed experiment were statistically analyzed to test the research hypothesis. The “control” and “treatment” samples were statistically dependent for a given aircraft type because they involved the same pilot subjects. To account for the correlation between the “control” and “treatment” samples, a generalized linear mixed model approach was followed. A separate model was built for each aircraft type. The pilot effects were incorporated as random effects whereas the wing configuration and airport location were incorporated as fixed effects into the models. The number of observations met

the minimum sample size requirements for the generalized linear mixed model. A Laplace approximation method was followed to compute the coefficient estimates in the models. Both the wing configuration and treatment effects were found significant at a Type I Error rate of 0.05 in the mixed model for the A320 aircraft. On the other hand, only the treatment effect was found significant at a Type I Error rate of 0.05 in the mixed model for the 737-800 aircraft. The goodness-of-fit of both models were verified using the Hosmer and Lemeshow Test. Using the coefficient estimates in the mixed models, the predicted probability of safe touchdown on a runway is computed based on different levels of the fixed effects. Interpretation of the mixed models showed that:

- When the A320 pilots were guided with the ATC commands, the predicted probability of safe touchdown on a runway increased significantly from 0.51 to 0.99 in wing configuration "1+F", and from 0.13 to 0.94 in "clean" configuration compared to when they were not guided during the engines-out landing attempts.
- When the 737-800 pilots were guided with the ATC commands, the predicted probability of safe touchdown on a runway increased significantly from 0.36 to 0.82 compared to when they were not guided during the engines-out landing attempts.

Thus, at a Type I Error rate of 0.05, the results provided strong evidence in favor of the hypothesis that the adaptive flight planner would significantly increase the probability of a safe touchdown in the event of total loss of thrust. The ATC commands generated by the adaptive flight planner increased the probability of safe touchdown in the simulated total-loss-of-thrust scenarios because:

- The ATC commands enabled prompt selection of a landing site within the aircraft's glide range.
- The ATC commands assisted the pilots in performing energy-preserving maneuvers to the intended landing site.

With the increased probability of safe touchdown on a runway, the probability of casualty and hull loss was also significantly reduced through the deployment of the adaptive flight planner.

The research hypothesis tested in this study can open the door for how commercial aircraft manufacturers approach the growing hazard of total loss of thrust. With the emergent threat of bird strikes and the prevalence of twin-engine aircraft that has reduced engine redundancy, commercial aircraft manufacturers may undertake steps to incorporate the proposed adaptive flight planner into future glass cockpit technologies.

11.8 Future Research

This study demonstrated that the probability of safe touchdown in the event of total loss of thrust can be significantly increased with the deployment of the adaptive flight planner that guides pilots to a reachable landing site through simple ATC commands. The effectiveness of the adaptive flight planner was demonstrated for wing configurations "1+F" and "UP" on the Airbus A320 aircraft, and for flap settings "5" and "UP" on the Boeing 737-800 aircraft. The budget allocated for the study did not allow for assessing the effectiveness of the adaptive flight planner for other aircraft models and/ or other wing configurations. For future research, the following are recommended:

- The effectiveness of the adaptive flight planner can be tested for other takeoff configurations, which include wing configurations “2” and “3” on the A320 aircraft, and for flap settings “10” and “15” on the 737-800 aircraft.
- The adaptive flight planner can be developed for twin-engine wide-body jets such as the Airbus A330 and Boeing 777 aircraft, and the effectiveness of the adaptive flight planner on wide-body jets can be compared with that on narrow-body jets.
- In light of the findings, the existing dual-engine failure checklists for twin-engine airliners can be reviewed and extended to specifically address the total-loss-of-thrust emergency at a low altitude.
- The kinematic methodology can be elaborated to provide guidance on excess altitude dissipation for emergency situations, in which the aircraft altitude is greater than the minimum altitude required for reaching the intended touchdown location.
- Flight simulation tests can be performed to assess engines-out glide performance in the presence of cross wind. Thereby, the effect of rudder deployment on engines-out glide ratio can be measured, and the adaptive flight planner can incorporate the effects of crosswind in real-time trajectory optimization.

REFERENCES

[1] R. A. Dolbeer, S. E. Wright, J. Weller and M. J. Begier, "Wildlife Strikes to Civil Aircraft in the United States 1990-2012," Federal Aviation Administration National Wildlife Strike Database Serial Report Number 19, Washington, DC, 2013.

[2] "Rise in Airplane-Bird Strikes Threatens Flight Safety," NBC News, Washington, 2013.

[3] "Aviation Safety Network," Flight Safety Foundation, 2013. [Online]. Available: http://aviation-safety.net/database/record.php?id=19880915-0. [Accessed 11 June 2013].

[4] F. S. Foundation, "Military Boeing 707 Strikes Birds After Liftoff; Damage to Engines No. 1 and No. 2 Results in Loss of Power and Impact with Terrain," *Accident Prevention,* vol. 53, no. 11, November 1996.

[5] NTSB, "Foreign Notification Aviation. NTSB ID: ENG10WA002," National Transportation Safety Board, Washington, D.C., 2010.

[6] NTSB, "Foreign Notification Aviation. NTSB ID: DCA09RA010," National Transportation Safety Board, Washington, D.C., 2010.

[7] NTSB, "Loss of Thrust in Both Engines After Encountering a Flock of Birds and Subsequent Ditching on the Hudson River. US Airways Flight 1549 Airbus A320-214, N106US. Weehawken, New Jersey. January 15, 2009," National Transportation Safety Board, Washington, D.C., 2010.

[8] L. Lawal, "Dana Air Aircraft Suffers Bird Strike in Lagos," Nigeria Masterweb Daily News, 22 April 2010. [Online]. Available: http://nigeriamasterweb.com/blog/index.php/2010/04/22/dana_air_aircraft_suffers_bird_strike_in. [Accessed 1 September 2013].

[9] Code of Federal Regulations (CFR), "33.76 Bird Ingestion," in *Title 14: Aeronautics and Space, Part 33 -*

Airworthiness Standards: Aircraft Engines, Washington, D.C., U.S. Government Publishing Office, 2011.

[10] Code of Federal Regulations (CFR), "33.75 Safety Analysis," in *Title 14: Aeronautics and Space, Part 33 - Airworthiness Standards: Aircraft Engines*, Washington, D.C., U.S. Government Publishing Office, 2007.

[11] RITA, "Passengers: All Carriers, All Airports," Research and Innovative Technology Administration, Washington, 2013.

[12] RITA, "Air Carriers : T-100 Segment (US Carriers Only)," Research and Innovative Technology Administration, 2013. [Online]. Available: http://www.transtats.bts.gov/Oneway.asp?Display_Flag=0&Percent_Flag=0. [Accessed 6 September 2013].

[13] RITA, "Sum : Non-Stop Segment Passengers Transported by AircraftType for 2013," Bureau of Transportation Statistics, Washington, 2014.

[14] The Boeing Company, "ETOPS Expansion," *AERO 04,* 1998.

[15] Airbus Industrie, "A340 Family," Airbus Industries, October 2013. [Online]. Available: http://www.airbus.com/aircraftfamilies/passengeraircraft/a340family/. [Accessed 25 November 2013].

[16] P. M. Peeters, J. Middel and A. Hoolhorst, "Fuel efficiency of commercial aircraft: An overview of historical and future trends," National Aerospace Laboratory (NLR), Amsterdam, Netherlands, 2005.

[17] K. Holland, "Dana Air Claims Bird Strike Cause for MD-83 Crash, Others Disagree," Airnation.net, 10 June 2012. [Online]. Available: http://airnation.net/2012/06/10/dana-air-bird-strike-cause-md-83-crash/. [Accessed 31 August 2013].

[18] G. D'Amato, Director, *Hudson River Runway.* [Film]. Canada: Cineflix Media, 2011.

[19] FAA, Airline Transport Pilot and Aircraft Type Rating Practical Test Standards for Airplane, Washington, D.C.: U.S. Department of Transportation, Federal Aviation Administration, Flight Standards Service, 2008, pp. 1,43.

[20] Code of Federal Regulations (CFR), "61.157 Flight Proficiency," in *Title 14: Aeronautics and Space, Part 61 - Certification: Pilots, Flight Instructors, and Ground Instructors*, Washington, D.C., D.C.: U.S. Government Printing Office, 2014.

[21] 14 CFR 25.671d, *Evaluation of All-Engines Failed Condition,* 2010.

[22] K. Holland, "Dana Air Claims Bird Strike Cause for MD-83 Crash, Others Disagree," Airnation.net, 10 June 2012. [Online]. Available: http://airnation.net/2012/06/10/dana-air-bird-strike-cause-md-83-crash/. [Accessed August 2013].

[23] J. D. Anderson, Fundamentals of Aerodynamics, 4th Edition ed., New York, NY: McGraw-Hill, 2007.

[24] The Boeing Company, "Commercial Airplanes: Out-of-Production," The Boeing Company, 2013. [Online]. Available: http://www.boeing.com/boeing/commercial/out_of_production.page. [Accessed 26 November 2013].

[25] American Airlines, "American's Fleet Modernization Plan Enhances Customers' Travel Experience," 2012.

[26] Airbus Industrie, "A320 Orders &Deliveries," Airbus, 2015. [Online]. Available: http://www.airbus.com/aircraftfamilies/passengeraircraft/a320family/a320/. [Accessed 7 February 2015].

[27] The Boeing Company, "The Boeing Next-Generation 737-800," The Boeing Company, 2013. [Online]. Available: http://www.boeing.com/boeing/commercial/737family/737_800back.page?. [Accessed 11 August 2013].

[28] The Boeing Company, "737-700 Technical Characteristics," The Boeing Company, 2013. [Online]. Available: http://www.boeing.com/boeing/commercial/737family/pf/pf_700tech.page?. [Accessed 11 August 2013].

[29] The Boeing Company, "737-800 Technical Characteristics," The Boeing Company, 2013. [Online]. Available: http://www.boeing.com/boeing/commercial/737family/pf/pf_800tech.page. [Accessed 11 August 2013].

[30] Airbus Industrie, "A320 Dimensions & Key Data," Airbus, 2013. [Online]. Available: http://www.airbus.com/aircraftfamilies/passengeraircraft/a320family/a320/specifications/. [Accessed 11 August 2013].

[31] Airbus Industrie, "Key Documents, 2013 Airbus Results Table," 2014. [Online]. Available: http://www.airbus.com/presscentre/corporate-information/key-documents/. [Accessed 6 December 2014].

[32] The Boeing Company, "Recent Annual Orders, Orders and Deliveries," 2014. [Online]. Available: http://active.boeing.com/commercial/orders/index.cfm. [Accessed 6 December 2014].

[33] NTSB, "Aircraft Accident Report - Southern Airways, Inc. , DC-9-31, N1335U, New Hope, Georgia, April 4, 1977," National Transportation Safety Board, Bureau of Accident Investigation, Washington, D.C., 1978.

[34] NTSB , "NTSB Identification: FTW88IA109," National Transportation Safety Board, Washintgon, D.C., 1991.

[35] O. Forssberg, S.-E. Sigfridsson, N. Benker, H. Elinder, R. Lundin and J. Mansfeld, "Air Traffic Accident on 27 December 1991 at Gottröra, AB County," Swedish Civil Aviation Administration, Norrköping, 1993.

[36] Associated Press, "Delta Pilot Loses License Over Plane's Power Loss," The New York Times, 9 August 1987. [Online]. Available: http://www.nytimes.com/1987/08/09/us/delta-pilot-loses-license-over-plane-s-power-loss.html. [Accessed 9 September 2013].

[37] Flight Safety Foundation, "Accident Description," 2013. [Online]. Available: http://aviation-safety.net/database/record.php?id=19890108-0. [Accessed 9 September 2013].

[38] Flight Safety Foundation, "Accident Description," 2013. [Online]. Available: http://aviation-safety.net/database/record.php?id=19710906-0. [Accessed 18 August 2013].

[39] AAPID, "All Engines-out Landing Due to Fuel Exhaustion, Air Transat, Airbus A330-243 marks C-GITS, Lajes, Azores,

Portugal, 24 August 2001," Aviation Accidents Prevention and Investigation Department of Portugal, 2003.

[40] Ethiopian Civil Aviation Authority Flight Safety Department, "Ethiopian Airlines B767 (ET-AIZ) Aircraft Accident in the Federal Islamic Republic of the Comoros, in the Indian Ocean on November 23, 1996," Ethiopian Civil Aviation Authority Flight Safety Department, Addis Ababa, 1998.

[41] B. Tootell, All Four Engines Have Failed, MacMillan Education Australia, 1986.

[42] R. Witkin, "Jet Lands Safely After Engines Stop in Flight Through Volcanic Ash," The New York Times, 16 December 1989. [Online]. Available: http://www.nytimes.com/1989/12/16/us/jet-lands-safely-after-engines-stop-in-flight-through-volcanic-ash.html. [Accessed 9 September 2013].

[43] D. F. Rogers, "Possible "Impossible" Turn," *Journal of Aircraft,* vol. 32, no. 2, pp. 392-395, April 1995.

[44] J. Hoffren and T. Raivio, "Optimal Maneuvering After Engine Failure," in *Atmospheric Flight Mechanics Conference*, Minneapolis, 2000.

[45] D. C. Hyde, "Minimum-Altitude-Loss Gliding Turns with Terminal Constraints (Return to Runway After Engine Failure)," in *AIAA Atmospheric Flight Mechanics Conference and Exhibit*, San Francisco, 2005.

[46] I. Shapira and J. Ben-Asher, "Range Maximization for Emergency Landing After Engine Cutoff," *Journal of Aircraft,* vol. 42, no. 5, pp. 1296-1306, September-October 2005.

[47] E. M. Atkins, I. A. Portillo and M. J. Strube, "Emergency Flight Planning Applied to Total Loss of Thrust," *Journal of Aircraft,* vol. 43, no. 4, pp. 1205-1216, 2006.

[48] K. Brinkman and H. G. Visser, "Optimal Turn-Back Manoeuvre After Engine Failure In a Single-Engine Aircraft During Climb-Out," *Journal of Aerospace Engineering,* vol. 221, pp. 17-27, 1 January 2007.

[49] T. Peng, Z. Shuguang, J. Lei and T. Zhi, "A Novel Emergency Flight Path Planning Strategy for Civil

Airplanes in Total Loss of Thrust," in *The 2nd International Symposium on Aircraft Airworthiness (ISAA 2011)*, Beijing, 2011.

[50] A. Adler, A. Bar-Gill and N. Shimkin, "Optimal Flight Paths for Engine-Out Emergency Landing," in *Proceedings of the 2012 24th Chinese Control and Decision Conference, CCDC 2012*, Taiyuan, 2012.

[51] H. Wu, N. C. Cho, H. Bouadi, L. Zhong and F. Mora-Camino, "Dynamic Programming for Trajectory Optimization of Engine-out Transportation Aircraft," in *24th Chinese Control and Decision Conference*, Taiyuan, 2012.

[52] NTSB (Foreign Source), "NTSB Identification: DCA12RA084," National Transportation Safety Board, Washington, D.C., 2012.

[53] M. Williams, "The 156-tonne Gimli Glider," *Flight Safety Australia,* pp. 22-27, July-August 2003.

[54] DGCA, "Civil Aviation Aircraft Accident Summary for the Year 1993," Directorate General of Civil Aviation, 1994. [Online]. Available: http://www.dgca.nic.in/accident/acc93.pdf. [Accessed 9 August 2013].

[55] R. A. Dolbeer, "Height Distribution of Birds Recorded by Collisions with Civil Aircraft," *Air Safety Week,* vol. 19, no. 43, 7 11 2005.

[56] M. Zalakevicius, "Bird Strike Analysis in Lithuania," *Acta Ornithologica Lituanica,* Vols. 9-10, pp. 87-90, 1994.

[57] V. Jacoby, "Analysis of Bird Collision with Planes and Possibility of Utilization of the Bird Strike Prevention Measures," in *Bird Strike Committee Europe (BSCE), 20th Meeting, Helsinki, Finland, May 21st-25th, 1990, Working Papers*, Helsinki, 1990.

[58] NTSB, "Aircraft Accident Report: Overseas National Airways, Inc., Douglas DC-9, N935F Operating as Antilliaanse Luchtvaart Maatschappij Flight 980 Near St. Croix, Virgin Islands, May 2, 1970," National Transportation Safety Board, Washington, D.C., 1971.

[59] "Paraffin Caused One-Eleven Crash," *Flight International,* p. 444, 5 October 1972.

[60] Flight Safety Foundation, "Accident Description," 2013. [Online]. Available: http://aviation-safety.net/database/record.php?id=19761207-0. [Accessed 18 August 2013].

[61] NTSB, "Aircraft Accident Report - United Airlines, Inc., McDonnell-Douglas DC-8-61, N8082U, Portland, Oregon, December 28, 1978," National Transportation Safety Board, Bureau of Accident Investigation, Washington, D.C., 1979.

[62] "1988: Bad for Schedules," *Flight International,* p. 51, 21 January 1989.

[63] Flight Safety Foundation, "Accident Description," 2013. [Online]. Available: http://aviation-safety.net/database/record.php?id=20041014-1. [Accessed 18 August 2013].

[64] J. Brooke, "After Trek From Brazil Crash, Survivor Says 46 of 54 Live," *The New York Times,* 6 September 1989.

[65] NTSB, "Aircraft Accident Report: Avianca, the Airline of Columbia Boeing 707-321B, HK 2016 Fuel Exhaustion, Cove Neck, New York, January 25 1990," National Transportation Safety Board, Washington, D.C., 1991.

[66] B. R. Guttery, Encyclopedia of African Airlines, Jefferson, NC: McFarland Company, Inc., Publishers, 1998, p. 147.

[67] Flight Safety Foundation, "Accident Description," 2013. [Online]. Available: http://aviation-safety.net/database/record.php?id=19940926-0. [Accessed 18 August 2013].

[68] NTSB , "NTSB Identification: DCA00WA068," National Transportation Safety Board, Washington, D.C., 2000.

[69] NTSC, "Aircraft Accident Report: PT. Garuda Indonesia GA421 B737-300 PK-GWA Bengawan Solo River, Serenan Village, Central Java, 16 Jnauary 2002," National Transportation Safety Committee, 2006.

[70] NTSB, "Crash of Pinnacle Airlines Flight 3701 Bombardier CL-600-2B19, N8396A, Jefferson City, Missouri, October 14,

2004," National Transportation Safety Board, Washington, D.C., 2007.

[71] R. A. Price, "Glide Range Depiction for Electronic Flight Instrument Displays". USA Patent US6573841 B2, 3 June 2003.

[72] H. C. Smith, The Illustrated Guide to Aerodynamics, New York: TAB Books/ McGraw-Hill, 1992.

[73] Stanford University, "Engine Placement," 2013. [Online]. Available: http://adg.stanford.edu/aa241/propulsion/engineplacement.html. [Accessed 26 November 2013].

[74] F. A. Administration, "FAA Wildlife Strike Database," 31 1 2013. [Online]. Available: http://wildlife.faa.gov/database.aspx. [Accessed 02 2013].

[75] RITA, "Sum : Non-Stop Segment Passengers Transported by AircraftType for 2013," Bureau of Transportation Statistics, Washington, 2014.

[76] D. G. Garson, Missing Values Analysis & Data Imputation, Statistical Associates Publishers - Blue Book Series, 2012.

[77] R. J. A. Little, "A Test of Missing Completely at Random for Multivariate Data with Missing Values," *Journal of the American Statistical Association:Theory and Methods,* vol. 43, no. 404, pp. 1198-1202, December 1988.

[78] D. B. Rubin, "Multiple Imputation for Nonresponse in Surveys," John Wiley & Sons, Inc., New York, 1987.

[79] B.-J. Lee and L. C. Marsh, "Sample Selection Bias Correction for Missing Observations," *Oxford Bulletin of Economics and Statistics,* vol. 62, no. 2, pp. 305-322, 2000.

[80] J. Siddique and T. R. Belin, "Using an Approximate Bayesian Bootstrap to Multiply Impute Nonignorable Missing Data," *Computational Statistics and Data Analysis,* vol. 53, pp. 405-415, 2008.

[81] J. Siddique and T. R. Belin, "Multiple Imputation Using an Iterative Hot-Deck with Distance-Based Donor Selection," *Statistics in Medicine,* vol. 27, pp. 83-102, 2008.

[82] J. Siddique and T. R. Belin, "MIDAS: A SAS Macro for Multiple Imputation," *Journal of Statistical Software,* vol. 29, no. 9, February 2009.

[83] L. M. Collins, J. L. Schafer and C. M. Kam, "A Comparison of Inclusive and Restrictive Strategies in Modern Missing Data Procedures," *Psychological Methods,* vol. 6, pp. 330-351, 2001.

[84] A. Agresti, "Inference for Logistic Regression," in *Introduction to Categorical Data Analysis*, New Jersey: John Wiley & Sons, 2007, pp. 106-108.

[85] A. Agresti, "Fitting Generalized Linear Models," in *An Introduction to Categorical Data Analysis*, Hoboken, NJ: John Wiley & Sons, Inc., 2007, pp. 88-89.

[86] A. Agresti, "Strategies in Model Selection," in *An Introduction to Categorical Data Analysis*, Hoboken, NJ: John Wiley & Sons, Inc., 2007, pp. 139-141.

[87] Z. J. Shen, *Nested Multiple Imputation,* Cambridge, MA: Department of Statistics, Harvard University, 2000.

[88] D. W. Hosmer and S. Lemeshow, Applied Logistic Regression, Second Edition ed., Hoboken, NJ: John Wiley & Sons, Inc., 2000.

[89] D. Sullivan and R. Andridge, *Hosmer-Lemeshow Goodness-of-Fit Test for Multiply Imputed Data,* San Diego, CA: American Statistical Association, 2012.

[90] X.-L. Meng and D. B. Rubin, "Performing Likelihood Ratio Tests with Multiply-Imputed Data Sets," *Biometrika,* vol. 79, no. 1, pp. 103-111, March 1992.

[91] R. A. Dolbeer, "Birds and Aircraft - Fighting for Airspace in Ever More Crowded Skies," *Human-Wildlife Conflicts,* vol. 3, no. 2, pp. 165-166, 2009.

[92] R. Nicholson and W. S. Reed, "Strategies for Prevention of Bird-Strike Events," *Aero Quaterly,* pp. 17-24, March 2011.

[93] J. L. Dunn and J. Alderfer, National Geographic Field Guide to the Birds of North America, Fifth Edition ed., Washington, D.C.: National Geographic Society, 2006.

[94] Airbus Industrie, "A Glance at Airbus' Key Dates," Airbus, 2013. [Online]. Available: http://www.airbus.com/company/history/the-timeline/. [Accessed 10 August 2013].

[95] G. Norris and M. Wagner, Airbus, Osceola, WI: MBI Publishing Company, 1999.

[96] Airbus Industrie, A318/ A319/ A320/ A321 Flight Crew Operating Manual, Vols. 1-4, Toulouse: Airbus Industrie, Inc., 2002.

[97] Airbus Industrie, Getting to Grisps with Aircraft Performance, Toulouse: Airbus Flight Operations & Line Assistance, 2002.

[98] "Measurement of Airspeed," in *Jet Transport Performance Methods*, Seattle, WA: Performance Training Group, Flight Operations Engineering, Boeing Commercial Airplanes, 2009, pp. 6.1-6.11.

[99] "Drag Analysis," in *Jet Transport Performance Methods*, Performance Training Group, Flight Operations Engineering, Boeing Commercial Airplanes, 2009, pp. 11.7-11.8.

[100] Nordian AS, "Lift/Drag," in *Principles of Flight*, Sandefjord, Nordian AS, 2008, pp. 4-5.

[101] FAA, "Principles of Flight," in *Pilot's Handbook of Aeronautical Knowledge*, Oklahoma City, OK: U.S. Department of Transportation, Federal Aviation Administration, 2008, p. 3.2.

[102] Joint Aviation Requirements: JAR-FSTD A: Aeroplane Flight Simulation Training Devices, Hoofddorp: Joint Aviation Authorities, 2008, pp. 1-B-1.

[103] Joint Aviation Requirements: JAR-FSTD A: Aeroplane Flight Simulation Training Devices, Hoofddorp: Joint Aviation Authorities, 2008, pp. 1-C-7 - 1-C-25.

[104] H. Fong, Artist, *Airbus A320 Wingtip Fence.* [Art]. 2012.

[105] Airbus Industrie, "Takeoff Optimization Principle," in *Getting to Grisps with Aircraft Performance*, Toulouse, Airbus Flight Operations & Line Assistance, 2002, p. 192.

[106] International Civil Aviation Organization, "Review of Noise Abatement Procedure Research & Development and Implementation Results," International Civil Aviation Organization, 2007.

[107] Airbus Industrie, "Aircraft Limitations," in *Getting to Grisps with Aircraft Performance*, Toulouse, Airbus Flight Operations & Line Assistance, 2002, p. 31.

[108] Airbus Industrie, "Landing," in *Getting to Grisps with Aircraft Performance*, Toulouse, Airbus Flight Operations & Line Assistance, 2002, p. 113.

[109] Airbus Industrie, "Takeoff," in *Getting to Grips with Aircraft Performance*, Toulouse, Flight Operations Support & Line Assistance, 2002, p. 63.

[110] Airbus Industrie , "Takeoff Speeds," in *Getting to Grisps with Aircraft Performance*, Toulouse, Airbus Flight Operations & Line Assistance, 2002, p. 48.

[111] M. Bugaj, "The Basic Analysis of Control Systems on Commercial Aircraft," *Perner's Contacts,* vol. VI, no. 5, pp. 29-35, December 2011.

[112] Airbus Industrie , "Landing," in *Getting to Grisps with Aircraft Performance*, Toulouse, Airbus Flight Operations & Line Assistance, 2002, p. 113.

[113] B. Truslove, "Kegworth air disaster: Plane crash survivors' stories," *BBC News,* 8 January 2014.

[114] The Boeing Company, "The Boeing Next-Generation 737 Family - Productive, Progressive, Flexible, Familiar," The Boeing Company, 2013. [Online]. Available: http://www.boeing.com/boeing/commercial/737family/background.page. [Accessed 10 August 2013].

[115] The Boeing Company, "The Boeing Logbook: 1997-2001," The Boeing Company, 2013. [Online]. Available: http://www.boeing.com/boeing/history/chronology/chron16.page. [Accessed 10 August 2013].

[116] The Boeing Company, "737-600 Technical Characteristics," 2013. [Online]. Available: http://www.boeing.com/boeing/commercial/737family/pf/pf_600tech.page?. [Accessed 11 August 2013].

[117] The Boeing Company, "The Boeing 737-900ER," The Boeing Company, 2013. [Online]. Available: http://www.boeing.com/boeing/commercial/737family/pf/pf_900ER_back.page. [Accessed 11 August 2013].

[118] The Boeing Company, "Orders and Deliveries, User-Defined Forms," The Boeing Company, February 2015. [Online]. Available: http://active.boeing.com/commercial/orders/index.cfm?content=userdefinedselection.cfm&pageid=m15527. [Accessed February 2015].

[119] W. Roberson and J. A. Johns, "Fuel Conservation Strategies: Descent and Approach," *Aeromagazine,* pp. 25-27, Qtr_02 2010.

[120] W. Roberson and J. A. Johns, "Fuel Conservation Strategies: Takeoff and Climb," *Aeromagazine,* pp. 25-28, Qtr_4 2008.

[121] M. van der Lande, Artist, *Between heaven and earth.* [Art]. 2006.

[122] W. Blake, "Speeds," in *Jet Transport Performance Methods*, Oklahoma City, OK: Performance Training Group, Flight Operations Engineering, Boeing Commercial Airplanes, 2009, pp. 17.27-17.30.

[123] FAA, "Climb Via/ Descend Via Speed Clearances: Frequently Asked Questions," 14 2 2014. [Online]. Available: http://www.faa.gov/about/office_org/headquarters_offices/avs/offices/afs/afs400/afs470/pbn/media/rnav1_rnp1_rnav2/climb_descend_via_faq.pdf. [Accessed 9 2 2015].

[124] The Boeing Company, "Maneuvers," in *737-600/700/800/900/900ER Flight Crew Training Manual*, 8 ed., The Boeing Company, 2008, p. 7.12.

[125] The Boeing Company, "F.A.R. Landing Runway Length Requirements," in *737 Airplane Characteristics for Airport Planning*, Seattle, WA: Boeing Commercial Airplanes, 2011, p. 290.

[126] Airbus Industrie, "Airbus' Sharklets delivering efficiency to operators around the world," 18 June 2013. [Online]. Available: http://www.airbus.com/newsevents/news-events-single/detail/airbus-sharklets-delivering-efficiency-to-operators-around-the-world/. [Accessed 7 April 2015].

[127] H. J. Kelly, E. M. Cliff and F. H. Lutze, "Boost-Glide Range-Optimal Guidance," *Optimal Control Applications & Methods,* vol. 3, pp. 293-298, 1982.

[128] S. Weisberg, "Multiple Regression," in *Applied Linear Regression*, Hoboken, NJ: John Wiley & Soncs, Inc., 2014, pp. 51-69.

[129] D. K. Wilde, "Computing Clothoid Segments for Trajectory Generation," in *2009 IEEE/RSJ International Conference on Intelligent Robots and Systems, IROS 2009*, St. Louis, 2009.

[130] K. Knopp, "The Expansions of the So-Called Elementary Functions," in *Theory and Application of Infinite Series*, New York, NY: Dover Publications, Inc., 1990, pp. 198-208.

[131] W. Blake, "The Atmosphere," in *Jet Transport Performance Methods*, Oklahoma City, OK: Performance Training Group, Flight Operations Engineering, Boeing Commercial Airplanes, 2009, p. 4.8.

[132] D. Simon, Evolutionary Optimization Algorithms, Hoboken, NJ: John Wiley & Sons, Inc., 2013.

[133] K. V. Price, R. M. Storn and J. A. Lampinen, Differential Evolution: A Practical Approach to Global Optimization, Berlin: Springer-Verlag, 2005.

[134] Air Accidents Investigation Branch, "Report on the accident to Boeing 777-236ER, G-YMMM, at London Heathrow Airport on 17 January 2008," Department of Transport, Air Accidents Investigation Branch, Hampshire, 2010.

[135] Baltic Aviation Academy, "Dual Engine Failure during Climb-out on Airbus A320," Baltic Aviation Academy, Vilnius, 2013.

[136] D. C. Hyde, "Minimum-Altitude-Loss Gliding Turns with Terminal Constraints (Return to Runway After Engine

Failure)," in *AIAA Atmospheric Flight Mechanics Conference and Exhibit*, San Francisco, 2005.

[137] The Boeing Company, "Schiphol Airport," 2011. [Online]. Available: http://www.boeing.com/resources/boeingdotcom/commercial/noise/schiphol.html. [Accessed 11 April 2015].

[138] The Boeing Company, "Atatürk International Airport," February 2011. [Online]. Available: http://www.boeing.com/resources/boeingdotcom/commercial/noise/ataturk.html. [Accessed 11 April 2015].

[139] A. Agresti, "Models for Matched Pairs," in *An Introduction to Categorical Data Analysis*, Hoboken, NJ: John Wiley & Sons, Inc., 2007, pp. 244-250.

[140] A. Agresti, "Modeling Correlated, Clustered Responses," in *Introduction to Categorical Data Analysis*, Hoboken, NJ: John Wiley & Sons, Inc., 2007, pp. 276-278.

[141] A. Agresti, "Random Effects: Generalized Linear Mixed Models," in *An Introduction to Categorical Data Analysis*, Hoboken, NJ: John Wiley & Sons, Inc., 2007, pp. 297-302.

[142] E. Vittinghoff and C. E. McCulloch, "Relaxing the Rule of Ten Events per Variable in Logistic and Cox Regression," *American Journal of Epidemiology,* vol. 165, no. 6, pp. 710-718, 2006.

[143] R. D. Wolfinger, "Laplace's approximation for nonlinear mixed models," *Biometrika,* vol. 80, no. 4, pp. 791-795, December 1993.

[144] S. S. Shapiro and M. Wilk, "An Analysis of Variance Test for Normality (Complete Samples)," *Biometrika,* vol. 52, no. 3-4, pp. 591-611, 1965.

APPENDIX A. OPTIMUM LANDING TRAJECTORY SOLUTIONS FOR THE AIRBUS A320 AIRCRAFT

A.1 Solutions for the "Flaps" Scenario

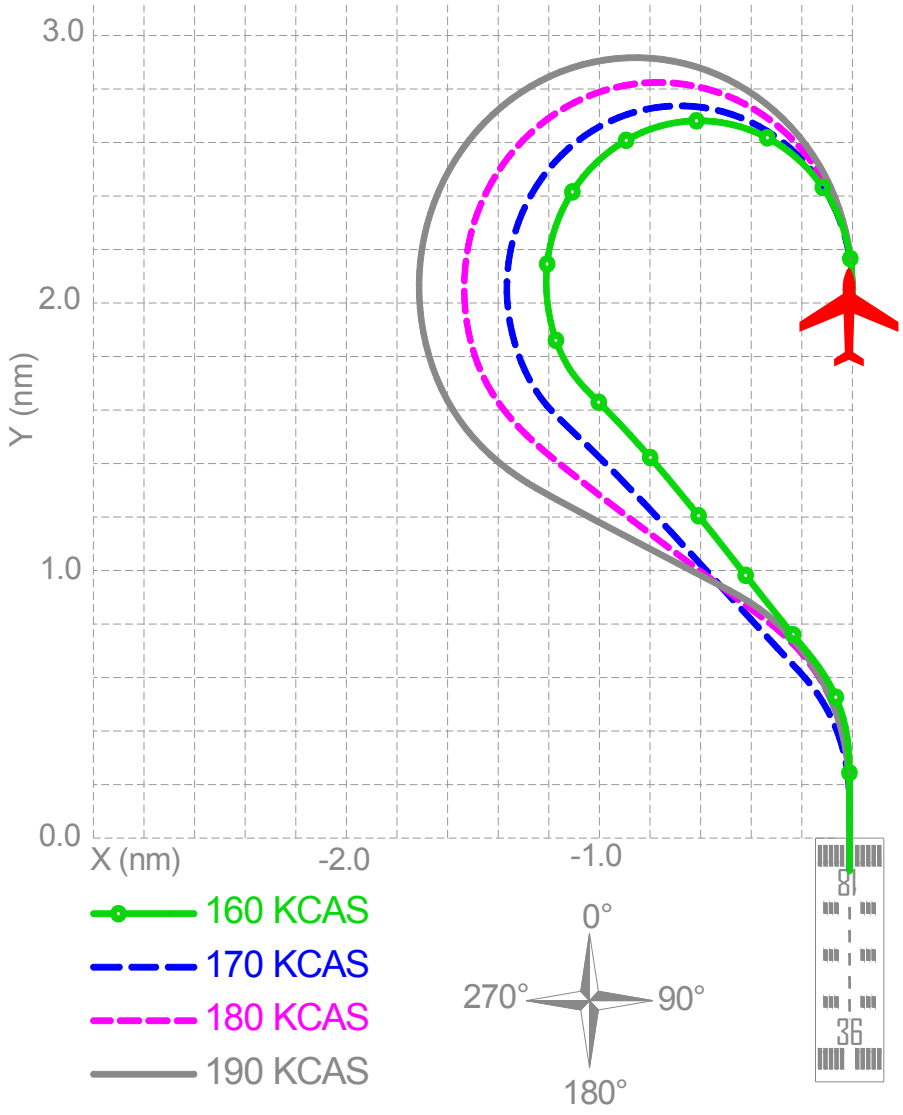

Figure A-1. Ground tracks of the predicted optimum engines-out landing trajectories for the "flaps" scenario (no wind).

Table A-1. Solutions from the segmented trajectory generation algorithm for the "flaps" scenario (no wind).

	Airspeed (KCAS)	160	170	180	190
Optimum Trajectory	S_{L_1} (nm)	0	0	0	0
	$\Delta\theta_1$ (°)	-221	-225	-234	-243
	ϕ_1 (°)	33	33	33	33
	S_{L_2} (nm)	1.2	1.2	1.0	0.7
	$\Delta\theta_2$ (°)	41	45	54	63
	ϕ_2 (°)	33	33	33	33
	S_{L_3} (nm)	0	0	0	0
	$\Delta\theta_3$ (°)	0	0	0	0
	ϕ_3 (°)	N/A	N/A	N/A	N/A
	S_{L_4} (nm)	0	0	0	0
Required Altitude Loss	Predicted (ft)	2660	2722	2824	3004
	Simulated* (ft)	2600	2667	2767	2917
	Absolute relative difference	2.3%	2.1%	2.1%	3.0%

**: Average result from three simulation runs. The result from each run is rounded up to the nearest 50 ft.*

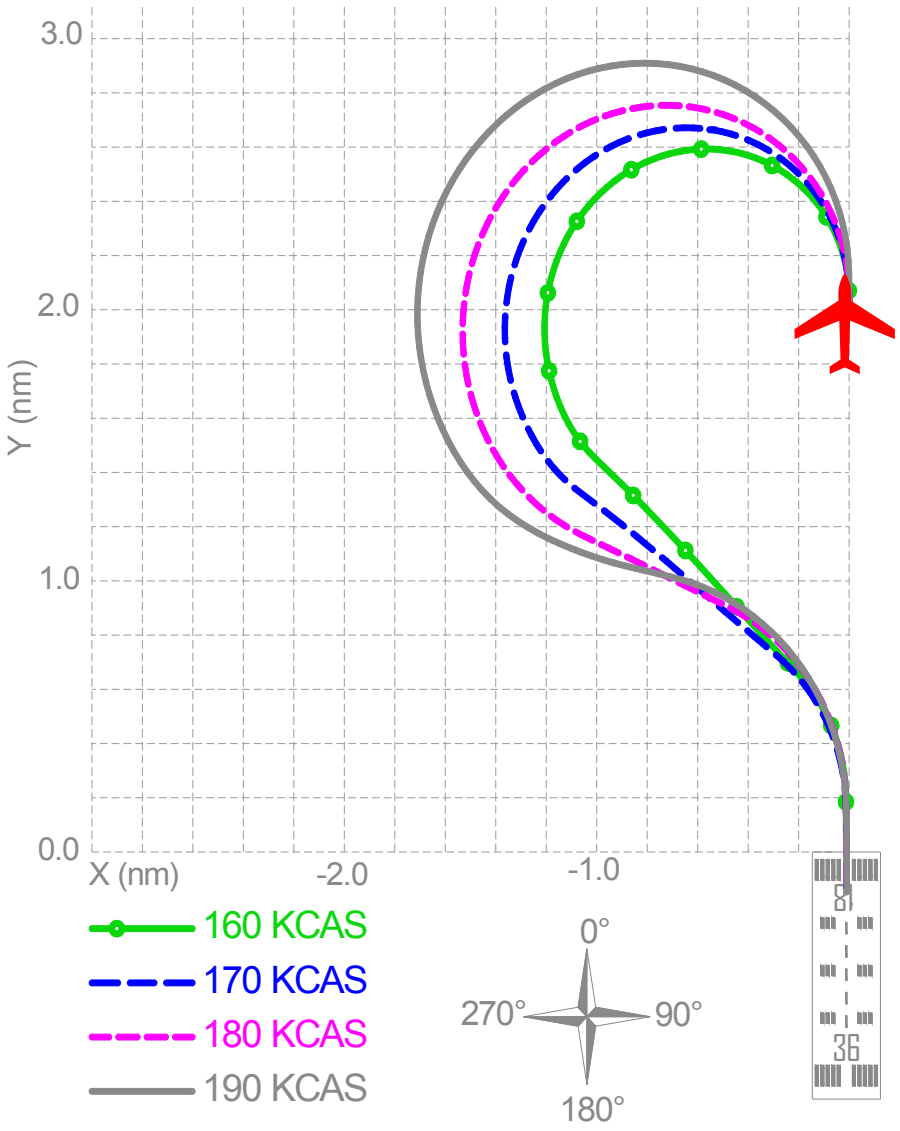

Figure A-2. Ground tracks of the predicted optimum engines-out landing trajectories for the "flaps" scenario (wind is 0° at 10 knots).

Table A-2. Solutions from the segmented trajectory generation algorithm for the "flaps" scenario (wind is 0° at 10 knots).

	Airspeed (KCAS)	160	170	180	190
Optimum Trajectory	S_{L_1} (nm)	0	0	0	0
	$\Delta\theta_1$ (°)	-228	-235	-248	-260
	ϕ_1 (°)	33	33	33	33
	S_{L_2} (nm)	1.0	0.8	0.5	0.2
	$\Delta\theta_2$ (°)	48	55	68	80
	ϕ_2 (°)	33	33	33	33
	S_{L_3} (nm)	0	0	0	0
	$\Delta\theta_3$ (°)	0	0	0	0
	ϕ_3 (°)	N/A	N/A	N/A	N/A
	S_{L_4} (nm)	0	0	0	0
Required Altitude Loss	Predicted (ft)	2576	2668	2806	3024
	Simulated* (ft)	2500	2583	2717	2933
	Absolute relative difference	3.0%	3.3%	3.3%	3.1%

**: Average result from three simulation runs. The result from each run is rounded up to the nearest 50 ft.*

A.2 Solutions for the "Clean" Scenario

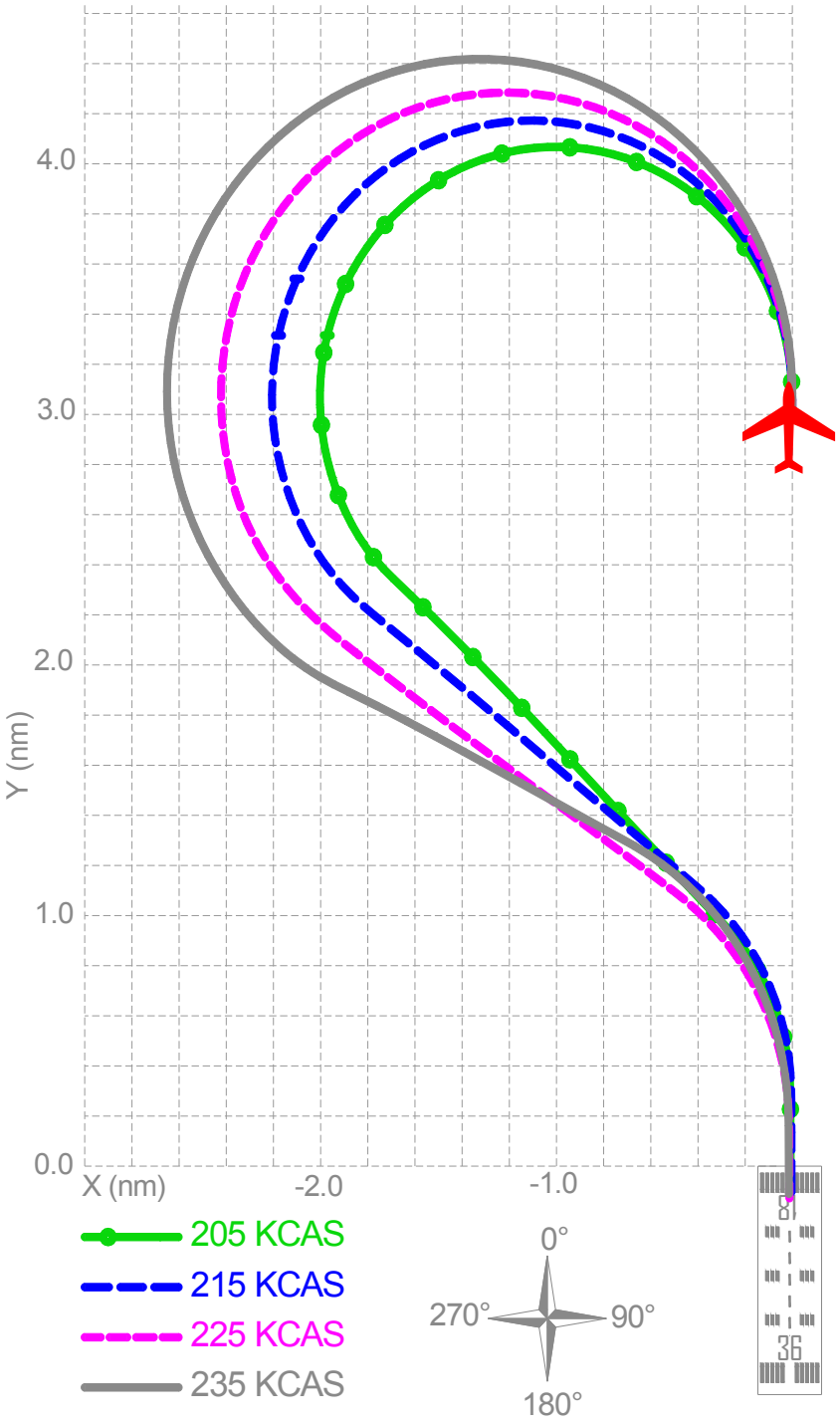

Figure A-3. Ground tracks of the predicted optimum engines-out landing trajectories for the "clean" scenario (no wind).

Table A-3. Solutions from the segmented trajectory generation algorithm for the "clean" scenario (no wind).

	Airspeed (KCAS)	205	215	225	235
Optimum Trajectory	S_{L_1} (nm)	0	0	0	0
	$\Delta\theta_1$ (°)	-225	-232	-235	-243
	ϕ_1 (°)	33	33	33	33
	S_{L_2} (nm)	1.8	1.7	1.6	1.2
	$\Delta\theta_2$ (°)	45	51	55	63
	ϕ_2 (°)	33	33	33	33
	S_{L_3} (nm)	0	0	0	0
	$\Delta\theta_3$ (°)	0	0	0	0
	ϕ_3 (°)	N/A	N/A	N/A	N/A
	S_{L_4} (nm)	0	0	0	0
Required Altitude Loss	Predicted (ft)	3098	3226	3443	3672
	Simulated* (ft)	3017	3167	3367	3583
	Absolute relative difference	2.7%	1.9%	2.3%	2.5%

**: Average result from three simulation runs. The result from each run is rounded up to the nearest 50 ft.*

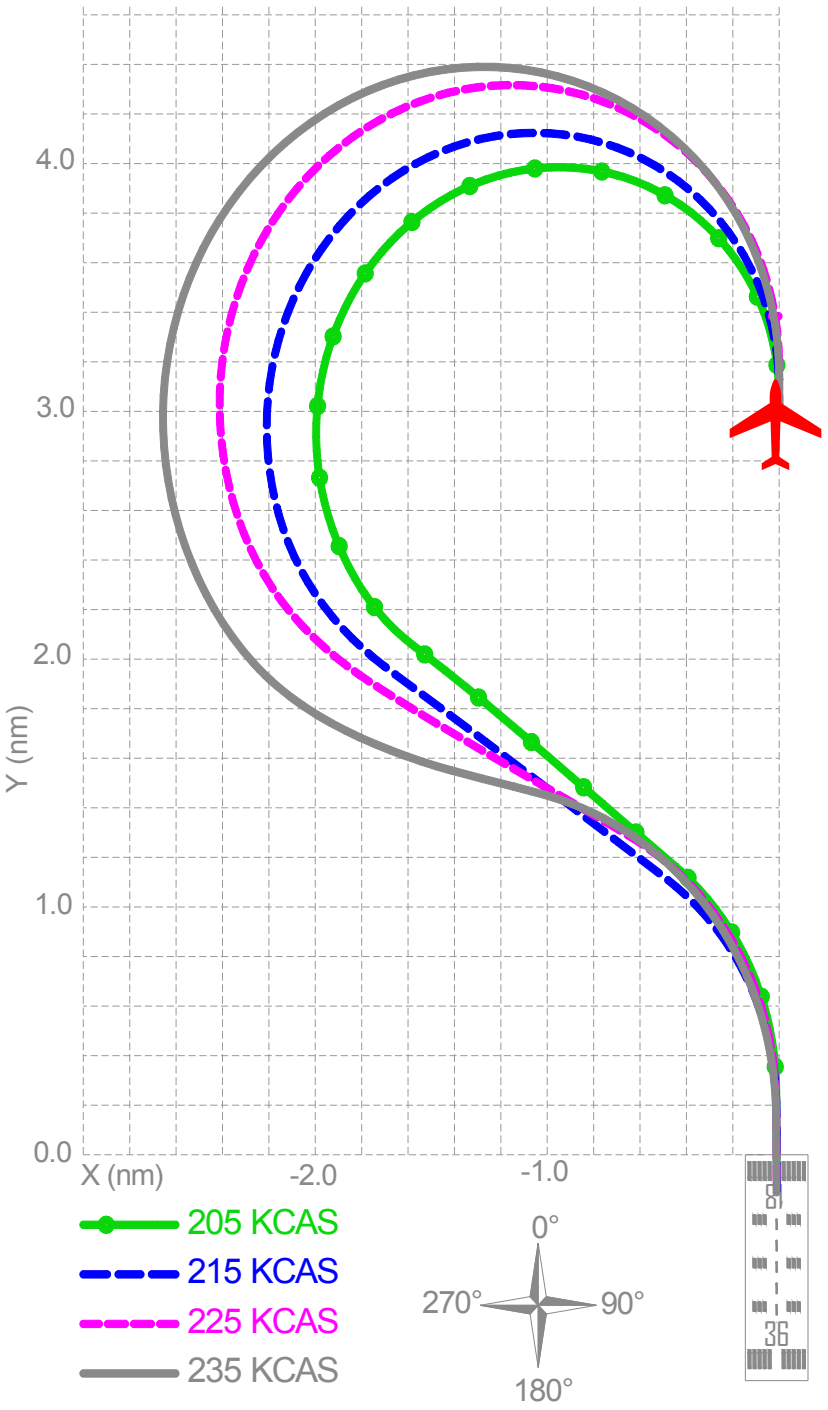

Figure A-4. Ground tracks of the predicted optimum engines-out landing trajectories for the "clean" scenario (wind is 0° at 10 knots).

Table A-4. Solutions from the segmented trajectory generation algorithm for the "clean" scenario (wind is 0° at 10 knots).

	Airspeed (KCAS)	205	215	225	235
Optimum Trajectory	S_{L_1} (nm)	0	0	0	0
	$\Delta\theta_1$ (°)	-234	-237	-243	-258
	ϕ_1 (°)	33	33	33	33
	S_{L_2} (nm)	1.3	1.2	1.1	0.4
	$\Delta\theta_2$ (°)	54	57	63	78
	ϕ_2 (°)	30	33	33	33
	S_{L_3} (nm)	0	0	0	0
	$\Delta\theta_3$ (°)	0	0	0	0
	ϕ_3 (°)	N/A	N/A	N/A	N/A
	S_{L_4} (nm)	0	0	0	0
Required Altitude Loss	Predicted (ft)	3046	3198	3376	3705
	Simulated* (ft)	2967	3100	3267	3583
	Absolute relative difference	2.7%	3.2%	3.3%	3.4%

**: Average result from three simulation runs. The result from each run is rounded up to the nearest 50 ft.*

APPENDIX B. OPTIMUM LANDING TRAJECTORY SOLUTIONS FOR THE BOEING 737-800 AIRCRAFT

B.1 Solutions for the "Flaps" Scenario

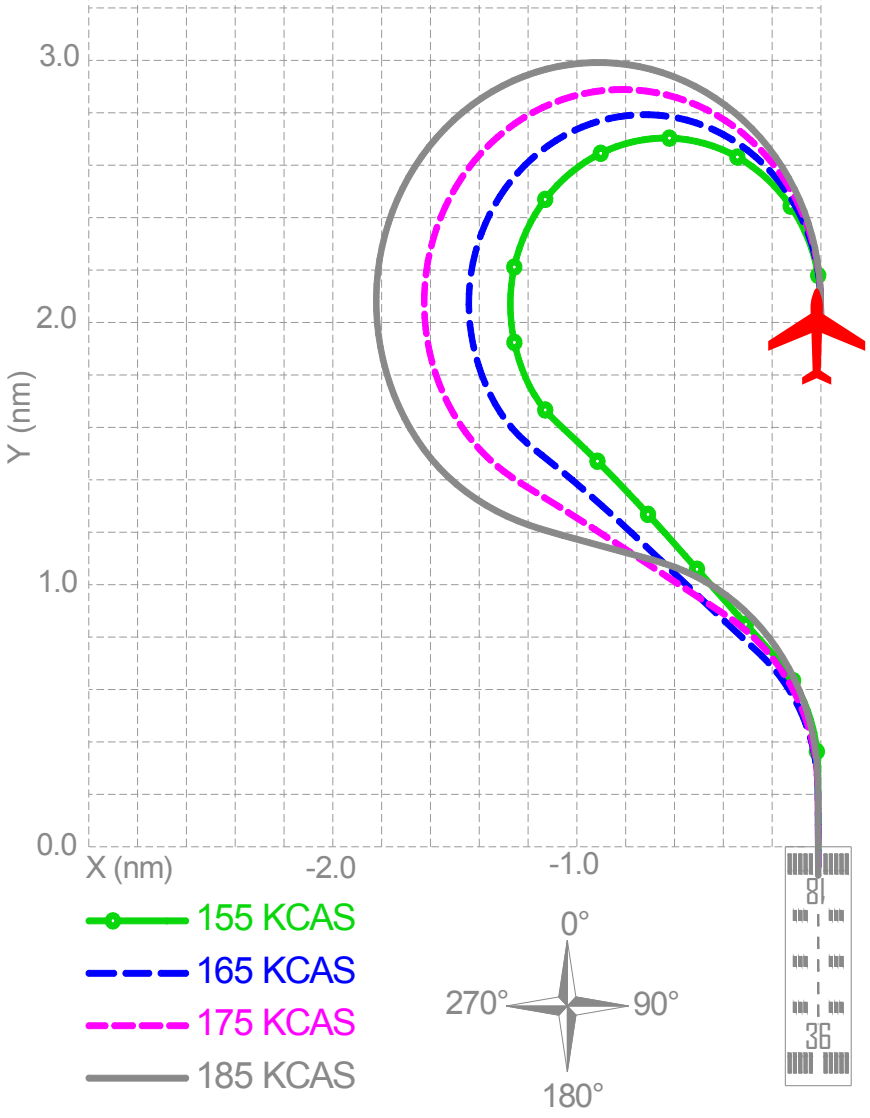

Figure B-1. Ground tracks of the predicted optimum engines-out landing trajectories for the "flaps" scenario (no wind).

Table B-1. Solutions from the segmented trajectory generation algorithm for the "flaps" scenario (no wind).

	Airspeed (KCAS)	155	165	175	185
Optimum Trajectory	S_{L_1} (nm)	0	0	0	0
	$\Delta\theta_1$ (°)	-225	-230	-239	-256
	ϕ_1 (°)	30	30	30	30
	S_{L_2} (nm)	1.1	1.1	0.8	0.3
	$\Delta\theta_2$ (°)	45	50	59	76
	ϕ_2 (°)	30	30	30	30
	S_{L_3} (nm)	0	0	0	0
	$\Delta\theta_3$ (°)	0	0	0	0
	ϕ_3 (°)	N/A	N/A	N/A	N/A
	S_{L_4} (nm)	0	0	0	0
Required Altitude Loss	Predicted (ft)	2394	2547	2695	2905
	Simulated* (ft)	2300	2433	2583	2783
	Absolute relative difference	4.1%	4.7%	4.3%	4.4%

**: Average result from three simulation runs. The result from each run is rounded up to the nearest 50 ft.*

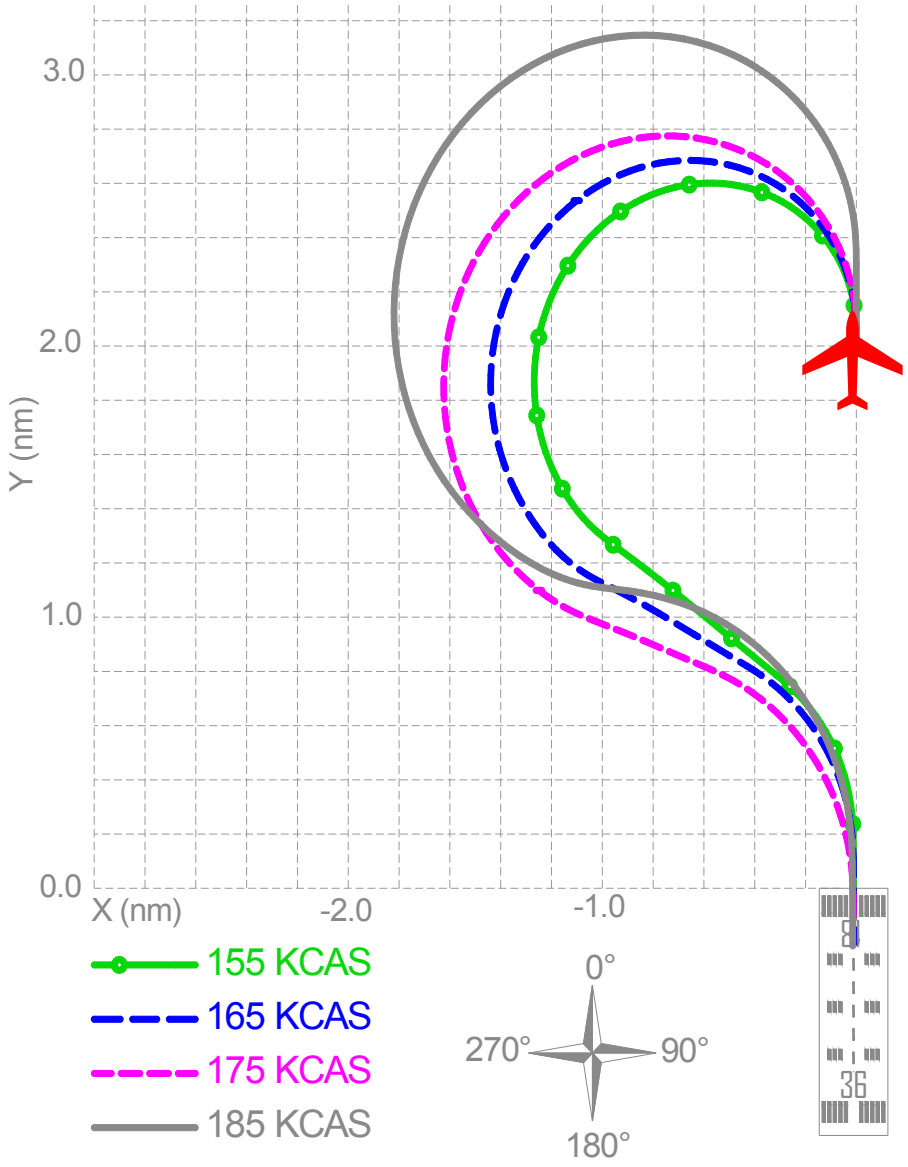

Figure B-2. Ground tracks of the predicted optimum engines-out landing trajectories for the "flaps" scenario (wind is 0° a 15 knots).

Table B-2. Solutions from the segmented trajectory generation algorithm for the "flaps" scenario (wind is 0° a 15 knots).

	Airspeed (KCAS)	155	165	175	185
Optimum Trajectory	S_{L_1} (nm)	0	0	0	0.3
	$\Delta\theta_1$ (°)	-238	-246	-253	-266
	ϕ_1 (°)	30	30	30	30
	S_{L_2} (nm)	0.7	0.5	0.4	0
	$\Delta\theta_2$ (°)	58	66	73	86
	ϕ_2 (°)	30	30	30	30
	S_{L_3} (nm)	0	0	0	0
	$\Delta\theta_3$ (°)	0	0	0	0
	ϕ_3 (°)	N/A	N/A	N/A	N/A
	S_{L_4} (nm)	0	0	0	0
Required Altitude Loss	Predicted (ft)	2329	2506	2601	2908
	Simulated* (ft)	2233	2400	2483	2767
	Absolute relative difference	4.3%	4.4%	4.7%	5.1%

**: Average result from three simulation runs. The result from each run is rounded up to the nearest 50 ft.*

B.2 Solutions for the "Clean" Scenario

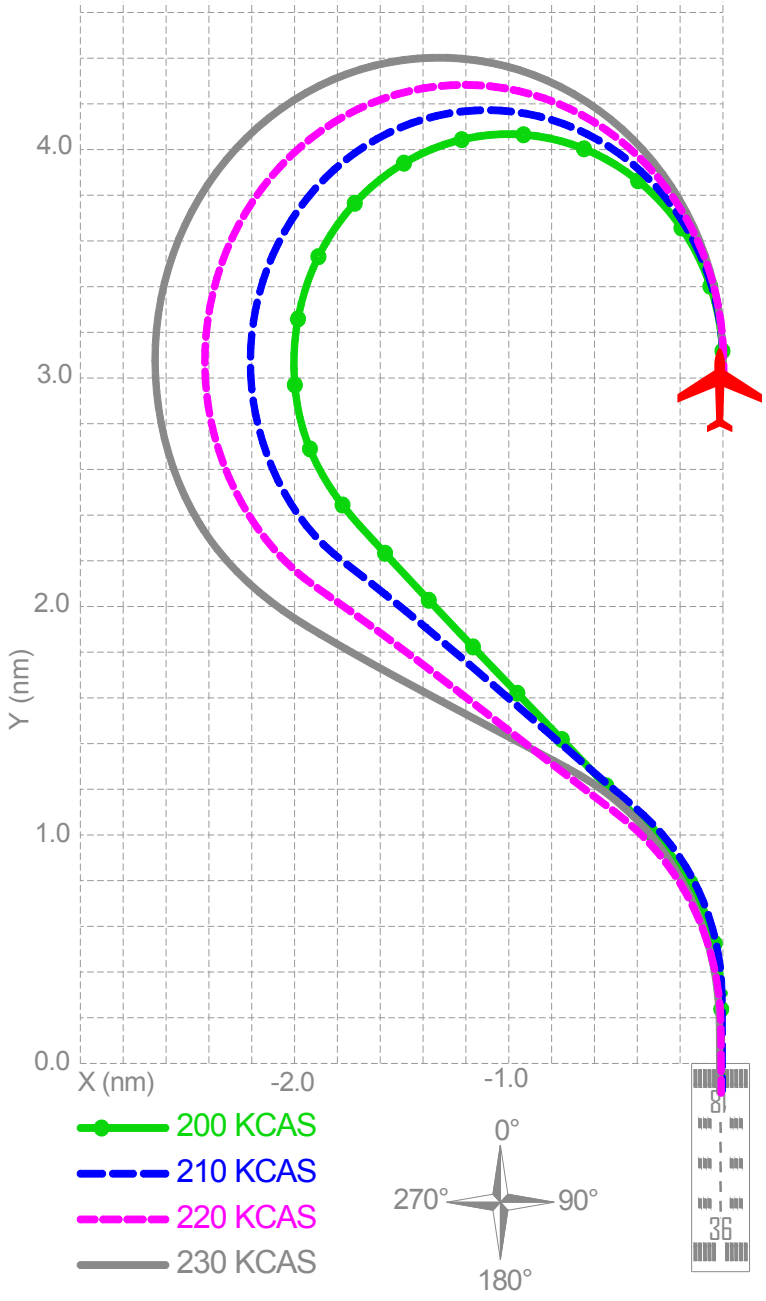

Figure B-3. Ground tracks of the predicted optimum engines-out landing trajectories for the "clean" scenario (no wind).

Table B-3. Solutions from the segmented trajectory generation algorithm for the "clean" scenario (no wind).

	Airspeed (KCAS)	200	210	220	230
Optimum Trajectory	S_{L_1} (nm)	0	0	0	0
	$\Delta\theta_1$ (°)	-229	-234	-240	-252
	ϕ_1 (°)	30	30	30	30
	S_{L_2} (nm)	1.7	1.5	1.3	0.8
	$\Delta\theta_2$ (°)	49	54	60	72
	ϕ_2 (°)	30	30	30	30
	S_{L_3} (nm)	0	0	0	0
	$\Delta\theta_3$ (°)	0	0	0	0
	ϕ_3 (°)	N/A	N/A	N/A	N/A
	S_{L_4} (nm)	0	0	0	0
Required Altitude Loss	Predicted (ft)	3003	3062	3202	3497
	Simulated* (ft)	2867	2917	3067	3350
	Absolute relative difference	4.7%	5.0%	4.4%	4.4%

**: Average result from three simulation runs. The result from each run is rounded up to the nearest 50 ft.*

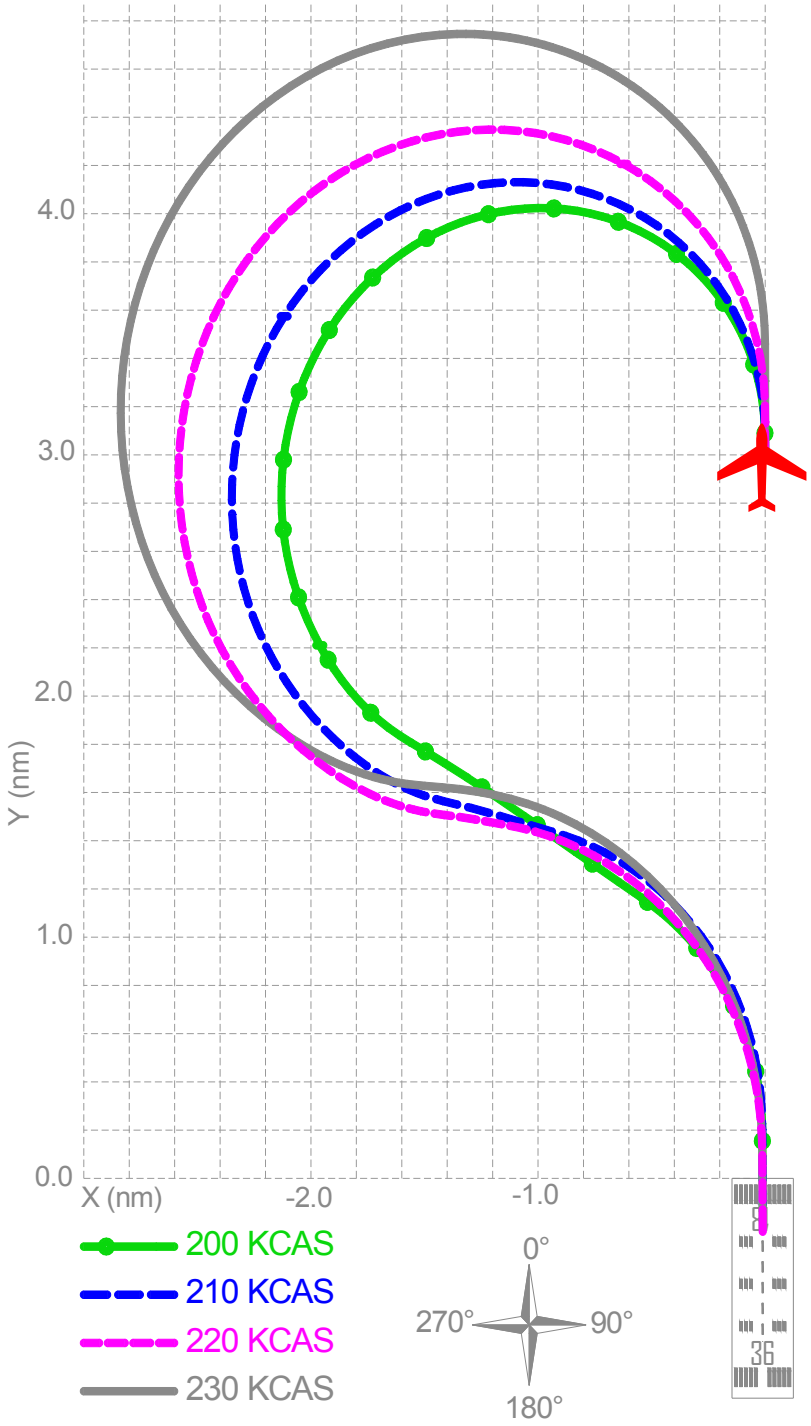

Figure B-4. Ground tracks of the predicted optimum engines-out landing trajectories for the "clean" scenario (wind is 0° a 15 knots).

Table B-4. Solutions from the segmented trajectory generation algorithm for the "clean" scenario (wind is 0° a 15 knots).

	Airspeed (KCAS)	200	210	220	230
Optimum Trajectory	S_{L_1} (nm)	0	0	0.1	0.4
	$\Delta\theta_1$ (°)	-241	-259	-265	-267
	ϕ_1 (°)	30	30	30	30
	S_{L_2} (nm)	1.0	0.3	0.1	0
	$\Delta\theta_2$ (°)	61	79	85	87
	ϕ_2 (°)	30	30	30	30
	S_{L_3} (nm)	0	0	0	0
	$\Delta\theta_3$ (°)	0	0	0	0
	ϕ_3 (°)	N/A	N/A	N/A	N/A
	S_{L_4} (nm)	0	0	0	0
Required Altitude Loss	Predicted (ft)	2868	2963	3213	3626
	Simulated* (ft)	2767	2850	3083	3483
	Absolute relative difference	3.7%	3.9%	4.2%	4.1%

**: Average result from three simulation runs. The result from each run is rounded up to the nearest 50 ft.*

APPENDIX C. OPTIMUM LANDING TRAJECTORY SOLUTIONS FOR THE SIMULATED TOTAL-LOSS-OF-THRUST SCENARIOS

Table C-1. Optimum landing trajectory solutions for the Airbus A320 aircraft (aircraft gross weight=70.0 tons).

	No. of Total-Loss-of-Thrust Scenario	1	2	3	4
	Wing Configuration	1+F	1+F	Up (Clean)	Up (Clean)
	Airport	Schiphol	Schiphol	Atatürk	Atatürk
	Takeoff Runway	36C	06	17L	05
	Landing Runway	18R	18L	05	17L
	Airspeed (KCAS)	160	160	205	205
Optimum Trajectory	S_{L_1} (nm)	0.5	0	0	0
	$\Delta\theta_1$ (°)	-182	-149	194	-176
	ϕ_1 (°)	33	33	33	33
	S_{L_2} (nm)	0.3	0.6	0.1	2.6
	$\Delta\theta_2$ (°)	2	-86	46	-64
	ϕ_2 (°)	33	33	10	33
	S_{L_3} (nm)	0	0.6	0.4	0
	$\Delta\theta_3$ (°)	0	0	0	0
	ϕ_3 (°)	N/A	N/A	N/A	N/A
	S_{L_4} (nm)	0	0	0	0
Required Altitude Loss	Predicted (ft)	1946	2291	2844	2949
	Simulated* (ft)	1900	2217	2767	2883
	Absolute relative difference	2.4%	3.3%	2.8%	2.3%

**: Average result from three simulation runs. The result from each run is rounded up to the nearest 50 ft.*

Table C-2. Optimum landing trajectory solutions for the Boeing 737-800 aircraft (aircraft gross weight=70.0 tons).

	No. of Total-Loss-of-Thrust Scenario	1	2	3	4
	Flap setting	5	5	Up (Clean)	Up (Clean)
	Airport	Schiphol	Schiphol	Atatürk	Atatürk
	Takeoff Runway	36C	06	17L	05
	Landing Runway	18R	18L	05	17L
	Airspeed (KCAS)	155	155	200	200
Optimum Trajectory	S_{L_1} (nm)	0.4	0	0	0
	$\Delta\theta_1$ (°)	-192	-148	168	-178
	ϕ_1 (°)	30	30	30	30
	S_{L_2} (nm)	0.1	0.3	0	2.5
	$\Delta\theta_2$ (°)	12	-87	72	-62
	ϕ_2 (°)	30	30	16	30
	S_{L_3} (nm)	0.2	0.6	1.4	0
	$\Delta\theta_3$ (°)	0	0	0	0
	ϕ_3 (°)	N/A	N/A	N/A	N/A
	S_{L_4} (nm)	0	0	0	0
Required Altitude Loss	Predicted (ft)	1748	1981	2814	2787
	Simulated* (ft)	1700	1917	2750	2700
	Absolute relative difference	2.8%	3.3%	2.3%	3.2%

**: Average result from three simulation runs. The result from each run is rounded up to the nearest 50 ft.*

APPENDIX D. OUTCOMES FROM THE DESIGNED EXPERIMENT

Table D-1. Simulation outcomes for the A320-200 aircraft.

No. of Pilot	No. of Simulated Scenario	Control or Treatment run?	Outcome	Runway Attempted for Landing	Notes
1	5	Control	Safe Landing	18R	
1	4	Control	Crash/ Hull Loss	23	Increased airspeed to green dot speed.
1	1	Control	Safe Landing	18R	
1	2	Control	Crash/ Hull Loss	22	
1	3	Control	Crash/ Hull Loss	05	Increased airspeed to green dot speed.
1	5	Treatment	Safe Landing	18R	
1	4	Treatment	Safe Landing	17L	
1	3	Treatment	Safe Landing	05	
1	1	Treatment	Safe Landing	18R	
1	2	Treatment	Safe Landing	18L	
2	4	Control	Crash/ Hull Loss	23	Increased airspeed to slightly less than green dot speed.
2	1	Control	Crash/ Hull Loss	18C	
2	2	Control	Crash/ Hull Loss	18L	Failure to follow optimum trajectory, turned back too sharp initially and missed the runway.
2	5	Control	Safe Landing	35L	Additional starting altitude enabled landing on 35L.
2	3	Control	Crash/ Hull Loss	05	Increased airspeed to slightly less than green dot speed.
2	5	Treatment	Safe Landing	18R	
2	4	Treatment	Safe Landing	17L	
2	3	Treatment	Safe Landing	05	
2	2	Treatment	Safe Landing	18L	
2	1	Treatment	Safe Landing	18R	
3	4	Control	Crash/ Hull Loss	23	
3	2	Control	Crash/ Hull Loss	22	
3	3	Control	Safe Landing	05	
3	5	Control	Safe Landing	35L	Additional 50-ft starting altitude enabled landing on 35L although it was not the optimum runway.
3	1	Control	Crash/ Hull Loss	18R	Turned back too soon, approached too high and overshot the runway.
3	3	Treatment	Safe Landing	05	
3	4	Treatment	Safe Landing	17L	
3	1	Treatment	Safe Landing	18R	
3	2	Treatment	Safe Landing	18L	
3	5	Treatment	Safe Landing	18R	

Table D-1 (continued). Simulation outcomes for the A320-200 aircraft.

No. of Pilot	No. of Simulated Scenario	Control or Treatment run?	Outcome	Runway Attempted for Landing	Notes
4	4	Control	Crash/ Hull Loss	23	
4	2	Control	Safe Landing	18L	
4	1	Control	Safe Landing	18R	
4	3	Control	Safe Landing	05	
4	5	Control	Safe Landing	18R	
4	5	Treatment	Safe Landing	18R	
4	3	Treatment	Safe Landing	05	
4	2	Treatment	Safe Landing	18L	
4	1	Treatment	Safe Landing	18R	
4	4	Treatment	Safe Landing	17L	
5	2	Control	Crash/ Hull Loss	22	
5	4	Control	Crash/ Hull Loss	23	Increased airspeed to green dot speed.
5	3	Control	Crash/ Hull Loss	05	Increased airspeed to green dot speed.
5	1	Control	Crash/ Hull Loss	18R	Turned back too soon, too high on final approach and overshot the runway.
5	5	Control	Safe Landing	18R	
5	3	Treatment	Safe Landing	05	
5	5	Treatment	Safe Landing	18R	
5	1	Treatment	Safe Landing	18R	
5	4	Treatment	Crash/ Hull Loss	17L	Wingtip collision during the final left turn at 33°-turn due to delayed response from the pilot.
5	2	Treatment	Safe Landing	18L	
6	4	Control	Crash/ Hull Loss	23	Used bank angles less than the optimum bank angle of 33°. Increased airspeed to green dot speed.
6	3	Control	Crash/ Hull Loss	05	Increased airspeed to green dot speed.
6	5	Control	Safe Landing	18R	
6	1	Control	Crash/ Hull Loss	18R	Turned back too soon, too high on approach and overshot the runway.
6	2	Control	Crash/ Hull Loss	22	
6	3	Treatment	Safe Landing	05	
6	1	Treatment	Safe Landing	18R	
6	2	Treatment	Safe Landing	18L	
6	5	Treatment	Safe Landing	18R	
6	4	Treatment	Safe Landing	17L	

Table D-2. Simulation outcomes for the 737-800 aircraft.

No. of Pilot	No. of Simulated Scenario	Control or Treatment run?	Outcome	Runway Attempted for Landing	Notes
1	3	Control	Crash/ Hull Loss	05	Used bank angles less than the optimum bank angle of 30°. Increased airspeed to maneuvering speed.
1	2	Control	Crash/ Hull Loss	22	Increased airspeed to slightly below maneuvering speed.
1	4	Control	Crash/ Hull Loss	23	Increased airspeed to slightly below maneuvering speed.
1	5	Control	Crash/ Hull Loss	05	Increased airspeed to maneuvering speed.
1	1	Control	Crash/ Hull Loss	18R	Turned back too soon, too high on approach and overshot the runway.
1	5	Treatment	Safe Landing	05	
1	4	Treatment	Crash/ Hull Loss	17L	Failure to maintain commanded constant optimum speed & optimum bank angle of 30°
1	3	Treatment	Crash/ Hull Loss	05	Failure to maintain commanded constant optimum speed.
1	2	Treatment	Safe Landing	18L	
1	1	Treatment	Safe Landing	18R	
2	3	Control	Safe Landing	05	
2	5	Control	Safe Landing	05	
2	1	Control	Crash/ Hull Loss	18R	Increased airspeed to over V_{LS}, but less than maneuvering speed.
2	4	Control	Safe Landing	17L	Increased airspeed to over V_{LS}, but less than maneuvering speed.
2	2	Control	Crash/ Hull Loss	18L	
2	3	Treatment	Safe Landing	05	
2	2	Treatment	Safe Landing	18L	
2	4	Treatment	Safe Landing	17L	
2	1	Treatment	Crash/ Hull Loss	18R	Failure to maintain commanded constant speed. Crashed short of runway.
2	5	Treatment	Safe Landing	05	
3	4	Control	Crash/ Hull Loss	23	Increased airspeed close to maneuvering speed.
3	3	Control	Crash/ Hull Loss	05	Used bank angles less than the optimum bank angle of 30°.
3	2	Control	Crash/ Hull Loss	18L	Increased airspeed close to maneuvering speed.
3	5	Control	Crash/ Hull Loss	35L	Increased airspeed close to maneuvering speed.
3	1	Control	Crash/ Hull Loss	18R	Turned back too soon, too high on approach and overshot the runway. Increased airspeed close to maneuvering speed.
3	4	Treatment	Crash/ Hull Loss	17L	
3	5	Treatment	Safe Landing	05	
3	2	Treatment	Safe Landing	18L	
3	1	Treatment	Safe Landing	18R	
3	3	Treatment	Safe Landing	05	

Table D-2 (continued). Simulation outcomes for the 737-800 aircraft.

No. of Pilot	No. of Simulated Scenario	Control or Treatment run?	Outcome	Runway Attempted for Landing	Notes
4	4	Control	Crash/ Hull Loss	23	Used bank angles less than the optimum bank angle of 30°. Increased airspeed to maneuvering speed.
4	1	Control	Crash/ Hull Loss	18C	
4	3	Control	Crash/ Hull Loss	05	Increased airspeed close to maneuvering speed.
4	2	Control	Safe Landing	18L	
4	5	Control	Safe Landing	05	
4	5	Treatment	Safe Landing	05	
4	2	Treatment	Safe Landing	18L	
4	3	Treatment	Safe Landing	05	
4	1	Treatment	Safe Landing	18R	
4	4	Treatment	Crash/ Hull Loss	17L	
5	2	Control	Crash/ Hull Loss	22	
5	1	Control	Safe Landing	18R	
5	4	Control	Crash/ Hull Loss	23	
5	3	Control	Safe Landing	05	
5	5	Control	Safe Landing	05	
5	2	Treatment	Safe Landing	18L	
5	5	Treatment	Safe Landing	05	
5	1	Treatment	Safe Landing	18R	
5	3	Treatment	Safe Landing	05	
5	4	Treatment	Safe Landing	17L	
6	2	Control	Crash/ Hull Loss	22	
6	3	Control	Safe Landing	05	
6	5	Control	Safe Landing	05	
6	4	Control	Safe Landing	17L	
6	1	Control	Crash/ Hull Loss	18C	
6	4	Treatment	Safe Landing	17L	
6	3	Treatment	Safe Landing	05	
6	2	Treatment	Safe Landing	18L	
6	1	Treatment	Safe Landing	18R	
6	5	Treatment	Crash/ Hull Loss	05	Runway overshoot - short runway.